From bacteria to cancer: exploiting metabolic networks for industrial and therapeutic purposes

Claudio Tomi Andrino, BSc

Thesis submitted to the University of Nottingham for the degree of Doctor of Philosophy

November 2022

Declaration

Unless otherwise acknowledged, the work presented in this thesis is my own. No part has been submitted for another degree in the University of Nottingham or any other institute of learning.



Claudio Tomi Andrino
November 2022

Abstract

Metabolic modelling has been used to facilitate industrial microbiology projects and identify potential drug targets for the last 15 years. Although originally modest, the reliability of simulations has greatly improved by the progressive inclusion of chemical, biological and medical information in the models. While the multidisciplinary nature of systems biology entails rich and novel perspectives to solve problems, it is accompanied by a general lack of standardisation and consensus on methodology. Therefore, establishing robust workflows requires (i) assessing and comparing the predictive capabilities of current approaches against experimental data, and (ii) combining the strong points of different strategies to minimize their limitations and generate useful data in a timely manner.

In this study, metabolic networks for a bacterium, a parasite and a type of cancer were inspected by means of flux balance analysis and network analysis. Firstly, a readily available toolbox integrating thermodynamics information into flux balance analysis was modified to increase the number of physicochemical parameters including more suitable equations to physiological conditions. Thermodynamics constraints are closely related to the quantitation of metabolites in the cell. However, the lack of a "one size fits all" extraction and quantitation method prevents from performing a systems-wide analysis, forcing the researcher to select ca. 50 compounds for a targeted method. Exploring the topology of the network allowed identifying a set of important metabolites with a high constraining power, thus providing a rationale to such selection.

Secondly, metabolic modelling was used to facilitate drug repurposing efforts. There is a plethora of neglected diseases or conditions yet to be efficiently treated, so screening readily available drugs for novel uses has been deemed a cheaper and faster option than developing drugs from scratch. Therefore, systems biology has been exploited to reduce the list of potential candidates to be tested, as well as to identify novel potential drug targets. Specifically, a novel topological feature was introduced and combined with multiple metabolic states predicted by flux balance analysis in a model for the parasite causing sleeping sickness. Comparing against the literature validated the predictive capabilities of such approach and identified an antiviral whose potential lethality was tested *in vitro*.

Thirdly, a more information-rich workflow was developed based on the previous results. Transcriptomics data for a brain tumour was exploited to generate contextualised human metabolic models. Network analyses pinpointed important reactions and topological features of interest, greatly reducing the list of potential drug targets to be considered. Consequently, an automated search of chemical-gene interactions and published results allowed identifying five compounds that had proven anti-proliferative and anti-invasion effects on other cancer types. Finally, *in vitro* testing on patient-derived cancer cell lines showed their potential for further studies and generated new research questions.

This study provides considerations and approaches to increase the reliability of metabolic modelling predictions, as well as a novel workflow to identify relevant potential drug targets yet to be explored and prioritise chemicals to assess their suitability as drugs in a timely manner.

Acknowledgements

This has been a thrilling 4-year long project on Systems Biology, in which I have worked and collaborated with plenty of people, from both wet and dry labs at different universities (Nottingham, Glasgow and Toulouse). I would like to express my gratitude to all of them for their quasi-infinite patience, as well as being helpful with my never-ending list of questions. It has been a great pleasure working with you all!

List of Figures

Figure 1-1. Generic metabolomics workflow 23
Figure 1-2. Small toy metabolic network 25
Figure 1-3. Stoichiometric modelling approaches 29
Figure 1-4. GSM reconstruction and FBA 31
Figure 1-5. Solution space for network comprising three reactions 32
Figure 1-6. Flux space solutions 33
Figure 1-7. Simple metabolic network 36
Figure 1-8. Tiny web 38
Figure 1-9. Examples of geographical choke points 40
Figure 2-1. Calculation of the parameter $\boldsymbol{A}$ 544
Figure 2-2. Comparison of flux values among FBA, TFA and ^{13}C-MFA 63
Figure 2-3. Anaplerotic node for *E. coli* 67
Figure 3-1. Simplex lattice design $\mathbf{3,4}$ for objective function weight values distribution 82
Figure 3-2. Strategies to identify reactions of interest 84
Figure 3-3. Kennedy pathway and sphingolipid metabolism, taking place in the cytosol and the smooth endoplasmic reticulum lumen as defined in the GSM 89
Figure 3-4. Partial polyamine biosynthesis and NADPH-dependent disulfide-reducing system, taking place in the cytosol as defined in the GSM 91
Figure 4-1. TISMAN (*Transcriptomics-Informed Stoichiometric Modelling And Network analysis*), the workflow developed in this study 105
Figure 4-2. FastCC and FASTCORE algorithms 107
Figure 4-3. Strategies to identify gene targets for drug repurposing 109
Figure 4-4. Comparison of genes of interest identified in this study against published works 115
Figure 4-5. *In vitro* assessment of identified compounds for drug repurposing as validation of *in silico* workflow 122

List of Tables

Table 1-1. Scientific and technical milestones relevant for this thesis. 18
Table 2-1. Comparison of frequently used approaches in fluxomics. 48
Table 2-2. Factors considered in mod-matTFA. 53
Table 2-3. List of side compounds 58
Table 2-4. Relative factor importance 61
Table 2-5. Quantified metabolites at the top 50% of PageRank (PR) based analysis 65
Table 2-6. Flux pattern changes between ^{13}C-MFA and TFA predictions69
Table 3-1. Protein homologs in *H. sapiens* 94
Table 4-1. Selected chemicals from the priority list for *in vitro* testing. 120

Abbreviations

^{13}C-DMFA	Dynamic 13 C Metabolic Flux Analysis
^{13}C-MFA	13 C Metabolic Flux Analysis
^{13}C-NMFA	Nonstationary 13 C Metabolic Flux Analysis
DMFA	Dynamic Metabolic Flux Analysis
FBA	Flux Balance Analysis
GBM	Glioblastoma
GCE	Glioblastoma Contrast-Enhanced core
GIN	Glioblastoma INvasive margin
GSC	Glioblastoma Stem Cells
GSM	Genome Scale Model
MFA	Metabolic Flux Analysis
ORG	Outer Radial Glia
PAM	Partitioning Around Medoids
RG	Radial Glia
TCGA	The Cancer Genome Atlas
TISMAN	Transcriptomics-Informed Stoichiometric Modelling And Network analysis
VRG	Ventricular Radial Glia

Table of Contents

DECLARATION III

ABSTRACT V

ACKNOWLEDGEMENTS VIII

LIST OF FIGURES X

LIST OF TABLES XI

ABBREVIATIONS XII

1. INTRODUCTION 17

1.1. FROM EARLY BIOTECHNOLOGY TO SYSTEMS BIOLOGY 18
1.2. FLUXOMICS. THE STOICHIOMETRIC PARADIGM. 24
1.3. TOPOLOGY OF METABOLIC NETWORKS 36
1.4. AIM AND SIGNIFICANCE 41

2. PHYSICOCHEMICAL AND METABOLIC CONSTRAINTS FOR THERMODYNAMICS-BASED STOICHIOMETRIC MODELLING UNDER MESOPHILIC GROWTH CONDITIONS 43

2.1. ABSTRACT 45
2.2. INTRODUCTION 46
2.3. MATERIALS AND METHODS 52
2.3.1. METABOLIC NETWORK, MAPPING OF METABOLIC FLUXES AND EXPERIMENTAL DATA 52
2.3.2. GENERATION OF EXPERIMENTAL DESIGN 52
2.3.3. ASSESSMENT OF FLUXOMICS AND METABOLOMICS PREDICTIVE CAPABILITIES 56
2.3.4. THERMODYNAMICS-ENRICHED NETWORK ANALYSIS 57
2.4. RESULTS AND DISCUSSION 60
2.4.1. EVALUATION OF THE RELIABILITY OF PREDICTED FLUX AND CONCENTRATION VALUES 60
2.4.2. IDENTIFICATION OF CENTRAL METABOLITES TO FURTHER CONSTRAIN THE MODEL 64
2.4.3. REACTION DIRECTIONALITIES IN THE CENTRAL CARBON METABOLISM 66
2.5. CONCLUSIONS 72

3. METABOLIC MODELLING-BASED DRUG REPURPOSING AND POTENTIAL DRUG TARGET IDENTIFICATION IN *TRYPANOSOMA BRUCEI* 74

3.1. ABSTRACT 76
3.2. INTRODUCTION 77
3.3. MATERIALS AND METHODS 81
3.3.1. METABOLIC NETWORK AND CONSTRAINTS 81
3.3.2. FLUX BALANCE ANALYSIS AND PROBLEM DEFINITION 81
3.3.3. IDENTIFICATION OF POTENTIAL DRUG TARGETS AND INHIBITORS 83
3.3.4. DRUG SENSITIVITY TESTING 85
3.4. RESULTS AND DISCUSSION 86
3.4.1. ALLOWABLE SOLUTION SPACE, REACTION ESSENTIALITY AND CHOKE POINTS 86
3.4.2. PRIORITISATION OF POTENTIAL DRUG TARGETS 87
3.4.3. SELECTION OF INHIBITORS FOR HUMAN PROTEINS AND SENSITIVITY TESTING 93
3.5. CONCLUSIONS AND FUTURE WORK 95

4. METABOLIC MODELLING-BASED DRUG REPURPOSING IN GLIOBLASTOMA 97

4.1. ABSTRACT 99
4.2. INTRODUCTION 101
4.3. MATERIALS AND METHODS 104
4.3.1. WHAT TO TARGET 106
4.3.2. HOW TO TARGET 110
4.3.3. *IN VITRO* TESTING 111
4.4. RESULTS AND DISCUSSION 113
4.4.1. WORKFLOW DESIGN 113
4.4.2. IDENTIFICATION OF GENES OF INTEREST 114
4.4.3. SELECTION OF CHEMICALS AND *IN VITRO* TESTING 118

5. GENERAL DISCUSSION 125

5.1. KEY FINDINGS 126
5.2. LIMITATIONS AND FUTURE WORK 127
5.3. CONCLUDING REMARKS 131

BIBLIOGRAPHY 132

APPENDIX 166

SUPPORTING INFORMATION CHAPTER 2 **167**
SUPPORTING INFORMATION CHAPTER 3 **211**
SUPPORTING INFORMATION CHAPTER 4 **223**
OTHER CONTRIBUTIONS **241**
PUBLICATIONS **245**

1. Introduction

"We are seeing the cells of plants and animals more and more clearly as chemical factories, where the various products are manufactured in separate workshops. The enzymes act as the overseers. Our acquaintance with these most important agents of living things is constantly increasing."

Eduard Buchner,
Nobel Lecture in Chemistry (1907)

1.1. From early biotechnology to systems biology

Human societies across time and space have been shaped by a plethora of factors, where scientific and technical developments have played a central role in societal progress. From creating the art of bread-making several millennia ago to starting to tame tumours, an endless list of people have collaborated and/or fought over motivated by sheer curiosity or political and economic pressures (Table 1-1) (Page L and Motwani R 1998, Buchholz and Collins 2013).

Table 1-1. Scientific and technical milestones relevant for this thesis.

Time, scientist(s) or company	*Scientific event or technical progress*
6000-3500 BC	Beer, wine and bread production
c. 550 BC Parmenides	"*Nothing comes from nothing*"
14th century	Industrial acetic acid fermentation
1680 Leeuwenhoek	Invention of the microscope
1828 Wöhler	Synthesis of urea from inorganic substrates
1856 Pasteur	Research on fermentation. Microbiology born as a discipline
1859 Darwin	"*On the Origin of Species*"
1876 Gibbs	"*On the Equilibrium of Heterogeneous Substances*"
1894 Fischer	Specificity of enzymes: lock and key model
1897 Buchner	Cell-free fermentations: studying metabolic intermediates
1920 Warburg	Aerobic fermentation or Warburg effect in tumours
1928 Fleming	Discovery of penicillin action
1944 Pfizer	Industrial production of penicillin
1949 Monod	Equation for growth in batch culture
1952 Turing	"*The Chemical Basis of Morphogenesis*"
1953 Sanger	Amino acid sequence of insulin
1953 Watson, Crick and Franklin	Elucidation of the structure of DNA
1973 Cohen and Boyer	Gene cloning in *E. coli*
1978 Genentec	Production of recombinant human insulin
1988 Mullis	Polymerase chain reaction (PCR)
1990s	"*-omics*" approaches, development of bioinformatics
1998 Google	PageRank algorithm
2003	Human Genome Project complete

While Egyptians managed to produce beer (and impose a tax on it), it was Pasteur, a chemist, who first described the fermentations from a microbiological standpoint in the 19th century. Shortly after, important studies on glycolysis and aerobic fermentation at a cellular level followed (Buchholz and Collins 2013). Three decades later, the structure of DNA was described and insulin (a protein) was sequenced, becoming the first biotechnological product in the 1970s (Watson and Crick 1953, Buchholz and Collins 2013). Around that year, Alan Turing' seminal work on a mathematical model describing the formation of patterns in nature inspired other researchers to combine experimental biological data and modelling techniques (Schiffmann 2017).

Systems biology was then defined as the evolution of molecular biology, where the goal is to study and model all biological elements and their interactions (De Backer, De Waele et al. 2010). Therefore, the classical central dogma of molecular biology (bold) is extended to: "*DNA* → *mRNA* → *protein* → *protein interactions* → *informational pathways* → *informational networks* → *cells* → *tissues or networks of cells* → *an organism* → *populations* → *ecologies*" (Ideker, Galitski et al. 2001).

To that end, two distinct and complementary perspectives are combined: (i) top-down, based on systems-wide datasets (*-omics*) aiming at formulating hypotheses by an inductive approach, and (ii) bottom-up, where functional properties of a system can be deduced from its well-characterised elements (e.g. kinetic parameters) (Bruggeman and Westerhoff 2007, De Backer, De Waele et al. 2010). Specifically, characterising the metabolic state to generate reliable predictions requires feeding metabolomics data (top-down) into metabolic models (bottom-up) (Tomar and De 2013, Toya and Shimizu 2013, Rosato, Tenori et al. 2018).

Metabolic engineering has been suggested as a tool to solve multiple industrial, environmental and economic problems, but traditional methods (e.g. random mutagenesis or single gene modification plus screening) have proven to be inefficient in the long run (Jang, Park et al. 2012). However, progressing towards a systems biology framework allowing to integrate high-throughput measurements with theoretical methods requires overcoming several challenges (Stephanopoulos, Alper et al. 2004, Dai and Nielsen 2015).

Firstly, the lack of accessible, cheap and fast analytical techniques prevents researchers from undertaking such measurements (Yadav, De Mey et al. 2012). In addition, developing informative-rich methods require extensive optimisation focusing on specific growth conditions and organism (Winder, Dunn et al. 2008, Winder and Dunn 2011). Secondly, bioscientists generally lack the mathematical literacy necessary to efficiently design systems-wide experiments and properly process the data generated (Cassman 2005, Kreutz and Timmer 2009). Consequently, fostering collaborations among different groups and disciplines is needed for understanding and engineering the cellular metabolism (Tomar and De 2013, Toya and Shimizu 2013).

The interplay of living systems with their environment is dictated by the natural laws (invariant) and a biological program (subjected to natural selection) – it responds to a "dual causality". Therefore, organisms display a phenotype (including the metabolic state) which is influenced by the growth conditions, and varies with age (Palsson 2006, Bock 2017). Two main culturing approaches should be noted: batch ("non-steady state") and continuous culture ("steady state"). At steady state, the replication rate equals the death rate, so the population remains constant over time (Orth, Thiele et al. 2010).

In a batch culture all nutrients are available from the start, so concentration values are not constant and cells may be growing at different rates (Takhaveev and Heinemann 2018, Reinhart, Damjanovic et al. 2019). Conversely, a chemostat allows reaching a steady state by continuously adding a growth-limiting substrate and keeping a constant culture volume, which allows fixing a growth rate (Altamirano, Illanes et al. 2001, Hoskisson and Hobbs 2005, Winder, Dunn et al. 2011). Interestingly, cells in the exponential phase of a batch culture can be used as a proxy for a continuous culture (Maier 2009, Gottstein, Olivier et al. 2016). Metabolic modelling normally relies on the assumption of a metabolic steady state (production and consumption metabolic fluxes for each metabolite cancel out), which can be achieved after reaching a steady state in a chemostat or at the beginning of the exponential growth phase in a batch culture (Orth, Thiele et al. 2010, Long and Antoniewicz 2019). Therefore, growth conditions should be considered early on to ensure the compatibility of the experimental

data with the modelling strategy, for example when estimating production or consumption fluxes (Chen, Alonso et al. 2011, Kim, Achcar et al. 2015, Long and Antoniewicz 2019).

Since at the population steady state cells are divide and die at the same rate, quantitative data is actually a weighted average of all the metabolic states taking place along the cell cycle. In fact, concentration values of multiple biomolecules oscillate along the cell cycle (during which cell size varies (Wang and Levin 2009)), comprising transcripts (Schwabe, Formichetti et al. 2020), proteins (Herr, Boström et al. 2020), metabolites (Papagiannakis, Niebel et al. 2017), and NADP(P)H (Zhang, Milias-Argeitis et al. 2018). High cell density yeast cultures in chemostats show a metabolome-wide oscillation depending on the respiratory phase (Satroutdinov, Kuriyama et al. 1992, Murray, Beckmann et al. 2007).

The energy metabolism regulation determines the ATP levels: its synthesis is adjusted to fulfil the energetic demands (Ataullakhanov and Vitvitsky 2002). Unsurprisingly, microbial clonal populations have shown ATP concentration values differ among single cells in a chemostat (Yaginuma, Kawai et al. 2014), and oscillations of metabolic fluxes in the Krebs cycle (comprising intermediates for biosynthesis) are found in mammalian cells (Ahn, Kumar et al. 2017).

When the energy source is a limiting factor (such as in a chemostat), the aforementioned ATP requirements can be divided into growth (i.e. biomass formation) and maintenance (e.g. sustaining the active transport of ions). These parameters can be measured by linear fitting of uptake rates of a growth-limiting substrate *versus* growth rates allows, but the procedure requires a considerable amount of resources (Park, Kim et al. 2011).

When facing a nutritional imbalance (e.g. batch culture), cells will make use of energy-spilling reactions (such as a futile cycles) or secrete metabolites to allocate the excess of energy (Russell and Cook 1995, Xie and Wang 1996, Sauer and Eikmanns 2005). Specifically, consuming the secreted metabolites has been recently appointed as an evolutionary strategy allowing to maximise growth under different growth conditions (Rabbers, Gottstein et al. 2021). However, such regulatory processes are not currently integrated into systems-wide metabolic modelling approaches (Orth, Thiele et al. 2010).

Conversely, metabolomics can be used to gain insight into the regulation of metabolic networks (Nägele 2014). This field studies the complete set of low-molecular-weight molecules (<1.5 kDa) of living systems (and their environment) under certain growth conditions (Toya and Shimizu 2013, Pinu and Villas-Boas 2017). Methods can be targeted (quantitative) and untargeted (relative quantification along with qualitative analysis), where both complement each other (Aldridge and Rhee 2014, Kim, Achcar et al. 2015, Surrati, Linforth et al. 2016). For example, quantitative approaches inform about enzyme binding site occupancy, providing a starting point for metabolic engineering (e.g. recombinant expression of enzymes) and therapeutic approaches (such as exploring the usage of competing substrates) (Park, Rubin et al. 2016).

Since industrial projects aim at developing continuous bioprocesses, targeted metabolomics is applied to intra- and extracellular metabolites once the steady state of interest is reached (Taymaz-Nikerel, de Mey et al. 2009, Reinhart, Damjanovic et al. 2019). In general, metabolomics studies face two main challenges: (i) spectral data from pure standards is only available for ca. 5% of known metabolites (Frainay, Schymanski et al. 2018), and (ii) quantifying the whole set of metabolites with a single method is not feasible due to their chemical diversity and differences in thermostability (Rabinowitz and Kimball 2007, Patejko, Jacyna et al. 2017, Lu, Wang et al. 2018). Thus, a prioritisation criterion is needed upon the design of the workflow (Figure 1-1) (Hasunuma, Sanda et al. 2011, Kiparissides and Hatzimanikatis 2017).

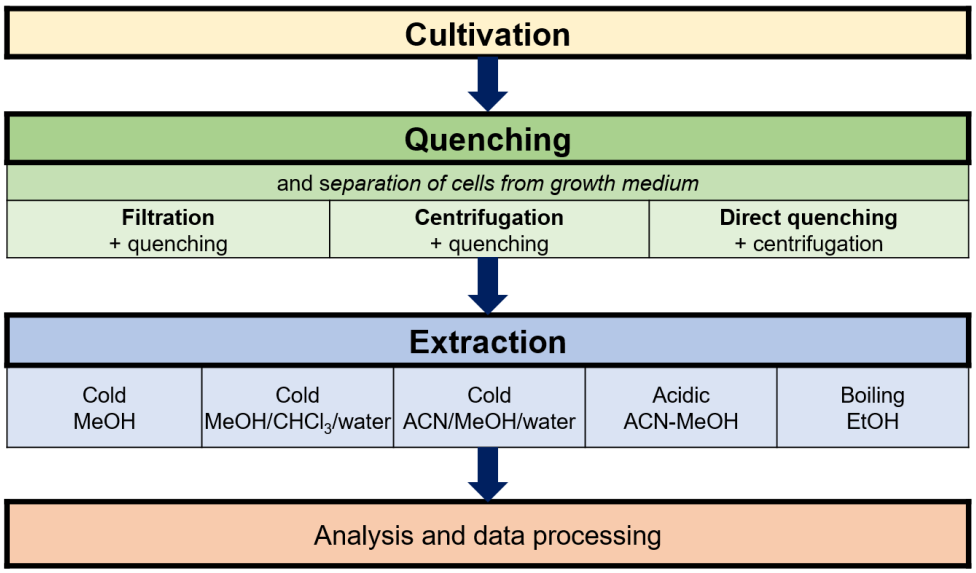


Figure 1-1. Generic metabolomics workflow, with a focus on intracellular metabolites. ACN = acetonitrile, $CHCl_3$ = chloroform, EtOH = ethanol, and MeOH = methanol. Adapted from (Patejko, Jacyna et al. 2017).

Biological properties of cells along with their response to the culture conditions affect the efficacy of the quenching step (i.e. arrest of metabolic/enzymatic activity) (van Gulik 2010). For instance, Gram-negative bacteria are more sensitive to an ion strength change of the washing solutions than Gram-positive ones (Gao and Xu 2015). Sampling and quenching should be fast enough to guarantee enzymatic inactivation, and the extraction step should minimise metabolite leakage and further interference with the analysis (e.g. ion-suppression) (Canelas, Ras et al. 2008, Winder, Dunn et al. 2008, Taymaz-Nikerel, de Mey et al. 2009, van Gulik 2010). Overall, protocols should be tested and optimised to produce reliable metabolomics data (top-down) to be fed into metabolic models (bottom-up) (Canelas, Ten Pierick et al. 2009, Toya and Shimizu 2013).

1.2. Fluxomics. The stoichiometric paradigm.

As stated above, characterising the metabolic state and determining the activity of a metabolic pathway generally requires integrating metabolomics data into metabolic models (Tomar and De 2013, Toya and Shimizu 2013, Rosato, Tenori et al. 2018). Metabolic fluxes (v_i) through a catalysed reaction can be defined as a function of both capacity (enzyme abundance) and kinetics-based (enzyme activity) components (Dauner 2010, Winter and Krömer 2013):

$$v_i = \overbrace{f(E_i}^{capacity} \underbrace{, k_i, S_i, P_i, I_i)}_{kinetics} \quad (1)$$

Firstly, the *capacity* aspect includes the enzyme concentration (E_i) of the reaction considered, and it is the outcome of the cell regulation at transcriptional and translational levels (Winter and Krömer 2013). Specifically, E_i values can be measured via quantitative proteomics (Bantscheff, Lemeer et al. 2012). Secondly, the *kinetics* component depends on: (i) the kinetic parameters of the reaction (k_i), (ii) the concentration of the substrate(s) (S_i), the concentration of the product(s) (P_i) and (iv) the concentration of effector molecules modulating enzymatic activity (I_i) (Winter and Krömer 2013). In addition, metabolic fluxes are also subjected to chemical equilibria, thermodynamics and regulatory processes (Horn and Jackson 1972, Henry, Broadbelt et al. 2007, Orth, Thiele et al. 2010).

Hundreds to thousands reactions and metabolites can be combined into a metabolic network suitable for metabolic engineering and modelling for therapeutic purposes (Csermely, Korcsmáros et al. 2013, King, Lu et al. 2016, Norsigian, Pusarla et al. 2020). Specifically, they can be defined as a system of ordinary differential equations describing the time course of metabolite concentration values (Figure 1-2) (Rosato, Tenori et al. 2018).

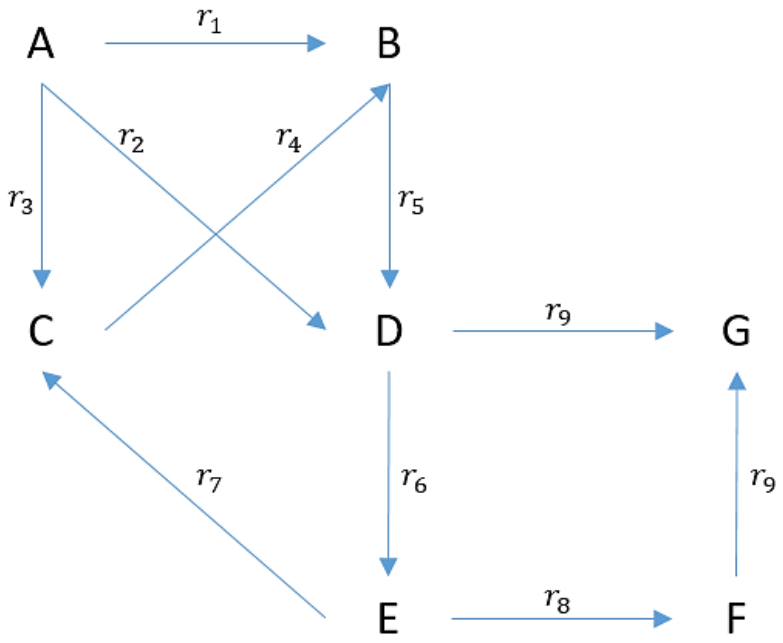


Figure 1-2. Small toy metabolic network, comprising 7 metabolites (A to G) and 9 reactions: $\boldsymbol{r_1}$: *A* → *B*, $\boldsymbol{r_2}$: *A* → *D*, $\boldsymbol{r_3}$: *A* → *C*, $\boldsymbol{r_4}$: *C* → *B*, $\boldsymbol{r_5}$: *B* → *D*, $\boldsymbol{r_6}$: *D* → *E*, $\boldsymbol{r_7}$: *E* → *C*, $\boldsymbol{r_8}$: *E* → *F*. Finally, r_9 is a bimolecular reaction defined as *D* + *F* → *G*, so it appears twice. Considering the rate of metabolite concentration change, the system can be defined by a set of Ordinary Differential Equations (ODEs): $^{dA}/_{dt} = -\boldsymbol{r_1}-\boldsymbol{r_2}-\boldsymbol{r_3}$; $^{dB}/_{dt} = \boldsymbol{r_1}+\boldsymbol{r_4}-\boldsymbol{r_5}$; $^{dC}/_{dt} = \boldsymbol{r_3}-\boldsymbol{r_4}+\boldsymbol{r_7}$; $^{dD}/_{dt} = \boldsymbol{r_2}+\boldsymbol{r_5}-\boldsymbol{r_6}-\boldsymbol{r_9}$; $^{dE}/_{dt} = \boldsymbol{r_6}-\boldsymbol{r_7}-\boldsymbol{r_8}$; $^{dF}/_{dt} = \boldsymbol{r_8}-\boldsymbol{r_9}$; and $^{dG}/_{dt} = \boldsymbol{r_9}$. Taken from (Tomi-Andrino, Norman et al. 2021).

Elucidating the metabolic fluxes in the system above could be done by different strategies. For instance, following a kinetics framework would require information regarding the kinetic parameters (k_i) and mechanism, with some approaches also exploiting metabolites levels (S_i, P_i and I_i) as well as the enzyme concentration (E_i) and thermodynamics and proteomics data (Saa and Nielsen 2017, Rosato, Tenori et al. 2018). Even though S_i, P_i, I_i and E_i values can be easily quantified, *in vitro*-determined kinetic parameters are either scarce or inadequate (Winter and Krömer 2013), and predicting parameters from experimental data remains a challenge (Davidi, Noor et al. 2016, Cuperlovic-Culf 2018, Dalwadi, Garavaglia et al. 2018).

Moreover, the variety of kinetic laws governing biochemical reactions (such as Michaelis-Menten or Ping Pong Bi Bi, to name a few) further hinders the applicability of this framework (Mendes, Hoops et al. 2009, Sriyudthsak, Shiraishi et al. 2016). Finally, the computational costs needed to analyse large metabolic networks limit its applicability (Cortassa, Caceres et al. 2015, Saa and Nielsen 2017). Nonetheless, user-friendly programs such as COPASI (COmplex PAthway SImulator) allows building and analysing small to medium-sized metabolic networks (Figure 1-2) (Hoops, Sahle et al. 2006).

Another approach worth mentioning is Metabolic Control Analysis (MCA), which has been used to gain insight into rate-limiting steps in metabolic engineering without requiring the kinetics of individual enzymes (Stephanopoulos, Alper et al. 2004). Specifically, control coefficients inform about the relationship between enzymes and fluxes or metabolite concentrations. Additionally, the MCA framework comprises elasticity coefficients, which describe the impact of changing a parameter (such as S_i, P_i or I_i) on the rate of reaction: they are partial derivatives of the rate equations for the chosen concentration values (i.e. specific of each steady state). However, the measurements needed and the computational costs associated to the analysis limit the application of MCA to small metabolic networks (Fell 1992, Snoep, Mendes et al. 1999, Tsouka, Ataman et al. 2021).

Given the aforementioned difficulties associated to solving Eq. 1, widely used strategies focus on measuring or modelling metabolic fluxes instead (Winter and Krömer 2013). To that end, this stoichiometric paradigm assumes a metabolic steady state (i.e. no changes in metabolite concentration, C, over time), so no dynamic nor kinetic data are needed (Eq. 2). In addition, modelling should ideally be applied to cells growing in a chemostat or in the exponential phase of a batch culture to ensure a balanced growth (Gottstein, Olivier et al. 2016).

$$\frac{dC}{dt} = S \times v \cong 0 \qquad (2)$$

Metabolic networks are modelled as a matrix S comprising (i) n metabolic and transport reactions (columns), and (ii) m metabolites, which act as substrates and/or products (rows) (Orth, Thiele et al. 2010). For the previous toy model (Figure 1-2), the ODEs can be rewritten as:

$$S = \begin{pmatrix} -1 & -1 & -1 & 0 & 0 & 0 & 0 & 0 & 0 \\ 1 & 0 & 0 & 1 & -1 & 0 & 0 & 0 & 0 \\ 0 & 0 & 1 & -1 & 0 & 0 & 1 & 0 & 0 \\ 0 & 1 & 0 & 0 & 1 & -1 & 0 & 0 & -1 \\ 0 & 0 & 0 & 0 & 0 & 1 & -1 & -1 & 0 \\ 0 & 0 & 0 & 0 & 0 & 0 & 0 & 1 & -1 \\ 0 & 0 & 0 & 0 & 0 & 0 & 0 & 0 & 1 \end{pmatrix}$$

In general, $n > m$, so the systems are underdetermined: there is no unique v fulfilling Eq. 2, but an infinite number of feasible sets. Therefore, measuring enough fluxes (uptake, production or growth) may be needed to achieve a determined system (or overdetermined $n \leq m$) and to identify a flux distribution of interest (Llaneras and Pico 2007, Trinh, Wlaschin et al. 2009, Klamt, Regensburger et al. 2017). The latter scenario applies to two main frameworks: elementary flux modes (EFMs, to study the structural properties of the network (Palsson 2006)) and metabolic flux analysis (MFA, to estimate the fluxes (Antoniewicz 2015)) Conversely, flux balance analysis (FBA) can be used to solve underdetermined systems (Orth, Thiele et al. 2010)).

An EFM is a minimal set of admissible fluxes able to perform a certain task in the system (e.g. cell growth) whilst maintaining a steady state (Schuster, Fell et al. 2000, Lacroix, Cottret et al. 2008). In general, a flux distribution can be decomposed into a sum of weighted elementary modes (Schuster, Fell et al. 2000). For example, microorganisms cultured in a chemostat show a low metabolic complexity, which can be modelled by using just 1 to 3 EFMs (de Groot, van Boxtel et al. 2019). Although identifying the EFMs has been successfully applied to metabolic engineering projects (Lopar, Špoljaric et al. 2014), analysing networks of more than ~60 reactions is a problem yet to be efficiently solved (Nolan, Fenley et al. 2006, Ullah, Yosafshahi et al. 2020). For instance, for a metabolic network comprising 318 reactions and 335 metabolites, c. 2 billion EFMs were identified (Hunt, Folsom et al. 2014).

The MFA framework comprises three techniques: stoichiometric MFA, ^{13}C-MFA and ^{13}C-NMFA (Figure 1-3) (Antoniewicz 2015). As mentioned above, uptake, production and growth fluxes are easily measurable and can be used to constrain the model. Stoichiometric MFA (or simply "MFA") allows estimating intracellular fluxes in a small metabolic network by least squares regression between predicted and measured fluxes (Jørgensen, Nielsen et al. 1995, Antoniewicz 2015). For smaller metabolic networks, it is possible to measure enough metabolic fluxes to obtain a determined system (Trinh, Wlaschin et al. 2009). Otherwise, strategies to work with underdetermined systems have also been suggested (Ouattara, Prot et al. 2012).

Shortly after, ^{13}C-MFA became the gold standard in the fluxomics field. Briefly, an isotopically labelled carbon molecule is provided as a carbon source: considering the mass isotopomer distribution of the produced proteinogenic amino acids (i.e. isomers differing in the position of isotopically labelled carbon atoms) allows elucidating more internal metabolic fluxes, thus increasing the number of unmeasured fluxes which can be estimated (Long and Antoniewicz 2019). Therefore, the metabolic network size was extended to ~70 reactions, large enough to cover the central carbon metabolism and gain insight into the effects of different substrates in the flux distribution (Kiefer, Heinzle et al. 2004, Alagesan, Minton et al. 2018).

However, ^{13}C-MFA is limited to heterotrophic growth, were carbon and energy are obtained from the same organic molecule (such as glucose). Studying autotrophic growth (CO_2 as carbon source, and light as the energy source, for instance) requires extra technical and computational efforts. A glucose molecule comprises six carbon atoms, the fate of which in metabolism is well-known, so it is possible to use the aforementioned mass isotopomer distribution to determine the fluxes. Conversely, information derived from a fully labelled substrate comprising a single carbon atom ($^{13}CO_2$) cannot be exploited by means of ^{13}C-MFA. To that end, ^{13}C-NMFA (non-stationary ^{13}C-MFA) was developed to measure the isotopic labelling of the amino acids of interest prior to reaching the isotopic steady state (i.e. fully labelled) (Noack, Noh et al. 2011, Antoniewicz 2015, Jazmin, Xu et al. 2017).

Given the technical and computational requirements, mixotrophic metabolism (i.e. isotopically labelled organic molecule plus CO_2) has been studied as a proxy instead (Alagesan, Minton et al. 2018). Similarly, dynamic MFA approaches are also limited by technical requirements (such as an ultra-rapid sampling device) (Noh, Gronke et al. 2007, Antoniewicz 2015). Interestingly, conclusions derived from EFM analysis and ^{13}C-MFA for bacterial and plant cells were well correlated, respectively (Beurton-Aimar, Beauvoit et al. 2011).

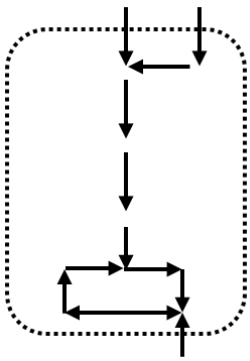
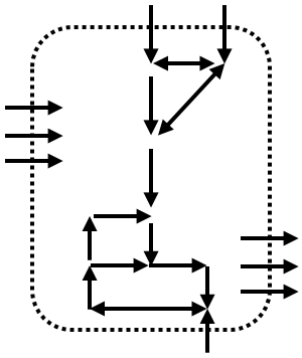
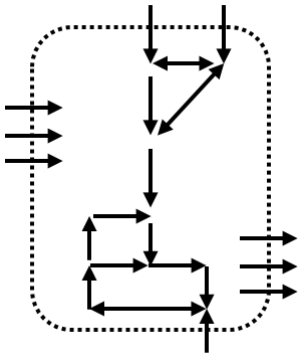
Stoichiometric flux analysis (MFA)	Isotope-based flux analysis (^{13}C-MFA and ^{13}C-NMFA)	Flux Balance Analysis (FBA)
		
Small-scale model (simplified)	Medium-scale model (central metabolism)	Large-scale model (GSM)
Minimize SSR s.t. $S \times v = 0$ $R \times v = r$	Minimize SSR s.t. $f_{isotopomer}(v, x) = 0$ $S \times v = 0$ $R \times v = r$	Maximize Z s.t. $S \times v = 0$ $\mathrm{LB} \leq v \leq \mathrm{UB}$

Figure 1-3. Stoichiometric modelling approaches. MFA and ^{13}C-MFA are both based on the minimization of the variance-weighted sum of squared residuals (SSR) between measured and predicted fluxes to solve the system. Using ^{13}C labelling provides extra constraints for flux estimation in ^{13}C-MFA. Conversely, FBA uses lower and upper bounds (LB and UB, respectively) to constraint the flux solution space and solves the system upon maximizing the objective function Z. Adapted from (Antoniewicz 2015) (and references therein).

Over time, metabolic networks have gained complexity and now include all the known genes, metabolic and transport reactions, and metabolites for a cell – these are termed genome scale models (GSMs) (Feist, Herrgård et al. 2009). The current *BiGG models* database version comprises c. 110 GSMs manually curated for prokaryotes and eukaryotes (Norsigian, Pusarla et al. 2020), which have been subjected to standardised testing (Lieven, Beber et al. 2020).

However, a plethora of strain-specific models or modified versions that do not adhere to the standard annotations or naming conventions are continuously published, but not indexed in such databases (Renz and Dräger 2021). Nevertheless, most GSMs follow the syntax and structure from the COBRA (COnstraint-Based Reconstruction and Analysis) toolbox community, comprising information required to run a FBA (Schellenberger, Que et al. 2011). Interestingly, GSMs have evolved into models integrating multi-scale processes (such as accounting for the dilution of macromolecules to daughter cells) but they are limited to a few species and are costly to analyse (Lloyd, Ebrahim et al. 2018).

Reconstructing and curating metabolic GSMs is an arduous process aiming at generating reliable simulations of the metabolic states. For instance, missing reactions may be filled by artificial ones to gain model consistency (Thiele and Palsson 2010). Other sources of uncertainty worth mentioning are (i) the gene-protein-reaction association rules, which map genes to reactions by means of a Boolean expression and is open to interpretation for isozymes, (ii) the poorly defined chemical composition of the culture media, which difficulties the experimental validation and limits the scope of the simulations, and (iii) the biomass formulation (Bernstein, Sulheim et al. 2021).

Modelling biomass formation requires making several assumptions. The cell composition and the associated ATP requirements are known to vary with the growth conditions (nutrient availability and culture type) (Feist, Scholten et al. 2006, Dikicioglu, Kırdar et al. 2015). For example, modelling autotrophic metabolism for a bacterium using experimental data from heterotrophic growth should be discouraged. Although there is no unique way to represent biomass formation, the ratio of the components is always considered. In MFA, intermediates from the central metabolism are

used as a proxy for biomass precursors by means of an artificial reaction, where the energetic costs are neglected (Antoniewicz 2015, Gopalakrishnan and Maranas 2015).

Conversely, using a GSM provides a more detailed view of biomass formation. Biomass precursors can be either (i) consumed by independent transport reactions (Hartman, Fell et al. 2014), or (ii) combined into a single biomass reaction (including the growth associated maintenance energy) with a metabolic flux μ equivalent to the specific growth rate. Following the COBRA consensus (Feist, Scholten et al. 2006, Feist and Palsson 2010, Schellenberger, Que et al. 2011):

$$\sum_{i=1}^{z} stoichiometric\ coefficient_z \cdot BiomassPrecursor_z \xrightarrow{\mu} 1\ \text{gram of biomass}$$

Small-to-medium sized metabolic networks are determined or overdetermined, and can be consequently inspected by MFA-based techniques (Figure 1-3). Conversely, GSMs are generally underdetermined (i.e. more reactions than metabolites), so there is no unique solution and FBA is needed (Kauffman, Prakash et al. 2003). In addition, FBA plays an important role in GSM reconstruction and curation (Figure 1-3):

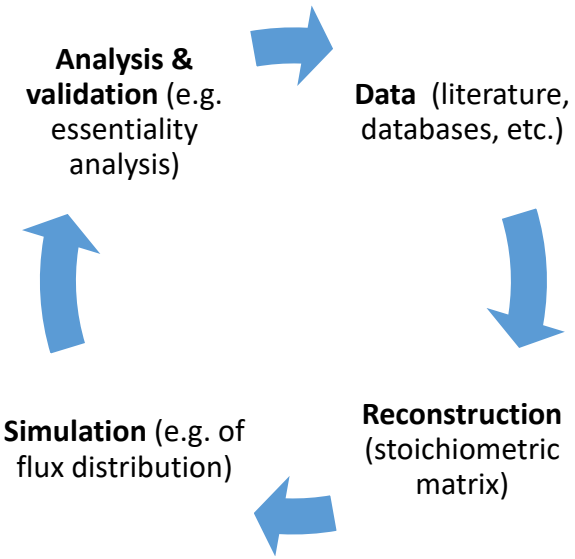


Figure 1-4. GSM reconstruction and FBA. Updating and curating GSMs considering new experiments is an iterative process (Gianchandani, Chavali et al. 2010, Thiele and Palsson 2010).

Briefly, the GSM is subjected to a series of constraints that define the allowable solution space, and the optimal solution is found upon maximising for an objective function Z by means of linear programming (LP) (Figure 1-5) (Budinich, Bourdon et al. 2017). Specifically, this method is used to solve problems involving a linear set of constrains (e.g. mass balance constraints) linear objective function (Z) (Palsson 2006). It should be noted other FBA-based methods include constraints such as protein synthesis rates (Yoo, Bestel-Corre et al. 2015), enzyme kinetics (Sánchez, Zhang et al. 2017), or enzyme usage (Mori, Hwa et al. 2016), but most studies still focus on standard FBA (Orth, Thiele et al. 2010).

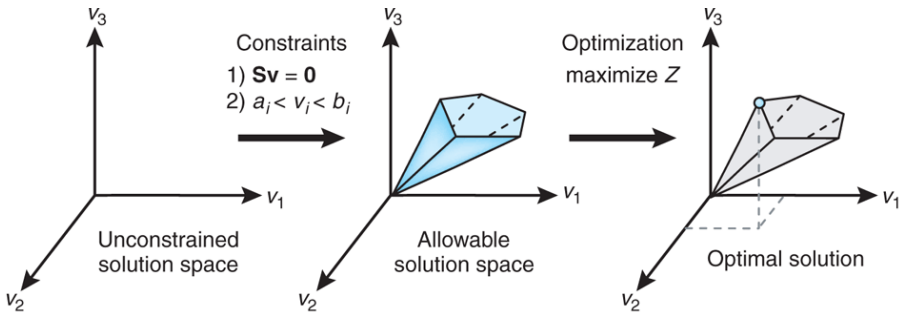


Figure 1-5. Solution space for network comprising three reactions. The allowable solution space is defined by 1) mass balance constraints (flux values guarantee a metabolic steady state) and 2) lower and upper bounds constraints for flux values (a_i and b_i, respectively). The optimal solution is found upon the maximisation of an objective function Z. Taken from (Orth, Thiele et al. 2010).

In the COBRA framework $Z = c^T v$, where v lists all reactions in the model, and c is a vector setting the weight of each reaction in the objective function (Figure 1-6). For the common metabolic engineering simulation where growth is the sought metabolic goal, c would have a value of 1 for the position of the biomass reaction (in v), and 0s in the remaining rows (Orth, Thiele et al. 2010).

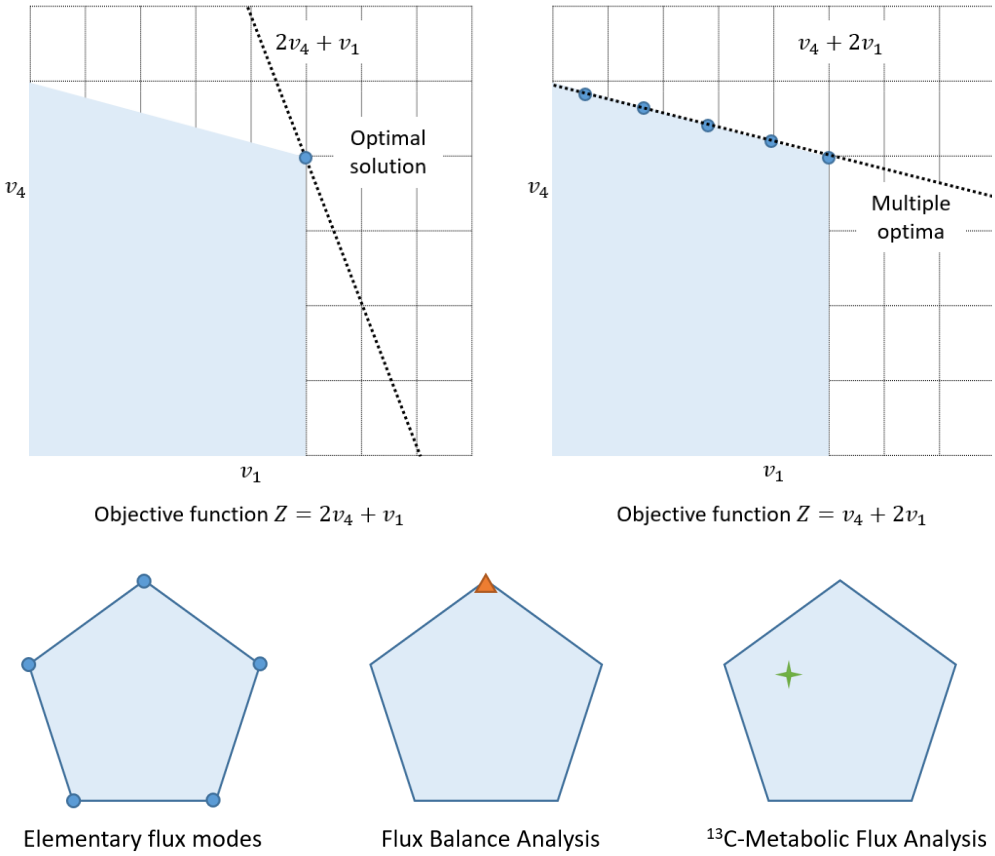


Figure 1-6. Flux space solutions. Different optimal solutions can be retrieved for the same flux space solution depending on the objective function (redrawn from (Kauffman, Prakash et al. 2003)). In addition, different fluxomics methods do not necessarily retrieve the same optimal solution(s) (redrawn from (Trinh, Wlaschin et al. 2009)).

While maximising the flux through the biomass reaction is the most commonly selected objective function (Feist and Palsson 2010), comparative studies showed that different objective functions are required for different growth conditions (Schuetz, Kuepfer et al. 2007). For example, minimizing the sum of fluxes (c would have a value of 1 for all reactions) would imply an efficient use of enzymes, incurring in lower biosynthetic costs (Holzhütter 2004, Dikicioglu, Kırdar et al. 2015). Interestingly, ^{13}C-MFA results from aerobic batch and continuous cultures of *E. coli* approached different regions of a flux space solution among three objective functions (maximisation of the biomass yield, maximisation of the ATP yield and minimization of the sum of fluxes) (Schuetz, Zamboni et al. 2012).

Since ^{13}C-MFA and FBA results do not necessarily agree (Figure 1-6), combining them would provide a wider view of cellular metabolism (Chen, Alonso et al. 2011). However, the costs associated to the former greatly limit its applicability (Long and Antoniewicz 2019). Therefore, FBA is normally used at preliminary stages, and different versions and purposes have been suggested.

FBA is used for a wide range of applications, from simulating mutant strains to improve product yields, to predicting gene essentiality as a proxy for gene silencing to facilitate the discovery of potential drug targets, or to gain insight into the metabolism of difficult to culture species, such as archaea (Orth, Thiele et al. 2010, Bordbar, Monk et al. 2014, Thor, Peterson et al. 2017). Gene essentiality can be easily predicted with the COBRA toolbox, by inspecting deletions which reduce the metabolic flux through the biomass reaction (i.e. impeding cell growth) (Schellenberger, Que et al. 2011).

To that end, large GSMs (e.g. human) require a "contextualization" step to properly model *in vivo* conditions: transcriptomics data is exploited to identify expressed genes, to later assume reactions catalysed by enzymes codified by them are active (Opdam, Richelle et al. 2017, Pires Pacheco, Bintener et al. 2019). Nevertheless, predicted gene essentiality has a limited reliability (Salvy and Hatzimanikatis 2020). Therefore, this approach should be combined with other methods to facilitate the drug discovery programs.

Other constraints of interest for FBA include thermodynamics, relative expression and relative metabolite abundance (Henry, Broadbelt et al. 2007, Salvy, Fengos et al. 2018, Pandey, Hadadi et al. 2019). Biological systems exchange matter and energy with the environment to generate energy flows – exergonic reactions require no energy input (they are spontaneous, $\Delta G_{ex} < 0$) and release free energy, which is used for endergonic reactions (or nonspontaneous, $\Delta G_{end} > 0$) to be carried out. Gibbs free energy (ΔG) is related to changes in the internal energy of a system, and can be used to predict the direction of a reversible reaction (the forward or backward may have $\Delta G < 0$).

However, reactions cannot be studied without the context of metabolic pathways: catabolic (exergonic, breakdown of molecules) and anabolic reactions (endergonic, build-up of molecules) are coupled in the

system, so that $\Delta G_{ex} + \Delta G_{end} < 0$ (Ataman and Hatzimanikatis 2015, Sherwood and Dalby 2018).

The Gibbs free energy of reaction $\Delta_r G^o$ equals $-RT \ln K$, where R refers to the gas constant ($8.31454\,\mathrm{JK^{-1}mol^{-1}}$) and K to reaction equilibrium constant (Sherwood and Dalby 2018). Alternatively, stoichiometric coefficients of reactants and products, and tabulated free energy of formation ($\Delta_f G^o$) values for each species can be used instead. This data is either measured or predicted at "standard conditions": temperature of 298.15K, 1 bar, zero ionic strength, pH 0 and concentration of 1M for all species (dilute aqueous solutions) (Alberty 2005, Jankowski, Henry et al. 2008). However, life operates in a myriad of physicochemical conditions (Merino, Aronson et al. 2019), so accounting for deviations in pH and ionic strength (but not for the temperature) from the standard conditions have been proposed (Salvy, Fengos et al. 2018). Specifically, the ionic strength is a measurement of both the quantity and the strength of the electrostatic interactions in the solution (Sherwood and Dalby 2018). Adjustments of the $\Delta_r G^o$ can be done by means of the extended Debye-Hückel equation or the Davies equation, depending on the ionic strength value of the solution (I < 0.1M and I < 0.5M, respectively) (Henry, Broadbelt et al. 2007, Simonin 2017). Thus, the direction for which some reactions become spontaneous may change (Sherwood and Dalby 2018), affecting the predicted flux distribution in the system.

GSMs include information about reaction reversibility, and the sign of the metabolic flux relates to how the reaction is defined in the model (Schellenberger, Que et al. 2011). Implementing said thermodynamic constraints into FBA requires reformulating the problem definition (Henry, Broadbelt et al. 2007). In Thermodynamics Flux Analysis (TFA), reversible reactions are split into a forward and a reverse reaction – upon identifying which direction is spontaneous ($\Delta_r G^o < 0$), an extra binary variable flagging the active reaction (or shutting both down) is needed (Soh and Hatzimanikatis 2014). Problems including such discontinuous variables cannot be solved by LP, so Mixed Integer Linear Programming (MILP) is used instead (Palsson 2006, Salvy, Fengos et al. 2018).

1.3. Topology of metabolic networks

Beyond the stoichiometric paradigm, other approaches exploiting the layout of metabolic networks have also been used for industrial and therapeutic purposes (Barabási and Oltvai 2004, Barabási, Gulbahce et al. 2011, Csermely, Korcsmáros et al. 2013). Analyses mainly focus on identifying well-connected nodes (either reactions or metabolites) by using centrality measures (Figure 1-7), or inspecting the network features generated among such elements (Csermely, Korcsmáros et al. 2013). Metabolic networks show a scale-free topology: while most metabolites participate in just one or two reactions, certain compounds are highly connected nodes (Wagner and Fell 2001, Barabási and Oltvai 2004).

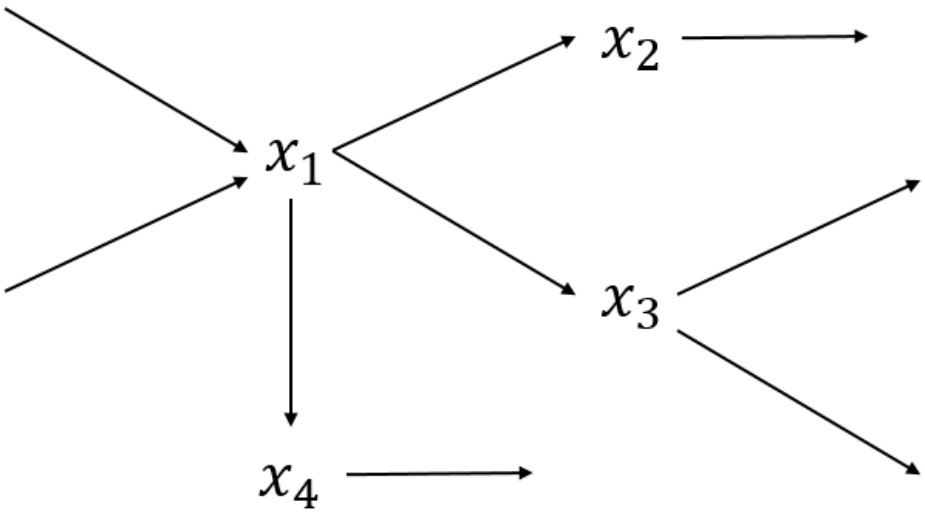


Figure 1-7. Simple metabolic network, where the nodes x_1, x_2, x_3 *and* x_4 represent metabolites with connectivities of 6, 2, 3 and 2 (respectively). Arrows refer to reactions (redrawn from (Palsson 2006)).

Several aspects should be considered prior to measuring the centrality of node. Firstly, the stoichiometric matrix needs to be converted into an adjacency matrix. The former stores a metabolic network by including reactions and metabolites (columns and rows, respectively). Conversely, an adjacency matrix informs of either whether two elements are connected or how many times they are linked (i.e. weight) – may they be metabolites or

reactions, but not both simultaneously (Palsson 2006, Orth, Thiele et al. 2010). Depending on directionality being considered or not, this matrix represents a directed or undirected graph (Liu, Hong et al. 2020). In fact, the problem of reversibility can be solved by feeding the directionalities derived from FBA into the matrix (Beguerisse-Díaz, Bosque et al. 2018). Furthermore, flux values have also been used to escalate weight values, which affects the centrality score (Yoon, Si et al. 2007, Beguerisse-Díaz, Bosque et al. 2018). Other flux-independent weighting policies to enrich metabolomics results have also been suggested in the literature (Frainay, Aros et al. 2018).

Secondly, should the adjacency matrix of interest be based on metabolites, it is important to remove those which would distort the characterisation of the network properties due to their high connectivity (Wagner and Fell 2001). These are termed *currency metabolites* (Li, Cao et al. 2019), *side compounds* (Frainay and Jourdan 2017), or *pool metabolites* (Beguerisse-Díaz, Bosque et al. 2018), and comprise chemicals such as ATP, NADP(H) and ions that are widely present in the metabolic network. Even though the set of metabolites to be removed directly impacts subsequent analyses (Wagner and Fell 2001), no consensus has been reached to define and remove them from the network.

Finally, there is a plethora of centrality measures to assess the "importance" of a node (Wang, Lü et al. 2014, Liu, Hong et al. 2020). Specifically, Google's PageRank (PR) algorithm has been successfully applied to both directed and undirected graphs (Page L and Motwani R 1998, Beguerisse-Díaz, Bosque et al. 2018). Briefly, this iterative algorithm calculates the probability of reaching a node when moving randomly through the network. Therefore, highly connected nodes would have a high PR score (Bianchini, Gori et al. 2005, Moler 2011). Even though a detailed description of the algorithm would be beyond the scope of this thesis, the following network can be considered as an illustrative example (Figure 1-8).

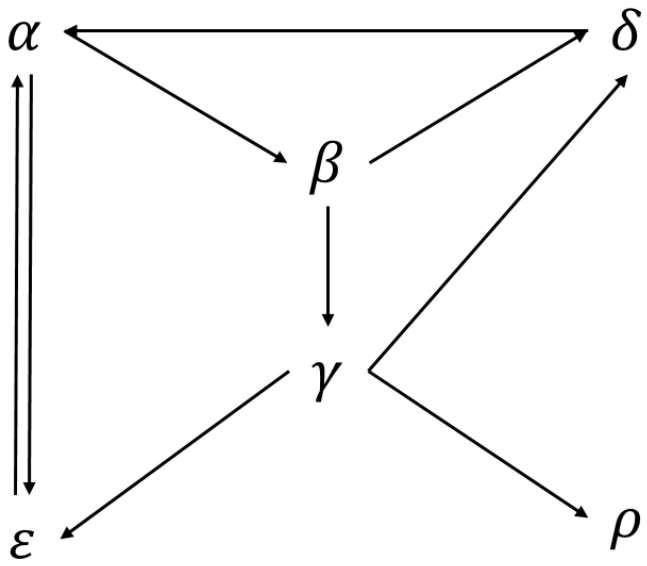


Figure 1-8. Tiny web. Redrawn from (Moler 2011).

MATLAB's in-built `centrality` function for PR scores calculation uses a matrix composed by the out-links (i.e., edges from the node). For the tiny web (Moler 2011):

$$\begin{pmatrix} 0 & 0 & 0 & 1 & 0 & 1 \\ 1 & 0 & 0 & 0 & 0 & 0 \\ 0 & 1 & 0 & 0 & 0 & 0 \\ 0 & 1 & 1 & 0 & 0 & 0 \\ 0 & 0 & 1 & 0 & 0 & 0 \\ 1 & 0 & 1 & 0 & 0 & 0 \end{pmatrix}$$

$$\begin{aligned} PR(\alpha) &= 0.3210 \\ PR(\beta) &= 0.1705 \\ PR(\gamma) &= 0.1066 \\ PR(\delta) &= 0.1368 \\ PR(\rho) &= 0.0643 \\ PR(\varepsilon) &= 0.2007 \\ \sum PR &= 1 \end{aligned}$$

Finally, using a simplified formula (Bianchini, Gori et al. 2005) and the PR(α) derived from the function above, it can be easily shown that:

$$PR(\beta) = \sum_{\beta}^{\alpha} \frac{PR(\alpha)}{outlinks(\alpha)} = 1\frac{0.3210}{2} = 0.1705$$

Interestingly, reactions with high centrality scores according to multiple metrics for an *E. coli* metabolic network proved to be essential (Kim, Ashlock et al. 2019). Similarly, reactions with low in-degree (i.e. few preceding reactions) and high PageRank were essential in *Mycobacterium tuberculosis, Plasmodium falciparum* and methicillin-resistant *Staphylococcus aureus* (Bánky, Iván et al. 2013).

Network features can be found at a local or mesoscopic level, depending on how many nodes participate. For instance, an overrepresented set of 3 to 6 nodes in a directed graph is known as "motif" (or "graphlet" for an undirected one) ((Csermely, Korcsmáros et al. 2013) and references therein). A larger number of nodes may group into a network community, and connections amongst them (such as "bridges" or "bottlenecks") may be interesting potential drug targets (Kim, Ashlock et al. 2019). For example, the "central hit strategy" has been suggested to fight off living systems showing a flexible metabolism (such as infectious agents or cancer cells), where important nodes and choke points are targeted. Specifically, choke points are reactions exclusively producing or consuming a metabolite, making them potential drug targets (Csermely, Korcsmáros et al. 2013).

Choke points play an important role in geopolitics and economics. In 480 BC, Leonidas led the Greek city-states against the Persian Empire by fortifying the Pass of Thermopylae (Figure 1-9), a path surrounded by mountains and the coastline (Martini 2009). This strategy made possible for 7,000 Greeks to defend against tens of thousands of Persian soldiers, and failed only after a traitor informed the invaders about an alternative route (Lohnes and Sommerville 2019).

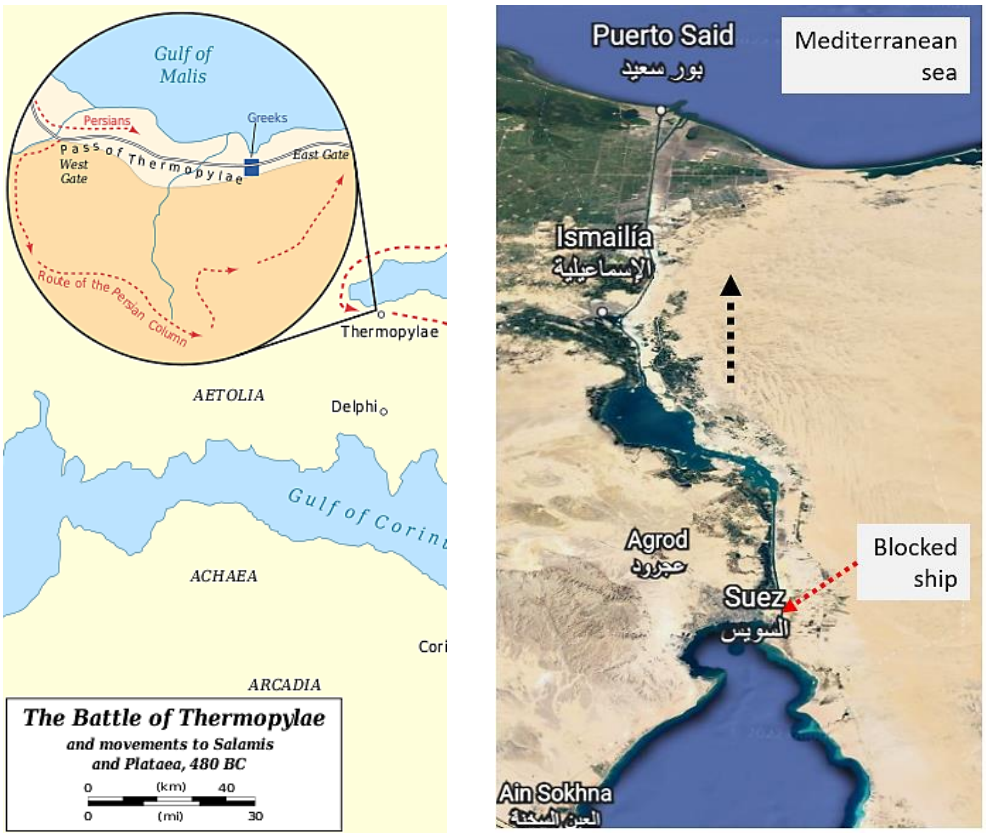


Figure 1-9. Examples of geographical choke points: pass of Thermopylae next to the Gulf of Malis in Greece (left, taken from (Martini 2009), *Maps Courtesy of the Department of History, United States Military Academy*) and the Suez Canal in Egypt (right, redrawn from (Nabil 2021)).

More than 2,000 years later, the global economy highly depends on a reduced number of narrow international waterways (Alexander 1992). One of the main West-East canals was blocked by a stuck cargo ship in 2021, causing hundreds of millions of dollars losses and forcing other ships to circumvent Africa to reach the European ports (Nabil 2021). Both cases show how the original objectives can be achieved if (i) an alternative pathway exists and (ii) resources can be allocated (such as a military column, time or money). Translated into a biological context, the existence of a viable alternative pathway can be assessed by inspecting gene essentiality with FBA (Orth, Thiele et al. 2010).

1.4. Aim and significance

This project exploited the metabolic networks of a bacterium, a parasite and a type of cancer for industrial and therapeutic purposes, showing a progression in complexity from the beginning. This document comprises three results chapters and Other contributions. Specifically, there is a varying degree of computational and experimental work, where the author has focused on the former and collaborated with experimental scientists for the latter.

Chapter 2 presents a thorough analysis of two different *in silico* methods tested against experimental data (metabolomics and ^{13}C-MFA) for the mesophile *E. coli*. Specifically, the matTFA toolbox (Salvy, Fengos et al. 2018) was modified to provide a broader range of physicochemical parameters, yielding 64 different combinations. Predicted concentration and flux values were compared against metabolomics and ^{13}C-MFA, respectively, to identify the set of parameters with the best predictive capabilities. Increasing the reliability of the simulations is instrumental to facilitate metabolic engineering projects. The chapter is a reformatted reprint of (Tomi-Andrino, Norman et al. 2021). A copy can be found in Publications.

Chapter 3 introduces a workflow based on reaction essentiality (via FBA) and network topology under multiple metabolic states to identify and prioritise potential drug targets for further genetic and/or pharmacological studies. Particularly, the concept of "double choke point" was introduced for the sake of a stringent search of reactions of interest to be targeted. Using a GSM for the well-studied parasite *Trypanosoma brucei* (Shameer, Logan-Klumpler et al. 2015) allowed validating the suitability of the workflow for drug repurposing studies by comparing the predicted drug targets against the literature. In addition, the lethality of an antiviral drug was tested *in vitro* by our collaborators at the University of Glasgow.

Finally, Chapter 4 focuses on expanding the previous workflow by conceptualising "extended choke points" and simultaneously searching for essential reactions, topologically important reactions and up-regulated genes. A generic human GSM was tailored to the studied tumour (glioblastoma, GBM) by exploiting publicly available transcriptomics data, resulting in two metabolic models. Reactions of interest were subjected to programmatic and/or manual searches in the literature and several chemical-gene

interactions databases to select compounds (drugs and natural products) yet to be tested for GBM. The effects of five chemicals on four patient-derived cell lines were tested with viability and invasion assays by our collaborators at the Children's Brain Tumour Drug Delivery Consortium (The University of Nottingham). This chapter was also published (Tomi-Andrino, Pandele et al. 2022). A copy can be found in Publications.

.

2. Physicochemical and metabolic constraints for thermodynamics-based stoichiometric modelling under mesophilic growth conditions

"How does the living organism avoid decay? The obvious answer is: by eating, drinking, breathing and (in the case of plants) assimilating. The technical term is called metabolism."

Erwin Schrödinger,
What is life? (1943)

Disclaimer: this chapter is a modified version of a Publication in Plos Computational Biology from January 2021 (Tomi-Andrino, Norman et al. 2021).

As explained in-text, the project is based on matTFA, a published and readily available MATLAB toolbox. A full list of the files used for this chapter can be found in S2 Table, where information about their source is given. Specifically, MATLAB functions to calculate physical parameters were created by Thomas Millat. These files are short scripts which simply implement a published equation (references can be found in the main text and in each file). The main script (*def_analysis_E_coli.m*) was created by CTA from the original matTFA code (Salvy, Fengos et al. 2018). Briefly, changes comprise: an increased number of parameters and parameter values, an automated analysis of all the combinations, and a comparison with ^{13}C-MFA and experimental metabolomics data was added, as well as ways to evaluate the goodness-of-fit and the concordance. Modifying the main file entailed changes in other scripts, as explained in S2 Table.

Conceptualisation: Claudio Tomi-Andrino, Thomas Millat
Data curation: Claudio Tomi-Andrino
Formal analysis: Claudio Tomi-Andrino, Rupert Norman
Methodology: Claudio Tomi-Andrino, Rupert Norman, Thomas Millat, Philippe Soucaille
Project administration: Claudio Tomi-Andrino
Resources: Klaus Winzer, David A. Barrett, John King, Dong-Hyun Kim
Software: Claudio Tomi-Andrino, Rupert Norman, Thomas Millat
Supervision: Klaus Winzer, David A. Barrett, John King, Dong-Hyun Kim
Writing – original draft: Claudio Tomi-Andrino
Writing – review & editing: Claudio Tomi-Andrino, Rupert Norman, Thomas Millat, Philippe Soucaille, Klaus Winzer, David A. Barrett, John King, Dong-Hyun Kim

2.1. Abstract

Metabolic engineering in the post-genomic era is characterised by the development of new methods for metabolomics and fluxomics, supported by the integration of genetic engineering tools and mathematical modelling. Particularly, constraint-based stoichiometric models have been widely studied: (i) flux balance analysis (FBA) (*in silico*), and (ii) metabolic flux analysis (MFA) (*in vivo*). Recent studies have enabled the incorporation of thermodynamics and metabolomics data to improve the predictive capabilities of these approaches. However, an in-depth comparison and evaluation of these methods is lacking.

This study presents a thorough analysis of two different *in silico* methods tested against experimental data (metabolomics and ^{13}C-MFA) for the mesophile *Escherichia coli*. In particular, a modified version of the recently published matTFA toolbox was created, providing a broader range of physicochemical parameters. Validating against experimental data allowed the determination of the best physicochemical parameters to perform the TFA (Thermodynamics-based Flux Analysis). An analysis of flux pattern changes in the central carbon metabolism between ^{13}C-MFA and TFA highlighted the limited capabilities of both approaches for elucidating the anaplerotic fluxes. In addition, a method based on centrality measures was suggested to identify important metabolites that (if quantified) would allow to further constrain the TFA. Finally, this study emphasised the need for standardisation in the fluxomics community: novel approaches are frequently released but a thorough comparison with currently accepted methods is not always performed.

2.2. Introduction

Metabolic engineering aims to improve microbial strains by considering comprehensive metabolic pathways in their entirety rather than overexpressing a single gene (Stephanopoulos, Alper et al. 2004). To improve the strains, hypothesis-driven studies have attempted to rationally identify gene targets and to evaluate the effects of those changes in the network (Kell and Oliver 2003, Dai and Nielsen 2015). However, the complex nature of cellular metabolism and its regulation demands a holistic understanding, i.e. a data-driven approach (Kell and Oliver 2003, Stephanopoulos, Alper et al. 2004, Dai and Nielsen 2015). Combining metabolic engineering with systems biology and mathematical modelling allows for an optimisation of entire cellular networks considering further downstream processes at early stages (Park, Lee et al. 2008).

This systematic framework exploits information regarding the metabolic state, which comprises the metabolome (complete set of low-molecular-weight metabolites (<1.5 kDa)) and the fluxome (or metabolic activity, distribution of rates of conversion/transport in the metabolic network) (Toya and Shimizu 2013, Kim, Achcar et al. 2015). Kinetic modelling can yield metabolic fluxes from metabolomics data, but lack of high-quality enzymatic parameters and computational limitations (e.g. time-consuming processes) hinder its application (van Eunen, Kiewiet et al. 2012, Tomar and De 2013, Cortassa, Caceres et al. 2015).

Performing an elementary flux mode analysis (EFMA) to decompose the metabolic network into minimal subsets allowing to maintain the steady state provides useful information (Zanghellini, Ruckerbauer et al. 2013). However, the combinatorial explosion makes the algorithm computationally expensive and therefore limits the size of the network that can be analysed (Jol, Kummel et al. 2012, Zanghellini, Ruckerbauer et al. 2013). Alternatively, stoichiometric modelling can provide a flux distribution for larger networks without any kinetic or metabolomics information (Feist, Herrgard et al. 2009).

Briefly, a metabolic (quasi) steady state for intracellular concentration values (C) is assumed, so that the stoichiometric matrix (S) (including the stoichiometric coefficients of metabolites in each reaction of the metabolic network) constrains the set of metabolic fluxes (υ) (Antoniewicz 2015):

$$\frac{dC}{dt} = S \times v \cong 0 \qquad (1)$$

Two main approaches to solve this equation can be found: (i) flux balance analysis (FBA), normally applied to large models (genome-scale model, GSM) (Orth, Thiele et al. 2010) or (ii) metabolic flux analysis (MFA), used for smaller metabolic networks (mainly the central carbon metabolism) (Table 2-1). FBA solves the underdetermined system represented in Eq. 1 by maximising or minimising the value of an assumed objective function (Orth, Thiele et al. 2010). A plethora of different objectives has been described in the literature (Schuetz, Kuepfer et al. 2007). Three of them can be highlighted: maximisation of biomass yield ($Y_{X/S}$, equal to the ratio growth rate/substrate uptake rate), maximisation of ATP yield, and minimisation of sum of fluxes, which have been suggested to compete in the regulation of bacterial metabolism (Schuetz, Zamboni et al. 2012). Hence, selecting an adequate one/multi-dimensional objective function when analysing a GSM will depend on the growth conditions to be simulated in FBA.

In general, measured extracellular metabolic rates (e.g. substrate uptake) are insufficient to properly constrain the intracellular metabolic fluxes (Antoniewicz 2015). In contrast, MFA is based on a least-squares-regression problem, normally solved by exploiting experimental mass isotopomer distribution (MID) of proteinogenic amino acids (^{13}C-MFA) (Antoniewicz 2015). Since this approach requires fewer assumptions and uses more experimental information than FBA, ^{13}C-MFA is considered to be the *gold standard* in fluxomics (Long and Antoniewicz 2019). However, current applicability (central carbon metabolism), and technical/computational complexity (particularly for autotrophic growth (Wiechert and Noh 2013)) limit its usage.

Table 2-1. Comparison of frequently used approaches in fluxomics. Parameter *A* is used in the extended Debye-Hückel equation. ^{13}C-MFA, ^{13}C metabolic flux analysis; FBA, flux balance analysis; GCM, group contribution method; GSM, genome-scale model; LP, linear programming; MILP, mixed-integer linear programming; TFA, thermodynamics-based flux analysis.

	^{13}C-MFA	FBA	TFA
Metabolic network size	small	GSM	GSM
Flux distribution	generated	generated	generated
Uptake rate	Yes	Yes	Yes
Specific growth rate, μ (h^{-1})	-	Yes	Yes
Gibbs free energy of formation (ΔG_f°)	-	-	Experimental (Alberty 2005), or GCM (Jankowski, Henry et al. 2008)
Temperature, *t* (℃)	-	-	25
Ionic strength, *I* (M)	-	-	0.25
Salinity, S (g/kg)	-	-	-
Adjustment method	-	-	Extended Debye-Hückel
Parameter *A*	-	-	T-dependent
Metabolite concentration values	-	-	Constraint or predicted
Problem formulation	Least square regression (Antoniewicz 2015)	LP (Orth, Thiele et al. 2010)	MILP (Salvy, Fengos et al. 2018)

Living systems maintain energy flows to carry out life process, which depend on a continuous exchange of matter and energy with the environment (Sherwood and Dalby 2018). However, the set of constraints characterising

stoichiometric modelling approaches (Eq. 1) is insufficient to guarantee thermodynamically feasible flux distributions (Vojinović and Von Stockar 2009, Salvy, Fengos et al. 2018). Both FBA and ^{13}C-MFA assume most reactions to be reversible (Hoppe, Hoffmann et al. 2007, Antoniewicz 2015): in the first case directionalities are dictated by the optimal flux distribution (which depends on the *a priori* chosen objective function (Orth, Thiele et al. 2010)), whereas in ^{13}C-MFA they are determined by the MIDs (Park, Rubin et al. 2016).

A reversible reaction will follow the forward or backwards direction depending on the Gibbs free energy (ΔG), which relates to changes in the internal energy of the system (Sherwood and Dalby 2018). By definition, the direction with an associated $\Delta G < 0$ is spontaneous (i.e. it requires no energy input) and will prevail over the reverse one (Henry, Broadbelt et al. 2007). Therefore, strategies based on setting an upper limit on the Gibbs energy dissipation rate (Niebel, Leupold et al. 2019), or fixing reaction directionalities (Fleming and Thiele 2011) have been suggested. Regarding EFMA, even though using thermodynamics reduces the aforementioned limitations due to combinatorial explosion, the network size is still a limiting factor (Gerstl, Jungreuthmayer et al. 2015). The flux-force relationship (thermodynamic displacement from the equilibrium (Ataman and Hatzimanikatis 2015)) links thermodynamic potentials and fluxes (Eq. 2):

$$\Delta_r G' = \Delta_r G'^o + RT \ln Q = RT \ln\left(Q/k_{eq}\right) = -RT \ln(J^+/J^-) \qquad (2)$$

where $\Delta_r G'$ and $\Delta_r G'^o$ are the Gibbs free energies of reactions (the latter referring to adjusted standard conditions), which can be derived from tabulated Gibbs free energies of formation and reaction stoichiometry (Alberty 2005). Q and K_{eq} are the ratio of products to reactant concentrations or activities (the latter at equilibrium), R to the gas constant ($8.31\ \mathrm{JK^{-1}mol^{-1}}$) and (J^+/J^-) is the relative forward-to-backward flux (Park, Rubin et al. 2016). It is also worth mentioning that $\Delta_r G'^o$ results from adjusting $\Delta_r G^o$ to physicochemical parameter values different from the standard conditions ones (temperature of 298.15K, 1 bar, zero ionic strength, pH 0 and concentration of 1M for all species (dilute aqueous solutions) (Alberty 2005, Jankowski, Henry et al. 2008). For instance, deviations in

ionic strength (I) values can be accounted for by using the extended Debye-Hückel equation or the Davies equation (for $I < 0.1$M and $I < 0.5$M, respectively) (Henry, Broadbelt et al. 2007, Simonin 2017).

Four main approaches exploiting thermodynamics data can be highlighted: (i) energy balance analysis (EBA), where pre-selecting $\Delta_r G'$ bounds leads to biased results (Beard, Babson et al. 2004), (ii) network-embedded thermodynamic (NET) analysis, that needs pre-assigned directionalities (e.g. obtained by FBA) and evaluates the thermodynamic consistency (Kümmel, Panke et al. 2006), (iii) max-min driving force (MDF), which needs a flux distribution as input data to predict metabolite concentration values (Flamholz, Noor et al. 2012), and (iv) thermodynamically-constrained FBA.

Two methods were developed in the latter approach: thermodynamics-based flux analysis (TFA), and an optimization problem allowing to obtain a thermodynamically flux-minimised (TR-fluxmin) solution. TFA directly yields a thermodynamically feasible FBA solution (e.g. by maximising $Y_{X/S}$) and simulates metabolomics data (Henry, Broadbelt et al. 2007, Salvy, Fengos et al. 2018). In contrast, TR-fluxmin is based on the minimisation of sum of fluxes in the system whilst applying a penalty score for *in silico* metabolite concentration values (Hoppe, Hoffmann et al. 2007).

MDF and TFA are generally performed using eQuilibrator (Flamholz, Noor et al. 2012) and matTFA (Salvy, Fengos et al. 2018). However, the former can only be applied to small networks upon pre-assigning flux values derived from an EFMA, while matTFA can be directly used to analyse a GSM. Briefly, TFA couples thermodynamic constraints (metabolite concentration values and $\Delta_r G'$) to reaction directionalities (Henry, Broadbelt et al. 2007, Orth, Thiele et al. 2010, Salvy, Fengos et al. 2018). Consequently, the predicted optimal solution consists of a flux distribution and a set of associated metabolite concentrations.

Nevertheless, certain potential shortcomings are worth mentioning: (i) it only considers a unique value for temperature (25 ℃), (ii) salinity (S) is not taken into account when calculating parameter A, and (iii) Gibbs free energy values are adjusted for ionic strength using the extended Debye-Hückel equation (Table 2-1). This could be an issue, since

the cytosol of *E. coli* is normally in the interval 0.15 – 0.20 M (Henry, Broadbelt et al. 2007) (and so, salinity is not null), and such equation is only valid for $I < 0.1$ M (Simonin 2017).

Considering the lack of systems-wide validations of the matTFA toolbox against experimental data, the aim of this study was to determine the impact of varying and adjusting the physicochemical parameters (*t, I* and S) on the predictive capabilities of TFA under mesophilic growth conditions. To that end, a modified matTFA was developed by increasing the number of parameters and parameter values that were originally considered (Salvy, Fengos et al. 2018). Finally, published ^{13}C-MFA and metabolomics data was used to test the predicted capabilities of each test to identify the best combination of factors. Specifically, flux pattern changes between *in vivo* and *in silico* fluxes in the central carbon metabolism were analysed, with a focus on the anaplerotic reactions. In addition, a method based on network analysis was developed, allowing to identify and prioritise important metabolites that (if quantified) would allow to further constrain the TFA.

2.3. Materials and methods

2.3.1. Metabolic network, mapping of metabolic fluxes and experimental data

Mesophilic growth conditions were studied by selecting a GSM for *Escherichia coli* (str. K-12 substr. MG1655): *i*JO1366, which has proven to predict phenotypes in a wide range of growth conditions (Orth, Conrad et al. 2011). For the sake of consistency, metabolomics and fluxomics data were obtained from the same experiment (S2-1 Dataset and S2-1 Table) (Ishii, Nakahigashi et al. 2007). Briefly, cells were grown in glucose-limited chemostats at 37 ℃ with minimal medium and a fixed specific growth rate (μ) of 0.20 h^{-1}. The experimental glucose uptake rate (2.93 mmol $gDCW^{-1}$ h^{-1}) was used as a constraint, leaving the default lower and upper bounds for transport reactions. Maximisation of the biomass yield was selected as the objective function, and no flux value was forced through the biomass reactions ($v_{biomass}$). Directionalities of resulting flux values from TFA were compared on a reaction-by-reaction case against *in vivo* fluxes from ^{13}C-MFA, for which a mapping and directionality correction step was needed (S2-1 Table).

2.3.2. Generation of experimental design

The original matTFA toolbox uses unique values for t and I (Salvy, Fengos et al. 2018), and S is not taken into account (Table 2-1). To explore their potential impact in the predictive capabilities, a modified matTFA (mod-matTFA) allowing to consider alternative parameters values and methods was created (Table 2-2). Specifically, six factors were considered: three relating to physicochemical conditions (t, I and S), and three to methodological aspects (adjusting equation, parameter A calculation and exploiting metabolomics data for constraining). For the sake of reproducibility (Sandve, Nekrutenko et al. 2013), the complete list of files used in this study was collected in S2 Table, and are publicly available in *Nottingham SBRC*'s GitHub profile (https://github.com/SBRCNottingham/Impact-of-Physicochemical-Parameters-on-thermodynamics-based-FBA). Analyses were performed using the COBRA toolbox (Schellenberger, Que et al. 2011) in MATLAB R2016b with the solver CPLEX 12.8.0 to ensure compatibility.

Table 2-2. Factors considered in mod-matTFA. Values 0/1 refer to the binary codification for the full factorial design (S3 Table). In total, 2^6 combinations were tested.

Temperature, t (°C)	(0): 25 (1): 37
Ionic strength, I (M)	(0): 0 (1): 0.25
Salinity, S (g/kg)	(0): 0 (1): 13.74
Adjustment method	(0): Extended Debye-Hückel equation (1): Davies equation
Parameter A	(0): T-dependent* (1): T,S-dependent
Metabolite concentration values	(0): Default matTFA (1): experimental data

*T is temperature in K. There is a 'default matTFA' constraint regarding set concentrations values for cofactors (AMP, ADP and ATP) as included in the original matTFA code. 'Experimental data' refers to the use of published metabolomics data (S2 Dataset), setting the lower and upper bound for the simulation as 90-110% of the concentration values.

Since I affects the Gibbs energy of formation, an adjustment from the reference state ($\Delta_f G_j^o$) was needed to obtain the standard transformed Gibbs energy of formation ($\Delta_f G_j'^o$) (Alberty 2005). In the original matTFA (Salvy, Fengos et al. 2018) and other studies (Flamholz, Noor et al. 2012, Niebel, Leupold et al. 2019) the extended Debye-Hückel equation was used to adjust the Gibbs free energy values, with a proven validity for $I < 0.1$ M (Simonin 2017) (Eq. 3). The parameter B was assumed to be constant, with a value of 1.6 $mol^{-1/2}L^{1/2}$ (Alberty 2005, Henry, Broadbelt et al. 2007). Mod-matTFA also explored the impact of using the Davies equation ($\beta = 0.3$) (Eq. 4) as an alternative adjustment approach, with a tested validity for $I < 0.5$ M (Simonin 2017).

$$\Delta_f G_j'^o(I) = \Delta_f G_j^o + N_H(j)RT\ln(10)\mathrm{pH} - RT\left(\frac{A\sqrt{I}}{1+B\sqrt{I}}\right)\left(z_j^2 - N_H(j)\right) \quad (3)$$

$$\Delta_f G_j'^o(I) = \Delta_f G_j^o + N_H(j)RT\ln(10)\mathrm{pH} - RT\left(\frac{A\sqrt{I}}{1+\sqrt{I}} - \beta I\right)\left(z_j^2 - N_H(j)\right) \quad (4)$$

Both formulas include terms correcting the pH and I, where $N_H(j)$ is the number of hydrogen atoms in species j, R is the gas constant, T is the absolute temperature and z_j refers to the charge of the species (Alberty

2005). Applying the Gibbs-Helmholtz equation would be necessary to account for temperature different from standard conditions, i.e. 25 °C, but the lack of measured changes in enthalpy (ΔH^o) for all the metabolites prevents from doing so (Atkins and Paula 2002). Hence, variations from 25 °C to 37 °C were assumed to be small, as shown elsewhere (Fleming, Thiele et al. 2009). The parameter A is normally assumed to be constant (Henry, Broadbelt et al. 2007) or calculated using a temperature-dependent function (Eq. 5) (Flamholz, Noor et al. 2012, Salvy, Fengos et al. 2018), and the impact of using a temperature/salinity-dependent function (Eq. 6) (Atkins and Paula 2002) was also tested in this study (Figure 2-1).

$$A\left(\mathrm{mol}^{-\frac{1}{2}}\mathrm{kg}^{\frac{1}{2}}\right) = 1.10708 - 1.54508 \times 10^{-3}T + 5.95584 \times 10^{-6}T^2 \quad (5)$$

$$A\left(\mathrm{mol}^{-\frac{1}{2}}\mathrm{kg}^{\frac{1}{2}}\right) = \frac{F^3\sqrt{2\varepsilon_0 R^3}}{4\pi\varepsilon_0 N_A} \times \left(\frac{\rho_{sw}(t,S)}{(\varepsilon_{sw}(t,S)T)^3}\right)^{\frac{1}{2}} \quad (6)$$

where the first term in Eq. (6) includes physical constants (Faraday's constant (F), vacuum permittivity (ε_0), gas constant (R) and Avogadro's constant (N_A)), and the second the temperature (T in K and t in °C), and salinity (S) dependent functions to calculate the density (ρ_{sw}) (Siedler and Peters 1986) and the relative permittivity (ε_{sw}) (Meissner and Wentz 2004) for seawater (S2-2 Table).

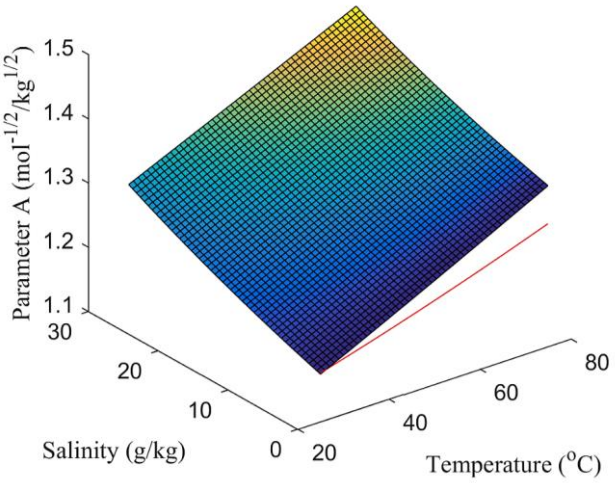


Figure 2-1. Calculation of the parameter $\boldsymbol{A}$. The red line refers to the temperature-dependent function (Eq. 5), whereas the surface is the temperature/salinity-dependent function (Eq. 6).

In general, consistency in units between parameters A ($mol^{-1/2}kg^{1/2}$) and B ($mol^{-1/2}L^{1/2}$) is achieved by assuming 1 kg = 1 L. In this study, an expression for seawater (Eq. 7) (Millero and Leung 1976) was used to estimate a salinity value by considering a buoyant density (ρ) for bacterial cells of 1.11 kg/L (Baldwin, Myer et al. 1995). For I, a value of 0.25 M was used (Table 2-2).

$$I(\mathrm{M}) \times \rho\left(\frac{\mathrm{kg}}{\mathrm{L}}\right) = \frac{19.92 \times \mathrm{S}}{1000 - 1.005 \times \mathrm{S}} \qquad 7$$

Certain aspects regarding the full factorial design could entail potential limitations which should be considered. It comprised 6 factors with two values or categories, yielding 64 combinations. This led to 16 incongruent tests, where an ionic strength of 0 M was analysed along with a salinity of 13.74 g/kg. However, it should be noted that salinity is only considered to calculate the aforementioned Parameter A, for which two different strategies to calculate such parameter were considered (a temperature-dependent and a temperature and salinity-dependent, Figure 2-2), thus further reducing the number of potentially conflicting conditions from 16 to 8. Overall, including such combinations was simply deemed necessary to assess the relevance of adjusting for salinity when running matTFA under mesophilic conditions, and whether the method was sensitive enough to these parameters or not. Nevertheless, further studies considering non-mesophilic species (e.g., living in environments with high salinity) should be considered to further explore the impact of adjusting such parameters on the simulations.

Another potential limitation worth exploring is the selection of an ionic strength value of 0.25 M for the cytoplasm of *E. coli*. Even though the estimated value is in the range 0.15-0.20 M, modelling approaches such as matTFA use the aforementioned ionic strength instead. Thus, enabling a comparison against mod-matTFA required keeping the consistency. A more detailed Discussion can be found in section 5.2.

2.3.3. Assessment of fluxomics and metabolomics predictive capabilities

Mesophilic growth conditions for *E. coli* were selected as a case study to explore the impact of metabolic and physiochemical constraints on the predictive capabilities of TFA at the fluxomics and metabolomics level. Accordingly, 64 different factor combinations (Table 2-2) were tested using mod-matTFA. It is important to note that not all test yielded a solution where cell growth was achieved (i.e. $v_{biomass} > 0$ mmol $gDCW^{-1}$ h^{-1}). Since different factor combinations converged into the same set of solutions, tests were characterised at the fluxomics and metabolomics levels by considering either the full set of values, or the subset with an experimental counterpart.

Results yielding feasible solutions were also compared against ^{13}C-MFA flux values (S2-1 Table) and experimental metabolomics data (S2-1 Dataset), respectively. A goodness-of-fit analysis based on the Pearson correlation coefficient (r) was performed, as shown in (Pandey, Hadadi et al. 2019). In order to identify the test(s) with the best predictive capabilities at both levels, they were separately ranked according to two criteria: (i) correlation coefficient at the fluxomics level, and (ii) correlation coefficient at the metabolomics level.

The concordance between results was assessed by the Kendall's W statistics (S2-2 Table), where a value of 0 means no agreement of ranking position with respect to each criterion, and a value of 1 indicates total agreement. This statistics is a normalisation of the Friedman test, which simply tests whether samples are from the same population or not (Field 2009). Finally, a joint ranking after weighting the ranking position according to each criterion was considered (the higher the score, the better the correlation in both the fluxomics and metabolomics levels).

Finally, the relative importance of each factor (S2-3 Table) in the prediction of fluxomics and metabolomics data was determined by means of the Classification And Regression Trees (CART) algorithm using Minitab 19 (Ghiasi, Zendehboudi et al. 2020). Briefly, this technique classifies data in a binary tree upon calculating the splitting criterion (Gini's impurity index) for each predictor (i.e. the factors used in this study) (Kuzilek, Kremen et al. 2014). This index measures the misclassification error, so the best predictor

in classifying the results will have the highest relative importance (Breiman, Friedman et al. 1984, Jaworski, Duda et al. 2018).

2.3.4. Thermodynamics-enriched network analysis

The constraining capacity of metabolites is not uniform, and depends on their connectivity in the network (Kiparissides and Hatzimanikatis 2017, Salvy, Fengos et al. 2018). To further constrain the model, a priority list of metabolites to be quantified should be considered when designing the metabolomics protocol. In this study, the suitability of the selected dataset for this purpose was analysed (S2-1 Dataset). The importance of each metabolite in the network was measured by means of PageRank as implemented in MATLAB. This algorithm was developed by Google (Page L and Motwani R 1998) and has been recently applied to metabolic networks (Frainay, Aros et al. 2018).

Ubiquituous compounds in a metabolic network bias the centrality measures (Wagner and Fell 2001, Beguerisse-Díaz, Bosque et al. 2018, Frainay, Aros et al. 2018). These are known as *side compounds* (also known as "currency" or "pool" compounds), and even though there is no clear definition they normally comprise cofactors, ion, metabolites participating in energy metabolism, among others. The selection of compounds for this study is shown below (Table 2-3).

Non-redundant flux distributions from TFA were selected and subjected to network simplification and correction. Briefly, only active metabolites and reactions were kept, and stoichiometric coefficients were corrected so that they reflected the flux direction of each reaction. Centrality measures require a graph G, defined as a pair $G = (V, E)$, where the vertices (or nodes) V are the metabolites, and the edges E the reactions connecting them. The stoichiometric matrix was converted into an adjacency matrix using an in-house script (S2-1 Appendix), which was later used to generate a G ready for the PageRank analysis. The final list of metabolites was ranked by their centrality score, focusing on the top 50%. Specifically, metabolites for which concentration values were available and used for the assessment of the predictive capabilities were selected for inspection (Ishii, Nakahigashi et al. 2007).

Table 2-3. List of side compounds, including ions, acyl-carrier-proteins (ACP), cofactors and currency metabolites.

MetSymbol	MetName	MetSymbol	MetName
2dmmql8_c	2-Demethylmenaquinol 8	hpmeACP_c	3-Hydroxypimeloyl-[ACP] methyl ester
2fe1s_c	[2Fe-1S] desulfurated iron-sulfur cluster	imp_c	IMP
2fe2s_c	[2Fe-2S] iron-sulfur cluster	iscs_c	IscS sulfur acceptor protein
3fe4s_c	[3Fe-4S] damaged iron-sulfur cluster	iscssh_c	IscS with bound sulfur
3hcpalm9eACP_c	(R)-3-hydroxy-cis-palm-9-eoyl-[ACP]	iscu_c	IscU scaffold protein
3hmrsACP_c	(R)-3-Hydroxytetradecanoyl-[ACP]	iscu-2fe2s_c	IscU with bound [2Fe-2S] cluster
3ocpalm9eACP_c	3-oxo-cis-palm-9-eoyl-[ACP]	iscu-2fe2s2_c	IscU with two bound [2Fe-2S] clusters
3omrsACP_c	3-Oxotetradecanoyl-[ACP]	iscu-4fe4s_c	IscU with bound [4Fe-4S] cluster
4fe4s_c	[4Fe-4S] iron-sulfur cluster	k_c	Potassium
6hmhpt_c	6-hydroxymethyl dihydropterin	lipopb_c	Lipoate (protein bound)
6hmhptpp_c	6-hydroxymethyl-dihydropterin (...)	malACP_c	Malonyl-[acyl-carrier protein]
ACP_c	Acyl carrier protein	meoh_c	Methanol
adocbl_c	Adenosylcobalamin	mg2_c	Magnesium
adp_c	ADP	mn2_c	Manganese
ahdt_c	2-Amino-4-hydroxy-6-(...)	moadamp_c	MoaD Protein with bound AMP
amp_c	AMP	moadcoo_c	MoaD Protein with carboxylate
aps_c	Adenosine 5	moadcosh_c	MoaD Protein with thiocarboxylate
atp_c	ATP	mobd_c	Molybdate
bmoco_c	Bis-molybdenum cofactor	moco_c	Molybdenum cofactor
bmoco1gdp_c	Bis-molybdopterin mono-guanine (...)	mococdp_c	Molybdopterin cytosine dinucleotide
bmocogdp_c	Bis-molybdopterin guanine dinucleotide	mocogdp_c	Molybdopterin guanine dinucleotide
ca2_c	Calcium	mpt_c	Molybdopterin
cbl1_c	Cob(I)alamin	mptamp_c	Adenylated molybdopterin
cbp_c	Carbamoyl phosphate	mql8_c	Menaquinol 8
cdp_c	CDP	myrsACP_c	Myristoyl-ACP (n-C14:0ACP)
cl_c	Chloride	na1_c	Sodium
cmp_c	CMP	nad_c	Nicotinamide adenine dinucleotide
co2_c	CO2	nadh_c	Nicotinamide adenine dinucleotide - reduced
coa_c	Coenzyme A	nadp_c	Nicotinamide adenine dinucleotide phosphate
cobalt2_c	Co2+	nadph_c	Nicotinamide adenine dinucleotide phosphate - reduced
cpmp_c	Cyclic pyranopterin monophosphate	nh4_c	Ammonium
ctp_c	CTP	ni2_c	Nickel
cu2_c	Copper	nicrnt_c	Nicotinate D-ribonucleotide
ddcaACP_c	Dodecanoyl-ACP (n-C12:0ACP)	o2_c	O2 O2
dhpmp_c	Dihydroneopterin monophosphate	ocACP_c	Octanoyl-ACP (n-C8:0ACP)
dnad_c	Deamino-NAD+	octapb_c	Octanoate (protein bound)

dpcoa_c	Dephospho-CoA	octeACP_c	Cis-octadec-11-enoyl-[acyl-carrier protein] (n-C18:1)
dscl_c	Dihydrosirohydrochlorin	ogmeACP_c	3-Oxo-glutaryl-[acyl-carrier protein] methyl ester
dtdp_c	DTDP	opmeACP_c	3-Oxo-pimeloyl-[acyl-carrier protein] methyl ester
dtmp_c	DTMP	palmACP_c	Palmitoyl-ACP (n-C16:0ACP)
dttp_c	DTTP	pap_c	Adenosine 3',5'-bisphosphate
egmeACP_c	Enoylglutaryl-[ACP] methyl ester	paps_c	3'-Phosphoadenylyl sulfate
epmeACP_c	Enoylpimeloyl-[ACP] methyl ester	pdx5p_c	Pyridoxine 5'-phosphate
fad_c	Flavin adenine dinucleotide oxidized	pi_c	Phosphate
fadh2_c	Flavin adenine dinucleotide reduced	pimACP_c	Pimeloyl-[acyl-carrier protein]
fe2_c	Fe2+ mitochondria	pmeACP_c	Pimeloyl-[acyl-carrier protein] methyl ester
fe3_c	Iron (Fe3+)	ppi_c	Diphosphate
flxr_c	Flavodoxin reduced	pppi_c	Inorganic triphosphate
flxso_c	Flavodoxin semi oxidized	pyam5p_c	Pyridoxamine 5'-phosphate
fmn_c	FMN	pydam_c	Pyridoxamine
gdp_c	GDP	pydx_c	Pyridoxal
glyc_c	Glycerol	pydx5p_c	Pyridoxal 5'-phosphate
glycogenn1_c	Glycogen	pydxn_c	Pyridoxine
gmeACP_c	Glutaryl-[ACP] methyl ester	q8_c	Ubiquinone-8
gmp_c	GMP	q8h2_c	Ubiquinol-8
grxox_c	Glutaredoxin (oxidized)	quln_c	Quinolinate
grxrd_c	Glutaredoxin (reduced)	scl_c	Sirohydrochlorin
gthox_c	Oxidized glutathione	sheme_c	Siroheme C42H36FeN4O16
gthrd_c	Reduced glutathione	so3_c	Sulfite
gtp_c	GTP	so4_c	Sulfate
h_c	H+	t3c9palmeACP_c	Trans-3-cis-9-palmitoleoyl-[acyl-carrier protein]
h2o_c	H2O H2O	tdeACP_c	Cis-tetradec-7-enoyl-[acyl-carrier protein] (n-C14:1)
h2o2_c	Hydrogen peroxide	thf_c	5,6,7,8-Tetrahydrofolate
h2s_c	Hydrogen sulfide	thmmp_c	Thiamin monophosphate
hco3_c	Bicarbonate	thmpp_c	Thiamine diphosphate
hdeACP_c	Cis-hexadec-9-enoyl-[ACP] (n-C16:1)	trdox_c	Oxidized thioredoxin
hemeO_c	Heme O	trdrd_c	Reduced thioredoxin
hgmeACP_c	3-Hydroxyglutaryl-[ACP] methyl ester	udp_c	UDP
		ump_c	UMP
		zn2_c	Zinc

2.4. Results and discussion

2.4.1. Evaluation of the reliability of predicted flux and concentration values

A full factorial design comprising 2^6 tests (Table 2-2) was applied in TFA to constrain the GSM *i*JO1366 (Orth, Conrad et al. 2011), selecting the maximisation of biomass yield as the objective function. An experimental glucose uptake rate was set (2.93 mmol $gDCW^{-1}$ h^{-1}), reaching a $\mu \approx 0.28$ h^{-1} (the experimental was 0.20 h^{-1}) for all FBA and TFA tests. Overall, 26/64 tests were unsuccessful (no cell growth), and the remaining 38/64 converged into common optimal solutions (S2-4 Table). At the fluxomics level, a single flux distribution was achieved in FBA for all tests, whereas for TFA a different number of non-redundant solutions were found: 5 (when considering all reactions) or 4 (only those with an experimental counterpart).

Likewise, at the metabolomics level, the 38 tests were reduced to 9 optimal solutions. Results were tested against available experimental data (^{13}C-MFA and metabolomics (Ishii, Nakahigashi et al. 2007)) by calculating the Pearson correlation coefficient. Therefore, each successful test was characterised by the optimal solutions it achieved and the correlation coefficients at both the fluxomics and metabolomics levels.

The importance of each factor was assessed by means of decision trees (CART in Minitab 19) (Table 2-4). Briefly, models were built considering categorical predictors (the factors after the codification (S2-3 Table)) and responses: the importance of a factor measured the improvement on the model when using it to split the data (Figure S2-1). Accordingly, the relative importance was calculated with respect to the best predictor (Table 2-4).

The I (M) was the top one for all responses except for *TFA (full)*, where it equalised t (°C) at 95.7 % and was second to the adjustment method. In all cases, using either default concentrations values for AMP, ADP and ATP (as included in the original matTFA), or experimental data made no difference. As a result, tests only differing in this factor showed the same correlations with experimental data (S2-4 Table).

Table 2-4. Relative factor importance. The type of analysis depended on the nature of the response: *classification* was selected for TFA (full), TFA (match ^{13}C-MFA), concentration values (full) and concentration values (match experimental), and *regression* for r (fluxomics) and r (metabolomics). The former was suited for categorical responses (i.e. which solution is achieved, as shown in S4 Table), and the latter for continuous responses (for Pearson's r, from -1 to +1).

	TFA (full)	TFA (match ^{13}C-MFA)	Concentration values (full)	Concentration values (match exp)	r (fluxomics)	r (metabolomics)
t (°C)	95.7	50.0	50.0	50.0	29.8	60.4
I (M)	95.7	100.0	100.0	100.0	100.0	100.0
S (g/kg)	19.9	7.8	27.5	27.5	-	-
Parameter ***A***	-	1.0	50.0	50.0	2.6	-
Adjustment method	100.0	52.1	44.4	44.4	52.3	0.9
[met]	-	-	-	-	-	-

Correlation coefficients for FBA in all tests was r ≈ 0.76, whereas for TFA it varied within the range from 0.90 to 0.95. A reaction-by-reaction comparison of flux directionalities in central metabolism showed inherent differences between ^{13}C-MFA and FBA/TFA, as discussed in the last section of this study. At the metabolomics level, correlation coefficient for the different tests ranged from 0.08 to 0.18 (S2-4 Table). Tests were ranked independently by both criteria, showing a notable agreement in their positions (Kendall's W ≈ 0.81).

Scoring the position according to each criterion allowed creating a joint ranking to identify the test(s) with the best predictive capability at both levels ((S2-4 Table).). Four tests held the first position, since they all converged into the same optimal solutions (S2-4 Table). Specifically, t = 37 °C, I = 0.25 M and the Davies equations as adjustment method were used. Following the relative factor importance (Table 2-4), correlation coefficients were not affected by S and the selection of concentrations values.

This analysis showed that adjusting the physicochemical parameters to the experimental conditions did improve the predictive capabilities of TFA (S2-4 Table), but certain technical limitations at both levels need to be discussed. The nature of ^{13}C-MFA only allows determining the flux distribution in the central carbon metabolism by considering amino acid synthesis (Antoniewicz 2015), which has been noted to be very robust against changes in the intermediate metabolite concentrations (Costenoble, Muller et al. 2007, Toya, Ishii et al. 2010). The recent discovery of non-enzymatic metabolism-like reactions suggests that current metabolic networks evolved from prebiotic reaction sequences. Therefore, a well-established flux distribution in the central pathways can be expected (Ralser 2018).

Predicted flux values were compared against ^{13}C-MFA data from (Ishii, Nakahigashi et al. 2007) (Figure 2-3). Certain reactions were predicted to be inactive but experimental data showed otherwise. This was caused due to intrinsic differences in problem definitions, as further explained in next sections. Overall, only 36/1705 metabolic fluxes showed a variance among TFA tests greater than zero, of which 6 reactions had an experimental counterpart to compare against (S2 Dataset). Optimal solutions for all tests were similar (reducing the discerning capacity), which explained the overall high correlation coefficients with experimental data for all of them. Therefore, results from the comparison of predicted and experimental metabolite concentration values are paramount to better understand the impact of varying the physicochemical parameters.

Regarding the metabolomics level, the 9 non-redundant solutions were subjected to a similar analysis. Likewise, only 46/972 metabolites had a variance among tests greater than zero (S2-3 Dataset), out of which 7 were quantified: L-aspartate, phosphoenolpyruvate, ATP, L-valine, pyruvate, $NADP^+$, and FAD. Reliable quantitation of energy-carrying molecules and redox cofactors is not easily achievable, given the inherent cell dynamics (e.g. cell cycle and cell size variations) and degradation during extraction (Goodwin 1969, Rabinowitz and Kimball 2007, Massie, Blasius et al. 2010, Yaginuma, Kawai et al. 2014, Gao and Xu 2015, Barber, Ho et al. 2017, Lu, Wang et al. 2018, Takhaveev and Heinemann 2018, Zhang, Milias-Argeitis et al. 2018). Since the correlation coefficients were calculated using a dataset

blind to highly variable metabolites (e.g. 3-phosphohydroxypyruvate ranged four orders of magnitude), resulting values were similar for different factor combinations (Table 2-4). Thus, said metabolites should be quantified to deconvolute the impact of using default or experimental concentration values in the predictive capabilities.

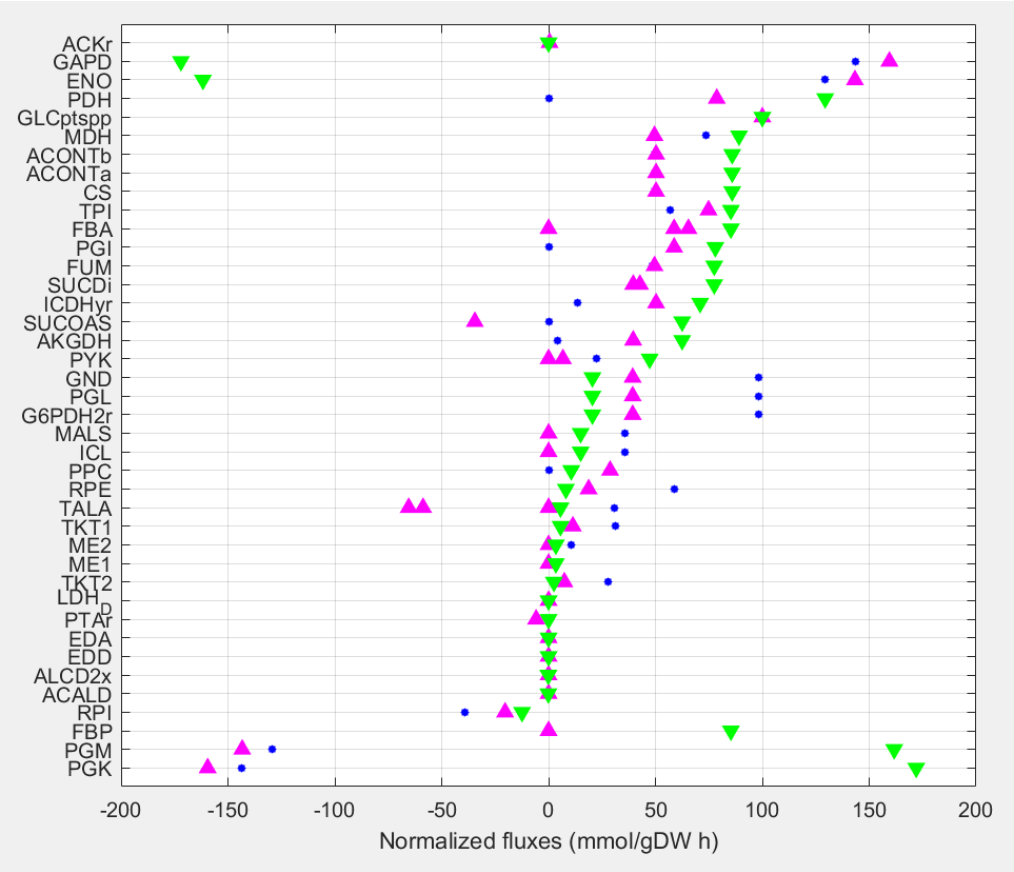


Figure 2-3. Comparison of flux values among FBA (blue circle), TFA (magenta up triangle, up to 4 per reaction depending on the optimal solution (S2-4 Table)) and ^{13}C-MFA (green down triangle).

Other limitations refer to the design of the tool itself. This method does not consider other complex phenomena affecting the thermodynamic feasibility of metabolic pathways, such as Mg complexation with metabolites, or compound dissociation into more than two protonated species (Vojinović and Von Stockar 2009, Salvy, Fengos et al. 2018) (as shown in the file *calcDGspecies.m*). In addition, Gibbs free energy values are relaxed when no feasible solution is found, so the constraining power of experimental

metabolite concentration values is reduced (Salvy, Fengos et al. 2018). Related to this, an approach allowing to identify metabolites to further constrain the model was developed in this study (next section). Finally, it should be noted that to apply matTFA to thermophilic species (e.g. *Thermus thermophilus*, a potential non-model metabolic engineering platform (Crosby, Laemthong et al. 2019)), recent methods to adjust Gibbs free energies to high temperatures should be considered (Dun, Zhang et al. 2018).

2.4.2. Identification of central metabolites to further constrain the model

Successful tests converged into 5 solutions at the fluxomics level (S4 Table), which are structurally equivalent. Therefore, a single stoichiometric matrix was considered for further analysis. After the simplification step (removal of inactive metabolites and reactions, as well as side compounds) 622/1805 metabolites were left in the network. The experimental dataset included information about 44 metabolites (S1 Dataset), out of which 34 were also considered in the simplified network, and the rest was discarded as side compounds.

PageRank scores were calculated, allowing to identify metabolites in the top 50% for which experimental data was available (Table 2-5). Overall, 18/34 quantified metabolites were in the top 50%, with only 7 in the top 10%. The lack of high centrality for most metabolites explains the aforementioned result, where tests only differing in the set of concentrations values used as a constraint (default ATP/ADP/AMP or experimental) led to the same optimal solution (e.g. tests 20 and 52, Table 2-4).

The priority list is led by L-glutamate, pyruvate, 2-oxoglutarate (not quantified), D-fructose-6-P and glyceraldehyde 3-phosphate (not quantified). Both L-glutamate and 2-oxoglutarate participate in the assimilation of nitrogen in *E. coli*, where the former also plays a role as nitrogen donor in the biosynthesis of nucleic acids (van Heeswijk, V. Westerhoff et al. 2013). The latter along with the rest (except for glyceraldehyde 3-phosphate), and acetyl-CoA are important biosynthetic precursors used in modelling (Wagner and Fell 2001). Accordingly, other metabolites participating in central pathways such as glycolysis (glyceraldehyde 3-phosphate, dihydroxyacetone phosphate, etc.) and protein biosynthesis (amino acids) were also identified.

Table 2-5. Quantified metabolites from (Ishii, Nakahigashi et al. 2007) in the top 50% of PageRank (PR) based analysis. The last position in the ranking (#622) was L-Tyrosine (PR score = 0.0004), which had been quantified. The full list can be found in (S2-4 Dataset).

Quantile	Ranking position	Metabolite	Node	PR score
10%	1	L-Glutamate	glu-L_c	0.0172
	2	Pyruvate	pyr_c	0.0126
	4	D-Fructose 6-phosphate	f6p_c	0.0079
	6	Acetyl-CoA	accoa_c	0.0071
	7	L-Methionine	met-L_c	0.0071
	23	Succinyl-CoA	succoa_c	0.0046
	44	L-Serine	ser-L_c	0.0034
30%	69	Dihydroxyacetone phosphate	dhap_c	0.0029
	70	L-Tryptophan	trp-L_c	0.0029
	88	Phosphoenolpyruvate	pep_c	0.0026
	103	S-Adenosyl-L-methionine	amet_c	0.0024
	129	L-Alanine	ala-L_c	0.0021
	157	L-Histidine	his-L_c	0.0020
	161	D-Glucose 1-phosphate	g1p_c	0.0019
	177	L-Proline	pro-L_c	0.0019
	181	3-Phospho-D-glycerate	3pg_c	0.0018
50%	249	D-Fructose 1,6-bisphosphate	fdp_c	0.0016
	258	L-Leucine	leu-L_c	0.0015

Important metabolites highlighted here agree with results from the seminal work by Wagner et al. (Wagner and Fell 2001), where they used a smaller network (317 vs. 931 reactions). Due to computational costs, other attempts specifically focusing on the constraining capacity with regards to TFA (Thermodynamics-based Metabolite Sensitivity Analysis, TMSA) are also limited by the network size (156 reactions in (Kiparissides and Hatzimanikatis 2017)).

In particular, this approach identified pyruvate as the most significant metabolite in terms of reducing the variability in the thermodynamic properties of reactions, and attributed it to its high connectivity in the network. Other important compounds included phosphate, NAD^+, NADH, CO_2, menaquinol-8, menaquinone-8 and D-lactate. All but the latter were classified as side compounds for this study (and therefore excluded), since

the centrality measures are biased by ubiquitous metabolites (Frainay, Aros et al. 2018).

The impact of the inherent dynamics (cell cycle and cell ageing) has been pointed out as a source of metabolic heterogeneity in clonal microbial populations (Takhaveev and Heinemann 2018). In a chemostat, cells are maintained at the exponential growth phase, but the cell cycle is not synchronised across single cells unless forced (Goodwin 1969, Massie, Blasius et al. 2010). In *E. coli*, concentration values for NAD(P)H oscillate along the cell cycle (Zhang, Milias-Argeitis et al. 2018), and ATP concentration values show an asymmetric distribution across single cells in a continuous culture (Yaginuma, Kawai et al. 2014). From a metabolomics point of view, an unbiased extraction and quantitation method is yet to be developed (Gao and Xu 2015). Particularly, ATP/ADP/AMP quantitation require specific culture conditions (Rabinowitz and Kimball 2007), and nicotinamides parallel protocols to avoid degradation. Overall, the method developed here generated a priority list to be considered when selecting a metabolomics protocol aiming at providing data to further constrain a model in TFA.

2.4.3. Reaction directionalities in the central carbon metabolism

Finally, flux pattern changes between *in vivo* and *in silico* fluxes in the central carbon metabolism were analysed, with a particular focus on the anaplerotic reactions. The 'anaplerotic node' (Figure 2-4) comprises carboxylation and decarboxylation reactions of metabolites participating in the tricarboxylic acid (TCA), which are used for the biosynthesis of amino acids (Sauer and Eikmanns 2005). Given the fact similar MIDs (from proteinogenic amino acids) can be obtained from different precursors, ^{13}C-MFA has been noted to show a limited capability to elucidate fluxes around the anaplerotic node (Fischer, Zamboni et al. 2004, Toya, Ishii et al. 2010, Kappelmann, Wiechert et al. 2015). In order to evaluate changes in reaction directionalities, the available *in vivo* fluxes were tested against their equivalents in the simulated TFA flux distributions (S2-1 Table). Overall, 13/40 flux directions disagree between approaches (Table 2-6).

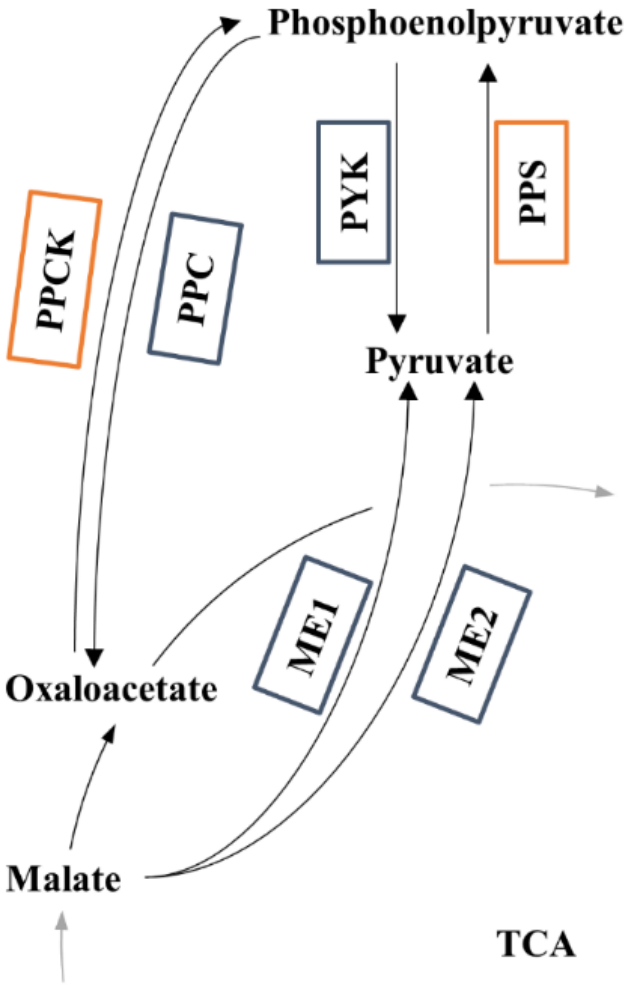


Figure 2-4. Anaplerotic node for *E. coli*. Set of carboxylation/decarboxylation reactions including phosphoenolpyruvate, pyruvate, oxaloacetate, and malate. Arrows indicate the expected direction of carbon fluxes. Boxes refer to reactions: blue when they are defined in both the GSM and the metabolic network used for ^{13}C-MFA, and orange when they are exclusively considered in the GSM. In the latter case no mapping was possible (S2-1 Table).

Discrepancies in flux pattern between methods are caused by both differences in the structure of the metabolic networks and the way the problem is defined (Table 2-1). On the one hand, *i*JO1366 includes 8 reactions concerning the anaplerotic node and the glyoxylate shunt: PPC and PPCK (between phosphoenolpyruvate and oxaloacetate), PYK and PPS (between phosphoenolpyruvate and pyruvate), ME1 and ME2 (between pyruvate and malate) (Figure 2-4), and finally ICL and MALS (from isocitrate to malate, via glyoxylate).

In contrast, the metabolic network used for the ^{13}C-MFA did not consider PPCK and PPS (S1 Table), which could affect the determination of fluxes to/from phosphoenolpyruvate. Since ^{13}C-MFA is based on lumped reactions, branched pathways are not taken into account (Antoniewicz 2015). Thus, having a smaller range of alternative pathways than FBA/TFA may affect the estimation of flux values.

On the other hand, *in silico* flux distributions are the result of optimising the system according to the chosen objective function. Accordingly, when maximising the biomass production (which requires ATP), FBA and TFA promote pathways that reduce wasting ATP in the optimal solution (Orth, Thiele et al. 2010). For instance, PPCK (ATP-consuming reaction) carried no flux, but PPC did (for FBA, TFA and ^{13}C-MFA). In contrast, experimental data from *E. coli* grown on glucose has proven that both PPC and PPCK (which constitute a *futile cycle*) are active and play a role in metabolic regulations (Yang, Hua et al. 2003).

Given the fact that ICL and ME1/ME2 do not generate any ATP, fluxes may be shut down in the simulated flux distributions (as shown in (Toya, Ishii et al. 2010)). Interestingly, ICL and ME2 were active in FBA, suggesting thermodynamic constraints favoured an alternative route. In this sense, it should be noted that stochastic events or regulatory processes have been suggested to provoke a variation of the fluxes through PPCK and ME1/ME2 (Nanchen, Schicker et al. 2006).

FBA/TFA also faced problems regarding the overflow metabolism: a low amount of acetate was predicted to be produced (PTAr and ACKr), as opposed to the lack of flux according to ^{13}C-MFA. Nevertheless, TFA correctly predicted flux through PDH and PGI, whereas FBA did not (S2-5 Dataset).

Table 2-6. Flux pattern changes between ^{13}C-MFA data and TFA predictions. Where +, flux in the forward direction; -, flux in the reverse direction; 0, no flux. Corrected direction, refers to the adjustments due to differences in reaction definitions between the simplified network used for ^{13}C-MFA and the GSM (S1 Table). For example the case of ALCD2x: in vivo flux (^{13}C-MFA) suggests production of ethanol, whereas the in silico one (GSM/TFA) predicts consumption of ethanol. Since reactions are defined in opposite directions, a correction becomes necessary.

Reaction (GSM)	Definition (GSM)	Definition (^{13}C-MFA)	Direction (^{13}C-MFA)	Corrected direction (^{13}C-MFA)	Direction (TFA)
ACALD	acald_c + coa_c + nad_c ↔ accoa_c + h_c + nadh_c	AcCoA → Ethanol	+	-	0
ACKr	ac_c + atp_c + h_c ↔ actp_c + adp_c	AcCoA → Acetate	0	0	+
ACONTb	acon-C_c + h2o_c <=> icit_c	CIT -> ICT	+	+	0/+
ALCD2x	etoh_c + nad_c ↔ acald_c + h_c + nadh_c	AcCoA → Ethanol	+	-	+
FBA	fdp_c ↔ dhap_c + g3p_c	F1,6P → DHAP + G3P	+	+	0/+
ICL	icit_c → glx_c + succ_c	ICT → Glyoxylate + SUC	+	+	0
ME1	mal-L_c + nad_c → co2_c + nadh_c + pyr_c	MAL → PYR + CO2	+	+	0
ME2	mal-L_c + nadp_c → co2_c + nadph_c + pyr_c	MAL → PYR + CO2	+	+	0
PFK	atp_c + f6p_c <=> adp_c + fdp_c	F6P -> F1,6P	+	+	0/+
PTAr	accoa_c + h_c + pi_c ↔ actp_c + coa_c	AcCoA → Acetate	0	0	-/0
PYK	adp_c + pep_c ↔ atp_c + pyr_c	PEP → PYR	+	+	0/+
SUCOAS	atp_c + coa_c + succ_c ↔ adp_c + pi_c + succoa_c	2-KG → SUC + CO2	+	+	-
TALA	g3p_c + s7p_c ↔ e4p_c + f6p_c	S7P + G3P ↔ E4P + F6P	+	+	-/0

Even though flux pattern changes between predicted and experimentally determined intracellular fluxes were present, TFA offered a reliable prediction of intracellular fluxes (S2-4 Table). This overall consistency has been noted in the literature by comparing an array of different objective functions and constraints (based on split ratios rather than on mapping on a reaction-by-reaction case) (Schuetz, Kuepfer et al. 2007). A combination of both approaches to overcome their limitations and different flux space solutions has also been suggested (Williams, Poolman et al. 2010, Chen, Alonso et al. 2011). However, fluxes concerning the TCA cycle, the glyoxylate shunt and acetate secretion have proven to be difficult to predict (Schuetz, Kuepfer et al. 2007), as also shown in this study. Similarly, other reactions are also affected by the substrate uptake rate: ALCD2x becomes unidirectional at high glucose levels (Niebel, Leupold et al. 2019).

In addition, the nonlinear dependency of the anaplerotic fluxes on the growth rate has been reported in the literature, limiting the reliability of conclusions from experiments using single dilution rates (Yang, Hua et al. 2003, Nanchen, Schicker et al. 2006). Particularly, metabolic fluxes through the aforementioned futile cycle are expected to be active under glucose-limited growth conditions (Sauer, Lasko et al. 1999), rather than being totally shut down (Figure 2-4). In this sense, a higher degree of consistency between predicted and experimental flux distributions could have been achieved by (i) focusing on data from cultures with high dilution rates, so that futile cycle activity is lowered and the flux distribution becomes closer to the optimal solution, or (ii) applying further constraints to properly model the anaplerotic reactions (Myoung Park, Yong Kim et al. 2010). The first option is limited by the lack of published data at both the metabolomics and fluxomics levels from the same experiment, and the second one by the lack of implementation.

Consequently, it was assumed that the high correlation coefficient achieved for TFA against *in vivo* fluxomics data ($r \approx 0.9$) was high enough to enable the analyses on the impact of varying the physicochemical parameters in the predictive capabilities. Studying flux pattern changes on a reaction-by-reaction basis also allowed to confirm previously reported limitations from both ^{13}C-MFA and FBA/TFA with regards to the anaplerotic node (Fischer, Zamboni et al. 2004, Myoung Park, Yong Kim et

al. 2010, Kappelmann, Wiechert et al. 2015). Thus, metabolites in the node are expected to be directly affected.

2.5. Conclusions

This study showed that the predictive capabilities of TFA can be slightly improved by using physicochemical parameters closer to the experimental conditions and adequate equations. Most of the available concentrations referred to metabolites whose predicted concentration values did not vary among the tests. This scenario prevented from comparing concentration which did vary, thus lowering the extent of the assessment. Therefore, a study focusing on quantifying said metabolites should be considered. To that end, we also proposed a method based on centrality measures to identify important metabolites allowing to further constrain the TFA and predicting more reliable concentration values. In contrast to previous attempts, our strategy is not limited by the size of the network and is computationally cheap. Therefore, a preliminary TFA could be considered when designing a metabolomics protocol to maximise the constraining power of the experimental concentration values. Overall, our study stressed the necessity of performing an in-depth assessment of available methods in the fluxomics field. For instance, interesting published potential solutions to known problems (e.g. elucidation of the anaplerotic fluxes) should be integrated with the widely used approaches. This should increase the degree of standardisation in the community, allowing to cross-validate novel strategies and improving the reliability of the simulated data.

3. Metabolic modelling-based drug repurposing and potential drug target identification in *Trypanosoma brucei*

"All models are wrong, but some are useful."

George E. P. Box (1978)

Disclaimer: this chapter was written following a scientific article structure.

Authors: Claudio Tomi-Andrino[1,2,3], Sanu Shameer[4], Supriya Khanra[5,], Klaus Winzer[2], John King[3], Michael P. Barrett[5,6] , Fabien Jourdan[7], and Dong-Hyun Kim[1]

[1] Centre for Analytical Bioscience, Advanced Materials and Healthcare Technologies Division, School of Pharmacy, University of Nottingham, Nottingham (NG7 2RD), United Kingdom
[2] Nottingham BBSRC/EPSRC Synthetic Biology Research Centre (SBRC), School of Life Sciences, BioDiscovery Institute, University of Nottingham, Nottingham (NG7 2RD), United Kingdom
[3] Nottingham BBSRC/EPSRC Synthetic Biology Research Centre (SBRC), School of Mathematical Sciences, University of Nottingham, Nottingham (NG7 2RD), United Kingdom
[4] Department of Plant Sciences, University of Oxford, Oxford (OX1 3RB), United Kingdom
[5] Wellcome Centre for Integrative Parasitology, Institute of Infection, Immunity and Inflammation, College of Medical, Veterinary and Life Sciences, University of Glasgow, Glasgow, United Kingdom
[6] Glasgow Polyomics, Wolfson Wohl Cancer Research Centre, Garscube Campus, College of Medical Veterinary and Life Sciences, University of Glasgow, Glasgow (G12 8TA), United Kingdom
[7] Toxalim (Research Centre in Food Toxicology), Université de Toulouse, INRAE, ENVT, INP-Purpan, UPS, 31300 Toulouse, France

The GSM used in this chapter was developed and shared by Sanu Shameer (Shameer, Logan-Klumpler et al. 2015). Experimental methods were performed by Supriya Khanra. The remaining modelling explained in this chapter was done by the author of this thesis. Klaus Winzer, John King, Michael P. Barrett, Fabien Jourdan and Dong-Hyun Kim provided useful comments during the writing process.

3.1. Abstract

The scarcity of suitable treatments for neglected tropical diseases has promoted drug repurposing efforts (i.e. new uses for readily available drugs). Systems biology approaches can identify potential drug targets in pathogens, facilitating drug discovery. Metabolic networks are particularly useful, where Genome-Scale Models (GSMs) comprise all known metabolic reactions (derived from associated genes when available). Such models can be subjected to Flux Balance Analysis (FBA) to predict essential genes, serving as a proxy for inhibiting enzymes or gene knockout.

This chapter used a GSM of relatively well studied parasite, *Trypanosoma brucei*, to assess the predictive capabilities of the workflow developed here. Briefly, multiple metabolic states were simulated in FBA to predict essential genes. In addition, the topology (i.e. arrangement of the elements in the metabolic network) of the resulting metabolic states were inspected to identify double choke points – reactions exclusively producing and consuming two different metabolites. Both lists were combined and ranked according to their occurrence, where only 33/240 reactions fulfilling both criteria were identified in at least half of the metabolic states. A literature search validated the workflow's capability to pinpoint enzymes already tested, which supported the suitability of analysing those not yet explored as potential drug targets. Given the expected lack of inhibitors for the enzymes of interest, readily available inhibitors for the human homologs were selected. While none of the three molecules showed any trypanocidal activity, one of them produced a poor inhibition of trypanosome growth. Nevertheless, the workflow generated a prioritised list of potential drug targets in an efficient and timely manner, proving its suitability to facilitate drug repurposing efforts and guide drug discovery programs (e.g. highlighting proteins for further genetic/structural characterisations) in an efficient and timely manner, something of particular relevance to the neglected tropical diseases and applicable to other diseases were metabolic enzymes play a central role.

3.2. Introduction

Human African Trypanosomiasis (HAT) is a neglected disease caused by *Trypanosoma brucei* subspecies (Dickie, Giordani et al. 2020). This parasite escapes the host immune system by sequentially replacing the variant surface glycoprotein (VSG) that coats the parasite in the bloodstream form (BSF) of its life cycle (Wiedemar, Zwyer et al. 2019). VSG accounts for 10% of total cell protein and shows an average half-life of 4.6h, thus requiring almost 5 days to fully renew the coat (Pinger, Chowdhury et al. 2017, Tinti, Güther et al. 2019, Melo do Nascimento, Egler et al. 2021). This protein is a homodimer attached to the parasite by a glycosylphosphatidylinositol (GPI) anchor, making it a key element for the expression of VSG (Böhme and Cross 2002, Garrison, Khan et al. 2021).

As a neglected tropical disease, the pharmaceutical industry has struggled to justify investment in new compounds, with costs to develop new drugs estimated to exceed a $1bn per compound. Notwithstanding, one molecule, a nitroheterocycle, fexinidazole (Mesu, Kalonji et al. 2018) – originally tested against trypanosomiasis in the 1980s then revisited in the twenty first century has recently been licensed for use against HAT. A second compound, acoziborole, one of a family of benzoxaboroles with good antitrypanosomal activity (Jacobs, Nare et al. 2011) has also advanced through clinical trials and is currently being considered for licensing at the European Medicines Agency (EMA). Development of both compounds was feasible due to the emergence of new non-profit models of drug development, here through the Drugs for Neglected Diseases initiative (DNDi) (Jean-Robert and Chang 2011).

In general, drug targets should be druggable (activity susceptible to modulation) and essential for the survival of the parasite (Pereira, Sayé et al. 2020). Providing structural data for potential targets is available, using virtual screening techniques allows reducing the number of candidates to be tested for inhibitory effect. However, proteins showing a high similarity to human homologs have been suggested to be discarded early on as drug targets (Chavali, D'Auria et al. 2012, Pereira, Sayé et al. 2020). Another route to bringing drugs forward is through repurposing of drugs already licensed for other conditions where trials have been conducted (Pushpakom, Iorio et al. 2019). Since most approved drugs interact with human proteins

(Chavali, Blazier et al. 2012), using the aforementioned homology criterion may mask interesting therapeutic approaches – the impact of inhibiting a particular enzyme can be different in different systems (e.g. non-lethal in humans and toxic for the parasite) (Csermely, Korcsmáros et al. 2013). In fact, a library of FDA approved compounds was already screened against *T. brucei* 15 years ago (Mackey, Baca et al. 2006). However, the time and costs associated to this approach have promoted the implementation of metabolic modelling methods to refine the list of compounds to be tested (Bintener, Pacheco et al. 2020).

The new compounds that have successfully passed clinical trials for HAT mentioned above were discovered either by re-visiting molecules discovered in earlier focused screens of nitroheterocycles in the case of fexinidazole, or else probing a library based on the benzoxaborole scaffold that was shown to have a variety of antimicrobial representatives for acoziborole. Other main strategies put to use in seeking new trypanocides have included (i) phenotypic screening, where the lethality of a chemical library is tested in whole cell assays against the parasites and targets for potent antimicrobials subsequently deconvoluted. This approach has found new classes of proteasome inhibitor (Khare, Nagle et al. 2016) and CLK1 protein kinase (Saldivia, Fang et al. 2020) with profound trypanocidal activity. (ii) Target based drug screening where assays for specific targets can be screened for inhibitors in large libraries as achieved for N-myristoyl transferase (Frearson, Brand et al. 2010). (iii) Virtual *in silico* screening using 3D structural data on targets to identify molecules predicted to bind to the enzyme's active site (Bertelli, El-Bastawissy et al. 2001, Pushpakom, Iorio et al. 2019, Pereira, Sayé et al. 2020).

Genome-wide RNA interference screening efforts provide in vivo gene essentiality data, which can also indicate potential drug targets (Glover, Alsford et al. 2015). Recent studies suggest gene essentiality and metabolic states vary with the context (genetic makeup, developmental stage and environmental conditions), sharing a core subset (Rancati, Moffat et al. 2018, Lewin, Stacy et al. 2019). Therefore, screening and modelling efforts should consider an array of conditions so as to identify relevant potential drug targets.

Beyond these approaches, network-aided drug development can be used to prioritise candidate targets, where protein-protein interaction networks are crucial (Csermely, Korcsmáros et al. 2013). In particular, 1,595 proteins with at least one experimentally proven interaction are known for *T. brucei* TREU927 (Gazestani, Yip et al. 2017), but 30% of the genes are annotated as encoding *hypothetical proteins* (Aslett, Aurrecoechea et al. 2010). Therefore, further characterisations are needed to effectively exploit this approach (Crozier, Tinti et al. 2017). Potential drug targets can also be predicted based on kinetic modelling of metabolic networks. Specifically, this approach has been successfully applied to *T. brucei*'s glycolysis (Haanstra, van Tuijl et al. 2008), with the pentose phosphate pathway added (Kerkhoven, Achcar et al. 2013) and polyamine metabolism (Gu, Reid et al. 2013). However, the fact this strategy requires experimentally determining kinetic parameters and cannot be applied to genome-wide models limits its applicability (Orth, Thiele et al. 2010, van Eunen, Kiewiet et al. 2012).

As an alternative, less information-demanding strategies have been proposed. Genome-Scale Models (GSM) comprise all metabolic and transport reactions, plus the associated genes (GPR: gene-protein-reactions) if available. Otherwise, reactions known to take place are included even though no gene(s) have yet been identified and annotated. GSM can be subjected to Flux Balance Analysis (FBA) to predict gene or reaction essentiality as a proxy for potential drug targets (Orth, Thiele et al. 2010, Failli, Paananen et al. 2019). Even though the GSM could also by inspected by Elementary Mode Analysis to predict drug targets, associated computational costs and the network size they can handle prevents from a suitable application (Parvatham and Veerakumari 2013, Kaltdorf, Srivastava et al. 2016). Other *in silico* methods explore the network topology to identify choke points: unique reactions responsible for producing or consuming an essential metabolite (Csermely, Korcsmáros et al. 2013). However, these strategies are normally applied separately, instead of combining their strengths and reduce the number of candidates for follow-up studies.

The objective of this study was twofold: (i) to explore a curated high level GSM for *T. brucei* based on TrypanoCyc (Shameer, Logan-Klumpler et al. 2015), and (ii) to develop a workflow based on metabolic modelling able to identify potential drug targets, by focusing on a well-studied parasite to

enable testing of the predictive capabilities against experimentally proven essential genes and druggable targets. GSMs have been assembled for other pathogens including *Mycobacterium tuberculosis* (Jamshidi and Palsson 2007), *Plasmodium falciparum* (Plata, Hsiao et al. 2010, Abdel-Haleem, Hefzi et al. 2018), *Trypanosoma cruzi* (Roberts, Robichaux et al. 2009, Shiratsubaki, Fang et al. 2020) and *Leishmania* (Chavali, Whittemore et al. 2008, Chavali, Blazier et al. 2012) and successful prediction of drug targets achieved. Here we take an approach that consisted of: (i) an exploration of different metabolic states, (ii) a stringent search of potential drug targets by combining FBA and choke points identification, and (iii) a prioritisation based on the occurrence over different optimal solutions in the causative agent of HAT, *T. brucei*.

3.3. Materials and methods

3.3.1. Metabolic network and constraints

A GSM derived from TrypanoCyc was used, comprising 1,690 reactions and 3,145 metabolites (Dataset S3-1) (Shameer, Logan-Klumpler et al. 2015, Totanes, Shameer et al. 2016). Uptake reactions for extracellular metabolites not found in blood serum (v. 4.0, https://serummetabolome.ca/) (Psychogios, Hau et al. 2011) were excluded: ceramide, carboxylate, zymosterol, UDP-alpha-D-galactose, and ((2 [[2,3bis(octadecanoyloxy) propylphosphonato]oxy]ethyl)trimethylazanium). The model was handled and analysed using the COBRA toolbox (Schellenberger, Que et al. 2011) along with the solver GNU Linear Programming Kit (GLPK) in MATLAB R2017b. The full script took 45 minutes to run on a 2.50 GHz laptop (Intel® Core™ i5-7200U Processor with 8 GB of RAM).

3.3.2. Flux balance analysis and problem definition

A gene or protein is deemed 'essential' when its absence disrupts the system, provoking cell death (*in vivo*) and reducing or impeding biomass production (*in silico*) (Nazarshodeh, Marashi et al. 2021). Therefore, predicted essentiality can be used as a proxy to find potential drug targets (Failli, Paananen et al. 2019). Specifically, a reaction was deemed essential whenever setting a metabolic flux of zero provoked a reduction ≥5% in the biomass reaction flux (using a flux distribution derived from running FBA and maximising for growth). Since essentiality varies with gene expression throughout the cell cycle and is affected by the growth conditions, multiple possible metabolic states should be expected (Lueong, Merce et al. 2016, Rancati, Moffat et al. 2018). Similarly, the available connections between metabolites (i.e. network topology) determines the feasible flux distributions (Palumbo, Colosimo et al. 2007).

Large metabolic networks comprise more reactions than metabolites, and the experimentally available fluxes (if any) normally refer to just the growth rate, or specific consumption or production rates. Therefore, FBA can be used to solve such an underdetermined problem (i.e. simulating a flux distribution), upon the optimization of objective function(s) along with their weight value(s). For instance, bacterial continuous cultures are normally modelled in FBA by maximising the biomass yield (Orth, Thiele et al. 2010).

Conversely, the microbial metabolism in batch culture is shaped by competing objectives, namely the maximisation of the biomass yield, the maximisation of the ATP yield and the minimisation of the sum of fluxes (Schuetz, Zamboni et al. 2012).

BSF *T. brucei* is continuously producing VSG to escape the immune system (Pinger, Chowdhury et al. 2017, Tinti, Güther et al. 2019, Melo do Nascimento, Egler et al. 2021). Therefore, three objective functions were selected for this study: maximisation of the biomass yield, maximisation of ATP production, and maximisation of GPI production (necessary for VSG expression on the surface (Böhme and Cross 2002)). In addition, a test where the sum of fluxes was minimised was also included, based on the assumption that cells tend to reduce costs associated to enzyme production (Holzhütter 2004, Cheung, Williams et al. 2013). The allowable solution space was explored by performing a mixture experiment (Figure 3-1) (Montgomery 2001).

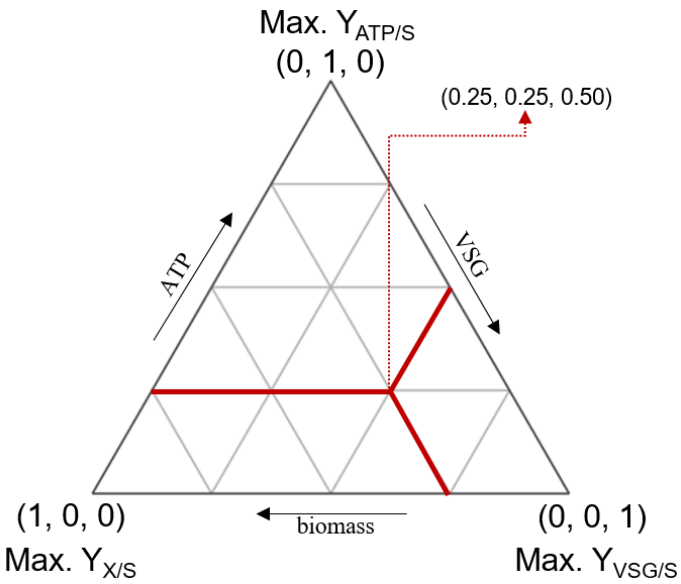


Figure 3-1. Simplex lattice design $\{3,4\}$ for objective function weight values distribution. Each outer vertex represents a case where a single objective function is selected: maximisation of the biomass yield ($Y_{X/S}$), maximisation of the ATP yield ($Y_{ATP/S}$), or maximisation of VSG yield ($Y_{VSG/S}$). For illustrative purposes the test comprising weight values (0.25, 0.25, 0.50) is shown. The 16th test (minimisation of the sum of fluxes) is not depicted here. Adapted from (Tomi-Andrino, Pandele et al. 2022).

Briefly, a $\{p, m\}$ simplex lattice design for $p = 3$ components (objective functions) and $m + 1$ ($m = 4$) equally spaced weight values (x_i) from 0 to 1 was used (Eq. 1), resulting in $N = 15$ tests (Eq. 2). In a triangle-shaped triangular lattice, each point (i.e. test) was defined by the coordinates (x_1, x_2, x_3) so that $\Sigma x_i = 1$ (Table S3-1).

$$x_i = 0, 0.25, 0.50, 0.75, 1 \quad (1)$$

$$\boldsymbol{N = \frac{(p + m - 1)!}{m!\,(p - 1)!}} \quad (2)$$

3.3.3. Identification of potential drug targets and inhibitors

Non-redundant optimal solutions derived from the FBA tests were used to generate specific models comprising only the active reactions (redefined as irreversible and imposing the predicted directionalities). These networks were explored to identify choke points – reactions exclusively responsible for producing or consuming certain essential metabolites in the network (Figure 3-2) (Csermely, Korcsmáros et al. 2013). To that end, single choke points (producing and consuming) are identified. This was done by characterising each metabolite according to how many reactions were participating in their production/consumption. Since models were redefined as explained above, updated stoichiometric coefficients informed about predicted directionalities. Finally, both lists were combined to highlight double choke points (Figure 3-2).

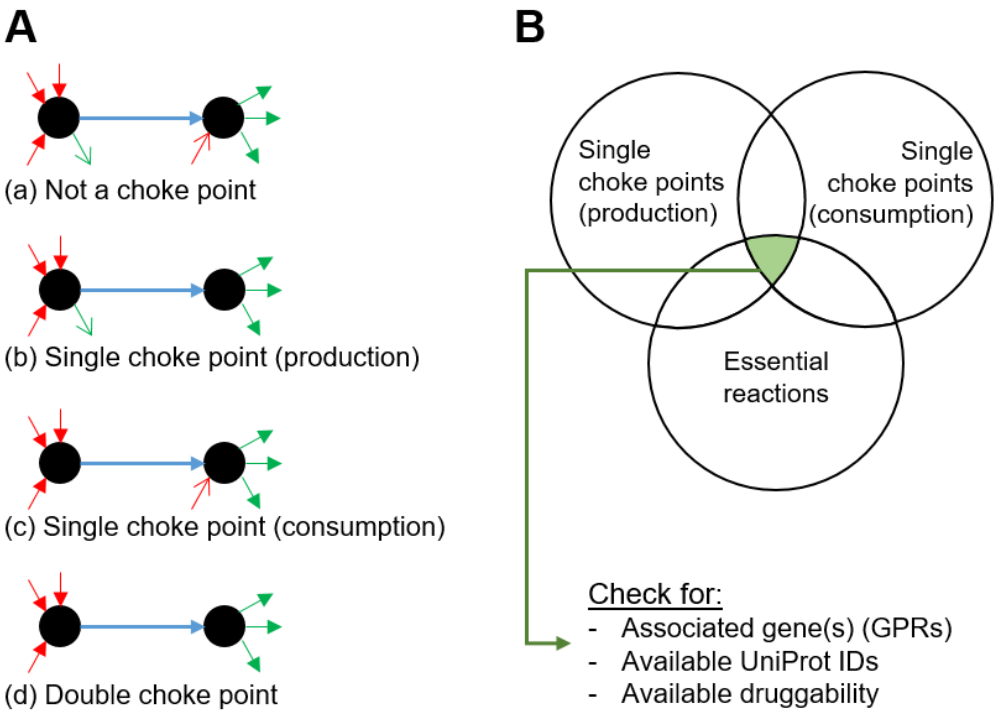


Figure 3-2. Strategies to identify reactions of interest. A: choke point reactions, where the dots refer to metabolites and the arrows to reactions. Middle blue arrow: reaction connecting both metabolites; red (inward): reactions producing a metabolite; green (outward): reactions consuming a metabolite. Case (a) is not a choke point since the blue reaction is not exclusively producing or consuming any of the two metabolites, (b) is a single choke point on the production side, as the second metabolite is produced just by the blue reaction, (c) is a single choke point on the consumption side, since the first metabolite is only consumed by one reaction, and (d) is a combination of (b) and (c). B: reactions of interest were double choke points and essential reactions at the same time. GPR: gene-protein-reactions, as defined in the GSM (Dataset S3-1).

In addition, transcriptomics data from TriTrypDB (release 46, 6/11/2019) was used to select reactions catalysed by enzymes depending on expressed genes in both life-cycle stages (Dataset S3-2) (Aslett, Aurrecoechea et al. 2010, Siegel, Hekstra et al. 2010). An enrichment analysis using STRING (v. 11.0) was performed to determine whether any pathways were over-represented in the analysis (Fig. S3-1) (Szklarczyk, Gable et al. 2019). It is important to note that the model included reactions presumed to take place, but without gene-protein-reactions associations (≈ 46%) (Dataset S3-1). Since 30% of this parasite's genes are annotated as *hypothetical protein* (Aslett, Aurrecoechea et al. 2010), further

characterisations are needed to effectively exploit this approach (Crozier, Tinti et al. 2017). Therefore, the prioritisation done here would guide further genetic characterisations.

Reactions of interest (Figure 3-2) over the non-redundant optimal solutions were grouped and ranked by their occurrence, selecting those appearing in at least half of the solutions. Potential drug targets were checked for associated genes, UniProt IDs (Aslett, Aurrecoechea et al. 2010, The UniProt Consortium 2019), druggability data (TDR Targets 6) (Landaburu, Berenstein et al. 2020), and any reported drugs or enzyme inhibitors described in the literature or DrugBank (v. 5.1.6, 2020-04-22) (Wishart, Feunang et al. 2018) that hit potential targets listed. Transport reactions were discarded due to targeting difficulties (The International Transporter Consortium 2010).

3.3.4. Drug sensitivity testing

After reviewing available drugs for native or homolog proteins, a readily available antiviral drug was selected to assess its trypanocidal activity: lamivudine (Sigma-Aldrich), using a highly potent trypanocide as control (diminazene aceturate, Sigma-Aldrich) (Dickie, Giordani et al. 2020). The IC_{50} values (drug concentration provoking a 50% growth reduction) were calculated following the alamarBlue assay, as described elsewhere (Creek, Nijagal et al. 2013). Briefly, bloodstream *T. brucei brucei* (Lister 427) were cultured in HMI-9 medium (Gibco) supplemented with 10% fetal bovine serum (Gibco) at 37 °C and 5% CO_2 (Khalaf, Huggan et al. 2014). Cells were seeded to a concentration of 2×10^4 cells ml^{-1} in 96-well microtiter plates, containing two-fold serial dilutions of each compound in triplicate. After 48 h of incubation, 20 µl of a 0.49 mM resazurin (Sigma-Aldrich) solution was added, and the cultures were incubated for another 24 h. Finally, fluorescence was measured at λexcitation = 530 nm and λemission = 590 nm with FLUOstar Optima Microplate Fluorometer (BMG LABTECH GmbH), and IC_{50} values were determined by nonlinear regression from the sigmoidal dose-inhibition curve in GraphPad Prism.

3.4. Results and discussion

3.4.1. Allowable solution space, reaction essentiality and choke points

FBA has traditionally been used in a metabolic engineering context, where cells are expected to continuously reproduce – so the "biomass reaction" is selected as the objective function. This rationale was extended to metabolic modelling-based approaches to identify potential drug targets, where the pathogen is assumed to use all its resources to maximize growth (Feist and Palsson 2010, Merigueti, Carneiro et al. 2019, Nazarshodeh, Marashi et al. 2021). Nevertheless, this straightforward analysis may fall short when simulating an infection. For example, *T. brucei* is known to also perform other biological activities, such as the renewal of the VSG coat (Wiedemar, Zwyer et al. 2019). While this scenario could be defined as a multi-objective linear problem where cells are specialized in each metabolic state (Budinich, Bourdon et al. 2017), it was reformulated as a single objective problem (solvable by FBA) and multiple tests were considered instead (Orth, Thiele et al. 2010).

To that end, multiple objective functions were selected by distributing weight values among them (weighted global criterion method), thus modelling several metabolic states. The allowable solution space of a GSM for *T. brucei* (Marler and Arora 2004, Shameer, Logan-Klumpler et al. 2015) was explored by means of running multiple FBA. Specifically, 16 tests were derived from a simplex lattice design $\{3,4\}$, where three main objective functions were considered: maximisation of the biomass yield ($Y_{X/S}$), maximisation of the ATP yield ($Y_{ATP/S}$), or maximisation of VSG yield ($Y_{VSG/S}$) (Table S3-1). Results converged into 13 non-redundant solutions (Table S3-2), which were subjected to reaction essentiality and choke point identification steps. Reactions were deemed of interest when they were: (i) essential, (ii) a choke point, and (iii) expressed in the bloodstream form (Aslett, Aurrecoechea et al. 2010, Siegel, Hekstra et al. 2010). Since 30% of this parasite's genes are annotated as *hypothetical protein* (Aslett, Aurrecoechea et al. 2010), reactions without gene associations were also selected, allowing to prioritise for further genetic characterisations.

Most published network-based approaches for drug target identification are based on either gene essentiality (via FBA) or choke point

identification (Csermely, Korcsmáros et al. 2013). Specifically, FBA generally focuses on a single objective function (Klobucar and Brown 2018) (the biomass reaction), as performed for the malaria-causing parasite (*P. falciparum*) (Fatumo, Plaimas et al. 2009, Plata, Hsiao et al. 2010), and for Chagas disease (*T. cruzi*) (Shiratsubaki, Fang et al. 2020). In contrast, here our workflow used (i) 13 optimal solutions for a wider coverage of metabolic states, and (ii) reaction essentiality, highlighting potentially relevant reactions for further characterisation.

Regarding choke point identification, current algorithms consider the whole GSM and both directions for reversible reactions, which generates long lists and hinders further prioritisation steps (Tyagi, Elfawal et al. 2019). Conversely, this study focused on using multiple solutions to reduce the stoichiometric matrices and identify fewer candidates. Ignoring inactive reactions (according to FBA) would remove alternative pathways, potentially creating choke points that would not be identified as such if considering the reversible reactions and the whole GSM. In addition, applying the essentiality criterion (proving it was not possible to compensate for their inhibition) allowed selecting relevant reactions for follow-up analyses.

3.4.2. Prioritisation of potential drug targets

The 240 reactions of interest (expressed in the BSF) over the non-redundant optimal solutions were grouped and ranked by their occurrence, where 33 appeared in at least 7 out of the 13 solutions (cut-off) (Table S3-3). Interestingly, two thirds of them have been studied as drug targets and/or tested, as explained below. The enrichment analysis identified pathways related to central carbon metabolism, lipid metabolism, and amino acid biosynthesis (Fig. S3-1). Firstly, inhibiting glycolytic reactions as a therapeutic approach is a well-explored strategy (Verlinde, Hannaert et al. 2001): enolase (Avilán, Gualdrón-López et al. 2011), phosphoglycerate mutase (Fuad, Fothergill-Gilmore et al. 2011) and phosphoglycerate kinase (Bressi, Choe et al. 2000) were identified (Table S3-3).

Secondly, lipidomics has been proposed as a route to find novel drug targets in this parasite (Guan and Mäser 2017). Regarding fatty acid metabolism, four fatty acyl CoA synthetases have been identified in this parasite (Jiang, Ingersoll et al. 2000), out of which two have been proposed

as potential drug targets and targeted by orlistat derivatives (an antiobesity drug) (Yang, Wang et al. 2012). The long-chain-fatty-acid-CoA ligase 5 (EC 6.2.1.3) plays an important role in fatty acid degradation during starvation in the procyclic stage (Allmann, Mazet et al. 2014), whereas *T. brucei*'s putative long-chain-fatty-acid-CoA ligase (Tb927.11.4490) has an ortholog in *Leishmania donovani* which has been proposed as a candidate drug target (Kaur, Tiwari et al. 2011).

Other interesting proteins participate in glycerolipid metabolism: the phospholipid:diacylglycerol acyltransferase-like protein (Tb927.11.13220) catalyses an acyl-CoA-independent triacylglycerol production that is not found in humans but has been characterised in plants and yeast (Dahlqvist, Ståhl et al. 2000). Even though alkyl-dihydroxyacetone phosphate synthase was identified as a pivotal enzyme in ether phospholipid biosynthesis more than two decades ago (Zomer, Opperdoes et al. 1995), no studies delving into its relevance as a potential drug could be found (Barros-Alvarez, Gualdrón-López et al. 2014).

More importantly, several enzymes participating in the Kennedy pathway (known to be essential (Farine, Niemann et al. 2015)) were selected (Figure 3-3). Choline kinase (Tb927.11.2090) and choline/ethanolamine kinase (Tb927.5.1140) are related to membrane formation and have been studied for bacterial infections, but no inhibitors are available (Zimmerman, Lacal et al. 2019). The two branches of the Kennedy pathway lead to the formation of phosphatidylethanolamine and phosphatidylcholine, and the ethanolamine branch was proposed to be essential to BSF *T. brucei* (Gibellini, Hunter et al. 2009). While both cholinephosphate cytidylyltransferase A (Tb927.10.12810) and ethanolamine phosphotransferase (EPT) (Tb927.10.13290) could be potential drug targets, no drugs have yet been developed.

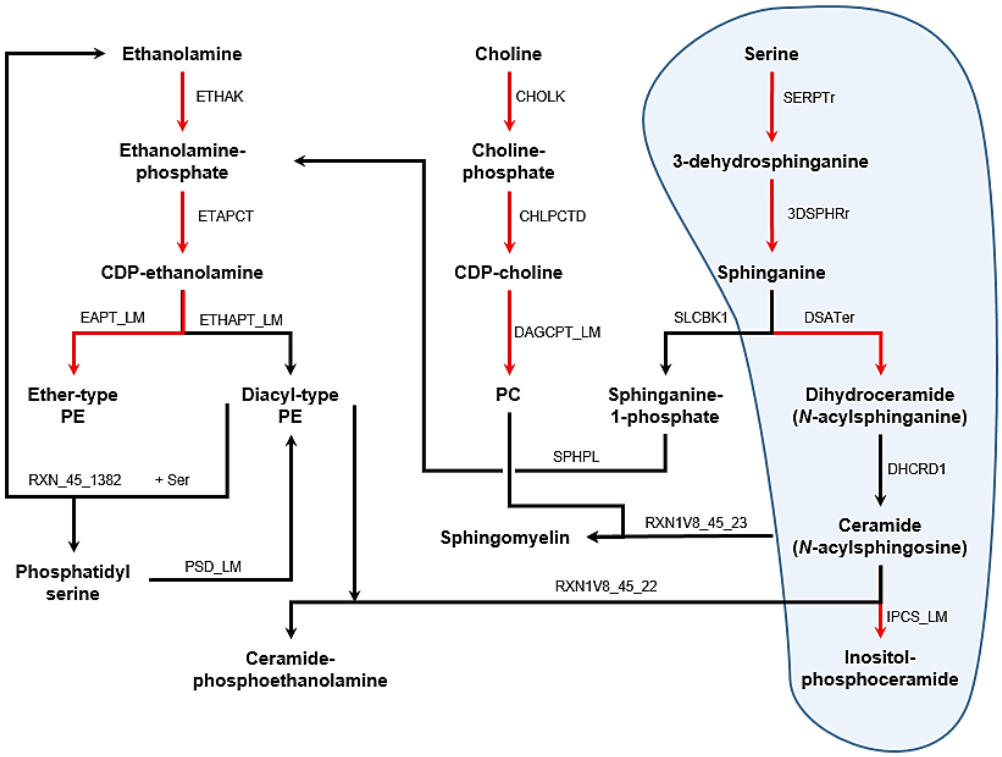


Figure 3-3. Kennedy pathway and sphingolipid metabolism, taking place in the cytosol and the smooth endoplasmic reticulum lumen (blue shade) as defined in the GSM (Dataset S3-1). Red arrows indicate reactions that fulfil the dual criteria of double choke point and essential reaction, appearing in at least half of the tests (7/13) (Table S3-3). From top left to bottom right: R_ETHAK, Tb927.11.2090, choline kinase (*EK1*); R_ETAPCT, Tb927.11.14140, ethanolamine-phosphate cytidylyltransferase (*ECT*); R_EAPT_LM, Tb927.10.13290, ethanolamine phosphotransferase (*EPT*); R_ETHAPT_LM, Tb927.10.8900, choline/ethanolamine phosphotransferase (*CEPT*); R_RXN__45__1382, Tb927.7.3760, phosphatidylserine synthase, putative; R_PSD_LM, Tb927.9.10080, phosphatidylserine decarboxylase, putative (*PSD*); R_CHOLK, Tb927.5.1140, choline/ethanolamine kinase (*C/EK1*); R_CHLPCTD, Tb927.10.12810, cholinephosphate cytidylyltransferase A, putative; R_DAGCPT_LM, Tb927.10.8900, choline/ethanolamine phosphotransferase (*CEPT*); R_SERPTr, Tb927.10.4050, serine palmitoyltransferase, putative; R_3DSPHRr, Tb927.10.4040, 3-keto-dihydrosphingosine reductase; R_SLCBK1, Tb927.7.1240, Sphingosine kinase; R_DSATer, Tb927.4.4740, Sphingosine N-acyltransferase, putative (*DHCS*); R_SPHPL, Tb927.6.3630, sphingosine 1-phosphate lyase, putative (*SPL*); R_DHCRD1, Tb927.6.3000, sphingolipid delta 4 desaturase, putative; R_RXN1V8__45__23, Tb927.9.9400, ceramide phosphorylethanolamine synthase; R_RXN1V8__45__22, Tb927.9.9390, sphingomyelin/ceramide phosphorylethanolamine synthase, bifunctional (*SLS3*);

R_IPCS_LM, Tb927.9.9390, sphingomyelin/ceramide phosphorylethanolamine synthase, bifunctional (*SLS3*).

Sphingolipid metabolism was also particularly targeted in the literature: (phyto)sphingosine kinase, sphingosine N-acyltransferase (Tb927.4.4740), phosphatidic acid phosphatase (Tb927.10.13930), 3 ketodihydrosphingosine reductase (Tb927.10.4040), sphingomyelin/ceramide phosphorylethanolamine synthase (Tb927.9.9390), and serine palmitoyltransferase (Tb927.10.4050). Inhibiting (phyto)sphingosine kinase by means of dimethyl sphingosine proved to be toxic for BSF cells (Pasternack, Sharma et al. 2015). Conversely, the other steps are yet to be deeply studied as drug targets and no drugs have been found: phosphatidic acid phosphatase (Pasternack, Sharma et al. 2015), 3-ketodihydrosphingosine reductase (Sutterwala, Creswell et al. 2007), sphingomyelin/ceramide phosphorylethanolamine synthase, and serine palmitoyltransferase (Mina and Denny 2018).

Finally, polyamine biosynthesis and the closely related dependent disulphide-reducing system (crucial to maintaining redox balance and to producing DNA precursors (Lu, Vodnala et al. 2013)) have been widely analysed (Figure 3-4). The reducing power (NADPH) is supplied by the oxidative section of the pentose phosphate pathway (PPP) in the cytosol (Kovářová and Barrett 2016). Kinetic modelling of the glycolysis and the PPP in the bloodstream form showed the potential of building metabolic models, albeit limited by the scarcity of kinetic parameters (Kerkhoven, Achcar et al. 2013).

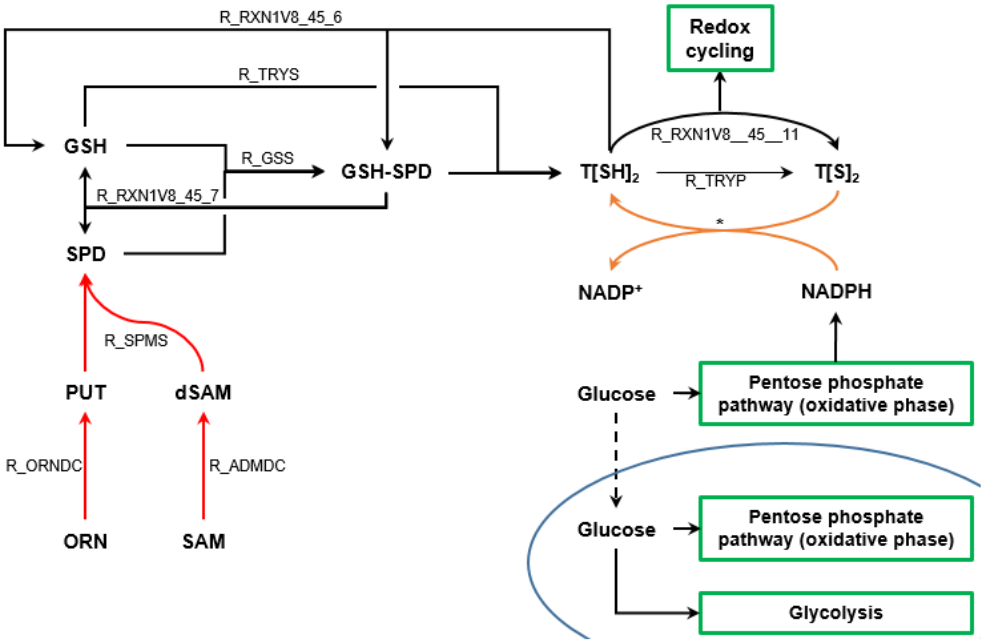


Figure 3-4. Partial polyamine biosynthesis and NADPH-dependent disulfide-reducing system, taking place in the cytosol as defined in the GSM (Dataset S3-1). Red arrows indicate reactions that fulfil the dual criteria of double choke point and essential reaction, appearing in at least half of the tests (7/13) (Table S3-3). The orange arrow (*) refers to trypanothione reductase (Tb927.10.10390):R_1__46__8__46__1__46__12__45__RXN (Dataset S3-1). This reaction fulfilled the dual criteria, but its occurrence was below the aforementioned cut-off (5/13). The blue oval represents the glycosome, and the dashed arrow the transport of glucose from the cytosol. From bottom left to top right: Orn, ornithine; PUT, putrescine; SAM, S-adenosylmethionine; dSAM, decarboxylated S-adenosylmethionine; SPD, spermidine; GSH, glutathione; GSH-SPD, glutathionylspermidine; $T[SH]_2$, reduced trypanothione; $T[S]_2$, oxidised trypanothione; $NADP^+$, nicotinamide adenine dinucleotide phosphate; NADPH, reduced nicotinamide adenine dinucleotide phosphate. Diagram modified from (Fairlamb and Cerami 1992, Kerkhoven, Achcar et al. 2013).

The pipeline failed to identify two of the most studied potential drug targets in this parasite: trypanothione synthetase (R_TRYS, Tb927.8.2410) and trypanothione reductase (Tb927.10.10390). Trypanothione synthetase is an interesting drug target as it is has been validated as essential (Spinks, Torrie et al. 2012), it is absent in the host and it is one of the main controlling steps in kinetic models, where a 63% inhibition would be necessary to halve the reduced trypanothione ($T[SH]_2$) synthesis flux.

Conversely, trypanothione reductase would need to be almost totally inhibited to reach the same effect (Olin-Sandoval, González-Chávez et al. 2012). In addition, reducing its activity *in vivo* stopped its growth and made cells avirulent (Krieger, Schwarz et al. 2000). Efficient and safe drugs for both of these targets are yet to be developed (Benítez, Medeiros et al. 2016, Mendonça, Coelho et al. 2018). While R_TRYS was an essential reaction, it did not (i) consume glutathione (GSH) in exclusivity, as glutathionylspermidine synthase (R_GSS, Tb11.12.0016) also participated, and (ii) produce $T[SH]_2$ in exclusivity: trypanothione reductase (R_TRYS, Tb927.8.2410) was involved too. Therefore, it did not fulfil the dual criteria and was not selected by the workflow. Interestingly, RNA interference tests for trypanothione synthetase showed growth arrest and loss viability, whereas knockingdown glutathionylspermidine synthase did not provoke a reduction in growth (Alsford, Turner et al. 2011). On the contrary, the reaction catalysed by trypanothione reductase did qualify as reaction of interest for certain optimal solutions, but its occurrence (5/13) was below the chosen cut-off. Similarly to trypanothione synthetase, trypanothione reductase interference experiments severely affected the parasite's growth and viability (Alsford, Turner et al. 2011). Finally, the reaction catalysed by tryparedoxin (R_TRYP, Tb927.3.3780) fulfilled the dual criteria with a low occurrence (4/13). Interestingly, previous kinetic modelling in *T. cruzi* supported its suitability as drug target (González-Chávez, Olin-Sandoval et al. 2015).

On the other hand, known drug targets in the polyamine pathway were correctly identified including: S-adenosylmethionine decarboxylase (R_ADMDC, Tb927.6.4410), a control point in the pathway (Willert and Phillips 2008); spermidine synthase (R_SPMS, Tb927.9.7770), an experimentally validated target (Xiao, McCloskey et al. 2009), and glutathione synthetase (Tb927.7.4000), whose absence provokes a reduction on growth (Alsford, Turner et al. 2011). In addition, the workflow successfully identified ornithine decarboxylase (R_ORNDC, Tb927.11.13730), which is targeted by eflornithine (Bacchi, Nathan et al. 1980), a first line treatment for HAT (Dickie, Giordani et al. 2020). Related to the glycine cleavage complex in this parasite, dihydrolipoyl dehydrogenase's homolog in *T. cruzi* has been appointed as a potential drug target due to its role in redox metabolism (dos Santos, Moreira et al. 2016).

Overall, the pipeline identified multiple well-studied drug targets, validating the potential of the other candidates. Therefore, reactions whose human counterpart are not choke points and parasitic proteins without homologs should be considered for further genetic and/or structural characterisation (Table S3-3).

3.4.3. Selection of inhibitors for human proteins and sensitivity testing

Given the fact most approved drugs target human proteins (Chavali, Blazier et al. 2012) and metabolic networks differ between the host and the parasite (Csermely, Korcsmáros et al. 2013), readily known inhibitors were selected. Prioritised reactions of interest (i.e. 33/240) were considered for homology analysis using PSI-BLAST (Schäffer, Aravind et al. 2001). Two searches were performed: (i) to identify human homologs for which inhibitors are available, and (ii) to identify native proteins which have been structurally characterised and should be considered for further virtual screening efforts.

Two human homologs with drugs entries in Drugbank were found: thymidylate synthase and phosphoglycerate kinase I (Table 3-1). While bifunctional dihydrofolate reductase thymidylate synthase (DHFR-TS, Tb927.7.5480) has been proposed as a drug target and *in vitro* enzyme inhibition with various well known antifolates was possible (Gibson, Dewar et al. 2016), the ability to kill trypanosomes with these inhibitors was dependent upon the abundance of thymidine or folate in medium (Creek, Nijagal et al. 2013), as these metabolite enable bypass of inhibition of the enzymes.

Phosphoglycerate kinase is part of glycolysis and has been studied as a potential drug target (Bressi, Choe et al. 2000). Three drugs targeting it can be highlighted, namely artenimol (dihydroartemisinin), acyclovir and lamivudine. As trypanosomes and Plasmodium are both blood dwelling protozoa, artemisinin, which is a major first line drug against malaria, was previously tested in *T. brucei* but showed no activity (Mishina, Krishna et al. 2007). This might not be surprising given biochemical differences between the two parasites including lack of haemoglobin digestion in trypanosomes, as this process is involved in activating artemisinins. Conversely, both

acyclovir and lamivudine are antiviral drugs. While acyclovir had no effects (Bouteille, Darde et al. 1988), no studies using lamivudine were found, so it was selected for this study.

Table 3-1. Protein homologs in *H. sapiens*. Homologs were identified by PSI-BLAST (database: nr, organism: human (taxid: 9606)), selecting top hits with E-value ≤ 0.005 and % identity $\geq 40\%$. UniProt IDs are included in brackets.

Protein in *T. brucei*	Homolog in *H. sapiens*	Inhibitors
Dihydrofolate reductase-thymidylate synthase (Q582G3)	Thymidylate Synthase (P04818)	Several (Gibson, Dewar et al. 2016)
Phosphoglycerate kinase (Q4GZG3)	Phosphoglycerate Kinase 1 (P00558)	Artenimol (dihydroartemisinin) (Mishina, Krishna et al. 2007) Acyclovir (Bouteille, Darde et al. 1988) Lamivudine

The drug sensitivity test for lamivudine yielded an IC_{50} value of 155.4 ± 2.3 µM. so it is a relatively poor inhibitor of trypanosome growth (diminazene used as a control yields an $IC_{50} = 0.087 \pm 0.004$ µM (Fig. S3-2)). This may relate to a number of issues, however, including limited ability to enter the parasites, different metabolic processing within the cells or differences inactive site of target enzymes or else differential impact on the metabolic network.

3.5. Conclusions and Future work

This study developed a workflow where modelling approaches (FBA and double choke point identification) have been combined and extended to identify potential drug targets in a timely manner, using a GSM of *T. brucei* to confirm and validate its predictive capabilities. Specifically, 240 reactions fulfilled both criteria (double choke point reactions related to a predicted essential gene), out of which 33 were identified in at least half (7/13) of the chosen metabolic states upon considering the bloodstream form of this parasite. A literature search pinpointed 12 reactions not yet explored as drug target for treating trypanosomiasis. Performing a homology analysis yielded two human protein counterparts, for which multiple inhibitors were found. Lamivudine, an antiviral drug for which no studies assessing its trypanocidal activity were found, was selected for sensitivity testing. While this drug had no lethal effect, the pipeline's capability to predict potential drug targets was validated by the identification of previously considered enzymes derived from traditional drug discovery procedures. Specifically, a prioritised list of several reactions and enzymes have been appointed for follow up genetic, structural and virtual screening analyses to widening the therapeutic approaches for HAT. Similarly, it could be applied to guide drug discovery efforts for less studied pathogens. In order to analyse other diseases such as cancer, different aspects should be considered. Exploring two large metabolic networks (healthy v cancerous) would require using transcriptomics data to contextualise the generic human metabolic network, creating two distinct solution spaces. Additionally, the rich variety of datasets would allow the integration of other omics in the workflow, further reducing the list of candidates to be tested and accelerating the drug discovery process.

4. Metabolic modelling-based drug repurposing in Glioblastoma

"As for the presence of large NGF [nerve growth factor] *sources in snake venom and male genital organs, they may be conceived as instances of bizarre evolutionary gene expression."*

Rita Levi-Montalcini,
Nobel Lecture in Physiology or Medicine (1986)

Disclaimer: this chapter is a modified version of a Publication in Scientific Reports from July 2022 (Tomi-Andrino, Pandele et al. 2022).

Authors: Claudio Tomi-Andrino [a, b, c], Alina Pandele [d], Klaus Winzer [b], John King [c], Ruman Rahman [d], Dong-Hyun Kim [a,*].

[a] Centre for Analytical Bioscience, Advanced Materials and Healthcare Technologies Division, School of Pharmacy, University of Nottingham, Nottingham, NG7 2RD, UK

[b] Nottingham BBSRC/EPSRC Synthetic Biology Research Centre (SBRC), School of Life Sciences, BioDiscovery Institute, University of Nottingham, Nottingham, NG7 2RD, UK

[c] Nottingham BBSRC/EPSRC Synthetic Biology Research Centre (SBRC), School of Mathematical Sciences, University of Nottingham, Nottingham, NG7 2RD, UK

[d] Children's Brain Tumour Research Centre, Biodiscovery Institute, School of Medicine, University of Nottingham, Nottingham, NG7 2RD, UK

All the metabolic modelling was done by CTA. AP did all the experimental work. RR contributed to refining the final list of chemicals to be tested. KW, JK, RR and DHK provided useful comments during the writing process.

4.1. Abstract

The manifestation of intra- and inter-tumour heterogeneity hinders the development of 'one size fits all' cancer treatments, thus requiring a tailored therapy for each cancer type. For the malignant brain tumour, glioblastoma (GBM), genetic and genomic abnormalities originate a series of hallmarks and properties that enable the proliferation and dissemination of cancer cells. Specifically, the reprogramming of cellular metabolism has been identified as a source of potential drug targets.

Drug discovery is a long and resource demanding process aiming at identifying and testing compounds early in the drug development pipeline. While drug repurposing efforts (i.e., focusing on readily available approved drugs) can be supported by a mechanistic rationale, strategies to further reduce and prioritise the list of potential candidates are still needed to facilitate feasible studies. Although –omics data is widely gathered in cancer studies, exploiting context-dependent information (such as transcriptomics), to guide the identification of potential drug targets limits its suitability to that end. Nevertheless, combining it with modelling approaches could help reducing the number of candidates to be further analysed and tested *in vitro*.

Flux Balance Analysis (FBA) is a metabolic modelling technique that mainly relies on the stoichiometry of the metabolic network. However, inspecting the network's topology typically neglects biologically relevant information. In this chapter, the approach introduced in Chapter 3 was modified to develop *Transcriptomics-Informed Stoichiometric Modelling And Network analysis* (TISMAN). Briefly, this method exploits transcriptomics data to generate GBM-like metabolic models from a generic human GSM and to identify upregulated genes in cancerous tissue (compared to a healthy counterpart). Inspecting the networks' topologies and simulating an array of metabolic states by FBAs yielded a prioritised list of c. 170 genes of interest, which agreed with published experimental and modelling results. Exploring multiple chemical-gene interaction databases and searching for yet to be tested compounds for GBM in the literature reduced the number of molecules to be tested *in vitro* to five: afuresertib, isorhamnetin, formononetin, pyrogallol and taxifolin. Specifically, 2/5 tested compounds as impaired metabolic viability, and 3/5 reduced invasion. These results validate the suitability of the *in silico* workflow to expedite compound prioritisation at a

drug discovery phase, thus facilitating drug repurposing programs. In addition, identified genes lacking targeting molecules should be considered in structural studies to develop novel compounds.

4.2. Introduction

Cancer is the first or second cause of premature death in 70% of countries (World Health Organization 2020). Tumours are characterised by multiple biological capabilities conferring cellular proliferation and metastasis (dissemination to other tissues and colonisation), where metabolic reprogramming is crucial to fulfil biosynthetic requirements underlying these phenotypes (Hanahan and Weinberg 2011). The disparity of oxygen and nutrient availability within the surrounding tumour microenvironment promotes different metabolic states amongst cells, which show a continuum in gene expression within sub-clonal populations (Hausser and Alon 2020). Consequently, metabolic dependencies and vulnerabilities are shaped by the cell lineage and the environment, rather than being universal (Chen, Cai et al. 2019).

Isocitrate dehydrogenase-1 wild-type Glioblastoma (GBM) is the most aggressive brain tumour in adults (Jemal, Siegel et al. 2010), characterised by a high degree of invasiveness through brain parenchyma (Petrecca, Guiot et al. 2013). Different subtypes and transcriptional subpopulations may co-exist within the same tumour, where a quiescent subpopulation of glioblastoma stem cells (GSC) can facilitate the development of radio- or chemo-resistance, leading to inevitable disease relapse (Chen, Li et al. 2012, Neftel, Laffy et al. 2019, Richards, Whitley et al. 2021). Therefore, novel therapeutic approaches should aim to target all cell lineages (Couturier, Ayyadhury et al. 2020), block GSC differentiation (Castellan, Guarnieri et al. 2021), or combine both strategies (Richards, Whitley et al. 2021). In particular, recent studies have shown the suitability of chemicals disrupting energy metabolism in GBM (Polson, Kuchler et al. 2018) or blocking de novo pyrimidine synthesis in GSC (Wang, Yang et al. 2019). Conversely, the application of immunotherapy and many drug compounds is hindered by the impermeability of the blood-brain-barrier (McCrorie, Vasey et al. 2020). Phenotypic screening of compound libraries can help identify putative drug candidates, albeit being a costly process and requiring further target deconvolution steps (Moffat, Vincent et al. 2017).

Although gene essentiality is used as a proxy for potential drug targeting, its context-dependent and evolvable nature hinders its usage: (i)

genetic ablation affects both the catalytic activity (which may not be essential) and any other function (e.g. essential structural); (ii) incomplete knockdown or off-target effects; (iii) genetic divergence of cell lines from the original tumour; (iv) metabolic response of cells to non-physiological growth conditions (Faubert, Li et al. 2017, Nilsson, Haanstra et al. 2018, Rancati, Moffat et al. 2018, Lin and Sheltzer 2020).

Whilst simulating ligand-target interactions (molecular docking) provides a shortlist of compounds to be tested, the scarcity of structural data limits its application (Adasme, Parisi et al. 2020). In addition, this approach prevents the identification of compounds indirectly affecting metabolism, for example by altering the expression levels of multiple genes (Bushweller 2019). Therefore, information-rich computational strategies to generate manageable lists of drug candidates should be considered as a viable complement to the drug discovery phase.

The set of metabolic fluxes (i.e., reaction rates) can be either estimated via ^{13}C metabolic flux analysis (^{13}C-MFA) for the central carbon metabolism or modelled by applying flux balance analysis (FBA) to a genome-scale model (GSM). A GSM consists of a stoichiometric matrix connecting metabolites (substrates and products) with reactions, where the latter are associated with genes following the gene-protein-reaction formalism (Schellenberger, Que et al. 2011). FBA predicts a flux distribution upon the optimization for a biological task (normally the biomass formation), represented by a reaction in the GSM (Orth, Thiele et al. 2010). Whilst ^{13}C-MFA mainly informs about the central carbon metabolism (Ahn, Kumar et al. 2017, Chen, Cai et al. 2019), transcriptomics data can be applied to obtain cell-specific models from GSMs and can predict in silico gene essentiality (Opdam, Richelle et al. 2017, Pires Pacheco, Bintener et al. 2019, Richelle, Joshi et al. 2019). In addition, other strategies based on network analysis can allow identifications of reactions that if inhibited, would potentially disrupt metabolism (Csermely, Korcsmáros et al. 2013).

To this end, we developed *Transcriptomics-Informed Stoichiometric Modelling And Network analysis* (TISMAN), based on our previous strategy (Chapter 3) by introducing a topological feature and including more biologically-rich information aiming at developing a workflow providing a stringent search of potential drug targets and compounds to be tested for

GBM as an exemplar disease type. Briefly, published data was exploited to build condition specific GBM metabolic models, which were analysed to identify and rank the reactions of interest according to different indicative criteria. Several chemical-gene interaction databases were used to identify and prioritise approved drugs or experimental compounds either directly targeting proteins or indirectly affecting the corresponding gene expression levels. Chemicals with a proven impact against other cancer types but which have not been tested for GBM, were prioritised for experimental validation using patient-derived GBM *in vitro* models.

4.3. Materials and methods

The workflow developed in this study comprised three main parts (Figure 4-1): (i) "what to target": identification of either metabolic or transport (e.g., between cellular compartments) reactions of interest; (ii) "how to target": identification of chemicals (readily available approved drugs or experimental compounds); (iii) *in vitro* validation of the selected compounds. Briefly, transcriptomics data from GBM tumours was used to: (a) contextualise a generic human GSM, yielding two GBM-specific models; (b) identify up regulated genes.

Next, the models were subjected to FBA to identify essential reactions, and the network topology was inspected to pinpoint certain features (choke points and centrality). Overall, the workflow aimed to identify proteins that if targeted, would potentially hinder cellular metabolism, impairing tumour proliferation and/or invasion. Chemicals targeting metabolism either directly (i.e., affecting the activity) or indirectly (i.e., affecting gene expression) were ranked, with five candidates prioritised for *in vitro* testing. Files and scripts for MATLAB and R can be found in Github (https://github.com/CTA-code/TISMAN).

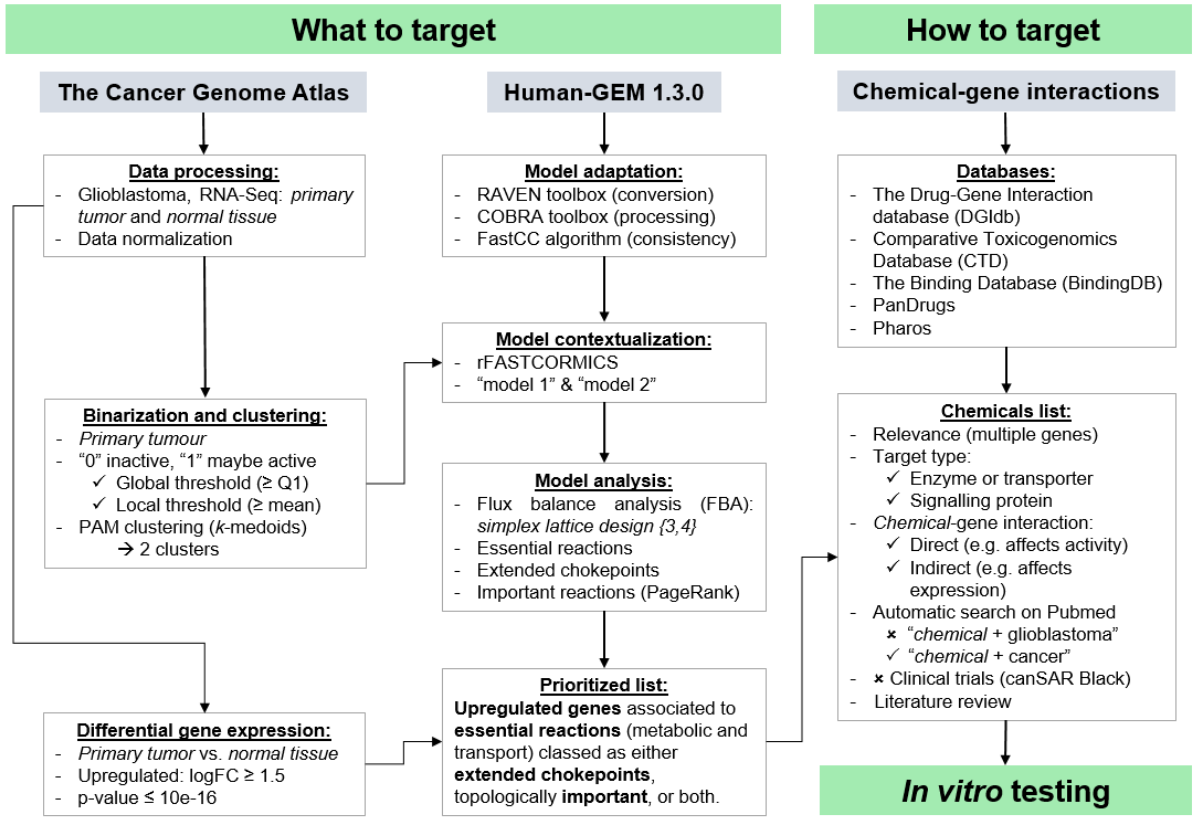


Figure 4-1. TISMAN (*Transcriptomics-Informed Stoichiometric Modelling And Network analysis*), the workflow developed in this study. It comprised three main parts (what to target, how to target and *in vitro* testing), where both MATLAB and R scripts were used.

4.3.1. What to target

Transcriptomics data analysis. Data processing: RNA-Seq data for GBM and healthy counterpart astrocytic tissue (herein referred to as 'primary tumour' and 'normal tissue') was obtained from The Cancer Genome Atlas (TCGA) database (https://portal.gdc.cancer.gov/) and processed using the R package TCGAbiolinks (Colaprico, Silva et al. 2016). This information was used for two independent steps, binarization and clustering. Expression data from primary tumour was binarized by considering two simultaneous thresholds: (i) global (≥ Q1) across all genes and samples, and (ii) local (≥ mean), which was gene-specific across samples. Genes were flagged as either maybe active ("1") or inactive ("0") if fulfilling both criteria or not, respectively, so that each sample was codified by a binary vector (Richelle, Joshi et al. 2019).

Next, R's PAM function (Partitioning Around Medoids, or k-medoids) was used to cluster the data into two groups (optimal number of clusters according to the Silhouette method), yielding a representative binary vector (or medoid) for each cluster (Schubert and Rousseeuw 2019). Both primary tumour and normal tissue data was used to determine the differential gene expression: genes with logFC ≥ 1.5 and p-value ≤ 10^{-16} were deemed upregulated in the tumour (Maié and Ticconi 2019).

Stoichiometric modelling and network analysis. Model adaptation: the latest version of a human genome-scale model (Human-GEM 1.3.0, comprising 13,417 reactions and 10,135 metabolites (Robinson, Kocabaş et al. 2020)) was converted and adapted to a COBRA toolbox paradigm by using the RAVEN toolbox (Agren, Liu et al. 2013) and the COBRA toolbox (Schellenberger, Que et al. 2011). Next, a consistent model was generated by FastCC prior to the contextualisation step, so that all reactions are active (i.e. nonzero flux) for at least one feasible flux distribution (Figure 4-2) (Vlassis, Pires Pacheco et al. 2014). Specifically, the consistent model includes 11,902 reactions and 8,458 metabolites.

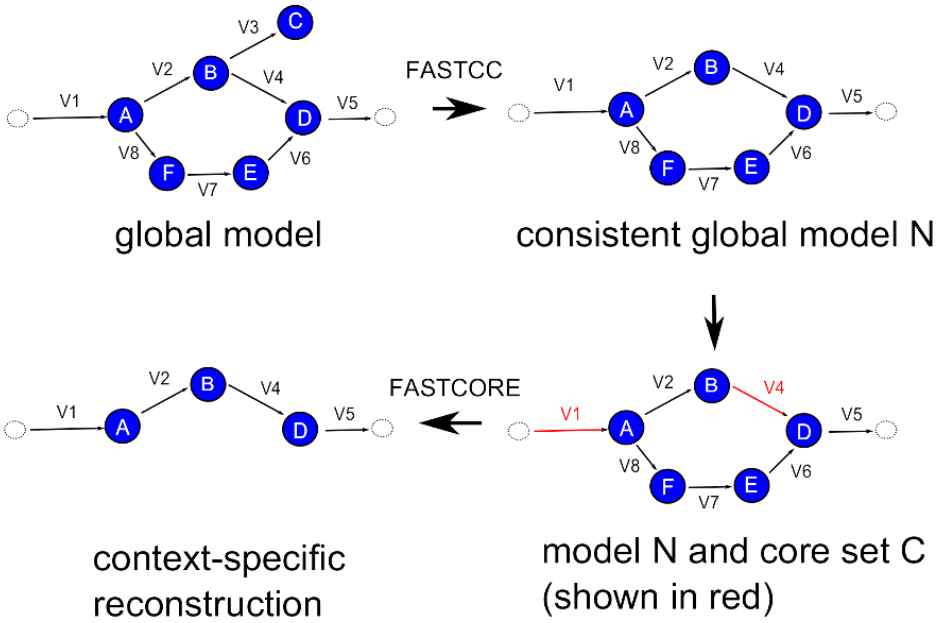


Figure 4-2. FastCC and FASTCORE algorithms. FastCC generates a consistent global model by removing reactions unable to carry nonzero flux values (due to gaps in the network). Next, the FASTCORE algorithm returns a context-specific reconstruction (subset of the global model) upon the selection of a core set of reactions as suggested by omics data, plus an additional set of reactions needed to reach consistency. Taken from (Vlassis, Pires Pacheco et al. 2014).

Model contextualisation: rFASTCORMICS (Pires Pacheco, Bintener et al. 2019), a modified version of FASTCORE (Figure 4-2), was used in this study. Briefly, the newest algorithm favours the inclusion of the core set in the context-specific reconstruction, thus providing more flexibility than FASTCORE (where the inclusion was enforced). For the GBM exemplar, the two previously generated medoids were used with rFASTCORMICS to build two cancer-specific models (COBRA toolbox v. 2, with IBM CPLEX 12.8 in MATLAB R2016b run in Windows 10 to ensure solver compatibility). Model analysis: an upper bound of 2 mmol/gDW-h was set for the oxygen uptake rate, as suggested for previous cancer models (Wagner, Venkataraman et al. 2011, Zielinski, Jamshidi et al. 2017).

A simplex lattice design for FBA was performed, where three objective functions and mixtures amongst were studied in 15 tests. This was achieved by varying the weight of the three reactions: maximisation of the biomass yield ('biomass_human'), maximisation of the ATP yield ('HMR_4358'), and maximisation of 1-phosphatidyl-1D-myo-inositol-4-phosphate production ('HMR_6552'), a lipid which induces curvature in the lipid membrane (Furse, Brooks et al. 2012). The latter reaction is catalysed by synaptojanin 2 (*SYNJ2*) a polyphosphoinositide phosphatase related to invasion in GBM (Chuang, Tran et al. 2004) and a mediator of metastasis in breast cancer (Ben-Chetrit, Chetrit et al. 2015). An extra case for the minimization of the sum of fluxes was considered, yielding 16 final tests (see Chapter 3, Materials and methods).

Since certain optimal solutions were the same, the number of non-redundant solutions for each model was calculated. Reactions of interest fulfilled several criteria: related to an upregulated gene in the tumour; essential reaction; extended choke point and/or topologically important. Considering the full GSM and the flux through the biomass reaction when maximising it in FBA, a reaction was deemed essential for a test (same network, different objective function(s)) when shutting it down (no flux through allowed) caused a $\geq 5\%$ reduction of said metabolic flux (see Chapter 3, Materials and methods).

Conversely, topological aspects were studied by exploring reduced metabolic networks. A condition-specific model was generated for each unique flux distribution produced by FBA, so that the stoichiometric matrix only comprised active elements (reactions and metabolites). Single choke points were identified as reactions associated exclusively with producing or consuming a metabolite. Double choke points were then defined as reactions associated exclusively with producing and consuming metabolites.

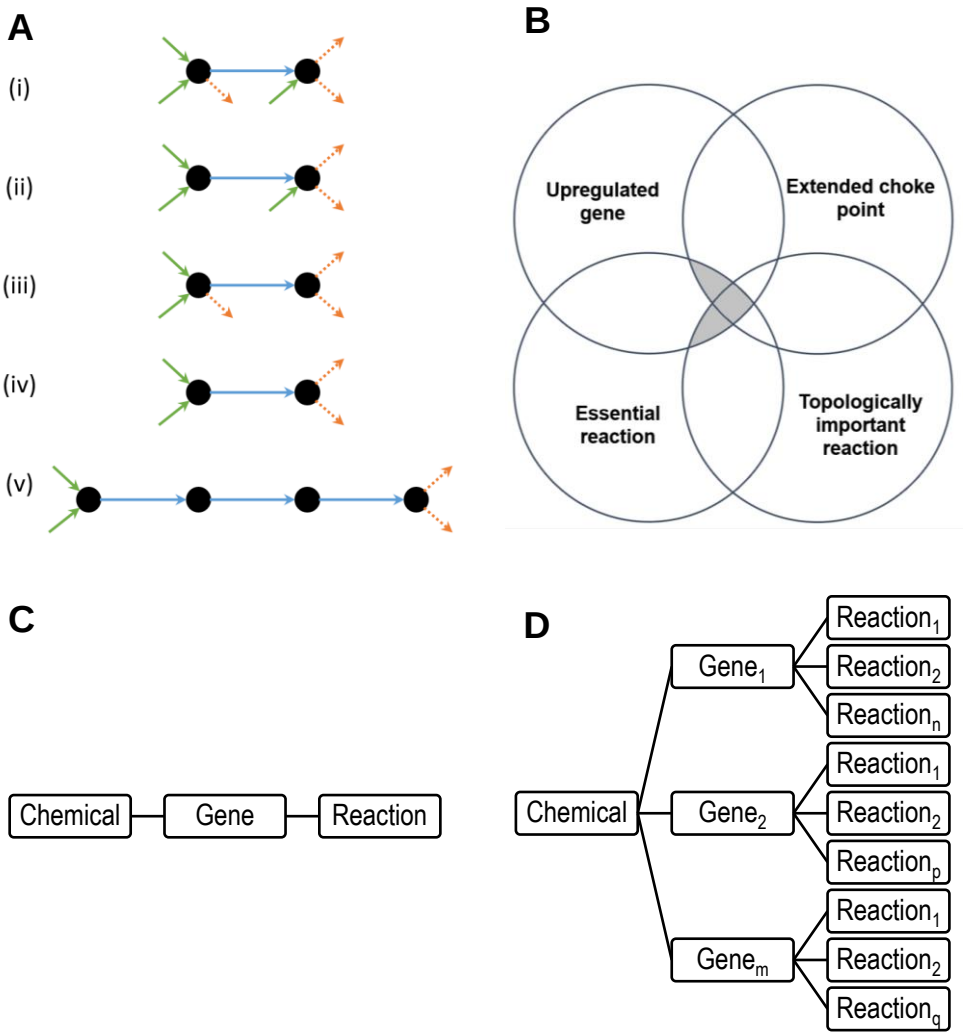


Figure 4-3. Strategies to identify gene targets for drug repurposing. (A) Examples of metabolites-reactions relationships (dots and arrows, respectively). The blue arrows represent the production of the metabolite on the right from the metabolite on the left. Inward green arrows refer to production reactions from metabolites not drawn, while outward orange dotted arrows represent consumption reactions. (i) Not a choke point, (ii) single choke point on the consumption side, (iii) single choke point on the production side, (iv) double choke point, and (v) extended choke point. (B) Venn diagram showing the subsets of reactions of interest. In all cases, reactions (metabolic or transport reactions) were essential and carried out by proteins related to upregulated genes, as well as identified as extended choke points and/or topologically important reactions. (C) Direct chemical-gene interaction, where a compound affects the activity of a single protein (e.g., an inhibitor). (D) Indirect chemical-gene interaction, where a single compound targets an element such as a signalling protein, that leads to changes in the expression levels of multiple genes, thus affecting several reactions in a pleiotropic manner.

To ensure a more stringent selection criterion, the concept of extended choke points was introduced, defined as double choke points surrounded by single choke points (consuming and producing) (Figure 4-3). Alternatively, topologically important reactions were identified by MATLAB's in-built PageRank function (Page L and Motwani R 1998). This analysis was applied to a directed graph (i.e., considering the flux direction) derived from an adjacency matrix, where the centrality of the nodes (reactions) was determined. Directly calculating the adjacency matrix from the stoichiometric matrix would yield a metabolite-centric graph (metabolites as nodes) (Tomi-Andrino, Norman et al. 2021). Therefore, an intermediate step converting the stoichiometric matrix into its conjugate transpose (reactions as nodes) was included prior to generating the adjacency matrix. Prioritised list: reactions of interest for each medoids were identified by independently selecting those identified as extended choke points in at least half of the non-redundant optimal solutions (occurrence), and those within the top 10% of central reactions according to PageRank. Finally, results from both medoids were combined by summation of occurrence or centrality scores, respectively.

4.3.2. How to target

Identification of relevant drugs and chemicals. Five databases comprising thousands of hits were used programmatically and/or manually: The Drug-Gene Interaction database (DGIdb) Nov 2020, v4.2.0 (Freshour, Kiwala et al. 2020); Comparative Toxicogenomics Database (CTD), Oct 2020 (Davis, Grondin et al. 2020); The Binding Database (BindingDB), Nov 2020 (Gilson, Liu et al. 2016); PanDrugs, version: 2018.11.7 (Piñeiro-Yáñez, Reboiro-Jato et al. 2018); and Pharos, version 3.2.0 (Sheils, Mathias et al. 2020). To exploit published chemical-gene interactions, a gene-centric list of potential candidates was generated from the reactions of interest. Since a gene may participate in several reactions, occurrence and centrality scores for each gene were normalised and separately summated. Similarly, as a chemical may target (directly or indirectly) one or several genes (Figure 4-3), drug-centric lists were created, and a final relevance score was calculated as the sum of occurrences and centrality scores. Automatic

searches on Pubmed were performed to identify which drugs have been tested for cancers (except for GBM), followed by a literature review and search for clinical trials in canSAR (Mitsopoulos, Di Micco et al. 2020) to finally select top five compounds for *in vitro* testing.

4.3.3. *In vitro* testing

Cell culture. Glioblastoma INvasive margin (GIN28, GIN31) and Glioblastoma Contrast-Enhanced core (GCE28, GCE31) cell lines have been previously derived at Queen's Medical Centre, Nottingham, authenticated using short tandem repeat genotyping (Table S1) and used at passages 21-29, 27-36, 15-23 and 28-37 respectively (Greco, Taresco et al. 2020, Vasey, Cavanagh et al. 2021). Cell lines were cultured using adherent T75 flasks (Corning) in Dulbecco's Modified Eagle Medium (Gibco) supplemented with 10% FBS (Sigma-Aldrich) and incubated under humidified growth conditions at 37°C and 5% CO_2.

Metabolic viability assay. All cell lines were seeded in 96 well plates (Costar) at $5x10^3$ cells/well and incubated for 24 h prior to treatment. Cells were treated with afuresertib (Selleckchem), isorhamnetin (Merck), formononetin (Merck), pyrogallol (Merck) and taxifolin (Merck) in a 16-point dose response (n = 6) over 72 hours, with concentrations ranging from 1µM to 500µM. Appropriate vehicle control (0.1% DMSO) and positive cell death control (10% DMSO) were used. Viability was assessed by adding 1:10 PrestoBlue (ThermoFisher) over 45 minutes and measuring resulting fluorescence at 544/590 nm (excitation/emission) on a FLUOstar Omega microplate reader (BMG LABTECH). Briefly, PrestoBlue is a resazurin-based solution – a redox-sensitive, non-toxic dye which turns red in colour due to the reducing environment of metabolically viable cells. Finally, fluorescence intensity was normalised against that of control wells to determine percent viability of drug-treated cells.

Invasion assay. The ability of the compounds to inhibit invasion was investigated for all cell lines using a Transwell collagen barrier assay: 24 well ThinCert™ 8 µm cell culture inserts (Greiner) were coated with 10 µg of mouse collagen IV (Cultrex, Trevigen) and incubated at 37°C overnight. Cells were seeded at 13,500 – 15,000 cells/insert in 0% FBS DMEM with added treatment and allowed to invade towards 10% FBS DMEM over 24 hours at

37°C and 5% CO_2. Invasion of untreated cells towards 10% and 0% FBS was used as controls. Following incubation, non-invading cells were removed from the top chamber using a cotton swab and media was replaced in the bottom chamber with 1:10 PrestoBlue in 0% DMEM and incubated for 45 minutes with fluorescence measured at 544/590nm. Number of invading cells was extrapolated from a standard curve comparing fluorescence intensity to cell seeding density (serially diluted from 20,000 to 234 cells/well). Finally, percentage invasion was calculated as the ratio of the number of invading cells to number of seeded cells.

Statistical analysis. Statistical data analysis and curve fitting was performed using GraphPad Prism (v8.4.3). Statistical significance was analysed via one-way ANOVA with $p < 0.05$ considered significant. Inhibitory concentration values (IC_{50} and IC_{25} for afuresertib and taxifolin, respectively) were generated from sigmoidal dose-response curves with upper and lower 95% confidence intervals.

4.4. Results and discussion

This study had three main outcomes: a widely applicable workflow based on metabolic modelling and network analysis (TISMAN), a list of potential drug targets for further investigation, and repurposing of drug compounds exerting inhibitory effects on GBM metabolic viability and invasion.

4.4.1. Workflow design

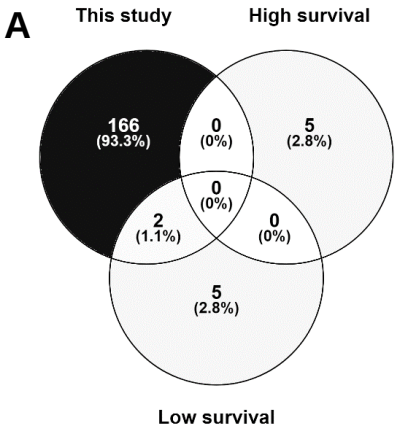
This workflow is an update of the version developed and tested for a parasite (Chapter 3), where criteria have been modified and extended in this study. Our previous method established dual criteria to identify reactions of interest (essential reaction and double choke point) appearing above a certain occurrence threshold over an array of metabolic states related to three biological properties (biomass yield, ATP yield and renewal of a protecting layer). The rationale behind this prioritisation approach is derived from the concept of targeting common underlying features of distinct phenotypes (McQuerry, Chang et al. 2017). In addition, the current version exploits differences at the transcriptional level between GBM and its healthy cellular counterpart, to highlight putative drug targets.

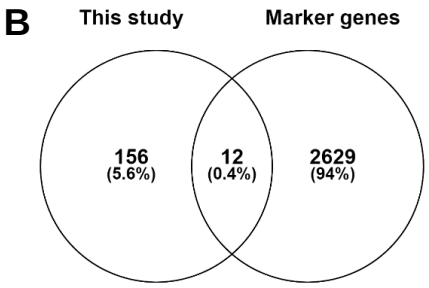
Accessible high throughput sequencing of biopsies transformed the usage of RNA-sequencing in neuro-oncology practice (Rogawski, Vitanza et al. 2017). Transcriptomics data was used to generate two contextualised models from a generic human GSM (Opdam, Richelle et al. 2017, Pires Pacheco, Bintener et al. 2019, Richelle, Joshi et al. 2019), and to identify upregulated genes in cancerous cells (Maié and Ticconi 2019). Specifically, GBMs comprise pro-tumourigenic subpopulations of stem cells able to develop resistance to therapy (Chen, Li et al. 2012, Neftel, Laffy et al. 2019, Wang, Sharma et al. 2020, Richards, Whitley et al. 2021). While using FBA to obtain in silico gene essentiality is not a novel idea (Orth, Thiele et al. 2010), defining an appropriate objective function for normal and cancerous tissues to elucidate differences cannot be easily done (Folger, Jerby et al. 2011, Hanahan and Weinberg 2011). Therefore, our analyses focused on cancer-specific models under an array of metabolic states and considering only reactions related to genes upregulated in GBM versus normal tissue. Conversely, recent metabolic modelling studies for GBM solely focused on the maximisation of biomass yield, but generated c. 140 patient-derived GSMs (Larsson, Uhlén et al. 2020).

4.4.2. Identification of genes of interest

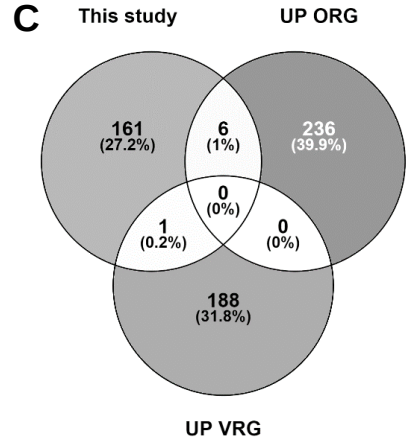
A final list of 168 upregulated genes associated with essential reactions classed as extended chokepoints and/or topologically important, was generated. Specifically, 74 genes contained hits in the chemical-gene interaction databases, whereas 94 genes did not (potential drug targets yet to be explored, Dataset S4-1). Given the genetic heterogeneity which manifests within GBM (Chen, Li et al. 2012, Neftel, Laffy et al. 2019, Wang, Sharma et al. 2020, Richards, Whitley et al. 2021), predicted genes of interest were compared against modelling and experimental approaches applied to cancerous tissue or specific subpopulations. In Larsson et al. (Figure 4-4), patient-derived GSMs for GBM were generated from transcriptomics data, and gene essentiality predicted by FBA (Larsson, Uhlén et al. 2020).

Two of the genes pinpointed for the low survival models agreed with our results: *ACOT8* (acyl-CoA thioesterase 8) and *GPAT4* (glycerol-3-phosphate acyltransferase 4), both related to lipid metabolism. The former is targeted by three drugs with antineoplastic activity which decrease its expression: doxorubicin (Jung, Lee et al. 2017, Vasey, Cavanagh et al. 2021), orlistat (Grube, Dünisch et al. 2014, You, Chen et al. 2019), and paclitaxel (Ganipineni, Ucakar et al. 2019, You, Chen et al. 2019). *GPAT4* is the only gene of the *GPAT* family expressed in the brain, and it has recently been identified as a potential drug target for treating obesity-associated depression (Huang, Wang et al. 2021).

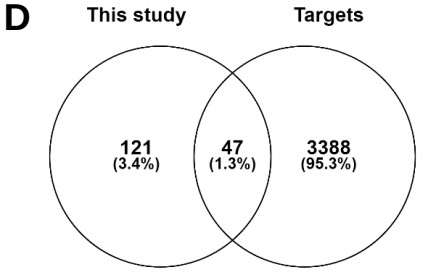




ACSF2 (ligase)
HADHB (acyltransferase)
ACSBG1 (ligase)
GUSB (glycosidase)
NUP107/NUP155/ NUP205/NUP210/NUP58 (transporter)
COX6A1 (oxidase)
PKM (kinase)
MGLL (phospholipase)



CYP4V2 (oxygenase)
ACSBG1 (ligase)
POLH (DNA metabolism)
FASN (synthase)
ABHD6 (lipase)
MGLL (phospholipase)



ACAA1 (acetyltransferase)
ACOX1 (oxidoreductase)
HADHB (acyltransferase)
ACOX3 (oxidoreductase)
SLC27A1/SLC27A4 (secondary carrier transporter)
HSD17B4 (oxidoreductase)
ACSL1/ ACSL3/ ACSL4/ ACSL5/ ACSL6 (ligase)
GAPDH (dehydrogenase)
MMAB (dehydrogenase)
NME1/NME2 (kinase)

Figure 4-4. Comparison of genes of interest identified in this study against published works: (A) Larsson et al. (Larsson, Uhlén et al. 2020), which highlighted essential genes for models for high and low survival, (B) Richards et al. (Richards, Whitley et al. 2021), where the list of marker genes comprises the top 50 genes for each one of the 86 intra-GSC clusters, (C) Wang et al. (Wang, Sharma et al. 2020), where upregulated genes for outer RG-like and ventricular RG-like (UP ORG and UP VRG, respectively) were considered, and (D) Liu et al. (Liu, Wu et al. 2015), where "targets" comprise both genes and miRNAs. Diagrams were made using Venny (Oliveros 2007-2015). Panels B, C and D include tables informing about the protein type (most of them are enzymes).

A subpopulation of GSC can facilitate developing resistance to therapy, promoting disease relapse (Chen, Li et al. 2012, Neftel, Laffy et al. 2019, Richards, Whitley et al. 2021). In Richards et al. (Richards, Whitley et al. 2021) certain marker genes for intra-GSC clusters were identified, some of which were also highlighted in this work as potential drug targets (Figure 4-4): *ACSF2* (acyl-CoA Synthetase Family Member 2), *MGLL* (monoglyceride lipase), and *PKM* (pyruvate kinase M1/2). Although *ACSF2* is functionally associated with fatty acid metabolism, *ACSF2* did not affect cell anchorage-dependent growth in U87 GBM cells (Pei, Sun et al. 2009). *MGLL* is highly expressed in the brain and in aggressive cancers and its role in self-renewal and tumorigenic behaviour has been demonstrated in murine models for GBM, where pharmacological inhibition of the translated protein showed promising results (Yin, Kim et al. 2020). Finally, overexpression of pyruvate kinase M1/2 is a trait occurring in brain tumours but not in other cancers, where it is involved in metabolic and signalling functions that promote cell proliferation, migration and chemoresistance. Knocking down *PKM* alters central carbon metabolism and decreases the activation of oncogenes, thus making it a viable therapy target (Verma, Cholia et al. 2021).

Other genes of interest also identified by both Richards et al. (Richards, Whitley et al. 2021) and this study, currently lack (i) extensive evidence of therapeutic relevance to treating cancer and/or (ii) cognate ligands or compounds affecting their expression levels (or updated chemical-gene interactions in databases): *ACSBG1* (acyl-CoA synthetase bubblegum family member 1), *COX6A1* (cytochrome c oxidase subunit 6A1), GUSB (glucuronidase beta), *HADHB* (acetyl-CoA acyltransferase), as well as multiple nucleoporins (*NUP58*, *NUP107*, *NUP155*, *NUP205* and *NUP201*).

A recent study in renal cell carcinoma cells showed that *ACSBG1* induces ferroptosis, an iron-dependent regulated cell death proposed as a therapeutic approach for cancer treatment (Xie, Sun et al. 2021). This mechanism plays a pro-tumourigenic effect in GBM by promoting necrosis, which is a sign of poor prognosis (Yee, Wei et al. 2020). Interestingly, depleting *ACSL4* (acyl-CoA synthetase long chain family member 4), a gene highlighted by the workflow, also inhibited tumour necrosis (Yee, Wei et al.

2020). *COX6A1*, has been reported as an anti-apoptotic gene in U373MG GBM cells, involved in mitochondrial energy metabolism (Eun, Woo et al. 2008). *HADHB* is involved in fatty acid β-oxidation, and gene knockdown in a colon carcinoma cell line decreased cell proliferation and increased sensitivity to the monoclonal antibody cetuximab (Hu, Yang et al. 2020). Regarding the aforementioned nucleoporins, even though there is a known link to cancer (Köhler and Hurt 2010), targeting membrane proteins remains a challenge due to the lack of robust models (The International Transporter Consortium 2010).

Radial glia (RG) cells are located in the ventricular zone during embryonic development and in the subventricular zone in the adult brain. In Wang et al., RG-like cells were found to play a role in the initiation or maintenance of adult GBM (Wang, Sharma et al. 2020). Specifically, two subpopulations of RG cells were identified: ventricular RG-like and outer RG-like, and upregulated RG genes are consistent with our results (Figure 4-4). Firstly, only one gene for ventricular RG-like was found in this study. *ACSL6* (acyl-CoA Synthetase Long Chain Family Member 6) is predominately expressed in the brain, where it participates in omega-3 fatty acid metabolism (crucial for correct brain function) (Fernandez, Kim et al. 2018). Conversely, six genes were highlighted as outer RG-like: *ABHD6* (Abhydrolase Domain-Containing Protein 6), *CYP4V2* (cytochrome P450 family 4 subfamily V member 2), *FASN* (fatty acid synthase), *POLH* (DNA polymerase eta), *MGLL* and *ACSBG1* (Wang, Sharma et al. 2020). ABHD6 is an endocannabinoid hydrolase with oncogenic functions, knockdown of which, reduces metastatic seeding in murine models (Tang, Xie et al. 2020, Miralpeix, Reguera et al. 2021). *CYP4V2* metabolizes fatty acids; however, as mutants with an impaired activity are the cause of multiple diseases (e.g. Bietti's crystalline dystrophy) (Jarrar and Lee 2019), this gene may not be a suitable drug target. Regarding *FASN*, it is known to be highly expressed in GBM, where its inhibition *in vitro* and *in vivo* by means of a saffron-derived compound induced cell death and impaired migration (Colapietro, Mancini et al. 2020). *POLH* is a DNA repair gene associated with correcting UV-induced damage, and its deficiency increases the risk of developing skin cancer (Di Lucca, Guedj et al. 2009). Conversely, ovarian cancer stem cells survive cisplatin treatment due to an enhanced *POLH*

expression, leading to tumour relapse (Srivastava, Han et al. 2015). Lastly, the remaining two genes identified as outer RG-like (*MGLL* and *ACSBG1*) are also marker genes for intra-GSC clusters, as discussed above.

Targeting transcription factors driving characteristic biological capabilities of cancer remains an attractive therapeutic approach (Bushweller 2019). 47/168 genes of interest had entries in RegNetwork (Figure 4-4), a database for regulatory information last updated in 2019 (Liu, Wu et al. 2015). Interestingly, 21 of these genes were related to the *MYC* family oncogene, which regulates a plethora of cellular functions and has been subjected to targeting studies at different levels (Chen, Liu et al. 2018). Specifically, *MYC* maintains GSC (Wang, Wang et al. 2008) and downregulating *MYC* promotes GBM autophagy (Ke, Zhang et al. 2020). Similarly, 13 genes are modulated by *PPARα* (Liu, Wu et al. 2015), a transcription factor whose depletion inhibits tumour cell proliferation and induces senescence (Chen, Wang et al. 2017).

Overall, genes of interest identified by the workflow agreed with published attempts to find potential drug targets for GBM. Therefore, the validation of its predictive capabilities should foster more research into the aforementioned genes whose relevance to GBM has been poorly studied (e.g., *ACSBG1*). Improving the workflow by adding more biological information (such as epigenomics, proteomics or survival data) would allow further refining of potential drug targets to enable *in vitro* and *in vivo* efficacy characterisations.

4.4.3. Selection of chemicals and *in vitro* testing

Gene-chemical interaction databases were used to identify relevant compounds, ranking them by the number of genes they interacted (directly and/or indirectly) with. Next, a literature search allowed selection based upon proven efficacy for other cancer types, but which have not yet been tested for GBM. A list of the top 30 chemicals identified can be found in Dataset S4-2, where a description, information about the mechanism of action and a potential application to GBM is provided. Upon scrutinizing such list, five chemicals were selected based on their potential effects on cell viability and invasion: afuresertib, pyrogallol, isorhamnetin, formononetin, and taxifolin (Table 4-1). Afuresertib is an orally bioavailable inhibitor of the

serine/threonine protein kinase Akt pathway (Spencer, Yoon et al. 2014) that can resensitise ovarian cancer to platinum-based chemotherapy (Blagden, Hamilton et al. 2019) and enhanced cisplatin treatment of mesothelioma cells (Yamaji, Ota et al. 2017). The PI3K/AKT/mTOR pathway is related to metabolism, proliferation and migration, and is generally active in GBM (Le Rhun, Preusser et al. 2019).

Pyrogallol is a natural polyphenol with antitumour effects in hepatocellular carcinoma via the upregulation of miR-134 (Ahn, Im et al. 2019). This microRNA is deregulated in GBM (U87 cells), and overexpressing it inhibited cell proliferation and invasion (Niu, Yang et al. 2013). Formononetin is an isoflavone affecting multiple signalling pathways with proven antitumourigenic properties in a rat glioma cell line (Ong, Shanmugam et al. 2019, Tay, Tan et al. 2019). 3-O-methylquercetin (isorhamnetin) is a flavonoid that inhibits cell proliferation and invasion, and induces apoptosis in multiple cancer types (Hu, Zhang et al. 2019). Finally, taxifolin (also a flavonoid) down-regulates β-catenin, thus promoting mesenchymal to epithelial transition – the reverse process is the epithelial to mesenchymal transition, related to metastasis. Specifically, this compound inhibited cell proliferation and invasion in breast cancer cell lines (Li, Hu et al. 2019). In addition, knocking down *PELP1*, a β-catenin coactivator, proved both elements to be crucial for GBM progression in a murine model (Sareddy, Pratap et al. 2019).

Table 4-1. Selected chemicals from the priority list for *in vitro* testing. Interactions for afuresertib were derived from CTD (Davis, Grondin et al. 2020), and interactions for all other compounds from DGIdb (Freshour, Kiwala et al. 2020). Gene relevance refers to the summation of the occurrence and the topological importance. As an illustrative example, the stoichiometry of a reaction related to ACSF2 can be found in Table S4-2. Afuresertib, pyrogallol and formononetin were selected from the higher part of the list, whereas isorhamnetin and taxifolin were at the bottom (full list in Dataset S4-2).

Position in priority list (Relevance)	Drug/ Chemical	Gene name	Gene symbol	Gene relevance	Interaction(s) (predicted "-")
4 (385)	Afuresertib	Acyl-CoA Synthetase Family Member 2	*ACSF2*	119	increases exp.
		Acyl-CoA Synthetase Long Chain Family Member 5	*ACSL5*	86	increases exp.
		Phenylalanyl-TRNA Synthetase Subunit Beta	*FARSB*	9	decreases exp.
		Lipin 1	*LPIN1*	9	increases exp.
		Metabolism Of Cobalamin Associated B	*MMAB*	26	increases exp.
		Patatin Like Phospholipase Domain Containing 2	*PNPLA2*	3	increases exp.
		DNA Polymerase Alpha 2, Accessory Subunit	*POLA2*	4	decreases exp.
		DNA Polymerase Delta 4, Accessory Subunit	*POLD4*	4	increases exp.
		Solute Carrier Family 27 Member 1. Long-chain fatty acid transport protein 1	*SLC27A1*	119	increases exp.
		Solute Carrier Family 29 Member 1. Equilibrative nucleoside transporter 1	*SLC29A1*	6	decreases exp.
8 (123)	Pyrogallol	Hydroxysteroid 17-Beta Dehydrogenase 10	*HSD17B10*	119	-
		DNA Polymerase Kappa	*POLK*	4	-
9 (119)	Formononetin	Hydroxysteroid 17-Beta Dehydrogenase 10	*HSD17B10*	119	-
13 (16)	3-O-methylquercetin (Isorhamnetin)	DNA Polymerase Beta	*POLB*	4	-
		DNA Polymerase Eta	*POLH*	4	-
		DNA Polymerase Iota	*POLI*	4	-
		DNA Polymerase Kappa	*POLK*	4	-
13 (16)	Taxifolin	DNA Polymerase Beta	*POLB*	4	-
		DNA Polymerase Eta	*POLH*	4	-
		DNA Polymerase Iota	*POLI*	4	-
		DNA Polymerase Kappa	*POLK*	4	-

Even though interesting candidates were identified in the databases, some instances referred to predicted interactions with DNA polymerases rather than stating the aforementioned actual effects (Table 4-1). Well-curated and maintained databases would greatly benefit drug repurposing efforts, and researchers should consider updating the chemical-gene interaction entries based upon new data.

Two *in vitro* tests were performed to assess the effects of the selected chemicals on metabolic viability and invasiveness of four patient-derived GBM cell lines, as a means to validate this innovative in silico pipeline. Afuresertib was identified as the most potent drug inhibiting proliferation (Figure 4-5A), while taxifolin showed a modest but significant effect on cell sensitisation (Figure 4-5B). No significant effect on proliferation was observed after treatment with isorhamnetin, formononetin and pyrogallol at 72h. Regarding the invasion assays (Figure 4-5C-F), afuresertib was the only compound to significantly inhibit invasion at IC_{50}, impairing invasion by 86.7% ($p < 0.001$) and 74.5% ($p < 0.0001$) in GIN28 and GIN31 GBM invasive margin cells respectively, and by 25.6% ($p = 0.017$) and 18% ($p = 0.028$) in corresponding GCE28 and GCE31 counterpart cell lines derived from the central tumour core. At 500μM, isorhamnetin significantly reduced invasion by 25.2% ($p = 0.0036$) in GIN28 and 34.2% ($p = 0.0011$) in GCE28. A significant reduction in invading cells was also observed in GIN28 and GCE28 cell lines upon treatment with formononetin at 500μM, impairing invasion by 26.8% ($p = 0.0042$) and 14.7% ($p = 0.0193$), respectively. While taxifolin demonstrated an antiproliferative effect across all cell lines, a significant effect on invasion was only observed in GCE28 ($p = 0.0034$) when used at 500 μM, reducing invasion to 15.5%.

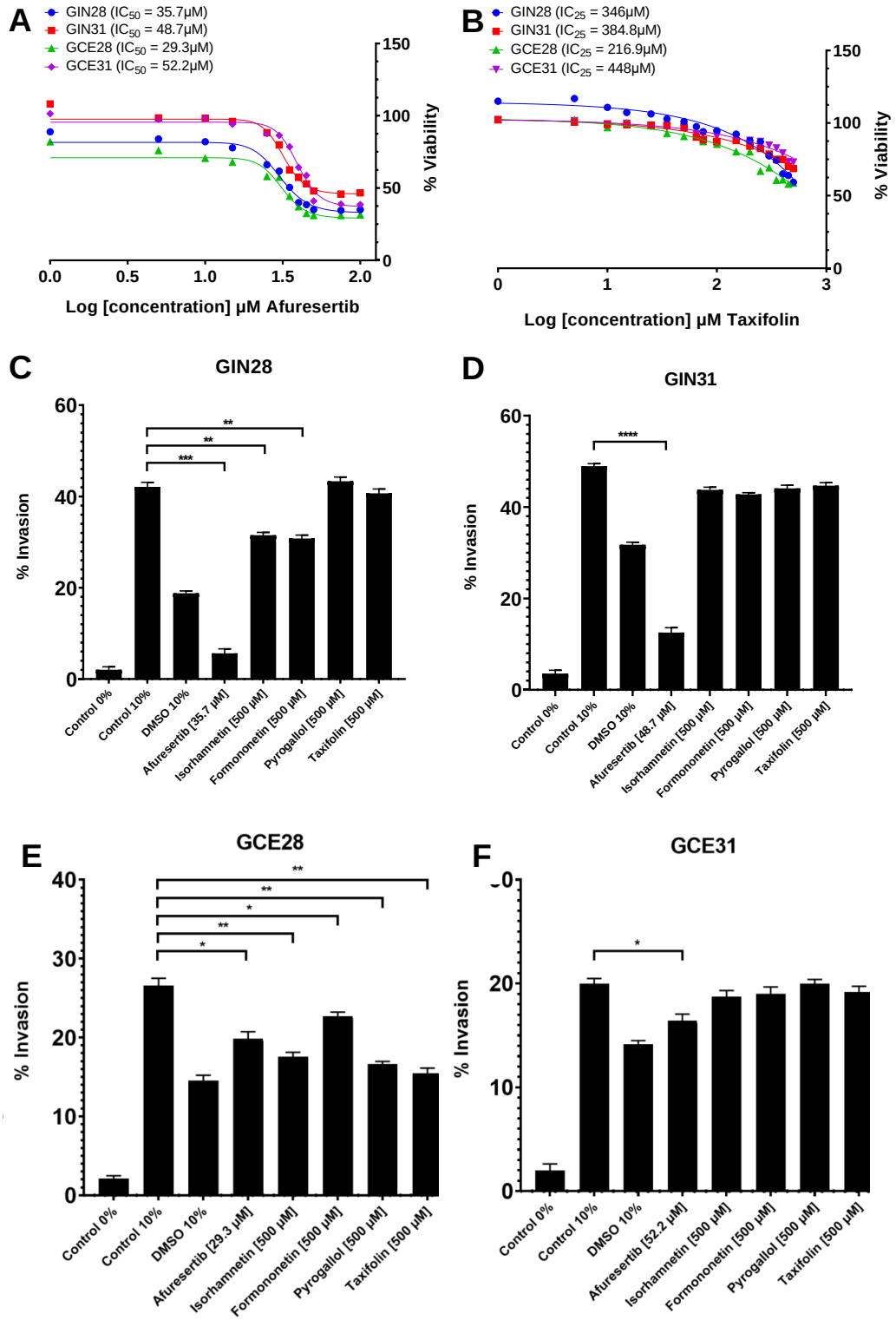


Figure 4-5. *In vitro* assessment of identified compounds for drug repurposing as validation of *in silico* workflow. [A-B] Metabolic viability was assessed for afuresertib (A) and taxifolin (B) in a 96-well 16-point dose response assay across

four patient-derived GBM lines. PrestoBlue was used to assess metabolic viability after 72hr and data is presented as the mean percent viability compared to DMSO-treated controls (n = 6). Afuresertib was identified as the most potent drug inhibiting proliferation at IC_{50} values of 35.7 μM, 48.7 μM, 29.3 μM and 52.2 μM for the GIN28, GIN31, GCE28 and GCE31 cell lines, respectively (A). Taxifolin showed a modest but significant effect on cell sensitisation generating IC_{25} values of 346 μM, 384.8 μM, 216.9 μM, 448 μM on GIN28, GIN31, GCE28 and GCE31 cell lines, respectively (B). [C-F] Effects on invasion in GBM invasive margin (GIN28, GIN31) and GBM Contrast-Enhanced core (GCE28, GCE31) cell lines following treatment with four compounds at 500 μM, and afuresertib at IC_{50} concentration. Invasion towards 0% FBS (Control 0%) on untreated cells and DMSO treated (DMSO 10%) controls were also included. Data is presented as mean percent invasion ± SEM compared to number of seeded cells after 24hr incubation. Significance was tested by one-way ANOVA (*$p < 0.05$, **$p < 0.01$, ***$p < 0.001$, **** $p < 0.0001$) comparing each data set to Control 10% (invasion towards 10% FBS; n = 3). Afuresertib was the only compound to significantly inhibit invasion at IC_{50} (GIN28 and GIN31), whereas taxifolin reduced invasiveness in GCE28 at 500 μM.

Therefore, afuresertib should be considered for *in vitro* studies to understand the underlying mechanisms to different responses, as well to assess the effect on GSCs, potentially leading to further *in vivo* studies to characterise its pre-clinical suitability. Collectively, *in vitro* assessment identified 2/5 tested compounds as impairing metabolic viability, and 3/5 tested compounds as impairing invasion. Considering both intra- and inter-tumour heterogeneity which manifests in GBM, and thereby the likely biological variation in TCGA transcriptomics data compared to the patient-derived GBM lines used in this study, validation of 40% and 60% of repurposed compounds for anti-proliferative and anti-invasion effects, represents an effective hit rate and validates this in silico workflow as a means to expedite compound prioritisation at a drug discovery phase. Furthermore, identified genes lacking targeting molecules should be considered in structural studies to enable and exploit molecular docking efforts. Overall, this validated workflow can be easily transferred to identify potential drug targets in other less-well studied cancer types.

5. General Discussion

"True Science teaches, above all, to doubt, and to be ignorant."

Miguel de Unamuno,
Tragic Sense of Life (1912)

5.1. Key findings

Chapter 2 is based on a publication (Tomi-Andrino, Norman et al. 2021). This study showed that (i) while the reliability of metabolic modelling is known to be improved by imposing thermodynamic constraints, adjusting the physicochemical parameters closer to the experimental conditions and using adequate equations yields better results, (ii) it was possible to design a computationally-cheap method (based on centrality measures) to identify important metabolites allowing to further constrain the solution space, as opposed to readily available methods, and (iii) the fluxomics community would benefit from standardising approaches to solve almost neglected known problem (such as the elucidation of the anaplerotic fluxes) and cross-validating novel strategies.

Chapter 3 introduced a workflow based on reaction essentiality (via FBA) and network topology under multiple metabolic states to identify and prioritise potential drug targets for further genetic and/or pharmacological studies and facilitate drug repurposing efforts. To that end, a GSM for a well-studied parasite was used to validate predicted drug targets against experimentally confirmed ones. In addition, the lethality of an antiviral drug was assessed *in vitro*. Overall, the workflow allowed identifying known drug targets, supporting its extension to integrating more biological information and analysing more complex metabolic networks.

Thus, Chapter 4 built on the previous workflow from Chapter 3 to exploit transcriptomics data from cancerous tissues (specifically glioblastoma) and further explore the network topology by introducing the concept of "extended choke point". In addition, it facilitated an automated search of chemical-gene interactions through multiple databases comprising thousands of hits, as well as publications in Pubmed to discard already tested chemical for glioblastoma. Five drugs or natural compounds were selected for *in vitro* testing (viability and invasion assays) on four patient-derived cell lines. In general, anti-proliferative and anti-invasion effects were shown by most of them, where afuresertib could be a promising compound to be considered for further studies. These results validated the suitability of the workflow both to identify potential drug targets yet to be explored and to simplify drug repurposing projects in a timely manner. This chapter was based on a publication (Tomi-Andrino, Pandele et al. 2022).

5.2. Limitations and future work

The studies in this thesis entail certain limitations (specifically covered in each chapter), which should be considered as future challenges allowing to improve the methods developed here. Chapter 2 explored the predictive capabilities of a published toolbox (Salvy, Fengos et al. 2018) by modifying the analysis and comparing against reported fluxomics and metabolomics data (Ishii, Nakahigashi et al. 2007). Limitations should be noted at the computational and experimental levels.

Firstly, the full factorial design should be considered. It comprised 6 factors with two values or categories, yielding $2^6 = 64$ combinations. This led to 16 incongruent tests, where an ionic strength of 0 M was analysed along with a salinity of 13.74 g/kg. However, it should be noted that salinity is only considered to calculate the Parameter A (used in both Debye-Hückel and Davies equations). Two different strategies to calculate such parameter were considered (a temperature-dependent and a temperature and salinity-dependent), thus further reducing the number of potentially conflicting conditions from 16 to 8. Overall, including such combinations was simply deemed necessary to assess the relevance of adjusting for salinity when running matTFA under mesophilic conditions, and whether the method was sensitive enough to these parameters or not. The relative importance analysis identified salinity as a factor having no impact when classifying the results. As a matter of fact, the joint ranking of correlation coefficients identified 4 tied tests at the top – all of them using an ionic strength of 0.25 M and the temperature-dependent equation to calculate the Parameter A, with half of them with a salinity value of 0 g/kg and the other with 13.74 g/kg. Therefore, there was no effective difference among those runs. Taken together, these results prove adjusting salinity did not affect the predictive capabilities of mod-matTFA, nor the assessment. Nevertheless, further studies considering non-mesophilic species (e.g., living in environments with high salinity) allowing to gather both ^{13}C-MFA and metabolomics data should be considered to further explore the impact of adjusting such parameters on the simulations.

Another potential limitation worth exploring is the selection of an ionic strength value of 0.25 M for the cytoplasm of *E. coli*. Even though the

estimated value is in the range 0.15-0.20 M, modelling approaches such as matTFA use the aforementioned ionic strength instead. Thus, enabling a comparison against mod-matTFA required keeping the consistency. As explained in the main text, this tool uses the Debye-Hückel equation beyond its range of applicability, which motivated testing the predictive capabilities when using a suitable equation. In this sense, the 4 tied tests at the top used the Davies equation instead, showing how selecting adequate methods improve the reliability of simulations.

For the sake of consistency between experimental datasets used to validate the predictions, ^{13}C-MFA and metabolomics results were gathered from the same study (Ishii, Nakahigashi et al. 2007). This significantly limited the assessment, since there was a lack of concentration values of interest to compare with. A follow-up study should set an *a priori* list of compounds to be quantified via metabolomics. To that end, a network-based method to identify important metabolites was also introduced in this study.

Secondly, both TFA (based on FBA) and ^{13}C-MFA have well-known shortcomings, such as elucidating fluxes in and around cycles, needing to simplify metabolic networks and making assumptions to apply thermodynamic constraints (Myoung Park, Yong Kim et al. 2010, Chen, Alonso et al. 2011). While of great relevance, solving structural problems in the fluxomics field was beyond the scope of this study, and the main focus was put on assessing and improving readily available tools.

FBA requires pre-selecting a 'metabolic goal' (in the form of an objective function) for the system, thus affecting which optimal solution is retrieved (Orth, Thiele et al. 2010). Relevant alternative strategies aiming at overcoming this potential caveat include sampling flux values (objective function-free approach) or simultaneously considering multiple objectives. While the former yields flux distributions different to those resulting from FBA, they must be manually checked (Herrmann, Dyson et al. 2019). This scenario could be of particular interest when exploring changing environmental conditions that may alter the metabolic goals of the system. However, maximising the biomass reaction has proven to be a solid objective function when modelling bacterial growth in a chemostat (Schuetz, Kuepfer et al. 2007). Consequently, this assumption has been extended and combined with other goals for metabolic engineering purposes, thus considering more

than one objective function at once (Schuetz, Zamboni et al. 2012). Such rationale was behind the methods developed in the following chapters.

A drug repurposing strategy based on FBA (using gene essentiality as a proxy for drug targets) and network analysis is introduced in Chapter 3, using a neglected disease as an exemplar. Even though the *T. brucei* GSM was two thirds the size of the *E. coli*, thermodynamic constraints were not considered since they were too restrictive for the current model version. In addition, recent analyses using such constraints in a highly-curated model of *E. coli* showed the limited reliability of predicted essentiality (regardless of the thermodynamic constraints) (Salvy and Hatzimanikatis 2020). Therefore, such shortcomings were assumed and compensated by considering multiple objective functions and focusing on highly recurrent essential genes. In parallel, exploiting the network structure by introducing the concept of "double choke point" further reduced the list of potential drug targets (Csermely, Korcsmáros et al. 2013). This approach contrasts with previous attempts at identifying choke points, where the full network was considered (as opposed to just predicted active reactions) (Shameer, Logan-Klumpler et al. 2015). Comparing predicted and experimentally studied potential drug target proved the reliability of the workflow. Two main limitations are worth mentioning. Firstly, 30% of genes are annotated as 'hypothetical proteins', and 46% of reactions lack gene-protein-reactions associations. Thus, follow-up studies are needed to further curate the GSM. To that end, this study also provided a list of prioritised reactions and enzymes (potential drug targets) that could serve as a starting point to parasitologists, geneticists and structural biologists. This would in turn facilitate overcoming the second limitation. While reported transcriptomics data (Aslett, Aurrecoechea et al. 2010, Siegel, Hekstra et al. 2010) was used qualitatively to discard non-expressed genes from the pipeline, an *ex profeso* study analysing both life-cycle genes would enable tailoring the GSM.

Finally, Chapter 4.builds on the previous chapter to develop TISMAN: *Transcriptomics-Informed Stoichiometric Modelling And Network analysis* (Tomi-Andrino, Pandele et al. 2022). In this case, thermodynamic constraints were not considered due to the size of the human metabolic network (c. 14,000 reactions), which prevented from a feasible integration with the other layers of information and an analysis in a timely manner.

Briefly, transcriptomics data characterising glioblastoma was exploited to generate context-specific models from the generic human GSM. Introducing the concept of "extended choke points" and combining it with centrality measures, allowed to reduce the list of potential candidates. This approach sufficed to identify and prioritise chemicals to be tested in only 3 days of processing, thus facilitating the drug repurposing effort. Specifically, half of the drugs proved to impair metabolic activity and/or invasion *in vitro*.

Beyond the aforementioned structural limitations of FBA and genome annotation, certain aspects are worth mentioning. Gene essentiality predictions via FBA are based on maximizing the biomass reaction. Consequently, inaccuracies in the biomass reaction lead to unreliable predictions (Dikicioglu, Kırdar et al. 2015). Modelling with context-specific cancer networks showed that metabolite composition of the biomass reaction affects both gene essentiality and rate growth predictions, but the stoichiometric coefficients only affect the latter (Moscardó García, Pacheco et al. 2021). Therefore, the lack of a GBM-specific biomass reaction should not be problematic when using TISMAN.

Published transcriptomics data was used in this study to obtain two tailored metabolic models and identify upregulated genes. Conversely, other approaches (such as INTEGRATE) exploit metabolomics data to further constrain the feasible space solution (Di Filippo, Pescini et al. 2022). While TISMAN solely relies on systematically reported data for a myriad of cancers, the latter requires specifically designing an experiment for a particular type. Nevertheless, these methods have different goals: TISMAN was conceived as a fast strategy to facilitate drug repurposing efforts, while INTEGRATE provides insight into the metabolic regulation of the selected cancers.

The aforementioned tailored metabolic models were independently subjected to TISMAN (simulating a variety of metabolic states), for an integration of potential drugs in the late stages. Alternatively, the intra-tumour heterogeneity (Altea-Manzano, Cuadros et al. 2020) could be considered early on when defining the problem. To that end, stoichiometric modelling developed for microbial communities (Khandelwal, Olivier et al. 2013, Zomorrodi and Segrè 2017) could be adapted to consider multiple subpopulations, thus extending the validity of any potential drug targets. Apart from transcriptomics data, the TCGA database

(https://portal.gdc.cancer.gov/) includes epigenomics data and survival rates, which would allow better discerning cancer subtypes than by using transcriptomics alone (Qi and Teschendorff 2022). Similarly, machine learning could be used to understand the evolutionary history of tumours, allowing to focus on key mutants when contextualizing the GSM (Caravagna, Heide et al. 2020). Overall, integrating TISMAN with other modelling frameworks would improve the reliability of predicted potential drug targets, thus extending its applicability from a drug repurposing perspective to the starting point of drug discovery programs.

5.3. Concluding remarks

Metabolic modelling is mainly limited by time and computational resources, which promoted searching for a productive compromise between costs and results. This thesis developed and explored the applicability of different strategies to exploit metabolic networks, yielding two main outcomes. Firstly, it brought closer metabolic modelling to experimental results, fostering future collaborations among different disciplines to deepen understanding of metabolism for industrial and therapeutic purposes. Secondly, it formed the basis of a fast workflow to facilitate drug repurposing efforts without requiring a high computational power and considerable amount of resources, thus promoting multi-omics characterisations and generating research questions from a novel perspective.

Bibliography

Abdel-Haleem, A. M., et al. (2018). "Functional interrogation of Plasmodium genus metabolism identifies species- and stage-specific differences in nutrient essentiality and drug targeting." PLoS Comput Biol **14**(1): e1005895.

Åberg, J. and M. B. Wallin (2014). "Evaluating a fast headspace method for measuring DIC and subsequent calculation of pCO2 in freshwater systems." Inland Waters **4**: 157-166.

Adasme, M. F., et al. (2020). "Structure-based Drug Repositioning: Potential and Limits." Semin Cancer Biol.

Agren, R., et al. (2013). "The RAVEN Toolbox and Its Use for Generating a Genome-scale Metabolic Model for Penicillium chrysogenum." PLoS Comput Biol **9**(3).

Ahadi, H. and S. Emami (2020). "Modification of 7-piperazinylquinolone antibacterials to promising anticancer lead compounds: Synthesis and in vitro studies." Eur J Med Chem **187**: 111970.

Ahn, E., et al. (2017). "Temporal fluxomics reveals oscillations in TCA cycle flux throughout the mammalian cell cycle." Molecular Systems Biology **13**(11): 953.

Ahn, H., et al. (2019). "Antitumor Effect of Pyrogallol via miR-134 Mediated S Phase Arrest and Inhibition of PI3K/AKT/Skp2/cMyc Signaling in Hepatocellular Carcinoma." Int J Mol Sci **20**(16).

Alagesan, S., et al. (2018). "13C-assisted metabolic flux analysis to investigate heterotrophic and mixotrophic metabolism in Cupriavidus necator H16." Metabolomics **14**(9).

Alberty, R. A. (2005). Thermodynamics of Biochemical Reactions, John Wiley & Sons.

Aldridge, B. B. and K. Y. Rhee (2014). "Microbial metabolomics: innovation, application, insight." Curr Opin Microbiol **19**: 90-96.

Alexander, L. M. (1992). "The role of choke points in the ocean context." Geojournal **26**(4): 503-509.

Allmann, S., et al. (2014). "Triacylglycerol Storage in Lipid Droplets in Procyclic Trypanosoma brucei." PLoS One **9**(12): e114628.

Alsford, S., et al. (2011). "High-throughput phenotyping using parallel sequencing of RNA interference targets in the African trypanosome." Genome Res **21**(6): 915-924.

Altamirano, C., et al. (2001). "Analysis of CHO cells metabolic redistribution in a glutamate-based defined medium in continuous culture." Biotechnol Prog **17**(6): 1032-1041.

Altea-Manzano, P., et al. (2020). "Nutrient metabolism and cancer in the in vivo context: a metabolic game of give and take." EMBO reports **21**(10): e50635.

Angius, G., et al. (2020). "Prexasertib, a checkpoint kinase inhibitor: from preclinical data to clinical development." Cancer Chemother Pharmacol **85**(1): 9-20.

Antoniewicz, M. R. (2015). "Methods and advances in metabolic flux analysis: a mini-review." J Ind Microbiol Biotechnol **42**(3): 317-325.

Aslett, M., et al. (2010). "TriTrypDB: A Functional Genomic Resource for the Trypanosomatidae." Nucleic Acids Research **38**: D457–D462.

Ataman, M. and V. Hatzimanikatis (2015). "Heading in the right direction: thermodynamics-based network analysis and pathway engineering." Curr Opin Biotechnol **36**: 176–182.

Ataullakhanov, F. I. and V. M. Vitvitsky (2002). "What determines the intracellular ATP concentration." Biosci Rep **22**(5-6): 501-511.

Atkins, P. and J. d. Paula (2002). Equilibrium electrochemistry. Atkins' physical chemistry. United States, Oxford University Press.

Attia, Y. M., et al. (2017). "The FXR Agonist, Obeticholic Acid, Suppresses HCC Proliferation & Metastasis: Role of IL-6/STAT3 Signalling Pathway." Sci Rep **7**(1): 12502.

Avilán, L., et al. (2011). "Enolase: A Key Player in the Metabolism and a Probable Virulence Factor of Trypanosomatid Parasites—Perspectives for Its Use as a Therapeutic Target." Enzyme Res. **2011**(932549).

Bacchi, C. J., et al. (1980). "Polyamine metabolism: a potential therapeutic target in trypanosomes." Science **210**(4467): 332-334.

Bahreyni-Toossi, M. T., et al. (2019). "microRNAs: Potential glioblastoma radiosensitizer by targeting radiation-related molecular pathways." Mutat Res **816-818**: 111679.

Baldwin, W. W., et al. (1995). "Buoyant density of Escherichia coli is determined solely by the osmolarity of the culture medium." Arch Microbiol **164**: 155-157.

Bánky, D., et al. (2013). "Equal opportunity for low-degree network nodes: a PageRank-based method for protein target identification in metabolic graphs." PLoS One **8**(1): e54204.

Bantscheff, M., et al. (2012). "Quantitative mass spectrometry in proteomics: critical review update from 2007 to the present." Anal Bioanal Chem **404**: 939-965.

Barabási, A.-L., et al. (2011). "Network medicine: a network-based approach to human disease." Nature Reviews Genetics **12**(1): 56-68.

Barabási, A.-L. and Z. N. Oltvai (2004). "Network biology: understanding the cell's functional organization." Nature Reviews Genetics **5**(2): 101-113.

Barber, F., et al. (2017). "Details matter: noise and model structure set the relationship between cell size and cell cycle timing." Front Cell Dev Biol **5**(92).

Barone, I., et al. (2018). "Activation of Farnesoid X Receptor impairs the tumor-promoting function of breast cancer-associated fibroblasts." Cancer Lett **437**: 89-99.

Barros-Alvarez, X., et al. (2014). "Glycosomal Targets for Anti-Trypanosomatid Drug Discovery." Curr. Med. Chem. **21**(1).

Bastiancich, C., et al. (2018). "Gemcitabine and glioblastoma: challenges and current perspectives." Drug Discov Today **23**(2): 416-423.

Beard, D. A., et al. (2004). "Thermodynamic constraints for biochemical networks." J Theor Biol **228**: 327-333.

Beguerisse-Díaz, M., et al. (2018). "Flux-dependent graphs for metabolic networks." NPJ Syst Biol Appl. **4**(32).

Ben-Chetrit, N., et al. (2015). "Synaptojanin 2 is a druggable mediator of metastasis and the gene is overexpressed and amplified in breast cancer." Sci. Signal. **8**(360).

Benítez, D., et al. (2016). "Identification of Novel Chemical Scaffolds Inhibiting Trypanothione Synthetase from Pathogenic Trypanosomatids." PLOS Neglected Tropical Diseases **10**(4): e0004617.

Bernstein, D. B., et al. (2021). "Addressing uncertainty in genome-scale metabolic model reconstruction and analysis." Genome Biology **22**(1): 64.

Bertelli, M., et al. (2001). "Selective inhibition of 6-phosphogluconate dehydrogenase from Trypanosoma brucei." J Comput Aided Mol Des **15**(5): 465-475.

Beurton-Aimar, M., et al. (2011) Comparison between elementary flux modes analysis and 13C-metabolic fluxes measured in bacterial and plant cells. BMC Systems Biology **5**, 95 DOI: 10.1186/1752-0509-5-95

Bianchini, M., et al. (2005). "Inside PageRank." ACM Trans. Internet Technol. **5**(1): 92–128.

Bintener, T., et al. (2020). "Towards the routine use of in silico screenings for drug discovery using metabolic modelling." Biochem. Soc.

Blagden, S. P., et al. (2019). "Phase IB Dose Escalation and Expansion Study of AKT Inhibitor Afuresertib with Carboplatin and Paclitaxel in Recurrent Platinum-resistant Ovarian Cancer." Clin Cancer Res **25**(5): 1472-1478.

Bock, W. J. (2017). "Dual Causality and the Autonomy of Biology." Acta Biotheor **65**(1): 63-79.

Böhme, U. and G. Cross (2002). "Mutational Analysis of the Variant Surface Glycoprotein GPI-anchor Signal Sequence in Trypanosoma Brucei." J Cell Sci. **115**(4): 805-816.

Bordbar, A., et al. (2014). "Constraint-based models predict metabolic and associated cellular functions." Nature Reviews Genetics **15**(2): 107-120.

Bouteille, B., et al. (1988). "[Action of drugs tested in an acellular medium and in mice infected with Trypanosoma brucei brucei]." Bull Soc Pathol Exot Filiales. **81**((3 Pt 2)): 533-542.

Breiman, L., et al. (1984). Classification And Regression Trees, Routledge.

Brennan, C., et al. (2013). "The Somatic Genomic Landscape of Glioblastoma." Cell **155**: 462–477.

Bressi, J., et al. (2000). "Adenosine Analogues as Inhibitors of Trypanosoma brucei Phosphoglycerate Kinase: Elucidation of a Novel Binding Mode for a 2-Amino-N6-Substituted Adenosine." J. Med. Chem. **43**: 4135-4150.

Bruggeman, F. J. and H. V. Westerhoff (2007). "The nature of systems biology." Trends in Microbiology **15**(1): 45-50.

Buchholz, K. and J. Collins (2013). "The roots--a short history of industrial microbiology and biotechnology." Appl Microbiol Biotechnol **97**(9): 3747-3762.

Budinich, M., et al. (2017). "A multi-objective constraint-based approach for modeling genome-scale microbial ecosystems." PLoS One **12**(2): e0171744.

Bushweller, J. H. (2019). "Targeting transcription factors in cancer — from undruggable to reality." Nature Reviews Cancer **19**(11): 611-624.

Canal Castro, C., et al. (2012). "Coumestrol has neuroprotective effects before and after global cerebral ischemia in female rats." Brain Research **1474**: 82-90.

Canelas, A. B., et al. (2008). "Leakage-free rapid quenching technique for yeast metabolomics." Metabolomics **4**(3): 226-239.

Canelas, A. B., et al. (2009). "Quantitative Evaluation of Intracellular Metabolite Extraction Techniques for Yeast Metabolomics." Anal Chem **81**: 7379-7389.

Caravagna, G., et al. (2020). "Subclonal reconstruction of tumors by using machine learning and population genetics." Nat Genet **52**(9): 898-907.

Cassman, M. (2005). "Barriers to progress in systems biology." Nature **438**(7071): 1079-1079.

Castellan, M., et al. (2021). "Single-cell analyses reveal YAP/TAZ as regulators of stemness and cell plasticity in glioblastoma." Nature Cancer **2**(2): 174-188.

Chavali, A., et al. (2012). "A metabolic network approach for the identification and prioritization of antimicrobial drug targets." Trends Microbiol **20**(3): 113-123.

Chavali, A. K., et al. (2012). "Metabolic network analysis predicts efficacy of FDA-approved drugs targeting the causative agent of a neglected tropical disease." BMC Syst Biol **6**: 27.

Chavali, A. K., et al. (2008). "Systems analysis of metabolism in the pathogenic trypanosomatid Leishmania major." Mol Syst Biol **4**: 177.

Chen, H., et al. (2018). "Targeting oncogenic Myc as a strategy for cancer treatment." Signal Transduction and Targeted Therapy **3**(1): 5.

Chen, J., et al. (2012). "A restricted cell population propagates glioblastoma growth after chemotherapy." Nature **488**(7412): 522-526.

Chen, M. K., et al. (2019). "Pinosylvin reduced migration and invasion of oral cancer carcinoma by regulating matrix metalloproteinase-2 expression and extracellular signal-regulated kinase pathway." Biomed Pharmacother **117**: 109160.

Chen, P.-H., et al. (2019). "Metabolic Diversity in Human Non-Small Cell Lung Cancer Cells." Mol. Cell **76**: 838–851.

Chen, X., et al. (2011). "Synergy between (13)C-metabolic flux analysis and flux balance analysis for understanding metabolic adaptation to anaerobiosis in E. coli." Metab Eng **13**(1): 38-48.

Chen, X., et al. (2017). "The Cdc2/Cdk1 inhibitor, purvalanol A, enhances the cytotoxic effects of taxol through Op18/stathmin in non-small cell lung cancer cells in vitro." Int J Mol Med **40**(1): 235-242.

Chen, Y., et al. (2017). "PPARα regulates tumor cell proliferation and senescence via a novel target gene carnitine palmitoyltransferase 1C." Carcinogenesis **38**(4): 474-483.

Cheng, A. N., et al. (2018). "Identification of Novel Cdc7 Kinase Inhibitors as Anti-Cancer Agents that Target the Interaction with Dbf4 by the Fragment Complementation and Drug Repositioning Approach." EBioMedicine **36**: 241-251.

Cheung, C., et al. (2013). "A method for accounting for maintenance costs in flux balance analysis improves the prediction of plant cell metabolic phenotypes under stress conditions." The Plant Journal **75**: 1050–1061.

Chuang, Y., et al. (2004). "Role of synaptojanin 2 in glioma cell migration and invasion." Cancer Res. **64**: 8271–8275.

Colapietro, A., et al. (2020). "Crocetin Extracted from Saffron Shows Antitumor Effects in Models of Human Glioblastoma." International Journal of Molecular Sciences **21**(2).

Colaprico, A., et al. (2016). "TCGAbiolinks: an R/Bioconductor package for integrative analysis of TCGA data." Nucleic Acids Res. **44**(e71).

Cortassa, S., et al. (2015). "From metabolomics to fluxomics: a computational procedure to translate metabolite profiles into metabolic fluxes." Biophysical Journal **108**(1): 163-172.

Costenoble, R., et al. (2007). "13C-Labeled metabolic flux analysis of a fed-batch culture of elutriated Saccharomyces cerevisiae." FEMS Yeast Res **7**(4): 511-526.

Couturier, C. P., et al. (2020). "Single-cell RNA-seq reveals that glioblastoma recapitulates a normal neurodevelopmental hierarchy." Nature Communications **11**(1): 3406.

Creek, D. J., et al. (2013). "Metabolomics guides rational development of a simplified cell culture medium for drug screening against Trypanosoma brucei." Antimicrobial agents and chemotherapy **57**(6): 2768-2779.

Crosby, J. R., et al. (2019). "Extreme thermophiles as emerging metabolic engineering platforms." Curr Opin Biotechnol **59**: 55-64.

Crozier, T., et al. (2017). "Prediction of Protein Complexes in Trypanosoma brucei by Protein Correlation Profiling Mass Spectrometry and Machine Learning." Molecular & Cellular Proteomics **16**(1): 2254-2267.

Csermely, P., et al. (2013). "Structure and dynamics of molecular networks: A novel paradigm of drug discovery A comprehensive review." Pharmacology & Therapeutics **138**: 333–408.

Cuperlovic-Culf, M. (2018). "Machine Learning Methods for Analysis of Metabolic Data and Metabolic Pathway Modeling." Metabolites **8**(4).

Dahlqvist, A., et al. (2000). "Phospholipid:diacylglycerol acyltransferase: An enzyme that catalyzes the acyl-CoA-independent formation of triacylglycerol

in yeast and plants." Proceedings of the National Academy of Sciences **97**(12): 6487.

Dai, Z. and J. Nielsen (2015). "Advancing metabolic engineering through systems biology of industrial microorganisms." Curr Opin Biotechnol **36**: 8-15.

Dalwadi, M. P., et al. (2018). "Applying asymptotic methods to synthetic biology: Modelling the reaction kinetics of the mevalonate pathway." Journal of Theoretical Biology **439**: 39–49.

Dash, A., et al. (2017). "Pharmacotoxicology of clinically-relevant concentrations of obeticholic acid in an organotypic human hepatocyte system." Toxicol In Vitro **39**: 93-103.

Dauner, M. (2010). "From fluxes and isotope labeling patterns towards in silico cells." Curr Opin Biotechnol **21**: 55-62.

Davidi, D., et al. (2016). "Global characterization of in vivo enzyme catalytic rates and their correspondence to in vitro k_{cat} measurements." Proceedings of the National Academy of Sciences **113**(12): 3401.

Davis, A., et al. (2020). "Comparative Toxicogenomics Database (CTD): update 2021." Nucleic Acid Res.

De Backer, P., et al. (2010). "Ins and Outs of Systems Biology vis-à-vis Molecular Biology: Continuation or Clear Cut?" Acta Biotheoretica **58**(1): 15-49.

de Groot, D. H., et al. (2019). "The number of active metabolic pathways is bounded by the number of cellular constraints at maximal metabolic rates." PLOS Computational Biology **15**(3): e1006858.

Di Filippo, M., et al. (2022). "INTEGRATE: Model-based multi-omics data integration to characterize multi-level metabolic regulation." PLoS Comput Biol **18**(2): e1009337.

Di Lucca, J., et al. (2009). "Variants of the xeroderma pigmentosum variant gene (POLH) are associated with melanoma risk." European Journal of Cancer **45**(18): 3228-3236.

Di Matteo, S., et al. (2019). "The FXR agonist obeticholic acid inhibits the cancerogenic potential of human cholangiocarcinoma." PLoS One **14**(1): e0210077.

Dickie, E. A., et al. (2020). "New Drugs for Human African Trypanosomiasis: A Twenty First Century Success Story." Trop. Med. Infect. Dis. **5**(29).

Dikicioglu, D., et al. (2015). "Biomass composition: the "elephant in the room" of metabolic modelling." Metabolomics **11**(6): 1690-1701.

Dip, R., et al. (2009). "Pleiotropic combinatorial transcriptomes of human breast cancer cells exposed to mixtures of dietary phytoestrogens." Food Chem Toxicol **47**(4): 787-795.

Dixon, N. M. and B. K. Douglas (1989). "The control and measurement of 'CO2' during fermentations." Journal of Microbiological Methods **10**: 155-176.

dos Santos, P., et al. (2016). "Molecular characterization of lipoamide dehydrogenase gene in Trypanosoma cruzi populations susceptible and resistant to benznidazole." Exp. Parasitol. **170**.

Dun, B., et al. (2018). "Temperature-Dependent Estimation of Gibbs Energies Using an Updated Group-Contribution Method." Biophys. J. **114**: 2691–2702.

Eun, S. Y., et al. (2008). "Identification of cytochrome c oxidase subunit 6A1 as a suppressor of Bax-induced cell death by yeast-based functional screening." Biochemical and Biophysical Research Communications **373**(1): 58-63.

Fahey, J. M., et al. (2019). "Upstream signaling events leading to elevated production of pro-survival nitric oxide in photodynamically-challenged glioblastoma cells." Free Radic Biol Med **137**: 37-45.

Failli, M., et al. (2019). "Prioritizing target-disease associations with novel safety and efficacy scoring methods." Sci Rep **9**(9852).

Fairlamb, A. and A. Cerami (1992). "Metabolism and functions of trypanothione in the kinetoplastida." Annu. Rev. Microbiol. **46**: 695-729.

Fan, X., et al. (2019). "Eupafolin Suppresses Esophagus Cancer Growth by Targeting T-LAK Cell-Originated Protein Kinase." Front Pharmacol **10**: 1248.

Farine, L., et al. (2015). "Phosphatidylethanolamine and phosphatidylcholine biosynthesis by the Kennedy pathway occurs at different sites in Trypanosoma brucei." Scientific Reports **5**(1): 16787.

Fatumo, S., et al. (2009). "Estimating novel potential drug targets of Plasmodium falciparum by analysing the metabolic network of knock-out strains in silico." Infection, Genetics and Evolution **9**: 351-358.

Faubert, B., et al. (2017). "Lactate Metabolism in Human Lung Tumors." Cell **171**: 358–371.

Feist, A. M., et al. (2009). "Reconstruction of biochemical networks in microorganisms." Nat Rev Microbiol **7**(2): 129-143.

Feist, A. M., et al. (2009). "Reconstruction of biochemical networks in microorganisms." Nature Reviews Microbiology **7**(2): 129-143.

Feist, A. M. and B. O. Palsson (2010). "The biomass objective function." Current Opinion in Microbiology **13**: 344-349.

Feist, A. M., et al. (2006). "Modeling methanogenesis with a genome-scale metabolic reconstruction of Methanosarcina barkeri." Molecular Systems Biology **2**(1): 2006.0004.

Fell, D. A. (1992). "Metabolic control analysis: a survey of its theoretical and experimental development." Biochem J **286 (Pt 2)**(Pt 2): 313-330.

Fernandez, R. F., et al. (2018). "Acyl-CoA synthetase 6 enriches the neuroprotective omega-3 fatty acid DHA in the brain." Proceedings of the National Academy of Sciences **115**(49): 12525.

Field, A. (2009). Discovering statistic using SPSS, SAGE Publications.

Fischer, E., et al. (2004). "High-throughput metabolic flux analysis based on gas chromatography–mass spectrometry derived 13C constraints." Anal Biochem **325**(2): 308-316.

Flamholz, A., et al. (2012). "eQuilibrator - the biochemical thermodynamics calculator." Nucleic Acids Res **40**: D770–D775.

Fleming, R. M. and I. Thiele (2011). "von Bertalanffy 1.0: a COBRA toolbox extension to thermodynamically constrain metabolic models." Bioinformatics **27**(1): 142-143.

Fleming, R. M., et al. (2009). "Quantitative assignment of reaction directionality in constraint-based models of metabolism: Application to Escherichia coli." Biophys Chem **145**: 47-56.

Folger, O., et al. (2011). "Predicting selective drug targets in cancer through metabolic networks." Mol Syst Biol **7**(501).

Frainay, C., et al. (2018). "MetaboRank: network-based recommendation system to interpret and enrich metabolomics results." Bioinformatics **35**(2): 274–283.

Frainay, C. and F. Jourdan (2017). "Computational methods to identify metabolic sub-networks based on metabolomic profiles." Brief Bioinform **18**(1): 43–56.

Frainay, C., et al. (2018). "Mind the Gap: Mapping Mass Spectral Databases in Genome-Scale Metabolic Networks Reveals Poorly Covered Areas." Metabolites **8**(3).

Frearson, J. A., et al. (2010). "N-myristoyltransferase inhibitors as new leads to treat sleeping sickness." Nature **464**(7289): 728-732.

Freshour, S., et al. (2020). "Integration of the Drug–Gene Interaction Database (DGIdb 4.0) with open crowdsource efforts." Nucleic Acid Res.

Fuad, F., et al. (2011). "Phosphoglycerate Mutase From Trypanosoma Brucei Is Hyperactivated by Cobalt in Vitro, but Not in Vivo." Metallomics **3**: 1310-1317.

Furse, S., et al. (2012). "Lipid membrane curvature induced by distearoyl phosphatidylinositol 4-phosphate." Soft Matter **8**(11): 3090-3093.

Ganipineni, L. P., et al. (2019). "Paclitaxel-loaded multifunctional nanoparticles for the targeted treatment of glioblastoma." J Drug Target **27**(5-6): 614-623.

Gao, P. and G. Xu (2015). "Mass-spectrometry-based microbial metabolomics: recent developments and applications." Anal Bioanal Chem **407**(3): 669-680.

Garrison, P., et al. (2021). "Turnover of Variant Surface Glycoprotein in Trypanosoma brucei Is a Bimodal Process." MBio **12**(4): e01725-01721.

Gazestani, V., et al. (2017). "TrypsNetDB: An integrated framework for the functional characterization of trypanosomatid proteins." PLoS Negl Trop Dis **11**(2).

Gerstl, M., et al. (2015). "tEFMA: computing thermodynamically feasible elementary flux modes in metabolic networks." Bioinformatics **31**(13): 2232–2234.

Ghiasi, M. M., et al. (2020). "Decision tree-based diagnosis of coronary artery disease: CART model." Comput Methods Programs Biomed **192**: 105400.

Gianchandani, E. P., et al. (2010). "The application of flux balance analysis in systems biology." WIREs Systems Biology and Medicine **2**(3): 372-382.

Gibellini, F., et al. (2008). "Biochemical characterization of the initial steps of the Kennedy pathway in Trypanosoma brucei: the ethanolamine and choline kinases." Biochem. J. **415**: 135–144.

Gibellini, F., et al. (2009). "The ethanolamine branch of the Kennedy pathway is essential in the bloodstream form of Trypanosoma brucei." Mol Microbiol **73**(5): 826-843.

Gibson, M., et al. (2016). "Trypanosoma brucei DHFR-TS Revisited: Characterisation of a Bifunctional and Highly Unstable Recombinant Dihydrofolate Reductase-Thymidylate Synthase." PLoS Negl Trop Dis **10**(5).

Gilson, M., et al. (2016). "BindingDB in 2015: A public database for medicinal chemistry, computational chemistry and systems pharmacology." Nucleic Acid Res. **44**: D1045–D1053.

Glover, L., et al. (2015). "Genome-scale RNAi screens for high-throughput phenotyping in bloodstream-form African trypanosomes." Nat. Protoc. **10**(1): 106-133.

González-Chávez, Z., et al. (2015). "Metabolic control analysis of the Trypanosoma cruzi peroxide detoxification pathway identifies tryparedoxin as a suitable drug target." Biochimica et Biophysica Acta (BBA) - General Subjects **1850**(2): 263-273.

Goodwin, B. C. (1969). "Synchronization of Escherichia coli in a chemostat by periodic phosphate feeding." Eur J Biochem **10**: 511-514.

Gopalakrishnan, S. and C. D. Maranas (2015). "13C metabolic flux analysis at a genome-scale." Metabolic Engineering **32**: 12-22.

Gottstein, W., et al. (2016). "Constraint-based stoichiometric modelling from single organisms to microbial communities." J. R. Soc. Interface **13**.

Greco, C., et al. (2020). "Development of Pyrazolo[3,4-d]pyrimidine Kinase Inhibitors as Potential Clinical Candidates for Glioblastoma Multiforme." ACS Med Chem Lett **11**(5): 657-663.

Grube, S., et al. (2014). "Overexpression of fatty acid synthase in human gliomas correlates with the WHO tumor grade and inhibition with Orlistat reduces cell viability and triggers apoptosis." J Neurooncol **118**(2): 277-287.

Grünig, D., et al. (2018). "Effect of the Catechol-O-Methyltransferase Inhibitors Tolcapone and Entacapone on Fatty Acid Metabolism in HepaRG Cells." Toxicol Sci **164**(2): 477-488.

Gu, X., et al. (2013). "Mathematical Modelling of Polyamine Metabolism in Bloodstream-Form Trypanosoma Brucei An Application to Drug Target Identification." PLoS One **8**(1).

Guan, X. and P. Mäser (2017). "Comparative sphingolipidomics of disease-causing trypanosomatids reveal unique lifecycle- and taxonomy-specific lipid chemistries." Sci Rep **7**(13617).

Haanstra, J. R., et al. (2008). "Compartmentation prevents a lethal turbo-explosion of glycolysis in trypanosomes." Proc Natl Acad Sci U S A **105**(46): 17718-17723.

Hanahan, D. and R. Weinberg (2011). "Hallmarks of Cancer: The Next Generation." Cell **144**: 646-674.

Hardy, K. and N. H. Hunt (2004). "Effects of a redox-active agent on lymphocyte activation and early gene expression patterns." Free Radic Biol Med **37**(10): 1550-1563.

Hartman, H. B., et al. (2014). "Identification of potential drug targets in Salmonella enterica sv. Typhimurium using metabolic modelling and experimental validation." Microbiology **160**(6): 1252-1266.

Hasunuma, T., et al. (2011). "Metabolic pathway engineering based on metabolomics confers acetic and formic acid tolerance to a recombinant xylose-fermenting strain of Saccharomyces cerevisiae." Microbial Cell Factories **10**(1): 2.

Hausser, J. and U. Alon (2020). "Tumour heterogeneity and the evolutionary trade-offs of cancer." Nat. Rev. Cancer **20**: 247-257.

Hayashi, T., et al. (2018). "Impact of a novel biomarker, T-LAK cell-originating protein kinase (TOPK) expression on outcome in malignant glioma." Neuropathology **38**(2): 144-153.

He, H., et al. (2020). "Chelerythrine induces apoptosis via ROS-mediated endoplasmic reticulum stress and STAT3 pathways in human renal cell carcinoma." J Cell Mol Med **24**(1): 50-60.

Henry, C. S., et al. (2007). "Thermodynamics-Based Metabolic Flux Analysis." Biophys J **92**: 1792–1805.

Herr, P., et al. (2020). "Cell Cycle Profiling Reveals Protein Oscillation, Phosphorylation, and Localization Dynamics." Mol Cell Proteomics.

Herrmann, H. A., et al. (2019). "Flux sampling is a powerful tool to study metabolism under changing environmental conditions." npj Systems Biology and Applications **5**(1): 32.

Holzhütter, H. G. (2004). "The principle of flux minimization and its application to estimate stationary fluxes in metabolic networks." Eur J Biochem **271**(14): 2905-2922.

Hoops, S., et al. (2006). "COPASI—a COmplex PAthway SImulator." Bioinformatics **22**(24): 3067–3074.

Hoppe, A., et al. (2007). "Including metabolite concentrations into flux balance analysis: thermodynamic realizability as a constraint on flux distributions in metabolic networks." BMC Syst Biol **1**(23).

Horn, F. and R. Jackson (1972). "General mass action kinetics." Arch. Ration. Mech. Anal. **47**: 81–116.

Hoskisson, P. A. and G. Hobbs (2005). "Continuous culture – making a comeback?" Microbiology **151**: 3153–3159.

Hotta, M., et al. (2019). "Farnesoid X receptor induces cell death and sensitizes to TRAIL-induced inhibition of growth in colorectal cancer cells through the up-regulation of death receptor 5." Biochem Biophys Res Commun **519**(4): 824-831.

Hu, J., et al. (2019). "ROS-mediated activation and mitochondrial translocation of CaMKII contributes to Drp1-dependent mitochondrial fission and apoptosis in triple-negative breast cancer cells by isorhamnetin and chloroquine." J Exp Clin Cancer Res **38**(1): 225.

Hu, T.-t., et al. (2020). "Detection of genes responsible for cetuximab sensitization in colorectal cancer cells using CRISPR-Cas9." Bioscience Reports **40**(10).

Huang, Y.-q., et al. (2021). "Hippocampal Glycerol-3-Phosphate Acyltransferases 4 and BDNF in the Progress of Obesity-Induced Depression." Frontiers in Endocrinology **12**(493).

Humphreys, C., et al. (2015). "Whole genome sequence and manual annotation of Clostridium autoethanogenum, an industrially relevant bacterium." BMC Genomics **16**(1085).

Hunt, K. A., et al. (2014). "Complete enumeration of elementary flux modes through scalable demand-based subnetwork definition." Bioinformatics **30**(11): 1569-1578.

Hwang, J. Y., et al. (2019). "Isolinderalactone regulates the BCL-2/caspase-3/PARP pathway and suppresses tumor growth in a human glioblastoma multiforme xenograft mouse model." Cancer Lett **443**: 25-33.

Ideker, T., et al. (2001). "A new approach to decoding life: systems biology." Annu Rev Genomics Hum Genet **2**: 343-372.

Iser, I. C., et al. (2017). "The Epithelial-to-Mesenchymal Transition-Like Process in Glioblastoma: An Updated Systematic Review and In Silico Investigation." Med Res Rev **37**(2): 271-313.

Ishii, N., et al. (2007). "Multiple high-throughput analyses monitor the response of E.coli to perturbations." Science **316**(5824): 593-597.

Jacobs, R. T., et al. (2011). "SCYX-7158, an orally-active benzoxaborole for the treatment of stage 2 human African trypanosomiasis." PLoS Negl Trop Dis **5**(6): e1151.

Jamshidi, N. and B. Palsson (2007). "Investigating the metabolic capabilities of Mycobacterium tuberculosis H37Rv using the in silico strain iNJ661 and proposing alternative drug targets." BMC Syst Biol **1**: 26.

Jang, Y. S., et al. (2012). "Engineering of microorganisms for the production of biofuels and perspectives based on systems metabolic engineering approaches." Biotechnol Adv **30**(5): 989-1000.

Jankowski, K., et al. (2008). "Group contribution method for thermodynamic analysis of complex metabolic networks." Biophys J **95**: 1487-1499.

Jarrar, Y. B. and S.-J. Lee (2019). "Molecular Functionality of Cytochrome P450 4 (CYP4) Genetic Polymorphisms and Their Clinical Implications." International Journal of Molecular Sciences **20**(17).

Jaworski, M., et al. (2018). "New Splitting Criteria for Decision Trees in Stationary Data Streams." IEEE Trans Neural Netw Learn Syst **29**(6): 2516-2529.

Jazmin, L. J., et al. (2017). "Isotopically nonstationary (13)C flux analysis of cyanobacterial isobutyraldehyde production." Metab Eng **42**: 9-18.

Jean-Robert, I. and S. Chang (2011). "Drugs for Neglected Diseases initiative model of drug development for neglected diseases: Current status and future challenges." Future Med. Chem. **3**(11): 1361-1371.

Jemal, A., et al. (2010). "Cancer statistics, 2010." CA Cancer J Clin **60**(5): 277-300.

Jiang, D. W., et al. (2000). "Trypanosoma brucei: Four Tandemly Linked Genes for Fatty Acyl-CoA Synthetases." Experimental Parasitology **96**(1): 16-22.

Jol, S., et al. (2012). "System-Level Insights into Yeast Metabolism by Thermodynamic Analysis of Elementary Flux Modes." PLoS Comput Biol **8**(3).

Jørgensen, H., et al. (1995). "Metabolic flux distributions in Penicillium chrysogenum during fed-batch cultivations." Biotechnol Bioeng **46**(2): 117-131.

Jung, S. H., et al. (2017). "Acyl-CoA thioesterase 7 is involved in cell cycle progression via regulation of PKCζ–p53–p21 signaling pathway." Cell Death & Disease **8**(5): e2793-e2793.

Kaltdorf, M., et al. (2016). "Systematic Identification of Anti-Fungal Drug Targets by a Metabolic Network Approach." Front. Mol. Biosci. **3**(22).

Kappelmann, J., et al. (2015). "Cutting the Gordian Knot: Identifiability of anaplerotic reactions in Corynebacterium glutamicum by means of (13) C-metabolic flux analysis." Biotechnol Bioeng **113**(3).

Karpel-Massler, G., et al. (2014). "PARP inhibition restores extrinsic apoptotic sensitivity in glioblastoma." PLoS One **9**(12): e114583.

Kast, R. E. and M. E. Halatsch (2012). "Matrix metalloproteinase-2 and -9 in glioblastoma: a trio of old drugs-captopril, disulfiram and nelfinavir-are inhibitors with potential as adjunctive treatments in glioblastoma." Arch Med Res **43**(3): 243-247.

Kauffman, K. J., et al. (2003). "Advances in flux balance analysis." Current Opinion in Biotechnology **14**(5): 491-496.

Kaur, J., et al. (2011). "Bioinformatic Analysis of Leishmania donovani Long-Chain Fatty Acid-CoA Ligase as a Novel Drug Target." Molecular Biology International **2011**: 278051.

Kazemi Noureini, S., et al. (2018). "Telomerase Inhibition by a New Synthetic Derivative of the Aporphine Alkaloid Boldine." Int J Mol Sci **19**(4).

Kazemi Noureini, S. and F. Tanavar (2015). "Boldine, a natural aporphine alkaloid, inhibits telomerase at non-toxic concentrations." Chem Biol Interact **231**: 27-34.

Ke, X. X., et al. (2020). "Deficiency of G9a Inhibits Cell Proliferation and Activates Autophagy via Transcriptionally Regulating c-Myc Expression in Glioblastoma." Front Cell Dev Biol **8**: 593964.

Kell, D. B. and S. G. Oliver (2003). "Here is the evidence, now what is the hypothesis? The complementary roles of inductive and hypothesis-driven science in the post-genomic era." BioEssays **26**: 99-105.

Kerkhoven, E. J., et al. (2013). "Handling Uncertainty in Dynamic Models: The Pentose Phosphate Pathway in Trypanosoma brucei." PLOS Computational Biology **9**(12): e1003371.

Khalaf, A. I., et al. (2014). "Structure-Based Design and Synthesis of Antiparasitic Pyrrolopyrimidines Targeting Pteridine Reductase 1." Journal of Medicinal Chemistry **57**(15): 6479-6494.

Khandelwal, R. A., et al. (2013). "Community Flux Balance Analysis for Microbial Consortia at Balanced Growth." PLoS One **8**(5): e64567.

Khare, S., et al. (2016). "Proteasome inhibition for treatment of leishmaniasis, Chagas disease and sleeping sickness." Nature **537**(7619): 229-233.

Kiefer, P., et al. (2004). "Comparative metabolic flux analysis of lysine-producing Corynebacterium glutamicum cultured on glucose or fructose." Appl Environ Microbiol **70**(1): 229-239.

Kim, D. H., et al. (2015). "LC-MS-based absolute metabolite quantification: application to metabolic flux measurement in trypanosomes." Metabolomics **11**(6): 1721-1732.

Kim, E.-Y., et al. (2019). "Identification of critical connectors in the directed reaction-centric graphs of microbial metabolic networks." BMC Bioinformatics **20**(1): 328.

Kim, J. E., et al. (2017). "Coumestrol Epigenetically Suppresses Cancer Cell Proliferation: Coumestrol Is a Natural Haspin Kinase Inhibitor." Int J Mol Sci **18**(10).

King, Z. A., et al. (2016). "BiGG Models: A platform for integrating, standardizing, and sharing genome-scale models." Nucleic Acids Res **44**: D515–D522.

Kiparissides, A. and V. Hatzimanikatis (2017). "Thermodynamics-based Metabolite Sensitivity Analysis in metabolic networks." Metab Eng **39**: 117-127.

Klamt, S., et al. (2017). "From elementary flux modes to elementary flux vectors: Metabolic pathway analysis with arbitrary linear flux constraints." PLOS Computational Biology **13**(4): e1005409.

Klobucar, K. and E. Brown (2018). "Use of genetic and chemical synthetic lethality as probes of complexity in bacterial cell systems." FEMS Microbiology Reviews **42**: 81-99.

Köhler, A. and E. Hurt (2010). "Gene regulation by nucleoporins and links to cancer." Mol Cell **38**(1): 6-15.

Korsnes, M. S. and R. Korsnes (2017). "Mitotic Catastrophe in BC3H1 Cells following Yessotoxin Exposure." Front Cell Dev Biol **5**: 30.

Kovářová, J. and M. P. Barrett (2016). "The Pentose Phosphate Pathway in Parasitic Trypanosomatids." Trends in Parasitology **32**(8): 622-634.

Kreutz, C. and J. Timmer (2009). "Systems biology: experimental design." The FEBS Journal **276**(4): 923-942.

Krieger, S., et al. (2000). "Trypanosomes lacking trypanothione reductase are avirulent and show increased sensitivity to oxidative stress." Molecular Microbiology **35**(3): 542-552.

Kümmel, A., et al. (2006). "Putative regulatory sites unraveled by network-embedded thermodynamic analysis of metabolome data." Mol Syst Biol.

Kuzilek, J., et al. (2014). "Independent Component Analysis and Decision Trees for ECG Holter Recording De-Noising." PLoS One **9**(6): e98450.

Lacroix, V., et al. (2008). "An Introduction to Metabolic Networks and Their Structural Analysis." IEEE/ACM Transactions on Computational Biology and Bioinformatics **5**(4): 594-617.

Lämmer, F., et al. (2019). "Cytosolic Hsp70 as a biomarker to predict clinical outcome in patients with glioblastoma." PLoS One **14**(8): e0221502.

Lan, L., et al. (2019). "Rhamnetin induces apoptosis in human breast cancer cells via the miR-34a/Notch-1 signaling pathway." Oncol Lett **17**(1): 676-682.

Landaburu, L., et al. (2020). "TDR Targets 6: driving drug discovery for human pathogens through intensive chemogenomic data integration." Nucleic Acids Research **48**: D992–D1005.

Larsson, I., et al. (2020). "Genome-Scale Metabolic Modeling of Glioblastoma Reveals Promising Targets for Drug Development." Frontiers in Genetics **11**(381).

Le Rhun, E., et al. (2019). "Molecular targeted therapy of glioblastoma." Cancer Treat. Rev. **80**.

Lee, E., et al. (2019). "The pleiotropic effects of TNFα in breast cancer subtypes is regulated by TNFAIP3/A20." Oncogene **38**(4): 469-482.

Lee, S., et al. (2016). "Geraniol suppresses prostate cancer growth through down-regulation of E2F8." Cancer Med **5**(10): 2899-2908.

Lewin, G., et al. (2019). "Large-scale identification of pathogen essential genes during coinfection with sympatric and allopatric microbes." PNAS **116**(39): 19685–19694.

Li, G., et al. (2019). "Structural and functional analyses of microbial metabolic networks reveal novel insights into genome-scale metabolic fluxes." Brief. Bioinform. **20**(4): 1590–1603.

Li, J., et al. (2019). "Taxifolin inhibits breast cancer cells proliferation, migration and invasion by promoting mesenchymal to epithelial transition via β-catenin signaling." Life Sci **232**: 116617.

Li, T., et al. (2018). "MicroRNA-320 Enhances Radiosensitivity of Glioma Through Down-Regulation of Sirtuin Type 1 by Directly Targeting Forkhead Box Protein M1." Transl Oncol **11**(2): 205-212.

Lieven, C., et al. (2020). "MEMOTE for standardized genome-scale metabolic model testing." Nat Biotechnol **38**(3): 272-276.

Lim, W., et al. (2017). "Coumestrol Inhibits Proliferation and Migration of Prostate Cancer Cells by Regulating AKT, ERK1/2, and JNK MAPK Cell Signaling Cascades." J Cell Physiol **232**(4): 862-871.

Lin, A. and J. M. Sheltzer (2020). "Discovering and validating cancer genetic dependencies: approaches and pitfalls." Nature Reviews Genetics **21**(11): 671-682.

Lino, M. M., et al. (2010). "Notch signaling in glioblastoma: a developmental drug target?" BMC Med **8**: 72.

Liu, X., et al. (2020). "Computational methods for identifying the critical nodes in biological networks." Briefings in Bioinformatics **21**(2): 486-497.

Liu, Z.-P., et al. (2015). "RegNetwork: an integrated database of transcriptional and post-transcriptional regulatory networks in human and mouse." Database **2015**.

Llaneras, F. and J. Pico (2007). "A procedure for the estimation over time of metabolic fluxes in scenarios where measurements are uncertain and/or insufficient." BMC Bioinformatics **8**: 421.

Lloyd, C. J., et al. (2018). "COBRAme: A computational framework for genome-scale models of metabolism and gene expression." PLoS Comput Biol **14**(7): e1006302.

Lohnes, K. and D. Sommerville (2019). "Battle of Thermopylae." Encyclopedia Britannica. Retrieved 12 April 2021, from https://www.britannica.com/event/Battle-of-Thermopylae-Greek-history-480-BC.

Long, C. P. and M. R. Antoniewicz (2019). "High-resolution 13C metabolic flux analysis." Nat Protoc **14**: 2856–2877.

Lopar, M., et al. (2014). "Study of metabolic network of Cupriavidus necator DSM 545 growing on glycerol by applying elementary flux modes and yield space analysis." Journal of Industrial Microbiology and Biotechnology **41**(6): 913-930.

Lu, J., et al. (2013). "Ebsulfur Is a Benzisothiazolone Cytocidal Inhibitor Targeting the Trypanothione Reductase of Trypanosoma brucei." J. Biol. Chem **288**(38): 27456–27468.

Lu, W., et al. (2018). "Extraction and Quantitation of Nicotinamide adenine dinucleotide redox cofactors." Antioxidants & redox signaling **28**(3): 167-179.

Lueong, S., et al. (2016). "Gene expression regulatory networks in Trypanosoma brucei: insights into the role of the mRNA-binding proteome." Molecular Microbiology **100**(3): 457–471.

Lv, L. X., et al. (2017). "Hispidin induces autophagic and necrotic death in SGC-7901 gastric cancer cells through lysosomal membrane permeabilization by inhibiting tubulin polymerization." Oncotarget **8**(16): 26992-27006.

Lv, W. L., et al. (2019). "Scutellarin inhibits hypoxia-induced epithelial-mesenchymal transition in bladder cancer cells." J Cell Physiol **234**(12): 23169-23175.

Mackey, Z. B., et al. (2006). "Discovery of trypanocidal compounds by whole cell HTS of Trypanosoma brucei." Chem Biol Drug Des **67**(5): 355-363.

Maié, T. and F. Ticconi (2019). "Analysis of Cancer Genome Atlas in R." from https://costalab.ukaachen.de/open_data/Bioinformatics_Analysis_in_R_2019/BIAR_D3/handout.html.

Maier, R. M. (2009). Bacterial growth. Environmental microbiology. R. M. Maier, I. L. Pepper and C. P. Gerba, Elsevier Academic Press**:** 37-54.

Major, L., et al. (2013). Coupled Enzyme Activity and Thermal Shift Screening of the Maybridge Rule of 3 Fragment Library Against Trypanosoma brucei Choline Kinase; A Genetically Validated Drug Target. Drug Discovery. H. A. El-Shemy, InTech.

Marler, R. T. and J. S. Arora (2004). "Survey of multi-objective optimization methods for engineering." Structural and Multidisciplinary Optimization **26**(6): 369-395.

Marrugal, Á., et al. (2019). "Impact of Heat Shock Protein 90 Inhibition on the Proteomic Profile of Lung Adenocarcinoma as Measured by Two-Dimensional Electrophoresis Coupled with Mass Spectrometry." Cells **8**(8).

Martini, F. (2009). "Map of the Battle of Thermopylae, 480 BC, 2nd Greco–Persian War, and the movements to Salamis and Plataea.". Retrieved 12 April 2021, from https://en.wikipedia.org/wiki/File:Battle_of_Thermopylae_and_movements_to_Salamis_and_Plataea_map-en.svg.

Maser, T., et al. (2017). "Tolcapone induces oxidative stress leading to apoptosis and inhibition of tumor growth in Neuroblastoma." Cancer Med **6**(6): 1341-1352.

Massie, T. M., et al. (2010). "Cycles, phase synchronization, and entrainment in single-species phytoplankton populations." P Natl Acad Sci USA **107**(9): 4236-4241.

McCrorie, P., et al. (2020). "Biomedical engineering approaches to enhance therapeutic delivery for malignant glioma." Journal of Controlled Release **328**: 917-931.

McFarland, B. C., et al. (2013). "Activation of the NF-κB Pathway by the STAT3 Inhibitor JSI-124 in Human Glioblastoma Cells." Cell Growth & Differentiation **11**(5): 494-505.

McQuerry, J. A., et al. (2017). "Mechanisms and clinical implications of tumor heterogeneity and convergence on recurrent phenotypes." Journal of molecular medicine (Berlin, Germany) **95**(11): 1167-1178.

Meissner, T. and F. J. Wentz (2004). "The complex dielectric constant of pure and sea water from microwave satellite observations." IEEE T Geosci Remote **42**(9): 1836-1849.

Melo do Nascimento, L., et al. (2021). "Functional insights from a surface antigen mRNA-bound proteome." eLife **10**: e68136.

Mendes, P., et al. (2009). Computational Modeling of Biochemical Networks Using COPASI. Systems Biology. I. V. Maly. USA, Humana Press. **500:** 17-59.

Mendonça, A. A. S., et al. (2018). "Relevance of Trypanothione Reductase Inhibitors on Trypanosoma cruzi Infection: A Systematic Review, Meta-Analysis, and In Silico Integrated Approach." Oxidative Medicine and Cellular Longevity **2018**: 8676578.

Merigueti, T. C., et al. (2019). "FindTargetsWEB: A User-Friendly Tool for Identification of Potential Therapeutic Targets in Metabolic Networks of Bacteria." Frontiers in Genetics **10**.

Merino, N., et al. (2019). "Living at the Extremes: Extremophiles and the Limits of Life in a Planetary Context." Front Microbiol **10**: 780.

Mesu, V., et al. (2018). "Oral fexinidazole for late-stage African Trypanosoma brucei gambiense trypanosomiasis: a pivotal multicentre, randomised, non-inferiority trial." Lancet **391**(10116): 144-154.

Millero, F. J. and W. H. Leung (1976). "Thermodynamics of seawater at one atmosphere." Am J Sci **276**: 1035-1077.

Mina, J. and W. Denny (2018). "Everybody needs sphingolipids, right! Mining for new drug targets in protozoan sphingolipid biosynthesis." Parasitology **145**: 134-147.

Miralpeix, C., et al. (2021). "Carnitine palmitoyltransferase 1C negatively regulates the endocannabinoid hydrolase ABHD6 in mice, depending on nutritional status." British Journal of Pharmacology **178**(7): 1507-1523.

Mishina, Y., et al. (2007). "Artemisinins Inhibit Trypanosoma cruzi and Trypanosoma brucei rhodesiense In Vitro Growth." Antimicrob Agents Chemother **51**(5): 1852–1854.

Mitsopoulos, C., et al. (2020). "canSAR: update to the cancer translational research and drug discovery knowledgebase." Nucleic Acids Research **49**(D1): D1074-D1082.

Moffat, J. G., et al. (2017). "Opportunities and challenges in phenotypic drug discovery: an industry perspective." Nat Rev Drug Discov **16**(8): 531-543.

Mohr, P. J., et al. (2015). CODATA Recommended Values of the Fundamental Physical Constants 2014. Gaithersburg, Maryland 20899-8420, USA, National Institute of Standards and Technology.

Moler, C. (2011). Google PageRank. Experiments with MATLAB.

Montgomery, D. C. (2001). Response Surface Methods and Other Approaches to Process Optimization. Design and Analysis of Experiments. United States of America, John Wiley & Sons, Inc.**:** 472-483.

Mori, M., et al. (2016). "Constrained Allocation Flux Balance Analysis." PLoS Comput Biol **12**(6): e1004913.

Morimoto, Y., et al. (2020). "Prexasertib increases the sensitivity of pancreatic cancer cells to gemcitabine and S-1." Oncol Rep **43**(2): 689-699.

Moscardó García, M., et al. (2021). "Importance of the biomass formulation for cancer metabolic modeling and drug prediction." iScience **24**(10).

Murray, D. B., et al. (2007). "Regulation of yeast oscillatory dynamics." Proceedings of the National Academy of Sciences of the United States of America **104**(7): 2241-2246.

Myoung Park, J., et al. (2010). "Prediction of metabolic fluxes by incorporating genomic context and flux-converging pattern analyses." P Natl Acad Sci USA **107**(33): 14931–14936.

Nabil, S. (2021). "Suez Canal reopens after giant stranded ship is freed." Retrieved 12 April 2021, from https://www.bbc.com/news/world-middle-east-56567985.

Nägele, T. (2014). "Linking metabolomics data to underlying metabolic regulation." Front Mol Biosci **1**: 22.

Nanchen, A., et al. (2006). "Nonlinear dependency of intracellular fluxes on growth rate in miniaturized continuous cultures of Escherichia coli." Appl Environ Microb **72**(2): 1164-1172.

Nazarshodeh, E., et al. (2021). "Structural systems pharmacology: A framework for integrating metabolic network and structure-based virtual screening for drug discovery against bacteria." PLoS One **16**(12): e0261267.

Neftel, C., et al. (2019). "An Integrative Model of Cellular States, Plasticity, and Genetics for Glioblastoma." Cell **178**(4): 835-849.e821.

Niebel, B., et al. (2019). "An upper limit on Gibbs energy dissipation governs cellular metabolism." Nat Metab **1**: 125–132.

Nilsson, A., et al. (2018). "Metabolite Depletion Affects Flux Profiling of Cell Lines." Trends Biochem. Sci. **43**(6): 395-397.

Niu, C. S., et al. (2013). "MiR-134 regulates the proliferation and invasion of glioblastoma cells by reducing Nanog expression." Int J Oncol **42**(5): 1533-1540.

Noack, S., et al. (2011). "Stationary versus non-stationary (13)C-MFA: a comparison using a consistent dataset." J Biotechnol **154**(2-3): 179-190.

Noh, K., et al. (2007). "Metabolic flux analysis at ultra short time scale: isotopically non-stationary 13C labeling experiments." J Biotechnol **129**(2): 249-267.

Nolan, R. P., et al. (2006). "Identification of distributed metabolic objectives in the hypermetabolic liver by flux and energy balance analysis." Metabolic Engineering: 30-45.

Norsigian, C. J., et al. (2020). "BiGG Models 2020: multi-strain genome-scale models and expansion across the phylogenetic tree." Nucleic Acids Res **48**(D1): D402-d406.

Olin-Sandoval, V., et al. (2012). "Drug target validation of the trypanothione pathway enzymes through metabolic modelling." The FEBS Journal **279**(10): 1811-1833.

Oliveros, J. C. (2007-2015). "Venny. An interactive tool for comparing lists with Venn's diagrams." from https://bioinfogp.cnb.csic.es/tools/venny/index.html.

Ong, S. K. L., et al. (2019). "Focus on Formononetin: Anticancer Potential and Molecular Targets." Cancers (Basel) **11**(5).

Opdam, S., et al. (2017). "A Systematic Evaluation of Methods for Tailoring Genome-Scale Metabolic Models." Cell systems **4**: 318–329.

Orth, J. D., et al. (2011). "A comprehensive genome-scale reconstruction of Escherichia coli metabolism—2011." Mol Syst Biol **7**(535).

Orth, J. D., et al. (2010). "What is flux balance analysis?" Nat Biotechnol **28**(3): 245-248.

Ouattara, D. A., et al. (2012). "Metabolomics-on-a-chip and metabolic flux analysis for label-free modeling of the internal metabolism of HepG2/C3A cells." Molecular BioSystems **8**: 1908–1920.

Ozfiliz-Kilbas, P., et al. (2018). "Cyclin-dependent kinase inhibitors, roscovitine and purvalanol, induce apoptosis and autophagy related to unfolded protein response in HeLa cervical cancer cells." Mol Biol Rep **45**(5): 815-828.

Page L, B. and W. Motwani R (1998). The PageRank Citation Ranking: Bringing Order to the Web. S. InfoLab. Stanford, CA, USA.

Palsson, B. O. (2006). Systems Biology. Properties of Reconstructed Networks, Cambridge University Press.

Palsson, B. Ø. (2006). Topological properties. Systems biology. Properties of reconstructed networks., Cambridge University Press**:** 107-117.

Palumbo, M., et al. (2007). "Essentiality is an emergent property of metabolic network wiring." FEBS Letters **581**: 2485–2489.

Pandey, V., et al. (2019). "Enhanced flux prediction by integrating relative expression and relative metabolite abundance into thermodynamically consistent metabolic models." PLoS Comput Biol **15**(5).

Pant, A., et al. (2019). "Farnesol induces fatty acid oxidation and decreases triglyceride accumulation in steatotic HepaRG cells." Toxicol Appl Pharmacol **365**: 61-70.

Papagiannakis, A., et al. (2017). "Autonomous Metabolic Oscillations Robustly Gate the Early and Late Cell Cycle." Mol Cell. **65**: 285–295.

Park, E. J., et al. (2013). "Suppression of Src/ERK and GSK-3/β-catenin signaling by pinosylvin inhibits the growth of human colorectal cancer cells." Food Chem Toxicol **55**: 424-433.

Park, J. H., et al. (2008). "Application of systems biology for bioprocess development." Trends Biotechnol **26**(8): 404-412.

Park, J. M., et al. (2011). "Genome-scale reconstruction and in silico analysis of the Ralstonia eutropha H16 for polyhydroxyalkanoate synthesis, lithoautotrophic growth, and 2-methyl citric acid production." BMC Systems Biology **5**: 101.

Park, J. O., et al. (2016). "Metabolite concentrations, fluxes and free energies imply efficient enzyme usage." Nat Chem Biol **12**.

Park, S. S., et al. (2018). "Pyrrolidine dithiocarbamate reverses Bcl-xL-mediated apoptotic resistance to doxorubicin by inducing paraptosis." Carcinogenesis **39**(3): 458-470.

Parmar, K., et al. (2019). "The CHK1 Inhibitor Prexasertib Exhibits Monotherapy Activity in High-Grade Serous Ovarian Cancer Models and Sensitizes to PARP Inhibition." Clin Cancer Res **25**(20): 6127-6140.

Parvatham, K. and L. Veerakumari (2013). "Drug target prediction using elementary mode analysis in Ascaris lumbricoides energy metabolism." Biotechnology and Bioprocess Engineering **18**(3): 491-500.

Pasternack, D., et al. (2015). "Sphingosine Kinase Regulates Microtubule Dynamics and Organelle Positioning Necessary for Proper G1/S Cell Cycle Transition in Trypanosoma brucei." MBio **6**(5).

Patejko, M., et al. (2017). "Sample preparation procedures utilized in microbial metabolomics: An overview." J Chromatogr B Analyt Technol Biomed Life Sci **1043**: 150-157.

Pearcy, N., et al. (2022). "A genome-scale metabolic model of Cupriavidus necator H16 integrated with TraDIS and transcriptomic data reveals metabolic insights for biotechnological applications." PLOS Computational Biology **18**(5): e1010106.

Pei, Z., et al. (2009). "Acyl-CoA synthetase VL3 knockdown inhibits human glioma cell proliferation and tumorigenicity." Cancer research **69**(24): 9175-9182.

Pereira, C., et al. (2020). "Computational approaches for drug discovery against trypanosomatid-caused diseases." Parasitology **1-23**.

Petrecca, K., et al. (2013). "Failure pattern following complete resection plus radiotherapy and temozolomide is at the resection margin in patients with glioblastoma." J Neurooncol **111**: 19-23.

Piñeiro-Yáñez, E., et al. (2018). "PanDrugs: a novel method to prioritize anticancer drug treatments according to individual genomic data." Genome Med. **10**(41).

Pinger, J., et al. (2017). "Variant surface glycoprotein density defines an immune evasion threshold for African trypanosomes undergoing antigenic variation." Nature Communications **8**(1): 828.

Pinu, F. R. and S. G. Villas-Boas (2017). "Extracellular Microbial Metabolomics: The State of the Art." Metabolites **7**(3).

Pires Pacheco, M., et al. (2019). "Identifying and targeting cancer-specific metabolism with network-based drug target prediction." EBioMedicine **43**: 98–106.

Plata, G., et al. (2010). "Reconstruction and flux-balance analysis of the Plasmodium falciparum metabolic network." Mol Syst Biol **6**: 408.

Polson, E. S., et al. (2018). "KHS101 disrupts energy metabolism in human glioblastoma cells and reduces tumor growth in mice." Science translational medicine **10**(454): eaar2718.

Psychogios, N., et al. (2011). "The Human Serum Metabolome." PLoS One **6**(2).

Pushpakom, S., et al. (2019). "Drug repurposing: progress, challenges and recommendations." Nat. Rev. Drug Discov. **18**: 41-58.

Qi, L. and A. E. Teschendorff (2022). "Cell-type heterogeneity: Why we should adjust for it in epigenome and biomarker studies." Clinical Epigenetics **14**(1): 31.

Qiu, C., et al. (2019). "Methylseleninic Acid Suppresses Breast Cancer Growth via the JAK2/STAT3 Pathway." Reprod Sci **26**(6): 829-838.

Rabbers, I., et al. (2021). "Selection for cell yield does not reduce overflow metabolism in E. coli." bioRxiv: 2021.2005.2024.445453.

Rabinowitz, J. D. and E. Kimball (2007). "Acidic Acetonitrile for Cellular Metabolome Extraction from Escherichia coli." Anal Chem **79**: 6167-6173.

Ralser, M. (2018). "An appeal to magic? The discovery of a non-enzymatic metabolism and its role in the origins of life." Biochem J **475**: 2577-2592.

Rancati, G., et al. (2018). "Emerging and evolving concepts in gene essentiality." Nature Reviews Genetics **19**(1): 34-49.

Reinhart, D., et al. (2019). "Bioprocessing of Recombinant CHO-K1, CHO-DG44, and CHO-S: CHO Expression Hosts Favor Either mAb Production or Biomass Synthesis." Biotechnol J **14**(3): e1700686.

Renz, A. and A. Dräger (2021). "Curating and comparing 114 strain-specific genome-scale metabolic models of Staphylococcus aureus." npj Systems Biology and Applications **7**(1): 30.

Richards, L. M., et al. (2021). "Gradient of Developmental and Injury Response transcriptional states defines functional vulnerabilities underpinning glioblastoma heterogeneity." Nature Cancer **2**(2): 157-173.

Richelle, A., et al. (2019). "Assessing key decisions for transcriptomic data integration in biochemical networks." PLoS Comput Biol **15**(7).

Rick, J., et al. (2019). "TMIC-22. IDENTIFICATION OF CANCER-ASSOCIATED FIBROBLASTS IN GLIOBLASTOMA and Defining Their Protumoral Effects." Neuro-Oncology **21**(Supplement_6): vi252-vi252.

Roberts, S. B., et al. (2009). "Proteomic and network analysis characterize stage-specific metabolism in Trypanosoma cruzi." BMC Syst Biol **3**: 52.

Robinson, J., et al. (2020). "An atlas of human metabolism." Sci. Signal. **13**(624).

Rogawski, D., et al. (2017). "Integrating RNA sequencing into neuro-oncology practice." Transl Res **189**: 93-104.

Romero, P., et al. (2004). "Computational prediction of human metabolic pathways from the complete human genome." Genome Biol **6**(I).

Rosato, A., et al. (2018). "From correlation to causation: analysis of metabolomics data using systems biology approaches." Metabolomics **14**(37).

Roy, R., et al. (2019). "Pongapin and Karanjin, furanoflavanoids of Pongamia pinnata, induce G2/M arrest and apoptosis in cervical cancer cells by differential reactive oxygen species modulation, DNA damage, and

nuclear factor kappa-light-chain-enhancer of activated B cell signaling." Phytother Res **33**(4): 1084-1094.

Rubiolo, J. A., et al. (2014). "Yessotoxin induces ER-stress followed by autophagic cell death in glioma cells mediated by mTOR and BNIP3." Cell Signal **26**(2): 419-432.

Russell, J. B. and G. M. Cook (1995). "Energetics of Bacterial Growth: Balance of Anabolic and Catabolic Reactions." Microbiological reviews **59**(1): 48-62.

Saa, P. A. and L. K. Nielsen (2017). "Formulation, construction and analysis of kinetic models of metabolism: A review of modelling frameworks." Biotechnol Adv **35**: 981-1003.

Saldivia, M., et al. (2020). "Targeting the trypanosome kinetochore with CLK1 protein kinase inhibitors." Nat Microbiol **5**(10): 1207-1216.

Salvy, P., et al. (2018). "pyTFA and matTFA a Python package and a Matlab toolbox for Thermodynamics-based Flux Analysis." Bioinformatics **35**(1): 167-169.

Salvy, P. and V. Hatzimanikatis (2020). "The ETFL formulation allows multi-omics integration in thermodynamics-compliant metabolism and expression models." Nat. Commun **11**(30).

Sánchez, B. J., et al. (2017). "Improving the phenotype predictions of a yeast genome-scale metabolic model by incorporating enzymatic constraints." Molecular Systems Biology **13**(8): 935.

Sander, R. (2015). "Compilation of Henry's law constants (version 4.0) for water as solvent." Atmospheric Chemistry and Physics **15**: 4399–4981.

Sandve, G. K., et al. (2013). "Ten Simple Rules for Reproducible Computational Research." PLoS Comput Biol **9**(10).

Sareddy, G. R., et al. (2019). "PELP1 promotes glioblastoma progression by enhancing Wnt/β-catenin signaling." Neurooncol Adv **1**(1): vdz042.

Satroutdinov, A. D., et al. (1992). "Oscillatory metabolism of Saccharomyces cerevisiae in continuous culture." FEMS Microbiol Lett **77**(1-3): 261-267.

Sauer, U. and B. J. Eikmanns (2005). "The PEP-pyruvate-oxaloacetate node as the switch point for carbon flux distribution in bacteria." FEMS Microbiol Rev **29**: 765-794.

Sauer, U., et al. (1999). "Metabolic flux ratio analysis of genetic and environmental modulations of Escherichia coli central carbon metabolism." J. Bacteriol. **181**(21): 6679-6688.

Schäffer, A., et al. (2001). "Improving the accuracy of PSI-BLAST protein database searches with composition-based statistics and other refinements." Nucleic Acids Res **29**(14): 2994–3005.

Schellenberger, J., et al. (2011). "Quantitative prediction of cellular metabolism with constraint-based models: the COBRA Toolbox v2.0." Nat Protoc **6**(9): 1290-1307.

Schiffmann, Y. (2017). "The non-equilibrium basis of Turing Instability and localised biological work." Progress in Biophysics and Molecular Biology **127**: 12-32.

Schubert, E. and P. J. Rousseeuw (2019). Faster k-Medoids Clustering: Improving the PAM, CLARA, and CLARANS Algorithms. Similarity Search and Applications, Cham, Springer International Publishing.

Schuetz, R., et al. (2007). "Systematic evaluation of objective functions for predicting intracellular fluxes in Escherichia coli." Molecular Systems Biology **3**(119).

Schuetz, R., et al. (2012). "Multidimensional optimality of microbial metabolism." Science **336**: 601-604.

Schuster, S., et al. (2000). "A general definition of metabolic pathways useful for systematic organization and analysis of complex metabolic networks." Nature Biotechnology **18**(3): 326-332.

Schwabe, D., et al. (2020). "The transcriptome dynamics of single cells during the cell cycle." Molecular Systems Biology **16**(11): e9946.

Shameer, S., et al. (2015). "TrypanoCyc: a community-led biochemical pathways database for Trypanosoma brucei." Nucleic Acids Research **43**(D1): D637-D644.

Sheils, T., et al. (2020). "TCRD and Pharos 2021: mining the human proteome for disease biology." Nucleic Acid Res.

Sherwood, D. and P. Dalby (2018). The bioenergetics of living cells. Modern Thermodynamics for Chemists and Biochemists, Oxford University Press.

Shin, H. J., et al. (2019). "A curcumin derivative hydrazinobenzoylcurcumin suppresses stem-like features of glioblastoma cells by targeting Ca(2+) /calmodulin-dependent protein kinase II." J Cell Biochem **120**(4): 6741-6752.

Shiratsubaki, I. S., et al. (2020). "Genome-scale metabolic models highlight stage-specific differences in essential metabolic pathways in Trypanosoma cruzi." PLoS Negl Trop Dis **14**(10): e0008728.

Siedler, G. and H. Peters (1986). Physical properties (general) of sea water. Oceanography. Berlin, Springer. **V/3a:** 233-264.

Siegel, T. N., et al. (2010). "Genome-wide analysis of mRNA abundance in two life-cycle stages of Trypanosoma brucei and identification of splicing and polyadenylation sites." Nucleic Acids Res **38**(15): 4946-4957.

Simonin, J.-P. (2017). "Thermodynamic consistency in the modeling of speciation in selfcomplexing electrolytes." Ind Eng Chem Res **56**: 9721-9733.

Snoep, J., et al. (1999). "Teaching Metabolic Control Analysis and kinetic modelling Towards a portable teaching module." The Biochemist **2**.

Soh, K. C. and V. Hatzimanikatis (2014). Constraining the Flux Space Using Thermodynamics and Integration of Metabolomics Data. Metabolic Flux Analysis: Methods and Protocols. J. O. Krömer, L. K. Nielsen and L. M. Blank. New York, NY, Springer New York**:** 49-63.

Song, J., et al. (2018). "Pinosylvin enhances leukemia cell death via down-regulation of AMPKα expression." Phytother Res **32**(10): 2097-2104.

Spencer, A., et al. (2014). "The novel AKT inhibitor afuresertib shows favorable safety, pharmacokinetics, and clinical activity in multiple myeloma." Blood **124**(14): 2190-2195.

Spinks, D., et al. (2012). "Design, synthesis and biological evaluation of Trypanosoma brucei trypanothione synthetase inhibitors." ChemMedChem **7**(1): 95-106.

Srivastava, A. K., et al. (2015). "Enhanced expression of DNA polymerase eta contributes to cisplatin resistance of ovarian cancer stem cells." Proc Natl Acad Sci U S A **112**(14): 4411-4416.

Sriyudthsak, K., et al. (2016). "Mathematical Modeling and Dynamic Simulation of Metabolic Reaction Systems Using Metabolome Time Series Data." Frontiers in Molecular Biosciences **3**(15).

Stechishin, O. D., et al. (2013). "On-target JAK2/STAT3 inhibition slows disease progression in orthotopic xenografts of human glioblastoma brain tumor stem cells." Neuro Oncol **15**(2): 198-207.

Stephanopoulos, G., et al. (2004). "Exploiting biological complexity for strain improvement through systems biology." Nat Biotechnol **22**(10): 1261-1267.

Subramaniam, N., et al. (2019). "Hepatoprotective effect of boldine against diethylnitrosamine-induced hepatocarcinogenesis in wistar rats." J Biochem Mol Toxicol **33**(12): e22404.

Surrati, A., et al. (2016). "Non-destructive characterisation of mesenchymal stem cell differentiation using LC-MS-based metabolite footprinting." Analyst **141**(12): 3776-3787.

Sutterwala, S., et al. (2007). "De Novo Sphingolipid Synthesis Is Essential for Viability, but Not for Transport of Glycosylphosphatidylinositol-Anchored Proteins, in African Trypanosomes." Eukaryotic Cell **6**: 454–464.

Szklarczyk, D., et al. (2019). "STRING v11: Protein-Protein Association Networks With Increased Coverage, Supporting Functional Discovery in Genome-Wide Experimental Datasets." Nucleic Acids Research **47**: D607–D613.

Takhaveev, V. and M. Heinemann (2018). "Metabolic heterogeneity in clonal microbial populations." Curr Opin Microbiol **45**: 30-38.

Tang, Z., et al. (2020). "Enhanced monoacylglycerol lipolysis by ABHD6 promotes NSCLC pathogenesis." EBioMedicine **53**: 102696.

Tay, K. C., et al. (2019). "Formononetin: A Review of Its Anticancer Potentials and Mechanisms." Front Pharmacol **10**: 820.

Taymaz-Nikerel, H., et al. (2009). "Development and application of a differential method for reliable metabolome analysis in Escherichia coli." Anal Biochem **386**(1): 9-19.

The International Transporter Consortium (2010). "Membrane transporters in drug development." Nat. Rev. Drug Discov. **9**: 215-236.

The UniProt Consortium (2019). "UniProt: a worldwide hub of protein knowledge." Nucleic Acids Res **47**: D506–D515.

Thiele, I. and B. O. Palsson (2010). "A protocol for generating a high-quality genome-scale metabolic reconstruction." Nat Protoc **5**(1): 93-121.

Thor, S., et al. (2017). "Genome-Scale Metabolic Modeling of Archaea Lends Insight into Diversity of Metabolic Function." Archaea **2017**: 9763848.

Tinti, M., et al. (2019). "Proteome turnover in the bloodstream and procyclic forms of Trypanosoma brucei measured by quantitative proteomics." Wellcome Open Research **4**(152).

Tomar, N. and R. K. De (2013). "Comparing methods for metabolic network analysis and an application to metabolic engineering." Gene **521**(1): 1-14.

Tomi-Andrino, C., et al. (2021). "Physicochemical and metabolic constraints for thermodynamics-based stoichiometric modelling under mesophilic growth conditions." PLOS Computational Biology **17**(1): e1007694.

Tomi-Andrino, C., et al. (2022). "Metabolic modeling-based drug repurposing in Glioblastoma." Scientific Reports **12**(1): 11189.

Totanes, F., et al. (2016). Understanding Protozoan Parasite Metabolism and Identifying Drug Targets through Constraint-Based Modeling.

Comprehensive Analysis of Parasite Biology: From Metabolism to Drug Discovery**:** 487-512.

Toya, Y., et al. (2010). "13C-metabolic flux analysis for batch culture of Escherichia coli and its pyk and pgi gene knockout mutants based on mass isotopomer distribution of intracellular metabolites." Biotechnol. Prog. **26**(4): 975-992.

Toya, Y. and H. Shimizu (2013). "Flux analysis and metabolomics for systematic metabolic engineering of microorganisms." Biotechnol Adv **31**(6): 818-826.

Trinh, C. T., et al. (2009). "Elementary Mode Analysis A Useful Metabolic Pathway Analysis Tool for Characterizing Cellular Metabolism." Appl Environ Microbiol **81**: 813–826.

Tsouka, S., et al. (2021). "Constraint-based metabolic control analysis for rational strain engineering." Metab Eng **66**: 191-203.

Tyagi, R., et al. (2019). "Identification of small molecule enzyme inhibitors as broadspectrum anthelmintics." Sci Rep **9**(9085).

Ullah, E., et al. (2020). "Towards scaling elementary flux mode computation." Brief Bioinform **21**(6): 1875-1885.

van Eunen, K., et al. (2012). "Testing Biochemistry Revisited: How In Vivo Metabolism Can Be Understood from In Vitro Enzyme Kinetics." PLoS Comput Biol **8**(4).

van Gulik, W. M. (2010). "Fast sampling for quantitative microbial metabolomics." Curr Opin Biotechnol **21**(1): 27-34.

van Heeswijk, W., et al. (2013). "Nitrogen Assimilation in Escherichia coli: Putting Molecular Data into a Systems Perspective." Microbiol. Mol. Biol. Rev. **77**(4): 628–695.

Vasey, C. E., et al. (2021). "Polymer Pro-Drug Nanoparticles for Sustained Release of Cytotoxic Drugs Evaluated in Patient-Derived Glioblastoma Cell Lines and In Situ Gelling Formulations." Pharmaceutics **13**(2).

Verlinde, C., et al. (2001). "Glycolysis as a Target for the Design of New Anti-Trypanosome Drugs." Drug Resistance Updates **4**: 50-65.

Verma, H., et al. (2021). "A short review on cross-link between pyruvate kinase (PKM2) and Glioblastoma Multiforme." Metabolic Brain Disease **36**(5): 751-765.

Vlassis, N., et al. (2014). "Fast Reconstruction of Compact Context-Specific Metabolic Network Models." PLoS Comput Biol **10**(1).

Vojinović, V. and U. Von Stockar (2009). "Influence of uncertainties in pH, pMg, activity coefficients, metabolite concentrations, and other factors on the analysis of the thermodynamic feasibility of metabolic pathways." Biotechnol Bioeng **103**(4): 780–795.

Wagner, A. and D. Fell (2001). "The small world inside large metabolic networks." Proc Biol Sci. **268**: 1803-1810.

Wagner, B., et al. (2011). "The Rate of Oxygen Utilization by Cells." Free Radic. Biol. Med **51**: 700–712.

Wang, G., et al. (2017). "Esculetin exerts antitumor effect on human gastric cancer cells through IGF-1/PI3K/Akt signaling pathway." Eur J Pharmacol **814**: 207-215.

Wang, J., et al. (2008). "c-Myc Is Required for Maintenance of Glioma Cancer Stem Cells." PLoS One **3**(11): e3769.

Wang, J. D. and P. A. Levin (2009). "Metabolism, cell growth and the bacterial cell cycle." Nature Reviews Microbiology **7**(11): 822-827.

Wang, P., et al. (2014). "Identification of Important Nodes in Directed Biological Networks: A Network Motif Approach." PLoS One **9**(8): e106132.

Wang, R., et al. (2020). "Adult Human Glioblastomas Harbor Radial Glia-like Cells." Stem Cell Reports **14**(2): 338-350.

Wang, X., et al. (2019). "Targeting pyrimidine synthesis accentuates molecular therapy response in glioblastoma stem cells." Science translational medicine **11**(504): eaau4972.

Watson, J. D. and F. H. C. Crick (1953). "The Structure of DNA." Cold Spring Harbor Symposia on Quantitative Biology **18**(0): 123-131.

Wiechert, W. and K. Noh (2013). "Isotopically non-stationary metabolic flux analysis: complex yet highly informative." Curr Opin Biotechnol **24**(6): 979-986.

Wiedemar, N., et al. (2019). "Expression of a specific variant surface glycoprotein has a major impact on suramin sensitivity and endocytosis in Trypanosoma brucei." FASEB BioAdvances(1): 595–608.

Willert, E. and M. Phillips (2008). "Regulated Expression of an Essential Allosteric Activator of Polyamine Biosynthesis in African Trypanosomes." PLoS Pathog **4**(10).

Williams, T. C. R., et al. (2010). "A genome-scale metabolic model accurately predicts fluxes in central carbon metabolism under stress conditions." Plant Physiol **154**: 311-323.

Winder, C. L. and W. B. Dunn (2011). "Fit-for-purpose quenching and extraction protocols for metabolic profiling of yeast using chromatography-mass spectrometry platforms." Methods Mol Biol **759**: 225-238.

Winder, C. L., et al. (2011). "TARDIS-based microbial metabolomics: time and relative differences in systems." Trends Microbiol **19**(7): 315-322.

Winder, C. L., et al. (2008). "Global Metabolic Profiling of Escherichia coli Cultures: an Evaluation of Methods for Quenching and Extraction of Intracellular Metabolites." Anal Chem **80**: 2939-2948.

Winter, G. and J. O. Krömer (2013). "Fluxomics – connecting 'omics analysis and phenotypes." Environmental microbiology **15**(7): 1901.

Wishart, D. S., et al. (2018). "DrugBank 5.0: a major update to the DrugBank database for 2018." Nucleic Acids Res. **46**: D1074–D1082.

Woods, C., et al. (2022). "Required Gene Set for Autotrophic Growth of Clostridium autoethanogenum." Applied and Environmental Microbiology **0**(0): e02479-02421.

World Health Organization (2020). WHO report on cancer. Setting priorities, investing wisely and providing care for all. Geneva.

Xiao, Y., et al. (2009). "RNA Interference-Mediated Silencing of Ornithine Decarboxylase and Spermidine Synthase Genes in Trypanosoma Brucei Provides Insight Into Regulation of Polyamine Biosynthesis." Eukaryot. Cell **8**(5): 747–755.

Xie, L. and D. I. C. Wang (1996). "Energy metabolism and ATP balance in animal cell cultivation using a stoichiometrically based reaction network." Biotechnology and Bioengineering **52**: 591-601.

Xie, S., et al. (2021). "Metabolic Control by Heat Stress Determining Cell Fate to Ferroptosis for Effective Cancer Therapy." ACS Nano **15**(4): 7179-7194.

Xu, W. T., et al. (2020). "Isoorientin induces the apoptosis and cell cycle arrest of A549 human lung cancer cells via the ROS-regulated MAPK, STAT3 and NF-κB signaling pathways." Int J Oncol **57**(2): 550-561.

Yadav, V. G., et al. (2012). "The future of metabolic engineering and synthetic biology: Towards a systematic practice." Metabolic Engineering **14**(3): 233-241.

Yaginuma, H., et al. (2014). "Diversity in ATP concentrations in a single bacterial cell population revealed by quantitative single-cell imaging." Sci. Rep **4**(6522).

Yamaji, M., et al. (2017). "Novel ATP-competitive Akt inhibitor afuresertib suppresses the proliferation of malignant pleural mesothelioma cells." Cancer Med **6**(11): 2646-2659.

Yang, B., et al. (2020). "Chelerythrine suppresses proliferation and metastasis of human prostate cancer cells via modulating MMP/TIMP/NF-κB system." Mol Cell Biochem **474**(1-2): 199-208.

Yang, C., et al. (2003). "Analysis of Escherichia coli anaplerotic metabolism and its regulation mechanisms from the metabolic responses to altered dilution rates and phosphoenolpyruvate carboxykinase knockout." Biotechnol Bioeng **84**(2): 129-144.

Yang, N., et al. (2017). "Scutellarin suppresses growth and causes apoptosis of human colorectal cancer cells by regulating the p53 pathway." Mol Med Rep **15**(2): 929-935.

Yang, P.-Y., et al. (2012). "Parasite-Based Screening and Proteome Profiling Reveal Orlistat, an FDA-Approved Drug, as a Potential Anti Trypanosoma brucei Agent[ ]." Chemistry – A European Journal **18**(27): 8403-8413.

Yee, P. P., et al. (2020). "Neutrophil-induced ferroptosis promotes tumor necrosis in glioblastoma progression." Nature Communications **11**(1): 5424.

Yin, J., et al. (2020). "ARS2/MAGL signaling in glioblastoma stem cells promotes self-renewal and M2-like polarization of tumor-associated macrophages." Nature Communications **11**(1): 2978.

Yoo, M., et al. (2015). "A Quantitative System-Scale Characterization of the Metabolism of Clostridium acetobutylicum." MBio **6**(6): e01808-01815.

Yoon, J., et al. (2007). "Modular decomposition of metabolic reaction networks based on flux analysis and pathway projection." Bioinformatics **23**(18): 2433-2440.

You, B. J., et al. (2019). "Orlistat Displays Antitumor Activity and Enhances the Efficacy of Paclitaxel in Human Hepatoma Hep3B Cells." Chem Res Toxicol **32**(2): 255-264.

Zafar, A., et al. (2018). "Deciphering the molecular mechanism underlying anticancer activity of coumestrol in triple-negative breast cancer cells." Toxicol In Vitro **46**: 19-28.

Zanghellini, J., et al. (2013). "Elementary flux modes in a nutshell: Properties, calculation and applications." Biotechnol. J. **8**: 1009–1016.

Zhang, W., et al. (2019). "Role of GDF15 in methylseleninic acid-mediated inhibition of cell proliferation and induction of apoptosis in prostate cancer cells." PLoS One **14**(9): e0222812.

Zhang, Z., et al. (2018). "Dynamic single-cell NAD(P)H measurement reveals oscillatory metabolism throughout the E. coli cell division cycle." Sci. Rep **8**(2162).

Zhao, H., et al. (2004). "Diverse effects of methylseleninic acid on the transcriptional program of human prostate cancer cells." Mol Biol Cell **15**(2): 506-519.

Zheng, Q., et al. (2014). "JAK2/STAT3 targeted therapy suppresses tumor invasion via disruption of the EGFRvIII/JAK2/STAT3 axis and associated focal adhesion in EGFRvIII-expressing glioblastoma." Neuro Oncol **16**(9): 1229-1243.

Zhou, Y., et al. (2019). "Crocin inhibits the migration, invasion, and epithelial-mesenchymal transition of gastric cancer cells via miR-320/KLF5/HIF-1α signaling." J Cell Physiol **234**(10): 17876-17885.

Zhu, X., et al. (2018). "Esculetin Attenuates the Growth of Lung Cancer by Downregulating Wnt Targeted Genes and Suppressing NF-κB." Arch Bronconeumol (Engl Ed) **54**(3): 128-133.

Zielinski, D., et al. (2017). "Systems biology analysis of drivers underlying hallmarks of cancer cell metabolism." Sci Rep **7**(41241).

Zimmerman, T., et al. (2019). "Choline Kinase Emerges as a Promising Drug Target in Gram-Positive Bacteria." Front. Microbiol. **6**(2146).

Zomer, A., et al. (1995). "Alkyl dihydroxyacetone phosphate synthase in glycosomes of Trypanosoma brucei." Biochimica et Biophysica Acta **1257**: 167-173.

Zomorrodi, A. R. and D. Segrè (2017). "Genome-driven evolutionary game theory helps understand the rise of metabolic interdependencies in microbial communities." Nature Communications **8**(1): 1563.

Zufferey, R., et al. (2017). "The Trypanosoma brucei dihydroxyacetonephosphate acyltransferase TbDAT is dispensable for normal growth but important for synthesis of ether glycerophospholipids." PLoS One **12**(7).

Appendix

"We demand rigidly defined areas of doubt and uncertainty!"

Douglas Adams,
The Hitchhiker's Guide to the Galaxy (1978)

Supporting information Chapter 2

S2-1 Appendix. Generation of directed graphs and side compounds.

a) Generation of directed graphs

Reconstructed metabolic networks model the interaction between substrates/products ('nodes') and the reactions connecting them ('edges') (Palsson 2006), as depicted below:

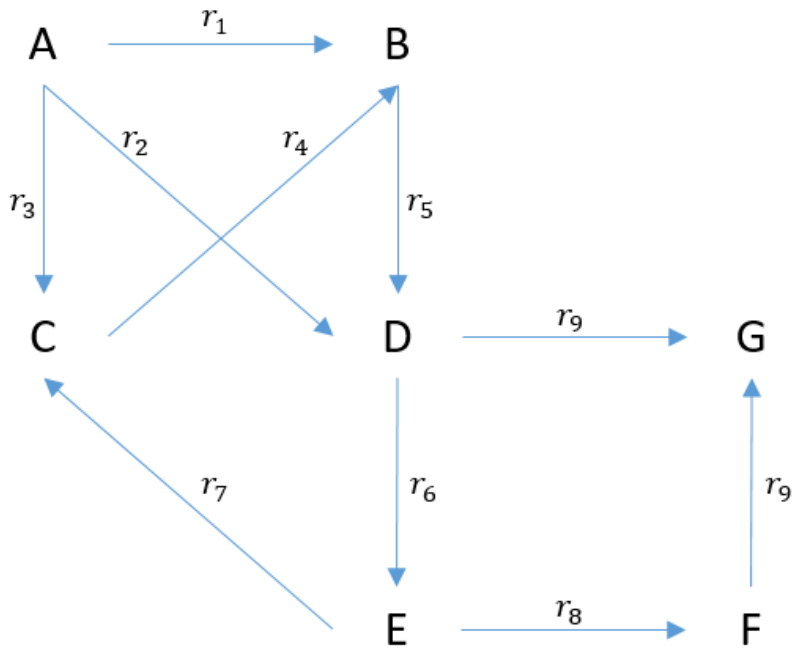


Fig. 1. Toy metabolic network, comprising 7 metabolites (A to G) and 9 reactions (r_1 to r_9). In particular, r_9 is a bimolecular reaction defined as $D + F \rightarrow G$.

Formally, these interactions can be described by means of a stoichiometric matrix S with m rows (metabolites) and n columns (reactions), where each element s_{ij} refers to the stoichiometric coefficient of metabolite m_i in reaction n_j.

$$S = \begin{pmatrix} -1 & -1 & -1 & 0 & 0 & 0 & 0 & 0 & 0 \\ 1 & 0 & 0 & 1 & -1 & 0 & 0 & 0 & 0 \\ 0 & 0 & 1 & -1 & 0 & 0 & 1 & 0 & 0 \\ 0 & 1 & 0 & 0 & 1 & -1 & 0 & 0 & -1 \\ 0 & 0 & 0 & 0 & 0 & 1 & -1 & -1 & 0 \\ 0 & 0 & 0 & 0 & 0 & 0 & 0 & 1 & -1 \\ 0 & 0 & 0 & 0 & 0 & 0 & 0 & 0 & 1 \end{pmatrix}$$

To study node connectivity and find the 'important' metabolites, S needs to be transformed into the adjacency matrix (A_x). In this case, both rows and columns refer to metabolites, and the value in the intersection is the number of times those two metabolites are connected (i.e. how many times they participate in the same reaction).

Depending on the considerations about the role of each metabolite in the reaction, two different scenario are found:

- *Undirected graph*: no information about the direction(s) of the reaction(s) are considered
- *Directed graph*: the direction(s) of the reaction(s) are considered

Centrality measures will be affected by the type of graph. In this study, the focus was on exploiting directionalities obtained from using thermodynamic constraints, so directed graphs were used. For the sake of completeness, both cases are explained here. A compound adjacency matrix for an undirected graph can be calculated as follows (Palsson 2006), where $\hat{S}$ is the binary form of S. For the toy model:

$$A_x^{undir} = \hat{S}\hat{S}^T$$

$$\hat{S} = \begin{pmatrix} 1 & 1 & 1 & 0 & 0 & 0 & 0 & 0 & 0 \\ 1 & 0 & 0 & 1 & 1 & 0 & 0 & 0 & 0 \\ 0 & 0 & 1 & 1 & 0 & 0 & 1 & 0 & 0 \\ 0 & 1 & 0 & 0 & 1 & 1 & 0 & 0 & 1 \\ 0 & 0 & 0 & 0 & 0 & 1 & 1 & 1 & 0 \\ 0 & 0 & 0 & 0 & 0 & 0 & 0 & 1 & 1 \\ 0 & 0 & 0 & 0 & 0 & 0 & 0 & 0 & 1 \end{pmatrix}$$

$$\hat{S}^T = \begin{pmatrix} 1 & 1 & 0 & 0 & 0 & 0 & 0 \\ 1 & 0 & 0 & 1 & 0 & 0 & 0 \\ 1 & 0 & 1 & 0 & 0 & 0 & 0 \\ 0 & 1 & 1 & 0 & 0 & 0 & 0 \\ 0 & 1 & 0 & 1 & 0 & 0 & 0 \\ 0 & 0 & 0 & 1 & 1 & 0 & 0 \\ 0 & 0 & 1 & 0 & 1 & 0 & 0 \\ 0 & 0 & 0 & 0 & 1 & 1 & 0 \\ 0 & 0 & 0 & 1 & 0 & 1 & 1 \end{pmatrix}$$

It is important to note that A_x^{undir} is symmetric, and elements in the diagonal $(a_x)_{ii}$ are equal to the number of reactions the metabolite m_i participates in.

$$A_x^{undir} = \begin{pmatrix} 3 & 1 & 1 & 1 & 0 & 0 & 0 \\ 1 & 3 & 1 & 1 & 0 & 0 & 0 \\ 1 & 1 & 3 & 0 & 1 & 0 & 0 \\ 1 & 1 & 0 & 4 & 1 & 1 & 1 \\ 0 & 0 & 1 & 1 & 3 & 1 & 0 \\ 0 & 0 & 0 & 1 & 1 & 2 & 1 \\ 0 & 0 & 0 & 1 & 0 & 1 & 1 \end{pmatrix}$$

With regards to A_x^{dir}, it can be manually obtained:

$$A_x^{dir} = \begin{pmatrix} 0 & 1 & 1 & 1 & 0 & 0 & 0 \\ 0 & 0 & 0 & 1 & 0 & 0 & 0 \\ 0 & 1 & 0 & 0 & 0 & 0 & 0 \\ 0 & 0 & 0 & 0 & 1 & 0 & 1 \\ 0 & 0 & 1 & 0 & 0 & 1 & 0 \\ 0 & 0 & 0 & 0 & 0 & 0 & 1 \\ 0 & 0 & 0 & 0 & 0 & 0 & 0 \end{pmatrix}$$

Since no straightforward method to calculate it from S could be found, an alternative approach was exploited. "Sweeping" elements in S allows gathering the indices of substrates ($s_{ij} < 0$) and products ($s_{ij} > 0$), which can be used as "coordinates" for A_x^{dir}: the connectivity $(a_x)_{ii}$ (considering the directionality) is determined by the intersection between the row (substrate) and the column (product). For example, r_4 corresponds to the element $(a_x)_{32}$, where the substrate is metabolite 'C' and the product metabolite 'B'. The plots below show how the A_x^{dir} generated by this algorithm matches the manual one.

In metabolic networks (such as *i*JO1366) there are reversible reactions, which are nonetheless defined in S following the most likely directionality. Therefore, a correction factor must be applied when considering genome-scale models, by taking the sign of the flux value after running the TFA. A directionality-corrected S can be generated, and used to obtain a A_x^{dir} ready for centrality measures.

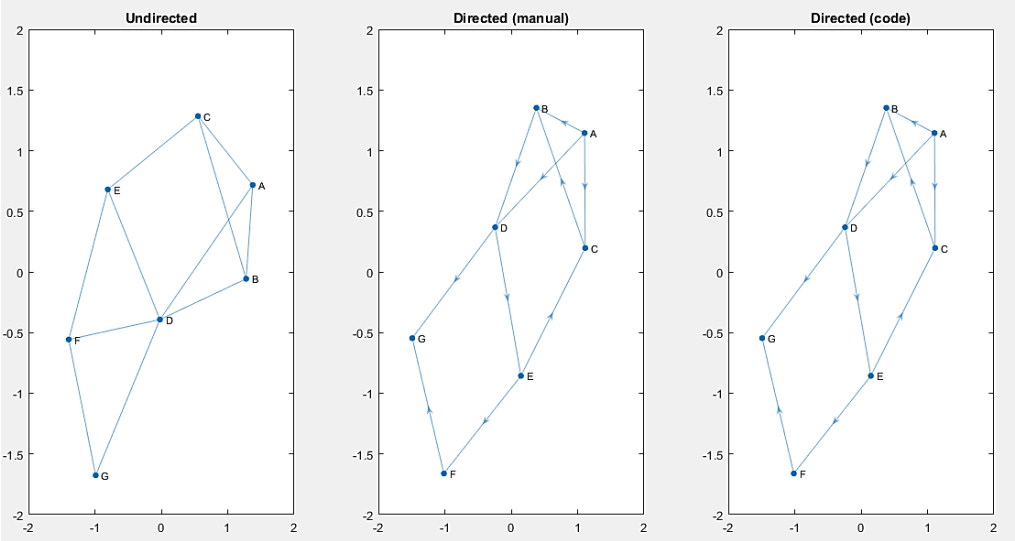
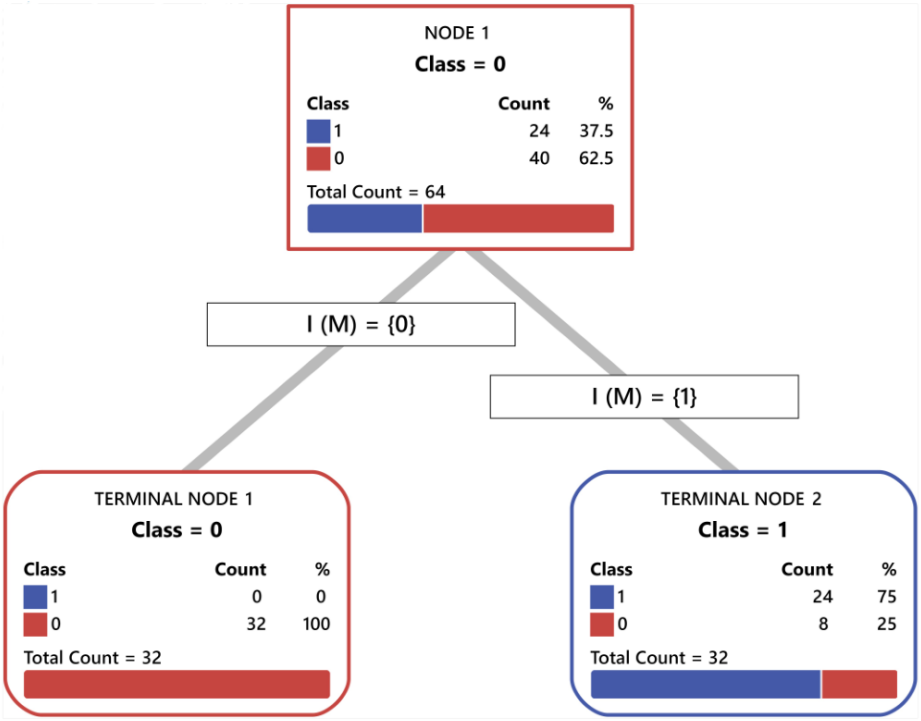


Fig. 2. Plots obtained from the same S. The 'undirected' graph was derived from A_x^{undir}, whereas A_x^{dir} was used for the second (manually obtained) and the third (script-derived) graphs. MATLAB's *graph* and *digraph* functions were used, respectively. It should be noted that in the undirected graph, the metabolite 'D' has 5 connections, as opposed to the 4 edges in the directed graph. This is due to the fact that r_9 is a bimolecular reaction, so even though both 'D' and 'F' are substrates, they appear as connected here.

S2-1 Figure. Optimal tree diagram.

Ionic strength (*I*) was the best predictor when classifying the simulated fluxomics and metabolomics data. Binary codification is the same followed in S2-3 Table. Retrieved from Minitab 19.



S2-1 Dataset. Metabolomics Keio database.

Subset of quantified metabolomics reported in Ishii et al. 2007 (Ishii, Nakahigashi et al. 2007) which are included in *this_tmodel.varNames* of the GSM processed in matTFA. Values for the wild type culture at 0.20 h-1 were considered. Values in mM.

Metabolites in GSM	RF02	RF03	RF04	RF05	RF06	Ave	SD	CV
for_e	0	0	0	0	0	0	0	0
pyr_e	0	0.000743	0.003766	0.000793	0.001536	0.001709	0.001418	0
ac_e	0	0.000304	0	0.005746	0.004466	0.002629	0.00291	0
glc-D_e	0	0.006328	0.010498	0.014081	0.004506	0.008853	0.004294	0
succoa_c				0.014863	0.003856	0.00936	0.007783	83.15573
succ_e	0	0.003411	0.027287	0.008771	0	0.009867	0.012161	0
trp-L_c			0.009387	0.012077		0.010732	0.001902	17.72346
dctp_c	0.035908	0.035415	0.017025	0.030495	0.008036	0.025376	0.012332	48.59865
fdp_c		0.031192			0.020667	0.025929	0.007442	28.70085
fad_c	0.035772	0.027334	0.037674	0.027943	0.004679	0.02668	0.01313	49.2115
met-L_c	0.034321	0.025815	0.030341	0.026168	0.042294	0.031788	0.006822	21.45989
ile-L_c			0.033148			0.033148		
tyr-L_c		0.027052	0.037769	0.045111	0.027892	0.034456	0.00861	24.98947
datp_c	0.075563	0.024847	0.058814	0.039253	0.002919	0.040279	0.028388	70.47688
f6p_c	0.054545	0.044968	0.05507	0.038978	0.025892	0.043891	0.012122	27.61802
phe-L_c	0.055718	0.051729	0.065726	0.054784	0.053513	0.056294	0.005481	9.735872
arg-L_c	0.043381	0.062449	0.057503	0.088754	0.032145	0.056846	0.021455	37.74285
g1p_c	0.015018	0.031685	0.033379	0.107071	0.130586	0.063548	0.051645	81.27036
his-L_c	0.059284	0.048775	0.052441	0.184068	0.047981	0.07851	0.059177	75.37569
nadp_c	0.095703	0.134635	0.110092	0.069918	0.026329	0.087336	0.041383	47.38414
pro-L_c	0.062523	0.071185	0.142775	0.116428	0.077862	0.094154	0.034109	36.22663
asn-L_c	0.073819	0.083396	0.102534	0.215597	0.084305	0.11193	0.058875	52.59935
leu-L_c		0.107227	0.120015			0.113621	0.009042	7.958331
pep_c	0.091135	0.174554			0.094574	0.120088	0.047201	39.30529
dhap_c					0.126233	0.126233		
pyr_c	0.128205					0.128205		
amet_c		0.166318	0.044188	0.203125	0.10756	0.130298	0.069601	53.41707
thr-L_c		0.088285	0.14715	0.264335	0.091457	0.147807	0.082255	55.64999
malcoa_c		0.181743	0.237499	0.173186	0.042678	0.158777	0.082485	51.95029
accoa_c	0.252281	0.262975	0.230366	0.182472	0.036411	0.192901	0.092788	48.10105
val-L_c		0.19869	0.181034	0.200864	0.222251	0.20071	0.016885	8.41252
s7p_c	0.216354	0.178013	0.333564	0.179788	0.200215	0.221587	0.064554	29.13255
pydx5p_c		0.243517				0.243517		

Metabolites in GSM	RF02	RF03	RF04	RF05	RF06	Ave	SD	CV
ctp_c	0.320167	0.370703	0.281761	0.259563	0.063668	0.259172	0.117145	45.19955
nadph_c			0.26743			0.26743		
gly_c	0.168028	0.156732	0.318135	0.596536	0.208347	0.289555	0.183071	63.22478
ser-L_c	0.201574	0.156231	0.342585	0.661201	0.181657	0.30865	0.209921	68.0128
ala-L_c	0.202503	0.182246	0.358487	0.627898	0.230268	0.320281	0.185146	57.80729
asp-L_c	0.241043	0.231043	0.336573	0.578863	0.25504	0.328512	0.146022	44.44954
lys-L_c	0.323442	0.388318	0.360666	0.198949	0.402221	0.334719	0.081644	24.39186
3pg_c	0.542791	0.746313		0.294777	0.441172	0.506263	0.189668	37.46425
adp_c	0.605284	0.889533	0.56421	0.579509	0.17272	0.562251	0.255442	45.43196
amp_c	0.65342	0.703891	0.699565	0.542918	0.253169	0.570593	0.188935	33.11214
gtp_c	0.676581	0.892424	0.588762	0.852358	0.126022	0.627229	0.306649	48.88953
utp_c	0.846153	0.887555	0.663136	0.647787	0.133982	0.635722	0.300142	47.21278
gln-L_c	0.569339	0.449426	0.494173	1.323343	0.370967	0.64145	0.387912	60.47426
nad_c	0.584897	0.762897	0.792675	1.251584	0.208828	0.720176	0.377244	52.3822
atp_c	1.262112	1.952016	1.30939	1.374135	0.263129	1.232156	0.609145	49.43735
glu-L_c	3.641547	3.019156	4.269149	3.263606	3.175011	3.473694	0.500219	14.40021

S2-2 Dataset. Variation of flux values among tests.

Showing reactions with a variance above the chosen tolerance ($> 10^{-4}$), Top 36/1705 reactions, where the green label refers to reactions for which ^{13}C-MFA is available. Columns 3-7 refer to the four non-redundant TFA-derived flux distributions.

#	Reaction	1(1)	2(3)	3(12)	5(20)	4(31)	VAR.S
1	NF_ACt2rpp	0.0E+00	-1.0E+02	0.0E+00	0.0E+00	-1.0E+02	3.0E+03
2	NF_ACt4pp	0.0E+00	1.0E+02	0.0E+00	0.0E+00	1.0E+02	3.0E+03
3	NF_NAt3pp	1.0E+02	1.0E+02	0.0E+00	0.0E+00	1.0E+02	3.0E+03
4	NF_PROt2rpp	0.0E+00	-1.4E-03	-1.0E+02	-1.0E+02	0.0E+00	3.0E+03
5	NF_PROt4pp	0.0E+00	1.4E-03	1.0E+02	1.0E+02	0.0E+00	3.0E+03
6	NF_CA2t3pp	0.0E+00	0.0E+00	1.0E+02	1.0E+02	0.0E+00	3.0E+03
7	NF_CAt6pp	-1.4E-03	-1.4E-03	-1.0E+02	-1.0E+02	-1.4E-03	3.0E+03
8	NF_GLYt2pp_copy2	-1.0E+02	0.0E+00	0.0E+00	0.0E+00	0.0E+00	2.0E+03
9	NF_GLYt4pp	1.0E+02	0.0E+00	0.0E+00	0.0E+00	0.0E+00	2.0E+03
10	NF_GLCtex_copy2	0.0E+00	2.9E+00	2.9E+00	2.9E+00	2.9E+00	1.7E+00
11	NF_GLCtex_copy1	2.9E+00	0.0E+00	0.0E+00	0.0E+00	0.0E+00	1.7E+00
12	NF_FBA	1.7E+00	0.0E+00	0.0E+00	2.0E+00	0.0E+00	1.0E+00
13	NF_PFK	1.7E+00	0.0E+00	0.0E+00	2.0E+00	0.0E+00	1.0E+00
14	NF_FBA3	3.0E-01	2.0E+00	2.3E+00	3.0E-01	2.0E+00	9.8E-01
15	NF_PFK_3	3.0E-01	2.0E+00	2.3E+00	3.0E-01	2.0E+00	9.8E-01
16	NF_TALA	0.0E+00	-1.7E+00	-2.0E+00	0.0E+00	-1.7E+00	9.8E-01
17	NF_ADK1	0.0E+00	8.9E-01	7.3E-01	7.3E-01	8.9E-01	1.4E-01
18	NF_PRPPS	-4.7E-01	2.6E-01	2.6E-01	2.6E-01	2.6E-01	1.1E-01
19	NF_PPM	-7.3E-01	0.0E+00	0.0E+00	0.0E+00	0.0E+00	1.1E-01
20	NF_R15BPK	7.3E-01	0.0E+00	0.0E+00	0.0E+00	0.0E+00	1.1E-01
21	NF_R1PK	7.3E-01	0.0E+00	0.0E+00	0.0E+00	0.0E+00	1.1E-01
22	NF_DHAPT	3.7E-01	3.7E-01	0.0E+00	0.0E+00	3.7E-01	4.2E-02
23	NF_F6PA	3.7E-01	3.7E-01	0.0E+00	0.0E+00	3.7E-01	4.2E-02
24	NF_PYK	0.0E+00	0.0E+00	3.7E-01	3.7E-01	0.0E+00	4.2E-02
25	NF_VALTA	0.0E+00	-2.8E-01	0.0E+00	-2.8E-01	-2.8E-01	2.3E-02
26	NF_VPAMTr	1.2E-01	-1.6E-01	1.2E-01	-1.6E-01	-1.6E-01	2.3E-02
27	NF_ALATA_L	-2.8E-01	0.0E+00	-2.8E-01	0.0E+00	0.0E+00	2.3E-02
28	NF_ACS	0.0E+00	1.6E-01	0.0E+00	0.0E+00	1.6E-01	7.9E-03
29	NF_PPK	-9.8E-01	-1.1E+00	-9.8E-01	-9.8E-01	-1.1E+00	7.9E-03
30	NF_ACKr	1.6E-01	0.0E+00	1.6E-01	1.6E-01	0.0E+00	7.9E-03
31	NF_PTAr	-1.6E-01	0.0E+00	-1.6E-01	-1.6E-01	0.0E+00	7.9E-03
32	NF_PAPSR	3.4E-02	6.9E-02	0.0E+00	0.0E+00	6.9E-02	1.2E-03
33	NF_TRDR	3.4E-02	6.9E-02	0.0E+00	0.0E+00	6.9E-02	1.2E-03
34	NF_GRXR	3.4E-02	0.0E+00	6.9E-02	6.9E-02	0.0E+00	1.2E-03
35	NF_GTHOr	3.4E-02	0.0E+00	6.9E-02	6.9E-02	0.0E+00	1.2E-03
36	NF_PAPSR2	3.4E-02	0.0E+00	6.9E-02	6.9E-02	0.0E+00	1.2E-03

S2-3 Dataset. Variation of concentration values among tests.

Showing metabolites with a variance above the chosen tolerance ($> 10^{-4}$) over the nine non-redundant sets of concentrations values. Top 7/972 metabolites, which do have an experimental counterpart from (Ishii, Nakahigashi et al. 2007) to compare with.

#	met	VAR.S
15	asp-L_c	6.12E-04
16	pep_c	5.60E-04
35	atp_c	2.77E-04
40	val-L_c	2.28E-04
41	pyr_c	2.19E-04
44	nadp_c	1.48E-04
46	fad_c	1.00E-04

S2-4 Dataset. PageRank scores.

Metabolites in the model with an experimental counterpart (Ishii, Nakahigashi et al. 2007) ranked according to their PR score: top 10% (green), top 30% (previous + amber), and top 50% (previous +red).

met name	node	PR score	pos
L-Glutamate	glu-L_c	0.017193	1
Pyruvate	pyr_c	0.012577	2
D-Fructose 6-phosphate	f6p_c	0.00794	4
Acetyl-CoA	accoa_c	0.007121	6
L-Methionine	met-L_c	0.007058	7
Succinyl-CoA	succoa_c	0.004591	23
L-Serine	ser-L_c	0.003406	44
Dihydroxyacetone phosphate	dhap_c	0.002905	69
L-Tryptophan	trp-L_c	0.002881	70
Phosphoenolpyruvate	pep_c	0.002605	88
S-Adenosyl-L-methionine	amet_c	0.002412	103
L-Alanine	ala-L_c	0.00214	129
L-Histidine	his-L_c	0.001968	157
D-Glucose 1-phosphate	g1p_c	0.001949	161
L-Proline	pro-L_c	0.001861	177
3-Phospho-D-glycerate	3pg_c	0.001844	181
D-Fructose 1,6-bisphosphate	fdp_c	0.001552	249
L-Leucine	leu-L_c	0.001522	258
L-Glutamine	gln-L_c	0.001122	338
DATP C10H12N5O12P3	datp_c	0.001113	342
DCTP C9H12N3O13P3	dctp_c	0.001113	343
Sedoheptulose 7-phosphate	s7p_c	0.001101	352
Glycine	gly_c	0.001097	354
L-Valine	val-L_c	0.000928	406
L-Lysine	lys-L_c	0.00091	412
L-Aspartate	asp-L_c	0.000903	413
L-Threonine	thr-L_c	0.00089	423
L-Arginine	arg-L_c	0.000859	427
Malonyl CoA C24H33N7O19P3S	malcoa_c	0.000714	483
L-Asparagine	asn-L_c	0.000561	516
L-Phenylalanine	phe-L_c	0.000426	605
L-Isoleucine	ile-L_c	0.000426	606
UTP C9H11N2O15P3	utp_c	0.000426	613
L-Tyrosine	tyr-L_c	0.000426	622

S2-5 Dataset. Comparison of flux distributions.

The optimal solution achieved by FBA was compared against the non-redundant solutions from TFA. Active in FBA, inactive in TFA: 68 (60 in the forward direction, 8 in the reverse). Inactive in FBA, active in TFA: 48 (30 in the forward direction, 18 in the reverse). Six of them were also measured via ^{13}C-MFA: ICL (971, isocitrate lyase), ME2 (1116, malic enzyme (NADP)), PDH (1316, pyruvate dehydrogenase). PGI (1343, glucose-6-phosphate isomerase), PPC (1438, phosphoenolpyruvate carboxylase) and SUCOAS (1582, succinyl-CoA synthetase (ADP-forming)).

#	Reaction name	FBA	1(1)	2(3)	3(12)	5(20)	4(31)
1	DM_4CRSOL	1.55E-04	1.79E-04	1.79E-04	1.79E-04	1.79E-04	1.79E-04
2	DM_5DRIB	1.62E-04	1.86E-04	1.86E-04	1.86E-04	1.86E-04	1.86E-04
3	DM_AMOB	1.39E-06	1.61E-06	1.61E-06	1.61E-06	1.61E-06	1.61E-06
4	DM_MTHTHF	9.30E-04	1.08E-03	1.08E-03	1.08E-03	1.08E-03	1.08E-03
5	DM_OXAM	1.00E-06	0.00E+00	0.00E+00	0.00E+00	0.00E+00	0.00E+00
6	Ec_biomass_iJO1366_WT_53p95M	6.93E-01	8.03E-01	8.03E-01	8.03E-01	8.03E-01	8.03E-01
7	DM_12ppd-R_e	2.00E-06	0.00E+00	0.00E+00	0.00E+00	0.00E+00	0.00E+00
8	DM_12ppd-S_e	1.00E-06	-2.84E-14	-2.84E-14	-2.84E-14	-2.84E-14	-2.84E-14
9	DM_15dap_e	1.00E-06	0.00E+00	0.00E+00	0.00E+00	0.00E+00	0.00E+00
10	DM_3hpp_e	1.00E-06	0.00E+00	0.00E+00	0.00E+00	0.00E+00	0.00E+00
11	DM_4abut_e	1.00E-06	0.00E+00	0.00E+00	0.00E+00	0.00E+00	0.00E+00
12	DM_5dglcn_e	1.00E-06	-2.84E-14	-2.84E-14	-2.84E-14	-2.84E-14	-2.84E-14
13	DM_5mtr_e	4.68E-03	5.42E-03	5.42E-03	5.42E-03	5.42E-03	5.42E-03
14	DM_LalaDgluMdap_e	1.00E-06	-2.84E-14	-2.84E-14	-2.84E-14	-2.84E-14	-2.84E-14
15	DM_LalaDgluMdapDala_e	1.00E-06	0.00E+00	0.00E+00	0.00E+00	0.00E+00	0.00E+00
16	DM_ac_e	1.00E-06	-2.84E-14	-2.84E-14	-2.84E-14	-2.84E-14	-2.84E-14
17	DM_acald_e	1.00E-06	-2.84E-14	-2.84E-14	-2.84E-14	-2.84E-14	-2.84E-14
18	DM_acolipa_e	0.00E+00	0.00E+00	0.00E+00	0.00E+00	0.00E+00	0.00E+00
19	DM_acser_e	1.00E-06	0.00E+00	0.00E+00	0.00E+00	0.00E+00	0.00E+00
20	DM_ade_e	1.00E-06	-2.84E-14	-2.84E-14	-2.84E-14	-2.84E-14	-2.84E-14
21	DM_adn_e	1.00E-06	0.00E+00	0.00E+00	0.00E+00	0.00E+00	0.00E+00
22	DM_agm_e	2.00E-06	-2.84E-14	-2.84E-14	-2.84E-14	-2.84E-14	-2.84E-14
23	DM_akg_e	1.00E-06	-2.84E-14	-2.84E-14	-2.84E-14	-2.84E-14	-2.84E-14
24	DM_ala-D_e	1.00E-06	-2.84E-14	-2.84E-14	-2.84E-14	-2.84E-14	-2.84E-14
25	DM_ala-L_e	1.00E-06	0.00E+00	0.00E+00	0.00E+00	0.00E+00	0.00E+00
26	DM_alaala_e	1.00E-06	-4.34E-19	0.00E+00	0.00E+00	0.00E+00	0.00E+00
27	DM_alltn_e	1.00E-06	-2.84E-14	-2.84E-14	-2.84E-14	-2.84E-14	-2.84E-14
28	DM_anhgm_e	1.00E-06	-2.84E-14	-2.84E-14	-2.84E-14	-2.84E-14	-2.84E-14
29	DM_arg-L_e	1.00E-06	-2.84E-14	-2.84E-14	-2.84E-14	-2.84E-14	-2.84E-14
30	DM_asn-L_e	1.00E-06	-5.68E-14	-5.68E-14	-5.68E-14	-5.68E-14	-5.68E-14
31	DM_asp-L_e	1.00E-06	-2.84E-14	-2.84E-14	-2.84E-14	-2.84E-14	-2.84E-14
32	DM_ca2_e	-3.43E-03	-3.98E-03	-3.98E-03	-3.98E-03	-3.98E-03	-3.98E-03
33	DM_cbl1_e	-1.55E-04	-1.79E-04	-1.79E-04	-1.79E-04	-1.79E-04	-1.79E-04
34	DM_cgly_e	1.00E-06	0.00E+00	0.00E+00	0.00E+00	0.00E+00	0.00E+00
35	DM_cit_e	1.00E-06	0.00E+00	0.00E+00	0.00E+00	0.00E+00	0.00E+00
36	DM_cl_e	-3.43E-03	-3.98E-03	-3.98E-03	-3.98E-03	-3.98E-03	-3.98E-03
37	DM_co2_e	2.06E+01	1.61E+01	1.61E+01	1.61E+01	1.61E+01	1.61E+01
38	DM_cobalt2_e	-1.66E-05	-1.93E-05	-1.93E-05	-1.93E-05	-1.93E-05	-1.93E-05
39	DM_colipa_e	1.00E-06	8.67E-19	0.00E+00	0.00E+00	0.00E+00	0.00E+00
40	DM_colipap_e	0.00E+00	0.00E+00	0.00E+00	0.00E+00	0.00E+00	0.00E+00
41	DM_cu2_e	-4.67E-04	-5.41E-04	-5.41E-04	-5.41E-04	-5.41E-04	-5.41E-04
42	DM_cys-L_e	1.00E-06	-2.84E-14	-2.84E-14	-2.84E-14	-2.84E-14	-2.84E-14
43	DM_cytd_e	1.00E-06	-2.84E-14	-2.84E-14	-2.84E-14	-2.84E-14	-2.84E-14
44	DM_dha_e	1.00E-06	-2.84E-14	-2.84E-14	-2.84E-14	-2.84E-14	-2.84E-14
45	DM_eca4colipa_e	0.00E+00	0.00E+00	0.00E+00	0.00E+00	0.00E+00	0.00E+00
46	DM_enlipa_e	2.00E-06	0.00E+00	0.00E+00	0.00E+00	0.00E+00	0.00E+00
47	DM_enter_e	1.00E-06	0.00E+00	0.00E+00	0.00E+00	0.00E+00	0.00E+00
48	DM_etha_e	1.00E-06	0.00E+00	0.00E+00	0.00E+00	0.00E+00	0.00E+00
49	DM_etoh_e	1.00E-06	-2.84E-14	-2.84E-14	-2.84E-14	-2.84E-14	-2.84E-14
50	DM_fe2_e	2.08E+00	-1.25E-02	-1.25E-02	-1.25E-02	-1.25E-02	-1.25E-02
51	DM_fe3_e	-2.09E+00	0.00E+00	0.00E+00	0.00E+00	0.00E+00	0.00E+00
52	DM_feenter_e	1.00E-06	0.00E+00	0.00E+00	0.00E+00	0.00E+00	0.00E+00
53	DM_for_e	1.00E-06	-2.84E-14	-2.84E-14	-2.84E-14	-2.84E-14	-2.84E-14
54	DM_g3pe_e	1.00E-06	-2.84E-14	-2.84E-14	-2.84E-14	-2.84E-14	-2.84E-14
55	DM_g3pg_e	1.00E-06	-2.84E-14	-2.84E-14	-2.84E-14	-2.84E-14	-2.84E-14

56	DM_glc_e	-8.16E+00	-8.16E+00	-8.16E+00	-8.16E+00	-8.16E+00	-8.16E+00
57	DM_glcn_e	1.00E-06	-2.84E-14	-2.84E-14	-2.84E-14	-2.84E-14	-2.84E-14
58	DM_glu-L_e	1.00E-06	-2.84E-14	-2.84E-14	-2.84E-14	-2.84E-14	-2.84E-14
59	DM_gly_e	1.00E-06	0.00E+00	0.00E+00	0.00E+00	0.00E+00	0.00E+00
60	DM_glyald_e	1.00E-06	-2.84E-14	-2.84E-14	-2.84E-14	-2.84E-14	-2.84E-14
61	DM_glyc_e	4.46E-03	-2.84E-14	-2.84E-14	-2.84E-14	-2.84E-14	-2.84E-14
62	DM_glyc-R_e	1.00E-06	-2.84E-14	-2.84E-14	-2.84E-14	-2.84E-14	-2.84E-14
63	DM_glycogenn1_c	-1.07E-01	-1.24E-01	-1.24E-01	-1.24E-01	-1.24E-01	-1.24E-01
64	DM_glyc3p_e	1.00E-06	-2.84E-14	-2.84E-14	-2.84E-14	-2.84E-14	-2.84E-14
65	DM_glyclt_e	1.00E-06	0.00E+00	-2.84E-14	0.00E+00	0.00E+00	0.00E+00
66	DM_gthrd_e	1.00E-06	0.00E+00	0.00E+00	0.00E+00	0.00E+00	0.00E+00
67	DM_gua_e	1.00E-06	0.00E+00	0.00E+00	0.00E+00	0.00E+00	0.00E+00
68	DM_h_e	8.37E+00	7.31E+00	7.31E+00	7.31E+00	7.31E+00	7.31E+00
69	DM_h2o_e	3.74E+01	3.68E+01	3.68E+01	3.68E+01	3.68E+01	3.68E+01
70	DM_h2s_e	1.00E-06	0.00E+00	0.00E+00	0.00E+00	0.00E+00	0.00E+00
71	DM_his-L_e	1.00E-06	-5.68E-14	-5.68E-14	-5.68E-14	-5.68E-14	-5.68E-14
72	DM_hom-L_e	1.00E-06	0.00E+00	0.00E+00	0.00E+00	0.00E+00	0.00E+00
73	DM_hxa_e	1.00E-06	-5.68E-14	-5.68E-14	-5.68E-14	-5.68E-14	-5.68E-14
74	DM_hxan_e	1.00E-06	-2.84E-14	-2.84E-14	-2.84E-14	-2.84E-14	-2.84E-14
75	DM_idon-L_e	2.00E-06	-2.84E-14	-2.84E-14	-2.84E-14	-2.84E-14	-2.84E-14
76	DM_ile-L_e	1.00E-06	-5.68E-14	-5.68E-14	-5.68E-14	-5.68E-14	-5.68E-14
77	DM_indole_e	1.00E-06	-2.84E-14	-2.84E-14	-2.84E-14	-2.84E-14	-2.84E-14
78	DM_ins_e	1.00E-06	0.00E+00	0.00E+00	0.00E+00	0.00E+00	0.00E+00
79	DM_k_e	-1.29E-01	-1.49E-01	-1.49E-01	-1.49E-01	-1.49E-01	-1.49E-01
80	DM_kdo2lipid4_e	1.00E-06	0.00E+00	0.00E+00	0.00E+00	0.00E+00	0.00E+00
81	DM_lac-D_e	1.00E-06	-2.84E-14	-2.84E-14	-2.84E-14	-2.84E-14	-2.84E-14
82	DM_lac-L_e	1.00E-06	-2.84E-14	-2.84E-14	-2.84E-14	-2.84E-14	-2.84E-14
83	DM_leu-L_e	1.00E-06	-5.68E-14	-5.68E-14	-5.68E-14	-5.68E-14	-5.68E-14
84	DM_lipa_e	1.00E-06	0.00E+00	0.00E+00	0.00E+00	0.00E+00	0.00E+00
85	DM_lipa_cold_e	1.00E-06	0.00E+00	0.00E+00	0.00E+00	0.00E+00	0.00E+00
86	DM_lys-L_e	1.00E-06	0.00E+00	0.00E+00	0.00E+00	0.00E+00	0.00E+00
87	DM_mal-L_e	1.00E-06	0.00E+00	0.00E+00	0.00E+00	0.00E+00	0.00E+00
88	DM_meoh_e	1.39E-06	1.61E-06	1.61E-06	1.61E-06	1.61E-06	1.61E-06
89	DM_mg2_e	-5.72E-03	-6.63E-03	-6.63E-03	-6.63E-03	-6.63E-03	-6.63E-03
90	DM_mn2_e	-4.56E-04	-5.28E-04	-5.28E-04	-5.28E-04	-5.28E-04	-5.28E-04
91	DM_mobd_e	-9.49E-05	-1.10E-04	-1.10E-04	-1.10E-04	-1.10E-04	-1.10E-04
92	DM_nh4_e	-7.28E+00	-8.44E+00	-8.44E+00	-8.44E+00	-8.44E+00	-8.44E+00
93	DM_ni2_e	-2.13E-04	-2.47E-04	-2.47E-04	-2.47E-04	-2.47E-04	-2.47E-04
94	DM_o2_e	-1.87E+01	-1.45E+01	-1.45E+01	-1.45E+01	-1.45E+01	-1.45E+01
95	DM_orn_e	1.00E-06	0.00E+00	0.00E+00	0.00E+00	0.00E+00	0.00E+00
96	DM_phe-L_e	1.00E-06	-2.84E-14	-2.84E-14	-2.84E-14	-2.84E-14	-2.84E-14
97	DM_pheme_e	1.00E-06	0.00E+00	0.00E+00	0.00E+00	0.00E+00	0.00E+00
98	DM_pi_e	-6.43E-01	-7.45E-01	-7.45E-01	-7.45E-01	-7.45E-01	-7.45E-01
99	DM_pro-L_e	1.00E-06	-2.84E-14	0.00E+00	-2.84E-14	0.00E+00	-2.84E-14
100	DM_ptrc_e	1.00E-06	0.00E+00	0.00E+00	0.00E+00	0.00E+00	0.00E+00
101	DM_pyr_e	1.00E-06	-2.84E-14	-2.84E-14	-2.84E-14	-2.84E-14	-2.84E-14
102	DM_quin_e	1.00E-06	-2.84E-14	-2.84E-14	-2.84E-14	-2.84E-14	-2.84E-14
103	DM_ser-L_e	1.00E-06	0.00E+00	0.00E+00	0.00E+00	0.00E+00	0.00E+00
104	DM_so4_e	-1.75E-01	-2.02E-01	-2.02E-01	-2.02E-01	-2.02E-01	-2.02E-01
105	DM_spmd_e	1.00E-06	0.00E+00	0.00E+00	0.00E+00	0.00E+00	0.00E+00
106	DM_succ_e	1.00E-06	-2.84E-14	-2.84E-14	-2.84E-14	-2.84E-14	-2.84E-14
107	DM_thr-L_e	1.00E-06	-2.84E-14	-2.84E-14	-2.84E-14	-2.84E-14	-2.84E-14
108	DM_thym_e	1.00E-06	0.00E+00	0.00E+00	0.00E+00	0.00E+00	0.00E+00
109	DM_thymd_e	1.00E-06	-2.84E-14	-2.84E-14	-2.84E-14	-2.84E-14	-2.84E-14
110	DM_trp-L_e	1.00E-06	-2.84E-14	-2.84E-14	-2.84E-14	-2.84E-14	-2.84E-14
111	DM_tyr-L_e	1.00E-06	-2.84E-14	-2.84E-14	-2.84E-14	-2.84E-14	-2.84E-14
112	DM_ura_e	1.00E-06	0.00E+00	0.00E+00	0.00E+00	0.00E+00	0.00E+00
113	DM_urea_e	1.00E-06	0.00E+00	0.00E+00	0.00E+00	0.00E+00	0.00E+00
114	DM_uri_e	1.00E-06	0.00E+00	0.00E+00	0.00E+00	0.00E+00	0.00E+00
115	DM_val-L_e	1.00E-06	-5.68E-14	-5.68E-14	-5.68E-14	-5.68E-14	-5.68E-14
116	DM_xan_e	1.00E-06	0.00E+00	0.00E+00	0.00E+00	0.00E+00	0.00E+00
117	DM_xtsn_e	1.00E-06	-2.84E-14	-2.84E-14	-2.84E-14	-2.84E-14	-2.84E-14
118	DM_zn2_e	-2.25E-04	-2.60E-04	-2.60E-04	-2.60E-04	-2.60E-04	-2.60E-04
119	12DGR120tipp	1.00E-06	0.00E+00	0.00E+00	0.00E+00	0.00E+00	0.00E+00
120	12DGR140tipp	1.00E-06	0.00E+00	0.00E+00	0.00E+00	0.00E+00	0.00E+00
121	12DGR141tipp	1.00E-06	0.00E+00	0.00E+00	0.00E+00	0.00E+00	0.00E+00
122	12DGR160tipp	2.00E-06	0.00E+00	0.00E+00	0.00E+00	0.00E+00	0.00E+00
123	12DGR161tipp	3.00E-06	0.00E+00	0.00E+00	0.00E+00	0.00E+00	0.00E+00
124	12DGR180tipp	3.00E-06	0.00E+00	0.00E+00	0.00E+00	0.00E+00	0.00E+00
125	12DGR181tipp	3.00E-06	0.00E+00	0.00E+00	0.00E+00	0.00E+00	0.00E+00
126	12PPDRtex	-2.00E-06	0.00E+00	0.00E+00	0.00E+00	0.00E+00	0.00E+00
127	12PPDRtpp	-2.00E-06	0.00E+00	0.00E+00	0.00E+00	0.00E+00	0.00E+00
128	12PPDStex	-1.00E-06	2.84E-14	2.84E-14	2.84E-14	2.84E-14	2.84E-14

129	12PPDStpp	-1.00E-06	2.84E-14	2.84E-14	2.84E-14	2.84E-14	2.84E-14
130	2AGPA120tipp	1.00E-06	0.00E+00	0.00E+00	0.00E+00	0.00E+00	0.00E+00
131	2AGPA140tipp	1.00E-06	0.00E+00	0.00E+00	0.00E+00	0.00E+00	0.00E+00
132	2AGPA141tipp	0.00E+00	0.00E+00	0.00E+00	0.00E+00	0.00E+00	0.00E+00
133	2AGPA160tipp	0.00E+00	0.00E+00	0.00E+00	0.00E+00	0.00E+00	0.00E+00
134	2AGPA161tipp	0.00E+00	0.00E+00	0.00E+00	0.00E+00	0.00E+00	0.00E+00
135	2AGPA180tipp	0.00E+00	0.00E+00	0.00E+00	0.00E+00	0.00E+00	0.00E+00
136	2AGPA181tipp	0.00E+00	0.00E+00	0.00E+00	0.00E+00	0.00E+00	0.00E+00
137	2AGPE120tipp	2.00E-06	0.00E+00	0.00E+00	0.00E+00	0.00E+00	0.00E+00
138	2AGPE140tipp	2.00E-06	0.00E+00	0.00E+00	0.00E+00	0.00E+00	0.00E+00
139	2AGPE141tipp	2.00E-06	0.00E+00	0.00E+00	0.00E+00	0.00E+00	0.00E+00
140	2AGPE160tipp	0.00E+00	0.00E+00	0.00E+00	0.00E+00	0.00E+00	0.00E+00
141	2AGPE161tipp	0.00E+00	0.00E+00	0.00E+00	0.00E+00	0.00E+00	0.00E+00
142	2AGPE180tipp	0.00E+00	0.00E+00	0.00E+00	0.00E+00	0.00E+00	0.00E+00
143	2AGPE181tipp	0.00E+00	0.00E+00	0.00E+00	0.00E+00	0.00E+00	0.00E+00
144	2AGPEAT120	1.00E-06	0.00E+00	0.00E+00	0.00E+00	0.00E+00	0.00E+00
145	2AGPEAT140	1.00E-06	0.00E+00	0.00E+00	0.00E+00	0.00E+00	0.00E+00
146	2AGPEAT141	1.00E-06	0.00E+00	0.00E+00	0.00E+00	0.00E+00	0.00E+00
147	2AGPEAT160	0.00E+00	0.00E+00	0.00E+00	0.00E+00	0.00E+00	0.00E+00
148	2AGPEAT161	0.00E+00	0.00E+00	0.00E+00	0.00E+00	0.00E+00	0.00E+00
149	2AGPEAT180	0.00E+00	0.00E+00	0.00E+00	0.00E+00	0.00E+00	0.00E+00
150	2AGPEAT181	0.00E+00	0.00E+00	0.00E+00	0.00E+00	0.00E+00	0.00E+00
151	2AGPG120tipp	2.00E-06	0.00E+00	0.00E+00	0.00E+00	0.00E+00	0.00E+00
152	2AGPG140tipp	2.00E-06	0.00E+00	0.00E+00	0.00E+00	0.00E+00	0.00E+00
153	2AGPG141tipp	2.00E-06	0.00E+00	0.00E+00	0.00E+00	0.00E+00	0.00E+00
154	2AGPG160tipp	0.00E+00	0.00E+00	0.00E+00	0.00E+00	0.00E+00	0.00E+00
155	2AGPG161tipp	0.00E+00	0.00E+00	0.00E+00	0.00E+00	0.00E+00	0.00E+00
156	2AGPG180tipp	0.00E+00	0.00E+00	0.00E+00	0.00E+00	0.00E+00	0.00E+00
157	2AGPG181tipp	0.00E+00	0.00E+00	0.00E+00	0.00E+00	0.00E+00	0.00E+00
158	2AGPGAT120	1.00E-06	0.00E+00	0.00E+00	0.00E+00	0.00E+00	0.00E+00
159	2AGPGAT140	1.00E-06	0.00E+00	0.00E+00	0.00E+00	0.00E+00	0.00E+00
160	2AGPGAT141	1.00E-06	0.00E+00	0.00E+00	0.00E+00	0.00E+00	0.00E+00
161	2AGPGAT160	0.00E+00	0.00E+00	0.00E+00	0.00E+00	0.00E+00	0.00E+00
162	2AGPGAT161	0.00E+00	0.00E+00	0.00E+00	0.00E+00	0.00E+00	0.00E+00
163	2AGPGAT180	0.00E+00	0.00E+00	0.00E+00	0.00E+00	0.00E+00	0.00E+00
164	2AGPGAT181	0.00E+00	0.00E+00	0.00E+00	0.00E+00	0.00E+00	0.00E+00
165	2MAHMP	1.00E-06	0.00E+00	0.00E+00	0.00E+00	0.00E+00	0.00E+00
166	3AMACHYD	1.00E-06	0.00E+00	0.00E+00	0.00E+00	0.00E+00	0.00E+00
167	3HAD100	9.91E-02	0.00E+00	0.00E+00	0.00E+00	0.00E+00	0.00E+00
168	3HAD120	3.00E-06	0.00E+00	0.00E+00	0.00E+00	0.00E+00	0.00E+00
169	3HAD121	9.91E-02	0.00E+00	0.00E+00	0.00E+00	0.00E+00	0.00E+00
170	3HAD140	2.00E-06	0.00E+00	0.00E+00	0.00E+00	0.00E+00	0.00E+00
171	3HAD141	9.91E-02	0.00E+00	0.00E+00	0.00E+00	0.00E+00	0.00E+00
172	3HAD160	8.41E-02	0.00E+00	0.00E+00	0.00E+00	0.00E+00	0.00E+00
173	3HAD161	9.91E-02	7.58E-02	7.58E-02	7.58E-02	7.58E-02	7.58E-02
174	3HAD180	0.00E+00	0.00E+00	0.00E+00	0.00E+00	0.00E+00	0.00E+00
175	3HAD181	3.37E-02	0.00E+00	0.00E+00	0.00E+00	0.00E+00	0.00E+00
176	3HAD40	3.00E-06	0.00E+00	0.00E+00	0.00E+00	0.00E+00	0.00E+00
177	3HAD60	3.00E-06	0.00E+00	0.00E+00	0.00E+00	0.00E+00	0.00E+00
178	3HAD80	3.00E-06	0.00E+00	0.00E+00	0.00E+00	0.00E+00	0.00E+00
179	3HPPtex	-1.00E-06	0.00E+00	0.00E+00	0.00E+00	0.00E+00	0.00E+00
180	3HPPtpp	1.00E-06	0.00E+00	0.00E+00	0.00E+00	0.00E+00	0.00E+00
181	3OAR100	9.91E-02	0.00E+00	0.00E+00	0.00E+00	0.00E+00	0.00E+00
182	3OAR120	3.00E-06	0.00E+00	0.00E+00	0.00E+00	0.00E+00	0.00E+00
183	3OAR121	9.91E-02	0.00E+00	0.00E+00	0.00E+00	0.00E+00	0.00E+00
184	3OAR140	2.26E-02	2.62E-02	2.62E-02	2.62E-02	2.62E-02	2.62E-02
185	3OAR141	9.91E-02	0.00E+00	0.00E+00	0.00E+00	0.00E+00	0.00E+00
186	3OAR160	8.41E-02	0.00E+00	0.00E+00	0.00E+00	0.00E+00	0.00E+00
187	3OAR161	9.91E-02	7.58E-02	7.58E-02	7.58E-02	7.58E-02	7.58E-02
188	3OAR180	0.00E+00	0.00E+00	0.00E+00	0.00E+00	0.00E+00	0.00E+00
189	3OAR181	3.37E-02	0.00E+00	0.00E+00	0.00E+00	0.00E+00	0.00E+00
190	3OAR40	3.00E-06	0.00E+00	0.00E+00	0.00E+00	0.00E+00	0.00E+00
191	3OAR60	3.00E-06	0.00E+00	0.00E+00	0.00E+00	0.00E+00	0.00E+00
192	3OAR80	3.00E-06	0.00E+00	0.00E+00	0.00E+00	0.00E+00	0.00E+00
193	3OAS100	9.91E-02	0.00E+00	0.00E+00	0.00E+00	0.00E+00	0.00E+00
194	3OAS120	3.00E-06	0.00E+00	0.00E+00	0.00E+00	0.00E+00	0.00E+00
195	3OAS121	9.91E-02	0.00E+00	0.00E+00	0.00E+00	0.00E+00	0.00E+00
196	3OAS140	2.26E-02	2.62E-02	2.62E-02	2.62E-02	2.62E-02	2.62E-02
197	3OAS141	9.91E-02	0.00E+00	0.00E+00	0.00E+00	0.00E+00	0.00E+00
198	3OAS160	8.41E-02	0.00E+00	0.00E+00	0.00E+00	0.00E+00	0.00E+00
199	3OAS161	9.91E-02	7.58E-02	7.58E-02	7.58E-02	7.58E-02	7.58E-02
200	3OAS180	0.00E+00	0.00E+00	0.00E+00	0.00E+00	0.00E+00	0.00E+00
201	3OAS181	3.37E-02	0.00E+00	0.00E+00	0.00E+00	0.00E+00	0.00E+00

202	3OAS60	3.00E-06	0.00E+00	0.00E+00	0.00E+00	0.00E+00	0.00E+00
203	3OAS80	3.00E-06	0.00E+00	0.00E+00	0.00E+00	0.00E+00	0.00E+00
204	3PEPTabcpp	1.00E-06	0.00E+00	0.00E+00	0.00E+00	0.00E+00	0.00E+00
205	3PEPTtex	-1.00E-06	2.84E-14	2.84E-14	2.84E-14	2.84E-14	2.84E-14
206	4PCP	1.00E-06	0.00E+00	0.00E+00	0.00E+00	0.00E+00	0.00E+00
207	4PCPpp	1.00E-06	0.00E+00	0.00E+00	0.00E+00	0.00E+00	0.00E+00
208	4PEPTabcpp	1.00E-06	0.00E+00	0.00E+00	0.00E+00	0.00E+00	0.00E+00
209	4PEPTtex	-1.00E-06	0.00E+00	0.00E+00	0.00E+00	0.00E+00	0.00E+00
210	5DGLCNR	-3.00E-06	0.00E+00	0.00E+00	0.00E+00	0.00E+00	0.00E+00
211	5DGLCNt2rpp	-1.00E-06	2.84E-14	2.84E-14	2.84E-14	2.84E-14	2.84E-14
212	5DGLCNtex	-1.00E-06	2.84E-14	2.84E-14	2.84E-14	2.84E-14	2.84E-14
213	5DOAN	1.62E-04	1.86E-04	1.86E-04	1.86E-04	1.86E-04	1.86E-04
214	5MTRtex	-4.68E-03	-5.42E-03	-5.42E-03	-5.42E-03	-5.42E-03	-5.42E-03
215	5MTRtpp	4.68E-03	5.42E-03	5.42E-03	5.42E-03	5.42E-03	5.42E-03
216	A5PISO	1.70E-02	1.96E-02	1.96E-02	1.96E-02	1.96E-02	1.96E-02
217	AACPS1	8.97E-02	6.55E-03	6.55E-03	6.55E-03	6.55E-03	6.55E-03
218	AACPS2	1.10E-05	7.58E-02	7.58E-02	7.58E-02	7.58E-02	7.58E-02
219	AACPS3	2.00E-06	9.74E-02	9.74E-02	9.74E-02	9.74E-02	9.74E-02
220	AACPS4	2.00E-06	0.00E+00	0.00E+00	0.00E+00	0.00E+00	0.00E+00
221	AACPS5	1.00E-06	3.91E-02	3.91E-02	3.91E-02	3.91E-02	3.91E-02
222	AACPS6	1.00E-06	0.00E+00	0.00E+00	0.00E+00	0.00E+00	0.00E+00
223	AACPS7	2.83E-02	3.27E-02	3.27E-02	3.27E-02	3.27E-02	3.27E-02
224	AACPS8	2.00E-06	0.00E+00	0.00E+00	0.00E+00	0.00E+00	0.00E+00
225	AACPS9	9.91E-02	2.41E-06	2.41E-06	2.41E-06	2.41E-06	2.41E-06
226	AACTOOR	7.00E-06	0.00E+00	0.00E+00	0.00E+00	0.00E+00	0.00E+00
227	AADDGT	0.00E+00	0.00E+00	0.00E+00	0.00E+00	0.00E+00	0.00E+00
228	ABTA	2.00E-06	0.00E+00	0.00E+00	0.00E+00	0.00E+00	0.00E+00
229	ABUTD	1.00E-06	0.00E+00	0.00E+00	0.00E+00	0.00E+00	0.00E+00
230	ABUTt2pp	1.00E-06	0.00E+00	0.00E+00	0.00E+00	0.00E+00	0.00E+00
231	ABUTtex	-1.00E-06	0.00E+00	0.00E+00	0.00E+00	0.00E+00	0.00E+00
232	ACACT1r	2.17E-01	2.52E-01	2.52E-01	2.52E-01	2.52E-01	2.52E-01
233	ACACT2r	2.17E-01	2.52E-01	2.52E-01	2.52E-01	2.52E-01	2.52E-01
234	ACACT3r	2.17E-01	2.52E-01	2.52E-01	2.52E-01	2.52E-01	2.52E-01
235	ACACT4r	1.18E-01	2.52E-01	2.52E-01	2.52E-01	2.52E-01	2.52E-01
236	ACACT5r	1.18E-01	2.52E-01	2.52E-01	2.52E-01	2.52E-01	2.52E-01
237	ACACT6r	8.97E-02	2.19E-01	2.19E-01	2.19E-01	2.19E-01	2.19E-01
238	ACACT7r	0.00E+00	1.36E-01	1.36E-01	1.36E-01	1.36E-01	1.36E-01
239	ACACT8r	0.00E+00	-3.91E-02	-3.91E-02	-3.91E-02	-3.91E-02	-3.91E-02
240	ACALD	1.00E-05	0.00E+00	0.00E+00	0.00E+00	0.00E+00	0.00E+00
241	ACALDtex	-1.00E-06	2.84E-14	2.84E-14	2.84E-14	2.84E-14	2.84E-14
242	ACALDtpp	-1.00E-06	2.84E-14	2.84E-14	2.84E-14	2.84E-14	2.84E-14
243	ACCOAC	5.37E-01	1.02E-01	1.02E-01	1.02E-01	1.02E-01	1.02E-01
244	ACCOAL	2.00E-06	0.00E+00	0.00E+00	0.00E+00	0.00E+00	0.00E+00
245	ACGAMK	8.00E-06	0.00E+00	0.00E+00	0.00E+00	0.00E+00	0.00E+00
246	ACGAMT	0.00E+00	0.00E+00	0.00E+00	0.00E+00	0.00E+00	0.00E+00
247	ACGK	2.27E-01	2.63E-01	2.63E-01	2.63E-01	2.63E-01	2.63E-01
248	ACGS	2.27E-01	2.63E-01	2.63E-01	2.63E-01	2.63E-01	2.63E-01
249	ACHBS	1.96E-01	2.27E-01	2.27E-01	2.27E-01	2.27E-01	2.27E-01
250	ACKr	4.10E-01	4.75E-01	4.75E-01	4.75E-01	4.75E-01	4.75E-01
251	ACLS	5.89E-01	6.82E-01	6.82E-01	6.82E-01	6.82E-01	6.82E-01
252	ACM6PH	8.00E-06	0.00E+00	0.00E+00	0.00E+00	0.00E+00	0.00E+00
253	ACMAMUT	0.00E+00	0.00E+00	0.00E+00	0.00E+00	0.00E+00	0.00E+00
254	ACOAD1f	-2.17E-01	-2.52E-01	-2.52E-01	-2.52E-01	-2.52E-01	-2.52E-01
255	ACOAD2f	-2.17E-01	-2.52E-01	-2.52E-01	-2.52E-01	-2.52E-01	-2.52E-01
256	ACOAD3f	-2.17E-01	-2.52E-01	-2.52E-01	-2.52E-01	-2.52E-01	-2.52E-01
257	ACOAD4f	-1.18E-01	-2.52E-01	-2.52E-01	-2.52E-01	-2.52E-01	-2.52E-01
258	ACOAD5f	-1.18E-01	-2.52E-01	-2.52E-01	-2.52E-01	-2.52E-01	-2.52E-01
259	ACOAD6f	-8.97E-02	-1.43E-01	-1.43E-01	-1.43E-01	-1.43E-01	-1.43E-01
260	ACOAD7f	0.00E+00	-1.36E-01	-1.36E-01	-1.36E-01	-1.36E-01	-1.36E-01
261	ACOAD8f	0.00E+00	0.00E+00	0.00E+00	0.00E+00	0.00E+00	0.00E+00
262	ACOATA	1.00E-06	0.00E+00	0.00E+00	0.00E+00	0.00E+00	0.00E+00
263	ACODA	2.27E-01	2.63E-01	2.63E-01	2.63E-01	2.63E-01	2.63E-01
264	ACOLIPAabctex	0.00E+00	0.00E+00	0.00E+00	0.00E+00	0.00E+00	0.00E+00
265	ACONTa	4.02E+00	4.10E+00	4.10E+00	4.10E+00	4.10E+00	4.10E+00
266	ACONTb	4.02E+00	4.10E+00	4.10E+00	4.10E+00	4.10E+00	4.10E+00
267	ACOTA	-2.27E-01	-2.63E-01	-2.63E-01	-2.63E-01	-2.63E-01	-2.63E-01
268	ACPPAT120	2.00E-06	0.00E+00	0.00E+00	0.00E+00	0.00E+00	0.00E+00
269	ACPPAT140	6.00E-06	0.00E+00	0.00E+00	0.00E+00	0.00E+00	0.00E+00
270	ACPPAT141	2.00E-06	0.00E+00	0.00E+00	0.00E+00	0.00E+00	0.00E+00
271	ACPPAT160	2.00E-06	4.87E-02	0.00E+00	0.00E+00	0.00E+00	0.00E+00
272	ACPPAT161	2.00E-06	0.00E+00	0.00E+00	0.00E+00	3.79E-02	3.79E-02
273	ACPPAT180	1.00E-06	0.00E+00	0.00E+00	0.00E+00	0.00E+00	0.00E+00
274	ACPPAT181	2.00E-06	1.95E-02	1.95E-02	0.00E+00	0.00E+00	1.95E-02

275	ACS	1.00E-06	0.00E+00	0.00E+00	0.00E+00	0.00E+00	0.00E+00
276	ACSERtex	-1.00E-06	0.00E+00	0.00E+00	0.00E+00	0.00E+00	0.00E+00
277	ACSERtpp	1.00E-06	0.00E+00	0.00E+00	0.00E+00	0.00E+00	0.00E+00
278	ACt2rpp	-2.00E-06	-1.00E+02	-1.00E+02	-1.00E+02	-1.00E+02	-1.00E+02
279	ACt4pp	1.00E-06	1.00E+02	1.00E+02	1.00E+02	1.00E+02	1.00E+02
280	ACtex	-1.00E-06	2.84E-14	2.84E-14	2.84E-14	2.84E-14	2.84E-14
281	ADA	1.00E-06	0.00E+00	0.00E+00	0.00E+00	0.00E+00	0.00E+00
282	ADCL	6.18E-04	7.16E-04	7.16E-04	7.16E-04	7.16E-04	7.16E-04
283	ADCS	6.18E-04	7.16E-04	7.16E-04	7.16E-04	7.16E-04	7.16E-04
284	ADD	1.00E-06	0.00E+00	0.00E+00	0.00E+00	0.00E+00	0.00E+00
285	ADEt2rpp	-1.00E-06	2.84E-14	2.84E-14	2.84E-14	2.84E-14	2.84E-14
286	ADEtex	-1.00E-06	2.84E-14	2.84E-14	2.84E-14	2.84E-14	2.84E-14
287	ADK1	1.76E+00	1.93E+00	-2.84E-14	1.31E+00	1.31E+00	-2.84E-14
288	ADK3	1.00E-06	-6.22E-01	2.04E+00	0.00E+00	0.00E+00	2.04E+00
289	ADK4	-1.00E-06	0.00E+00	0.00E+00	0.00E+00	0.00E+00	0.00E+00
290	ADMDC	4.68E-03	5.42E-03	5.42E-03	5.42E-03	5.42E-03	5.42E-03
291	ADNCYC	1.00E-06	0.00E+00	0.00E+00	0.00E+00	0.00E+00	0.00E+00
292	ADNK1	1.00E-06	6.68E-03	6.68E-03	6.68E-03	6.68E-03	6.68E-03
293	ADNUC	1.00E-06	0.00E+00	0.00E+00	0.00E+00	0.00E+00	0.00E+00
294	ADNt2pp	1.00E+02	0.00E+00	0.00E+00	0.00E+00	0.00E+00	0.00E+00
295	ADNt2rpp	-1.00E+02	0.00E+00	0.00E+00	0.00E+00	0.00E+00	0.00E+00
296	ADNtex	-1.00E-06	0.00E+00	0.00E+00	0.00E+00	0.00E+00	0.00E+00
297	ADPRDP	1.00E-06	0.00E+00	0.00E+00	0.00E+00	0.00E+00	0.00E+00
298	ADPT	5.77E-03	0.00E+00	0.00E+00	0.00E+00	0.00E+00	0.00E+00
299	ADSK	1.72E-01	1.99E-01	1.99E-01	1.99E-01	1.99E-01	1.99E-01
300	ADSL1r	2.01E-01	2.33E-01	2.33E-01	2.33E-01	2.33E-01	2.33E-01
301	ADSL2r	3.01E-01	3.49E-01	3.49E-01	3.49E-01	3.49E-01	3.49E-01
302	ADSS	2.01E-01	2.33E-01	2.33E-01	2.33E-01	2.33E-01	2.33E-01
303	AGDC	1.60E-05	0.00E+00	0.00E+00	0.00E+00	0.00E+00	0.00E+00
304	AGM3PA	1.00E-06	0.00E+00	0.00E+00	0.00E+00	0.00E+00	0.00E+00
305	AGM3PApp	1.00E-06	0.00E+00	0.00E+00	0.00E+00	0.00E+00	0.00E+00
306	AGM3PH	1.00E-06	0.00E+00	0.00E+00	0.00E+00	0.00E+00	0.00E+00
307	AGM3Pt2pp	1.00E-06	0.00E+00	0.00E+00	0.00E+00	0.00E+00	0.00E+00
308	AGM4PA	1.00E-06	0.00E+00	0.00E+00	0.00E+00	0.00E+00	0.00E+00
309	AGM4PApp	3.00E-06	0.00E+00	0.00E+00	0.00E+00	0.00E+00	0.00E+00
310	AGM4PCP	1.00E-06	0.00E+00	0.00E+00	0.00E+00	0.00E+00	0.00E+00
311	AGM4PCPpp	1.00E-06	0.00E+00	0.00E+00	0.00E+00	0.00E+00	0.00E+00
312	AGM4PH	2.00E-06	0.00E+00	0.00E+00	0.00E+00	0.00E+00	0.00E+00
313	AGM4Pt2pp	4.00E-06	0.00E+00	0.00E+00	0.00E+00	0.00E+00	0.00E+00
314	AGMH	5.00E-06	0.00E+00	0.00E+00	0.00E+00	0.00E+00	0.00E+00
315	AGMHE	2.26E-02	2.62E-02	2.62E-02	2.62E-02	2.62E-02	2.62E-02
316	AGMT	1.00E-06	0.00E+00	0.00E+00	0.00E+00	0.00E+00	0.00E+00
317	AGMt2pp	3.00E-06	0.00E+00	0.00E+00	0.00E+00	0.00E+00	0.00E+00
318	AGMtex	-2.00E-06	2.84E-14	2.84E-14	2.84E-14	2.84E-14	2.84E-14
319	AGPAT120	7.00E-06	0.00E+00	0.00E+00	0.00E+00	0.00E+00	0.00E+00
320	AGPAT140	6.00E-06	0.00E+00	0.00E+00	0.00E+00	0.00E+00	0.00E+00
321	AGPAT141	5.00E-06	0.00E+00	0.00E+00	0.00E+00	0.00E+00	0.00E+00
322	AGPAT160	4.20E-02	4.87E-02	4.87E-02	4.87E-02	4.87E-02	4.87E-02
323	AGPAT161	3.27E-02	3.79E-02	3.79E-02	3.79E-02	3.79E-02	3.79E-02
324	AGPAT180	0.00E+00	0.00E+00	0.00E+00	0.00E+00	0.00E+00	0.00E+00
325	AGPAT181	1.69E-02	1.95E-02	1.95E-02	1.95E-02	1.95E-02	1.95E-02
326	AGPR	-2.27E-01	-2.63E-01	-2.63E-01	-2.63E-01	-2.63E-01	-2.63E-01
327	AHCYSNS	9.30E-04	1.08E-03	1.08E-03	1.08E-03	1.08E-03	1.08E-03
328	AICART	3.65E-01	4.23E-01	4.23E-01	4.23E-01	4.23E-01	4.23E-01
329	AIRC2	3.01E-01	3.49E-01	3.49E-01	3.49E-01	3.49E-01	3.49E-01
330	AIRC3	-3.01E-01	-3.49E-01	-3.49E-01	-3.49E-01	-3.49E-01	-3.49E-01
331	AKGDH	3.59E-01	3.23E+00	3.23E+00	3.23E+00	3.23E+00	3.23E+00
332	AKGt2rpp	-1.00E-06	2.84E-14	2.84E-14	2.84E-14	2.84E-14	2.84E-14
333	AKGtex	-1.00E-06	2.84E-14	2.84E-14	2.84E-14	2.84E-14	2.84E-14
334	ALAALAD	1.00E-06	0.00E+00	0.00E+00	0.00E+00	0.00E+00	0.00E+00
335	ALAALAabcpp	2.28E-03	2.65E-03	2.65E-03	2.65E-03	2.65E-03	2.65E-03
336	ALAALAr	1.68E-02	1.95E-02	1.95E-02	1.95E-02	1.95E-02	1.95E-02
337	ALAALAtex	-1.00E-06	4.34E-19	0.00E+00	0.00E+00	0.00E+00	0.00E+00
338	ALAGLUE	0.00E+00	-2.84E-14	-2.84E-14	-2.84E-14	-2.84E-14	-2.84E-14
339	ALAR	1.68E-02	1.95E-02	1.95E-02	1.95E-02	1.95E-02	1.95E-02
340	ALATA_D2	1.00E-06	0.00E+00	0.00E+00	0.00E+00	0.00E+00	0.00E+00
341	ALATA_L	9.93E+01	-7.71E-01	-7.71E-01	0.00E+00	0.00E+00	-7.71E-01
342	ALATA_L2	1.00E-06	0.00E+00	0.00E+00	0.00E+00	0.00E+00	0.00E+00
343	ALAabcpp	1.00E-06	0.00E+00	0.00E+00	0.00E+00	0.00E+00	0.00E+00
344	ALAt2pp	1.00E-06	0.00E+00	0.00E+00	0.00E+00	0.00E+00	0.00E+00
345	ALAt2rpp	-4.00E-06	0.00E+00	0.00E+00	0.00E+00	0.00E+00	0.00E+00
346	ALAt4pp	1.00E-06	0.00E+00	0.00E+00	0.00E+00	0.00E+00	0.00E+00
347	ALAtex	-1.00E-06	0.00E+00	0.00E+00	0.00E+00	0.00E+00	0.00E+00

348	ALCD19	-1.00E-06	2.84E-14	2.84E-14	2.84E-14	2.84E-14	2.84E-14
349	ALCD2x	-1.00E-06	2.84E-14	2.84E-14	2.84E-14	2.84E-14	2.84E-14
350	ALDD2x	1.00E-06	0.00E+00	0.00E+00	0.00E+00	0.00E+00	0.00E+00
351	ALDD2y	1.00E-06	0.00E+00	0.00E+00	0.00E+00	0.00E+00	0.00E+00
352	ALLTAMH	2.00E-06	0.00E+00	0.00E+00	0.00E+00	0.00E+00	0.00E+00
353	ALLTN	2.00E-06	0.00E+00	0.00E+00	0.00E+00	0.00E+00	0.00E+00
354	ALLTNt2rpp	-1.00E-06	2.84E-14	2.84E-14	2.84E-14	2.84E-14	2.84E-14
355	ALLTNtex	-1.00E-06	2.84E-14	2.84E-14	2.84E-14	2.84E-14	2.84E-14
356	ALR2	1.00E-06	0.00E+00	0.00E+00	0.00E+00	0.00E+00	0.00E+00
357	ALR4x	1.00E-06	0.00E+00	0.00E+00	0.00E+00	0.00E+00	0.00E+00
358	AM3PA	2.00E-06	0.00E+00	0.00E+00	0.00E+00	0.00E+00	0.00E+00
359	AM4PA	1.00E-06	0.00E+00	0.00E+00	0.00E+00	0.00E+00	0.00E+00
360	AM4PCP	1.00E-06	0.00E+00	0.00E+00	0.00E+00	0.00E+00	0.00E+00
361	AMAOTr	1.39E-06	1.61E-06	1.61E-06	1.61E-06	1.61E-06	1.61E-06
362	AMMQLT8	1.55E-04	1.79E-04	1.79E-04	1.79E-04	1.79E-04	1.79E-04
363	AMPMS2	1.55E-04	1.79E-04	1.79E-04	1.79E-04	1.79E-04	1.79E-04
364	AMPN	1.00E-06	0.00E+00	0.00E+00	0.00E+00	0.00E+00	0.00E+00
365	AMPTASECG	5.00E-06	0.00E+00	0.00E+00	0.00E+00	0.00E+00	0.00E+00
366	ANHGMtex	-1.00E-06	2.84E-14	2.84E-14	2.84E-14	2.84E-14	2.84E-14
367	ANHMK	8.00E-06	0.00E+00	0.00E+00	0.00E+00	0.00E+00	0.00E+00
368	ANPRT	3.83E-02	4.44E-02	4.44E-02	4.44E-02	4.44E-02	4.44E-02
369	ANS	3.83E-02	4.44E-02	4.44E-02	4.44E-02	4.44E-02	4.44E-02
370	AOBUTDs	7.00E-06	0.00E+00	0.00E+00	0.00E+00	0.00E+00	0.00E+00
371	AOXSr2	1.39E-06	1.61E-06	1.61E-06	1.61E-06	1.61E-06	1.61E-06
372	AP4AH	1.00E-06	0.00E+00	0.00E+00	0.00E+00	0.00E+00	0.00E+00
373	AP4AS	1.00E-06	0.00E+00	0.00E+00	0.00E+00	0.00E+00	0.00E+00
374	APG3PAT120	1.00E-06	0.00E+00	0.00E+00	0.00E+00	0.00E+00	0.00E+00
375	APG3PAT140	5.00E-06	0.00E+00	0.00E+00	0.00E+00	0.00E+00	0.00E+00
376	APG3PAT141	1.00E-06	0.00E+00	0.00E+00	0.00E+00	0.00E+00	0.00E+00
377	APG3PAT160	1.00E-06	4.87E-02	0.00E+00	0.00E+00	0.00E+00	0.00E+00
378	APG3PAT161	1.00E-06	0.00E+00	0.00E+00	0.00E+00	3.79E-02	3.79E-02
379	APG3PAT180	0.00E+00	0.00E+00	0.00E+00	0.00E+00	0.00E+00	0.00E+00
380	APG3PAT181	1.00E-06	1.95E-02	1.95E-02	0.00E+00	0.00E+00	1.95E-02
381	APH120	1.00E-06	0.00E+00	0.00E+00	0.00E+00	0.00E+00	0.00E+00
382	APH140	1.00E-06	0.00E+00	0.00E+00	0.00E+00	0.00E+00	0.00E+00
383	APH141	1.00E-06	0.00E+00	0.00E+00	0.00E+00	0.00E+00	0.00E+00
384	APH160	1.00E-06	0.00E+00	0.00E+00	0.00E+00	0.00E+00	0.00E+00
385	APH161	1.00E-06	0.00E+00	0.00E+00	0.00E+00	0.00E+00	0.00E+00
386	APH180	1.00E-06	0.00E+00	0.00E+00	0.00E+00	0.00E+00	0.00E+00
387	APH181	1.00E-06	0.00E+00	0.00E+00	0.00E+00	0.00E+00	0.00E+00
388	APRAUR	3.09E-04	3.58E-04	3.58E-04	3.58E-04	3.58E-04	3.58E-04
389	ARBTNR1	1.00E-06	0.00E+00	0.00E+00	0.00E+00	0.00E+00	0.00E+00
390	ARBTNR2	1.00E-06	0.00E+00	0.00E+00	0.00E+00	0.00E+00	0.00E+00
391	ARBTNR3	1.00E-06	0.00E+00	0.00E+00	0.00E+00	0.00E+00	0.00E+00
392	ARBTNabcpp	6.00E-06	0.00E+00	0.00E+00	0.00E+00	0.00E+00	0.00E+00
393	ARBTNexs	6.00E-06	0.00E+00	0.00E+00	0.00E+00	0.00E+00	0.00E+00
394	ARBTNtex	6.00E-06	0.00E+00	0.00E+00	0.00E+00	0.00E+00	0.00E+00
395	ARBTNtonex	6.00E-06	0.00E+00	0.00E+00	0.00E+00	0.00E+00	0.00E+00
396	ARBTNtpp	6.00E-06	0.00E+00	0.00E+00	0.00E+00	0.00E+00	0.00E+00
397	ARBabcpp	1.00E-06	0.00E+00	0.00E+00	0.00E+00	0.00E+00	0.00E+00
398	ARBt2rpp	1.00E-06	0.00E+00	0.00E+00	0.00E+00	0.00E+00	0.00E+00
399	ARBt3ipp	2.00E-06	0.00E+00	0.00E+00	0.00E+00	0.00E+00	0.00E+00
400	ARGAGMt7pp	1.00E-06	0.00E+00	0.00E+00	0.00E+00	0.00E+00	0.00E+00
401	ARGDC	2.00E-06	0.00E+00	0.00E+00	0.00E+00	0.00E+00	0.00E+00
402	ARGDCpp	1.00E-06	0.00E+00	0.00E+00	0.00E+00	0.00E+00	0.00E+00
403	ARGORNt7pp	5.00E-06	0.00E+00	0.00E+00	0.00E+00	0.00E+00	0.00E+00
404	ARGSL	1.99E-01	2.31E-01	2.31E-01	2.31E-01	2.31E-01	2.31E-01
405	ARGSS	1.99E-01	2.31E-01	2.31E-01	2.31E-01	2.31E-01	2.31E-01
406	ARGabcpp	1.00E-06	0.00E+00	0.00E+00	0.00E+00	0.00E+00	0.00E+00
407	ARGt3pp	9.00E-06	0.00E+00	0.00E+00	0.00E+00	0.00E+00	0.00E+00
408	ARGtex	-1.00E-06	2.84E-14	2.84E-14	2.84E-14	2.84E-14	2.84E-14
409	ASAD	-7.25E-01	-8.40E-01	-8.40E-01	-8.40E-01	-8.40E-01	-8.40E-01
410	ASNN	1.00E-06	0.00E+00	0.00E+00	0.00E+00	0.00E+00	0.00E+00
411	ASNNpp	6.00E-06	0.00E+00	0.00E+00	0.00E+00	0.00E+00	0.00E+00
412	ASNS1	1.00E-06	0.00E+00	0.00E+00	0.00E+00	0.00E+00	0.00E+00
413	ASNS2	1.62E-01	1.88E-01	1.88E-01	1.88E-01	1.88E-01	1.88E-01
414	ASNabcpp	1.00E-06	0.00E+00	0.00E+00	0.00E+00	0.00E+00	0.00E+00
415	ASNt2rpp	-8.00E-06	5.68E-14	5.68E-14	5.68E-14	5.68E-14	5.68E-14
416	ASNtex	-1.00E-06	5.68E-14	5.68E-14	5.68E-14	5.68E-14	5.68E-14
417	ASP1DC	3.99E-04	4.63E-04	4.63E-04	4.63E-04	4.63E-04	4.63E-04
418	ASPCT	2.22E-01	2.57E-01	2.57E-01	2.57E-01	2.57E-01	2.57E-01
419	ASPK	7.25E-01	8.40E-01	8.40E-01	8.40E-01	8.40E-01	8.40E-01
420	ASPO3	1.00E-06	0.00E+00	0.00E+00	0.00E+00	0.00E+00	0.00E+00

421	ASPO4	1.00E-06	0.00E+00	0.00E+00	0.00E+00	0.00E+00	0.00E+00
422	ASPO5	1.00E-06	0.00E+00	0.00E+00	0.00E+00	0.00E+00	0.00E+00
423	ASPO6	1.58E-03	1.83E-03	1.83E-03	1.83E-03	1.83E-03	1.83E-03
424	ASPT	1.00E-06	0.00E+00	0.00E+00	0.00E+00	0.00E+00	0.00E+00
425	ASPTA	-1.98E+00	-2.29E+00	-2.29E+00	-2.29E+00	-2.29E+00	-2.29E+00
426	ASPabcpp	1.00E-06	0.00E+00	0.00E+00	0.00E+00	0.00E+00	0.00E+00
427	ASPt2_2pp	1.00E-06	0.00E+00	0.00E+00	0.00E+00	0.00E+00	0.00E+00
428	ASPt2_3pp	1.00E-06	0.00E+00	0.00E+00	0.00E+00	0.00E+00	0.00E+00
429	ASPt2pp	1.00E-06	0.00E+00	0.00E+00	0.00E+00	0.00E+00	0.00E+00
430	ASPt2rpp	1.00E-06	0.00E+00	0.00E+00	0.00E+00	0.00E+00	0.00E+00
431	ASPtex	-1.00E-06	2.84E-14	2.84E-14	2.84E-14	2.84E-14	2.84E-14
432	AST	1.00E-06	0.00E+00	0.00E+00	0.00E+00	0.00E+00	0.00E+00
433	ATHRDHr	-1.00E-06	0.00E+00	0.00E+00	0.00E+00	0.00E+00	0.00E+00
434	ATPHs	1.00E-06	0.00E+00	0.00E+00	0.00E+00	0.00E+00	0.00E+00
435	ATPM	1.00E-06	0.00E+00	0.00E+00	0.00E+00	0.00E+00	0.00E+00
436	ATPPRT	6.38E-02	7.39E-02	7.39E-02	7.39E-02	7.39E-02	7.39E-02
437	ATPS4rpp	4.86E+01	4.60E+01	4.60E+01	4.60E+01	4.60E+01	4.60E+01
438	BMOCOS	8.04E-05	9.32E-05	9.32E-05	9.32E-05	9.32E-05	9.32E-05
439	BMOGDS1	8.04E-05	9.32E-05	9.32E-05	9.32E-05	9.32E-05	9.32E-05
440	BMOGDS2	8.04E-05	9.32E-05	9.32E-05	9.32E-05	9.32E-05	9.32E-05
441	BPNT	1.72E-01	1.99E-01	1.99E-01	1.99E-01	1.99E-01	1.99E-01
442	BTS5	1.39E-06	1.61E-06	1.61E-06	1.61E-06	1.61E-06	1.61E-06
443	CA2t3pp	1.00E+02	1.00E+02	1.00E+02	1.00E+02	1.00E+02	1.00E+02
444	CA2tex	3.43E-03	3.98E-03	3.98E-03	3.98E-03	3.98E-03	3.98E-03
445	CADVtpp	1.00E-06	0.00E+00	0.00E+00	0.00E+00	0.00E+00	0.00E+00
446	CAt6pp	-1.00E+02	-1.00E+02	-1.00E+02	-1.00E+02	-1.00E+02	-1.00E+02
447	CBL1abcpp	1.55E-04	1.79E-04	1.79E-04	1.79E-04	1.79E-04	1.79E-04
448	CBL1tonex	1.55E-04	1.79E-04	1.79E-04	1.79E-04	1.79E-04	1.79E-04
449	CBLAT	1.55E-04	1.79E-04	1.79E-04	1.79E-04	1.79E-04	1.79E-04
450	CBMD	1.00E-06	0.00E+00	0.00E+00	0.00E+00	0.00E+00	0.00E+00
451	CBMKr	4.21E-01	4.88E-01	4.88E-01	4.88E-01	4.88E-01	4.88E-01
452	CBPS	1.00E-06	0.00E+00	0.00E+00	0.00E+00	0.00E+00	0.00E+00
453	CD2abcpp	1.00E-06	0.00E+00	0.00E+00	0.00E+00	0.00E+00	0.00E+00
454	CD2t3pp	1.00E-06	0.00E+00	0.00E+00	0.00E+00	0.00E+00	0.00E+00
455	CD2tpp	2.00E-06	0.00E+00	0.00E+00	0.00E+00	0.00E+00	0.00E+00
456	CDAPPA120	1.00E-06	0.00E+00	0.00E+00	0.00E+00	0.00E+00	0.00E+00
457	CDAPPA140	1.00E-06	0.00E+00	0.00E+00	0.00E+00	0.00E+00	0.00E+00
458	CDAPPA141	1.00E-06	0.00E+00	0.00E+00	0.00E+00	0.00E+00	0.00E+00
459	CDAPPA160	1.00E-06	0.00E+00	0.00E+00	0.00E+00	0.00E+00	0.00E+00
460	CDAPPA161	1.00E-06	0.00E+00	0.00E+00	0.00E+00	0.00E+00	0.00E+00
461	CDAPPA180	1.00E-06	0.00E+00	0.00E+00	0.00E+00	0.00E+00	0.00E+00
462	CDAPPA181	1.00E-06	0.00E+00	0.00E+00	0.00E+00	0.00E+00	0.00E+00
463	CDPMEK	4.59E-03	5.32E-03	5.32E-03	5.32E-03	5.32E-03	5.32E-03
464	CGLYabcpp	5.00E-06	0.00E+00	0.00E+00	0.00E+00	0.00E+00	0.00E+00
465	CGLYtex	-1.00E-06	0.00E+00	0.00E+00	0.00E+00	0.00E+00	0.00E+00
466	CHORM	2.18E-01	2.52E-01	2.52E-01	2.52E-01	2.52E-01	2.52E-01
467	CHORS	2.58E-01	2.99E-01	2.99E-01	2.99E-01	2.99E-01	2.99E-01
468	CHRPL	1.55E-04	1.79E-04	1.79E-04	1.79E-04	1.79E-04	1.79E-04
469	CITL	1.00E-06	0.00E+00	0.00E+00	0.00E+00	0.00E+00	0.00E+00
470	CITt3pp	2.00E-06	0.00E+00	0.00E+00	0.00E+00	0.00E+00	0.00E+00
471	CITt7pp	1.00E-06	0.00E+00	0.00E+00	0.00E+00	0.00E+00	0.00E+00
472	CITtex	-1.00E-06	0.00E+00	0.00E+00	0.00E+00	0.00E+00	0.00E+00
473	CLIPAabctex	1.00E-06	0.00E+00	0.00E+00	0.00E+00	0.00E+00	0.00E+00
474	CLPNH120pp	1.00E-06	0.00E+00	0.00E+00	0.00E+00	0.00E+00	0.00E+00
475	CLPNH140pp	1.00E-06	0.00E+00	0.00E+00	0.00E+00	0.00E+00	0.00E+00
476	CLPNH141pp	1.00E-06	0.00E+00	0.00E+00	0.00E+00	0.00E+00	0.00E+00
477	CLPNH160pp	1.00E-06	0.00E+00	0.00E+00	0.00E+00	0.00E+00	0.00E+00
478	CLPNH161pp	1.00E-06	0.00E+00	0.00E+00	0.00E+00	0.00E+00	0.00E+00
479	CLPNH180pp	2.00E-06	0.00E+00	0.00E+00	0.00E+00	0.00E+00	0.00E+00
480	CLPNH181pp	1.00E-06	0.00E+00	0.00E+00	0.00E+00	0.00E+00	0.00E+00
481	CLPNS120pp	1.00E-06	0.00E+00	0.00E+00	0.00E+00	0.00E+00	0.00E+00
482	CLPNS140pp	1.00E-06	0.00E+00	0.00E+00	0.00E+00	0.00E+00	0.00E+00
483	CLPNS141pp	1.00E-06	0.00E+00	0.00E+00	0.00E+00	0.00E+00	0.00E+00
484	CLPNS160pp	2.04E-03	2.36E-03	2.36E-03	2.36E-03	2.36E-03	2.36E-03
485	CLPNS161pp	1.59E-03	1.84E-03	1.84E-03	1.84E-03	1.84E-03	1.84E-03
486	CLPNS180pp	2.00E-06	0.00E+00	0.00E+00	0.00E+00	0.00E+00	0.00E+00
487	CLPNS181pp	8.19E-04	9.48E-04	9.48E-04	9.48E-04	9.48E-04	9.48E-04
488	CLt3_2pp	1.72E-03	1.99E-03	1.99E-03	1.99E-03	1.99E-03	1.99E-03
489	CLtex	3.43E-03	3.98E-03	3.98E-03	3.98E-03	3.98E-03	3.98E-03
490	CMPN	1.00E-06	0.00E+00	0.00E+00	0.00E+00	0.00E+00	0.00E+00
491	CMtex	1.00E-06	0.00E+00	0.00E+00	0.00E+00	0.00E+00	0.00E+00
492	CMtpp	1.00E-06	0.00E+00	0.00E+00	0.00E+00	0.00E+00	0.00E+00
493	CO2tex	-2.06E+01	-1.61E+01	-1.61E+01	-1.61E+01	-1.61E+01	-1.61E+01

494	CO2tpp	1.00E-06	-1.61E+01	-1.61E+01	-1.61E+01	-1.61E+01	-1.61E+01
495	COBALT2abcpp	1.00E-06	0.00E+00	0.00E+00	0.00E+00	0.00E+00	0.00E+00
496	COBALT2t3pp	1.00E-06	0.00E+00	0.00E+00	0.00E+00	0.00E+00	0.00E+00
497	COBALT2tex	1.66E-05	1.93E-05	1.93E-05	1.93E-05	1.93E-05	1.93E-05
498	COBALT2tpp	1.86E-05	1.93E-05	1.93E-05	1.93E-05	1.93E-05	1.93E-05
499	COLIPAKpp	0.00E+00	0.00E+00	0.00E+00	0.00E+00	0.00E+00	0.00E+00
500	COLIPAPabctex	0.00E+00	0.00E+00	0.00E+00	0.00E+00	0.00E+00	0.00E+00
501	COLIPAabcpp	5.65E-03	6.55E-03	6.55E-03	6.55E-03	6.55E-03	6.55E-03
502	COLIPAabctex	5.65E-03	6.55E-03	6.55E-03	6.55E-03	6.55E-03	6.55E-03
503	CPGNR1	1.00E-06	0.00E+00	0.00E+00	0.00E+00	0.00E+00	0.00E+00
504	CPGNR2	1.05E+00	0.00E+00	0.00E+00	0.00E+00	0.00E+00	0.00E+00
505	CPGNR3	1.00E-06	0.00E+00	0.00E+00	0.00E+00	0.00E+00	0.00E+00
506	CPGNUtex	2.09E+00	0.00E+00	0.00E+00	0.00E+00	0.00E+00	0.00E+00
507	CPGNUtpp	2.09E+00	0.00E+00	0.00E+00	0.00E+00	0.00E+00	0.00E+00
508	CPGNabcpp	2.09E+00	0.00E+00	0.00E+00	0.00E+00	0.00E+00	0.00E+00
509	CPGNexs	2.09E+00	0.00E+00	0.00E+00	0.00E+00	0.00E+00	0.00E+00
510	CPGNtonex	2.09E+00	0.00E+00	0.00E+00	0.00E+00	0.00E+00	0.00E+00
511	CPMPS	1.70E-04	1.98E-04	1.98E-04	1.98E-04	1.98E-04	1.98E-04
512	CPPPGO	3.09E-04	3.58E-04	3.58E-04	3.58E-04	3.58E-04	3.58E-04
513	CPPPGO2	1.00E-06	0.00E+00	0.00E+00	0.00E+00	0.00E+00	0.00E+00
514	CRNDabcpp	1.00E-06	0.00E+00	0.00E+00	0.00E+00	0.00E+00	0.00E+00
515	CRNDt2rpp	1.00E-06	0.00E+00	0.00E+00	0.00E+00	0.00E+00	0.00E+00
516	CRNabcpp	1.00E-06	0.00E+00	0.00E+00	0.00E+00	0.00E+00	0.00E+00
517	CRNt2rpp	-3.00E-06	0.00E+00	0.00E+00	0.00E+00	0.00E+00	0.00E+00
518	CRNt8pp	2.00E-06	0.00E+00	0.00E+00	0.00E+00	0.00E+00	0.00E+00
519	CS	4.02E+00	4.10E+00	4.10E+00	4.10E+00	4.10E+00	4.10E+00
520	CSND	2.00E-06	0.00E+00	0.00E+00	0.00E+00	0.00E+00	0.00E+00
521	CTBTabcpp	1.00E-06	0.00E+00	0.00E+00	0.00E+00	0.00E+00	0.00E+00
522	CTBTt2rpp	-1.00E-06	0.00E+00	0.00E+00	0.00E+00	0.00E+00	0.00E+00
523	CTECOAI6	1.00E-06	-7.58E-02	-7.58E-02	-7.58E-02	-7.58E-02	-7.58E-02
524	CTECOAI7	0.00E+00	2.84E-14	2.84E-14	2.84E-14	2.84E-14	2.84E-14
525	CTECOAI8	0.00E+00	-3.91E-02	-3.91E-02	-3.91E-02	-3.91E-02	-3.91E-02
526	CTPS2	1.08E-01	1.25E-01	1.25E-01	1.25E-01	1.25E-01	1.25E-01
527	CU2abcpp	1.00E-06	0.00E+00	0.00E+00	0.00E+00	0.00E+00	0.00E+00
528	CU2tex	4.67E-04	5.41E-04	5.41E-04	5.41E-04	5.41E-04	5.41E-04
529	CU2tpp	4.68E-04	5.41E-04	5.41E-04	5.41E-04	5.41E-04	5.41E-04
530	CYSDS	1.00E-06	0.00E+00	0.00E+00	0.00E+00	0.00E+00	0.00E+00
531	CYSS	1.72E-01	1.99E-01	1.99E-01	1.99E-01	1.99E-01	1.99E-01
532	CYSTL	1.08E-01	1.26E-01	1.26E-01	1.26E-01	1.26E-01	1.26E-01
533	CYSabc2pp	1.00E-06	0.00E+00	0.00E+00	0.00E+00	0.00E+00	0.00E+00
534	CYSabcpp	1.00E-06	0.00E+00	0.00E+00	0.00E+00	0.00E+00	0.00E+00
535	CYStex	-1.00E-06	2.84E-14	2.84E-14	2.84E-14	2.84E-14	2.84E-14
536	CYStpp	1.00E-06	0.00E+00	0.00E+00	0.00E+00	0.00E+00	0.00E+00
537	CYTBD2pp	1.00E-05	0.00E+00	0.00E+00	0.00E+00	0.00E+00	0.00E+00
538	CYTBDpp	1.00E-06	0.00E+00	0.00E+00	0.00E+00	0.00E+00	0.00E+00
539	CYTBO3_4pp	3.73E+01	2.90E+01	2.90E+01	2.90E+01	2.90E+01	2.90E+01
540	CYTD	1.00E-06	0.00E+00	0.00E+00	0.00E+00	0.00E+00	0.00E+00
541	CYTDH	1.00E-06	0.00E+00	0.00E+00	0.00E+00	0.00E+00	0.00E+00
542	CYTDK2	1.00E-06	0.00E+00	0.00E+00	0.00E+00	0.00E+00	0.00E+00
543	CYTDt2pp	1.00E+02	0.00E+00	0.00E+00	0.00E+00	1.00E+02	0.00E+00
544	CYTDt2rpp	-1.00E+02	2.84E-14	2.84E-14	2.84E-14	-1.00E+02	2.84E-14
545	CYTDtex	-1.00E-06	2.84E-14	2.84E-14	2.84E-14	2.84E-14	2.84E-14
546	CYTK1	1.14E-01	1.32E-01	1.32E-01	1.32E-01	1.32E-01	1.32E-01
547	CYTK2	1.00E-06	0.00E+00	0.00E+00	0.00E+00	0.00E+00	0.00E+00
548	D-LACt2pp	-1.00E-06	2.84E-14	2.84E-14	2.84E-14	2.84E-14	2.84E-14
549	D-LACtex	-1.00E-06	2.84E-14	2.84E-14	2.84E-14	2.84E-14	2.84E-14
550	DAAD	1.00E-06	0.00E+00	0.00E+00	0.00E+00	0.00E+00	0.00E+00
551	DADA	1.00E-06	0.00E+00	0.00E+00	0.00E+00	0.00E+00	0.00E+00
552	DADK	1.00E-06	0.00E+00	0.00E+00	0.00E+00	0.00E+00	0.00E+00
553	DAGK120	2.00E-06	0.00E+00	0.00E+00	0.00E+00	0.00E+00	0.00E+00
554	DAGK140	2.00E-06	0.00E+00	0.00E+00	0.00E+00	0.00E+00	0.00E+00
555	DAGK141	2.00E-06	0.00E+00	0.00E+00	0.00E+00	0.00E+00	0.00E+00
556	DAGK160	3.00E-06	0.00E+00	0.00E+00	0.00E+00	0.00E+00	0.00E+00
557	DAGK161	4.00E-06	0.00E+00	0.00E+00	0.00E+00	0.00E+00	0.00E+00
558	DAGK180	4.00E-06	0.00E+00	0.00E+00	0.00E+00	0.00E+00	0.00E+00
559	DAGK181	4.00E-06	0.00E+00	0.00E+00	0.00E+00	0.00E+00	0.00E+00
560	DALAt2pp	1.68E-02	1.95E-02	1.95E-02	1.95E-02	1.95E-02	1.95E-02
561	DALAtex	-1.00E-06	2.84E-14	2.84E-14	2.84E-14	2.84E-14	2.84E-14
562	DAPDC	2.31E-01	2.68E-01	2.68E-01	2.68E-01	2.68E-01	2.68E-01
563	DAPE	2.50E-01	2.90E-01	2.90E-01	2.90E-01	2.90E-01	2.90E-01
564	DAPtex	-1.00E-06	0.00E+00	0.00E+00	0.00E+00	0.00E+00	0.00E+00
565	DASYN120	7.00E-06	0.00E+00	0.00E+00	0.00E+00	0.00E+00	0.00E+00
566	DASYN140	6.00E-06	0.00E+00	0.00E+00	0.00E+00	0.00E+00	0.00E+00

567	DASYN141	6.00E-06	0.00E+00	0.00E+00	0.00E+00	0.00E+00	0.00E+00
568	DASYN160	4.20E-02	4.87E-02	4.87E-02	4.87E-02	4.87E-02	4.87E-02
569	DASYN161	3.27E-02	3.79E-02	3.79E-02	3.79E-02	3.79E-02	3.79E-02
570	DASYN180	3.00E-06	0.00E+00	0.00E+00	0.00E+00	0.00E+00	0.00E+00
571	DASYN181	1.69E-02	1.95E-02	1.95E-02	1.95E-02	1.95E-02	1.95E-02
572	DATPHs	1.00E-06	0.00E+00	0.00E+00	0.00E+00	0.00E+00	0.00E+00
573	DB4PS	6.18E-04	7.16E-04	7.16E-04	7.16E-04	7.16E-04	7.16E-04
574	DBTS	1.39E-06	1.61E-06	1.61E-06	1.61E-06	1.61E-06	1.61E-06
575	DCTPD	1.00E-06	0.00E+00	0.00E+00	0.00E+00	0.00E+00	0.00E+00
576	DCYTD	1.00E-06	0.00E+00	0.00E+00	0.00E+00	0.00E+00	0.00E+00
577	DDPA	2.58E-01	2.99E-01	2.99E-01	2.99E-01	2.99E-01	2.99E-01
578	DGK1	1.00E-06	0.00E+00	0.00E+00	0.00E+00	0.00E+00	0.00E+00
579	DHAD1	5.89E-01	6.82E-01	6.82E-01	6.82E-01	6.82E-01	6.82E-01
580	DHAD2	1.96E-01	2.27E-01	2.27E-01	2.27E-01	2.27E-01	2.27E-01
581	DHAPT	1.00E-06	0.00E+00	0.00E+00	0.00E+00	5.47E-01	5.47E-01
582	DHAtex	-1.00E-06	2.84E-14	2.84E-14	2.84E-14	2.84E-14	2.84E-14
583	DHAtpp	-1.00E-06	2.84E-14	2.84E-14	2.84E-14	2.84E-14	2.84E-14
584	DHBD	4.70E-04	5.37E-04	5.37E-04	5.37E-04	5.37E-04	5.37E-04
585	DHBS	4.76E-04	5.37E-04	5.37E-04	5.37E-04	5.37E-04	5.37E-04
586	DHBSH	6.00E-06	0.00E+00	0.00E+00	0.00E+00	0.00E+00	0.00E+00
587	DHDPRy	2.50E-01	2.90E-01	2.90E-01	2.90E-01	2.90E-01	2.90E-01
588	DHDPS	2.50E-01	2.90E-01	2.90E-01	2.90E-01	2.90E-01	2.90E-01
589	DHFR	1.78E-02	2.06E-02	2.06E-02	2.06E-02	2.06E-02	2.06E-02
590	DHFS	6.18E-04	7.16E-04	7.16E-04	7.16E-04	7.16E-04	7.16E-04
591	DHNAOT4	3.09E-04	3.58E-04	3.58E-04	3.58E-04	3.58E-04	3.58E-04
592	DHNCOAS	3.09E-04	3.58E-04	3.58E-04	3.58E-04	3.58E-04	3.58E-04
593	DHNCOAT	3.09E-04	3.58E-04	3.58E-04	3.58E-04	3.58E-04	3.58E-04
594	DHNPA2r	6.18E-04	7.16E-04	7.16E-04	7.16E-04	7.16E-04	7.16E-04
595	DHORD2	2.22E-01	0.00E+00	0.00E+00	0.00E+00	2.57E-01	0.00E+00
596	DHORD5	1.00E-06	0.00E+00	0.00E+00	0.00E+00	0.00E+00	0.00E+00
597	DHORDfum	1.00E-06	2.57E-01	2.57E-01	2.57E-01	0.00E+00	2.57E-01
598	DHORTS	-2.22E-01	-2.57E-01	-2.57E-01	-2.57E-01	-2.57E-01	-2.57E-01
599	DHPPDA2	3.09E-04	3.58E-04	3.58E-04	3.58E-04	3.58E-04	3.58E-04
600	DHPS2	6.18E-04	7.16E-04	7.16E-04	7.16E-04	7.16E-04	7.16E-04
601	DHPTDCs2	9.30E-04	1.08E-03	1.08E-03	1.08E-03	1.08E-03	1.08E-03
602	DHQS	2.58E-01	2.99E-01	2.99E-01	2.99E-01	2.99E-01	2.99E-01
603	DHQTi	2.58E-01	2.99E-01	2.99E-01	2.99E-01	2.99E-01	2.99E-01
604	DMATT	6.56E-04	7.61E-04	7.61E-04	7.61E-04	7.61E-04	7.61E-04
605	DMPPS	1.00E-06	7.61E-04	7.61E-04	5.32E-03	7.61E-04	7.61E-04
606	DMQMT	1.55E-04	1.79E-04	1.79E-04	1.79E-04	1.79E-04	1.79E-04
607	DNMPPA	6.18E-04	7.16E-04	7.16E-04	7.16E-04	7.16E-04	7.16E-04
608	DNTPPA	6.18E-04	7.16E-04	7.16E-04	7.16E-04	7.16E-04	7.16E-04
609	DOXRBCNtex	1.00E-06	0.00E+00	0.00E+00	0.00E+00	0.00E+00	0.00E+00
610	DOXRBCNtpp	1.00E-06	0.00E+00	0.00E+00	0.00E+00	0.00E+00	0.00E+00
611	DPCOAK	3.99E-04	4.63E-04	4.63E-04	4.63E-04	4.63E-04	4.63E-04
612	DPR	3.99E-04	4.63E-04	4.63E-04	4.63E-04	4.63E-04	4.63E-04
613	DRPA	7.00E-06	0.00E+00	0.00E+00	0.00E+00	0.00E+00	0.00E+00
614	DSERDHr	-1.00E-06	0.00E+00	0.00E+00	0.00E+00	0.00E+00	0.00E+00
615	DTMPK	1.72E-02	1.99E-02	1.99E-02	1.99E-02	1.99E-02	1.99E-02
616	DURIK1	1.00E-06	0.00E+00	0.00E+00	0.00E+00	0.00E+00	0.00E+00
617	DURIPP	1.00E-06	0.00E+00	0.00E+00	0.00E+00	0.00E+00	0.00E+00
618	DUTPDP	1.72E-02	1.99E-02	1.99E-02	1.99E-02	1.99E-02	1.99E-02
619	DXPRIi	4.59E-03	5.32E-03	5.32E-03	5.32E-03	5.32E-03	5.32E-03
620	DXPS	4.90E-03	5.68E-03	5.68E-03	5.68E-03	5.68E-03	5.68E-03
621	E4PD	1.55E-04	1.79E-04	1.79E-04	1.79E-04	1.79E-04	1.79E-04
622	EAR100x	1.00E-06	0.00E+00	0.00E+00	0.00E+00	0.00E+00	0.00E+00
623	EAR100y	1.00E-06	0.00E+00	0.00E+00	0.00E+00	0.00E+00	0.00E+00
624	EAR120x	2.00E-06	0.00E+00	0.00E+00	0.00E+00	0.00E+00	0.00E+00
625	EAR120y	1.00E-06	0.00E+00	0.00E+00	0.00E+00	0.00E+00	0.00E+00
626	EAR121x	9.91E-02	0.00E+00	0.00E+00	0.00E+00	0.00E+00	0.00E+00
627	EAR121y	1.00E-06	0.00E+00	0.00E+00	0.00E+00	0.00E+00	0.00E+00
628	EAR140x	1.00E-06	0.00E+00	0.00E+00	0.00E+00	0.00E+00	0.00E+00
629	EAR140y	1.00E-06	0.00E+00	0.00E+00	0.00E+00	0.00E+00	0.00E+00
630	EAR141x	9.91E-02	0.00E+00	0.00E+00	0.00E+00	0.00E+00	0.00E+00
631	EAR141y	1.00E-06	0.00E+00	0.00E+00	0.00E+00	0.00E+00	0.00E+00
632	EAR160x	8.41E-02	0.00E+00	0.00E+00	0.00E+00	0.00E+00	0.00E+00
633	EAR160y	1.00E-06	0.00E+00	0.00E+00	0.00E+00	0.00E+00	0.00E+00
634	EAR161x	9.91E-02	7.58E-02	7.58E-02	7.58E-02	7.58E-02	7.58E-02
635	EAR161y	1.00E-06	0.00E+00	0.00E+00	0.00E+00	0.00E+00	0.00E+00
636	EAR180x	0.00E+00	0.00E+00	0.00E+00	0.00E+00	0.00E+00	0.00E+00
637	EAR180y	0.00E+00	0.00E+00	0.00E+00	0.00E+00	0.00E+00	0.00E+00
638	EAR181x	3.37E-02	0.00E+00	0.00E+00	0.00E+00	0.00E+00	0.00E+00
639	EAR181y	1.00E-06	0.00E+00	0.00E+00	0.00E+00	0.00E+00	0.00E+00

640	EAR40x	2.00E-06	0.00E+00	0.00E+00	0.00E+00	0.00E+00	0.00E+00
641	EAR40y	1.00E-06	0.00E+00	0.00E+00	0.00E+00	0.00E+00	0.00E+00
642	EAR60x	2.00E-06	0.00E+00	0.00E+00	0.00E+00	0.00E+00	0.00E+00
643	EAR60y	1.00E-06	0.00E+00	0.00E+00	0.00E+00	0.00E+00	0.00E+00
644	EAR80x	2.00E-06	0.00E+00	0.00E+00	0.00E+00	0.00E+00	0.00E+00
645	EAR80y	1.00E-06	0.00E+00	0.00E+00	0.00E+00	0.00E+00	0.00E+00
646	ECA4COLIPAabctex	0.00E+00	0.00E+00	0.00E+00	0.00E+00	0.00E+00	0.00E+00
647	ECA4OALpp	0.00E+00	0.00E+00	0.00E+00	0.00E+00	0.00E+00	0.00E+00
648	ECAP1pp	0.00E+00	0.00E+00	0.00E+00	0.00E+00	0.00E+00	0.00E+00
649	ECAP2pp	0.00E+00	0.00E+00	0.00E+00	0.00E+00	0.00E+00	0.00E+00
650	ECAP3pp	0.00E+00	0.00E+00	0.00E+00	0.00E+00	0.00E+00	0.00E+00
651	ECAtpp	0.00E+00	0.00E+00	0.00E+00	0.00E+00	0.00E+00	0.00E+00
652	ECOAH1	2.17E-01	2.52E-01	2.52E-01	2.52E-01	2.52E-01	2.52E-01
653	ECOAH2	2.17E-01	2.52E-01	2.52E-01	2.52E-01	2.52E-01	2.52E-01
654	ECOAH3	2.17E-01	2.52E-01	2.52E-01	2.52E-01	2.52E-01	2.52E-01
655	ECOAH4	1.18E-01	2.52E-01	2.52E-01	2.52E-01	2.52E-01	2.52E-01
656	ECOAH5	1.18E-01	2.52E-01	2.52E-01	2.52E-01	2.52E-01	2.52E-01
657	ECOAH6	8.97E-02	2.19E-01	2.19E-01	2.19E-01	2.19E-01	2.19E-01
658	ECOAH7	0.00E+00	1.36E-01	1.36E-01	1.36E-01	1.36E-01	1.36E-01
659	ECOAH8	0.00E+00	3.91E-02	3.91E-02	3.91E-02	3.91E-02	3.91E-02
660	EDA	1.00E-06	0.00E+00	0.00E+00	0.00E+00	0.00E+00	0.00E+00
661	EDD	1.00E-06	0.00E+00	0.00E+00	0.00E+00	0.00E+00	0.00E+00
662	EDTXS1	5.65E-03	6.55E-03	6.55E-03	6.55E-03	6.55E-03	6.55E-03
663	EDTXS2	5.65E-03	6.55E-03	6.55E-03	6.55E-03	6.55E-03	6.55E-03
664	EDTXS3	1.00E-06	0.00E+00	0.00E+00	0.00E+00	0.00E+00	0.00E+00
665	EDTXS4	1.00E-06	0.00E+00	0.00E+00	0.00E+00	0.00E+00	0.00E+00
666	EGMEACPR	1.39E-06	1.61E-06	1.61E-06	1.61E-06	1.61E-06	1.61E-06
667	ENLIPAabctex	2.00E-06	0.00E+00	0.00E+00	0.00E+00	0.00E+00	0.00E+00
668	ENO	1.05E+01	1.17E+01	1.17E+01	1.17E+01	1.17E+01	1.17E+01
669	ENTCS	1.59E-04	1.79E-04	1.79E-04	1.79E-04	1.79E-04	1.79E-04
670	ENTERES	1.00E-06	0.00E+00	0.00E+00	0.00E+00	0.00E+00	0.00E+00
671	ENTERES2	1.00E-06	0.00E+00	0.00E+00	0.00E+00	0.00E+00	0.00E+00
672	EPMEACPR	1.39E-06	1.61E-06	1.61E-06	1.61E-06	1.61E-06	1.61E-06
673	ETHAAL	5.00E-06	0.00E+00	0.00E+00	0.00E+00	0.00E+00	0.00E+00
674	ETHAt2pp	1.00E-06	0.00E+00	0.00E+00	0.00E+00	0.00E+00	0.00E+00
675	ETHAtex	-1.00E-06	0.00E+00	0.00E+00	0.00E+00	0.00E+00	0.00E+00
676	ETOHtex	-1.00E-06	2.84E-14	2.84E-14	2.84E-14	2.84E-14	2.84E-14
677	ETOHtrpp	-1.00E-06	2.84E-14	2.84E-14	2.84E-14	2.84E-14	2.84E-14
678	F6PA	1.00E-06	0.00E+00	0.00E+00	0.00E+00	5.47E-01	5.47E-01
679	F6PP	1.00E-06	0.00E+00	0.00E+00	0.00E+00	0.00E+00	0.00E+00
680	FA100ACPHi	1.00E-06	0.00E+00	0.00E+00	0.00E+00	0.00E+00	0.00E+00
681	FA120ACPHi	1.00E-06	0.00E+00	0.00E+00	0.00E+00	0.00E+00	0.00E+00
682	FA140ACPHi	1.00E-06	0.00E+00	0.00E+00	0.00E+00	0.00E+00	0.00E+00
683	FA141ACPHi	1.00E-06	0.00E+00	0.00E+00	0.00E+00	0.00E+00	0.00E+00
684	FA160ACPHi	1.00E-06	0.00E+00	0.00E+00	0.00E+00	0.00E+00	0.00E+00
685	FA161ACPHi	1.00E-06	0.00E+00	0.00E+00	0.00E+00	0.00E+00	0.00E+00
686	FA80ACPHi	1.00E-06	0.00E+00	0.00E+00	0.00E+00	0.00E+00	0.00E+00
687	FACOAE100	1.00E-06	0.00E+00	0.00E+00	0.00E+00	0.00E+00	0.00E+00
688	FACOAE120	2.83E-02	3.27E-02	3.27E-02	3.27E-02	3.27E-02	3.27E-02
689	FACOAE140	8.97E-02	6.55E-03	6.55E-03	6.55E-03	6.55E-03	6.55E-03
690	FACOAE141	9.00E-06	7.58E-02	7.58E-02	7.58E-02	7.58E-02	7.58E-02
691	FACOAE160	0.00E+00	9.74E-02	9.74E-02	9.74E-02	9.74E-02	9.74E-02
692	FACOAE161	0.00E+00	0.00E+00	0.00E+00	0.00E+00	0.00E+00	0.00E+00
693	FACOAE180	0.00E+00	0.00E+00	0.00E+00	0.00E+00	0.00E+00	0.00E+00
694	FACOAE181	0.00E+00	3.91E-02	3.91E-02	3.91E-02	3.91E-02	3.91E-02
695	FACOAE60	3.00E-06	0.00E+00	0.00E+00	0.00E+00	0.00E+00	0.00E+00
696	FACOAE80	9.91E-02	2.41E-06	2.41E-06	2.41E-06	2.41E-06	2.41E-06
697	FACOAL120t2pp	1.30E-05	0.00E+00	0.00E+00	0.00E+00	0.00E+00	0.00E+00
698	FACOAL140t2pp	1.10E-05	0.00E+00	0.00E+00	0.00E+00	0.00E+00	0.00E+00
699	FACOAL141t2pp	1.00E-05	0.00E+00	0.00E+00	0.00E+00	0.00E+00	0.00E+00
700	FACOAL160t2pp	0.00E+00	0.00E+00	0.00E+00	0.00E+00	0.00E+00	0.00E+00
701	FACOAL161t2pp	0.00E+00	0.00E+00	0.00E+00	0.00E+00	0.00E+00	0.00E+00
702	FACOAL180t2pp	0.00E+00	0.00E+00	0.00E+00	0.00E+00	0.00E+00	0.00E+00
703	FACOAL181t2pp	0.00E+00	0.00E+00	0.00E+00	0.00E+00	0.00E+00	0.00E+00
704	FACOAL60t2pp	1.00E-06	0.00E+00	0.00E+00	0.00E+00	0.00E+00	0.00E+00
705	FADRx	9.78E-01	1.54E+00	1.54E+00	1.54E+00	1.54E+00	1.54E+00
706	FADRx2	1.00E-06	0.00E+00	0.00E+00	0.00E+00	0.00E+00	0.00E+00
707	FBA	4.75E+00	5.34E+00	0.00E+00	0.00E+00	4.79E+00	0.00E+00
708	FBA3	1.00E-06	9.01E-01	6.24E+00	6.24E+00	9.01E-01	5.69E+00
709	FBP	1.00E-06	0.00E+00	0.00E+00	0.00E+00	0.00E+00	0.00E+00
710	FCLT	3.10E-04	3.58E-04	3.58E-04	3.58E-04	3.58E-04	3.58E-04
711	FDH4pp	2.06E+01	0.00E+00	0.00E+00	0.00E+00	0.00E+00	0.00E+00
712	FDH5pp	1.00E-06	0.00E+00	0.00E+00	0.00E+00	0.00E+00	0.00E+00

713	FE2abcpp	1.00E-06	0.00E+00	0.00E+00	0.00E+00	0.00E+00	0.00E+00
714	FE2t2pp	1.00E-06	0.00E+00	0.00E+00	0.00E+00	0.00E+00	0.00E+00
715	FE2t3pp	2.08E+00	0.00E+00	0.00E+00	0.00E+00	0.00E+00	0.00E+00
716	FE2tex	-2.08E+00	1.25E-02	1.25E-02	1.25E-02	1.25E-02	1.25E-02
717	FE2tpp	1.00E-06	1.25E-02	1.25E-02	1.25E-02	1.25E-02	1.25E-02
718	FE3HOXR1	1.00E-06	0.00E+00	0.00E+00	0.00E+00	0.00E+00	0.00E+00
719	FE3HOXR2	1.00E-06	0.00E+00	0.00E+00	0.00E+00	0.00E+00	0.00E+00
720	FE3HOXR3	1.00E-06	0.00E+00	0.00E+00	0.00E+00	0.00E+00	0.00E+00
721	FE3HOXUtex	6.00E-06	0.00E+00	0.00E+00	0.00E+00	0.00E+00	0.00E+00
722	FE3HOXUtpp	6.00E-06	0.00E+00	0.00E+00	0.00E+00	0.00E+00	0.00E+00
723	FE3HOXabcpp	6.00E-06	0.00E+00	0.00E+00	0.00E+00	0.00E+00	0.00E+00
724	FE3HOXexs	6.00E-06	0.00E+00	0.00E+00	0.00E+00	0.00E+00	0.00E+00
725	FE3HOXtonex	6.00E-06	0.00E+00	0.00E+00	0.00E+00	0.00E+00	0.00E+00
726	FE3Ri	1.00E-06	0.00E+00	0.00E+00	0.00E+00	0.00E+00	0.00E+00
727	FE3abcpp	5.00E-06	0.00E+00	0.00E+00	0.00E+00	0.00E+00	0.00E+00
728	FE3tex	1.00E-06	0.00E+00	0.00E+00	0.00E+00	0.00E+00	0.00E+00
729	FECRMR1	1.00E-06	0.00E+00	0.00E+00	0.00E+00	0.00E+00	0.00E+00
730	FECRMR2	1.00E-06	0.00E+00	0.00E+00	0.00E+00	0.00E+00	0.00E+00
731	FECRMR3	1.00E-06	0.00E+00	0.00E+00	0.00E+00	0.00E+00	0.00E+00
732	FECRMUtex	6.00E-06	0.00E+00	0.00E+00	0.00E+00	0.00E+00	0.00E+00
733	FECRMUtpp	6.00E-06	0.00E+00	0.00E+00	0.00E+00	0.00E+00	0.00E+00
734	FECRMabcpp	6.00E-06	0.00E+00	0.00E+00	0.00E+00	0.00E+00	0.00E+00
735	FECRMexs	6.00E-06	0.00E+00	0.00E+00	0.00E+00	0.00E+00	0.00E+00
736	FECRMtonex	6.00E-06	0.00E+00	0.00E+00	0.00E+00	0.00E+00	0.00E+00
737	FEENTERR1	1.00E-06	0.00E+00	0.00E+00	0.00E+00	0.00E+00	0.00E+00
738	FEENTERR2	1.00E-06	0.00E+00	0.00E+00	0.00E+00	0.00E+00	0.00E+00
739	FEENTERR3	1.00E-06	0.00E+00	0.00E+00	0.00E+00	0.00E+00	0.00E+00
740	FEENTERabcpp	7.00E-06	0.00E+00	0.00E+00	0.00E+00	0.00E+00	0.00E+00
741	FEENTERexs	8.00E-06	0.00E+00	0.00E+00	0.00E+00	0.00E+00	0.00E+00
742	FEENTERtex	9.00E-06	0.00E+00	0.00E+00	0.00E+00	0.00E+00	0.00E+00
743	FEENTERtonex	7.00E-06	0.00E+00	0.00E+00	0.00E+00	0.00E+00	0.00E+00
744	FEENTERtpp	9.00E-06	0.00E+00	0.00E+00	0.00E+00	0.00E+00	0.00E+00
745	FEOXAMR1	1.00E-06	0.00E+00	0.00E+00	0.00E+00	0.00E+00	0.00E+00
746	FEOXAMR2	1.00E-06	0.00E+00	0.00E+00	0.00E+00	0.00E+00	0.00E+00
747	FEOXAMR3	1.00E-06	0.00E+00	0.00E+00	0.00E+00	0.00E+00	0.00E+00
748	FEOXAMUtex	6.00E-06	0.00E+00	0.00E+00	0.00E+00	0.00E+00	0.00E+00
749	FEOXAMUtpp	6.00E-06	0.00E+00	0.00E+00	0.00E+00	0.00E+00	0.00E+00
750	FEOXAMabcpp	6.00E-06	0.00E+00	0.00E+00	0.00E+00	0.00E+00	0.00E+00
751	FEOXAMexs	6.00E-06	0.00E+00	0.00E+00	0.00E+00	0.00E+00	0.00E+00
752	FEOXAMtonex	6.00E-06	0.00E+00	0.00E+00	0.00E+00	0.00E+00	0.00E+00
753	FEROpp	1.00E-06	0.00E+00	0.00E+00	0.00E+00	0.00E+00	0.00E+00
754	FESD1s	2.57E-03	2.98E-03	2.98E-03	2.98E-03	2.98E-03	2.98E-03
755	FESD2s	-1.00E-06	0.00E+00	0.00E+00	0.00E+00	0.00E+00	0.00E+00
756	FESR	5.14E-03	5.97E-03	5.97E-03	5.97E-03	5.97E-03	5.97E-03
757	FLDR2	1.16E+01	0.00E+00	0.00E+00	0.00E+00	0.00E+00	0.00E+00
758	FLVR	1.00E-06	0.00E+00	0.00E+00	0.00E+00	0.00E+00	0.00E+00
759	FLVRx	5.00E-06	0.00E+00	0.00E+00	0.00E+00	0.00E+00	0.00E+00
760	FMNAT	1.55E-04	1.79E-04	1.79E-04	1.79E-04	1.79E-04	1.79E-04
761	FMNRx	1.05E+00	0.00E+00	0.00E+00	0.00E+00	0.00E+00	0.00E+00
762	FMNRx2	1.00E-06	0.00E+00	0.00E+00	0.00E+00	0.00E+00	0.00E+00
763	FOMETRi	1.00E-06	0.00E+00	0.00E+00	0.00E+00	0.00E+00	0.00E+00
764	FORt2pp	1.00E-06	0.00E+00	0.00E+00	0.00E+00	0.00E+00	0.00E+00
765	FORtex	-1.00E-06	2.84E-14	2.84E-14	2.84E-14	2.84E-14	2.84E-14
766	FORtppi	2.06E+01	-2.84E-14	-2.84E-14	-2.84E-14	-2.84E-14	-2.84E-14
767	FRD2	0.00E+00	0.00E+00	0.00E+00	0.00E+00	0.00E+00	0.00E+00
768	FRD3	5.00E-06	0.00E+00	0.00E+00	0.00E+00	0.00E+00	0.00E+00
769	FTHFD	1.00E-06	0.00E+00	0.00E+00	0.00E+00	0.00E+00	0.00E+00
770	FTHFLi	1.00E-06	2.15E-03	0.00E+00	2.15E-03	2.15E-03	0.00E+00
771	FUM	3.97E+00	4.04E+00	4.04E+00	4.04E+00	4.04E+00	4.04E+00
772	FUSAtex	1.00E-06	0.00E+00	0.00E+00	0.00E+00	0.00E+00	0.00E+00
773	FUSAtpp	1.00E-06	0.00E+00	0.00E+00	0.00E+00	0.00E+00	0.00E+00
774	G1PACT	4.96E-02	5.74E-02	5.74E-02	5.74E-02	5.74E-02	5.74E-02
775	G1PTT	5.65E-03	6.55E-03	6.55E-03	6.55E-03	6.55E-03	6.55E-03
776	G1SAT	3.72E-03	4.30E-03	4.30E-03	4.30E-03	4.30E-03	4.30E-03
777	G3PAT120	6.00E-06	0.00E+00	0.00E+00	0.00E+00	0.00E+00	0.00E+00
778	G3PAT140	1.00E-06	0.00E+00	0.00E+00	0.00E+00	0.00E+00	0.00E+00
779	G3PAT141	4.00E-06	0.00E+00	0.00E+00	0.00E+00	0.00E+00	0.00E+00
780	G3PAT160	4.20E-02	0.00E+00	4.87E-02	4.87E-02	4.87E-02	4.87E-02
781	G3PAT161	3.27E-02	3.79E-02	3.79E-02	3.79E-02	0.00E+00	0.00E+00
782	G3PAT180	0.00E+00	0.00E+00	0.00E+00	0.00E+00	0.00E+00	0.00E+00
783	G3PAT181	1.68E-02	0.00E+00	0.00E+00	1.95E-02	1.95E-02	0.00E+00
784	G3PD2	-1.16E-01	-1.30E-01	-1.30E-01	-1.30E-01	-1.30E-01	-1.30E-01
785	G3PD5	1.00E-06	0.00E+00	0.00E+00	0.00E+00	0.00E+00	0.00E+00

786	G3PD6	1.00E-06	0.00E+00	0.00E+00	0.00E+00	0.00E+00	0.00E+00
787	G3PD7	1.00E-06	0.00E+00	0.00E+00	0.00E+00	0.00E+00	0.00E+00
788	G3PEabcpp	1.00E-06	0.00E+00	0.00E+00	0.00E+00	0.00E+00	0.00E+00
789	G3PEtex	-1.00E-06	2.84E-14	2.84E-14	2.84E-14	2.84E-14	2.84E-14
790	G3PGabcpp	1.00E-06	0.00E+00	0.00E+00	0.00E+00	0.00E+00	0.00E+00
791	G3PGtex	-1.00E-06	2.84E-14	2.84E-14	2.84E-14	2.84E-14	2.84E-14
792	G3PT	1.00E-06	0.00E+00	0.00E+00	0.00E+00	0.00E+00	0.00E+00
793	G5SADs	1.49E-01	1.73E-01	1.73E-01	1.73E-01	1.73E-01	1.73E-01
794	G5SD	1.49E-01	1.73E-01	1.73E-01	1.73E-01	1.73E-01	1.73E-01
795	G6PDA	1.00E-06	0.00E+00	0.00E+00	0.00E+00	0.00E+00	0.00E+00
796	G6PDH2r	8.02E+00	3.21E+00	3.21E+00	3.21E+00	3.21E+00	3.21E+00
797	G6PP	1.00E-06	0.00E+00	0.00E+00	0.00E+00	0.00E+00	0.00E+00
798	GALT1	5.65E-03	6.55E-03	6.55E-03	6.55E-03	6.55E-03	6.55E-03
799	GALUi	2.26E-02	2.62E-02	2.62E-02	2.62E-02	2.62E-02	2.62E-02
800	GAPD	1.17E+01	1.30E+01	1.30E+01	1.30E+01	1.30E+01	1.30E+01
801	GARFT	3.02E-01	3.49E-01	3.47E-01	3.49E-01	3.49E-01	3.47E-01
802	GART	1.00E-06	0.00E+00	2.15E-03	0.00E+00	0.00E+00	2.15E-03
803	GCALDD	6.18E-04	7.16E-04	7.16E-04	7.16E-04	7.16E-04	7.16E-04
804	GDPDPK	1.00E-06	0.00E+00	0.00E+00	0.00E+00	0.00E+00	0.00E+00
805	GDPMNH	1.00E-06	0.00E+00	0.00E+00	0.00E+00	0.00E+00	0.00E+00
806	GDPMNP	1.00E-06	0.00E+00	0.00E+00	0.00E+00	0.00E+00	0.00E+00
807	GDPTPDP	1.00E-06	0.00E+00	0.00E+00	0.00E+00	0.00E+00	0.00E+00
808	GF6PTA	4.95E-02	5.74E-02	5.74E-02	5.74E-02	5.74E-02	5.74E-02
809	GGGABADr	1.00E-06	0.00E+00	0.00E+00	0.00E+00	0.00E+00	0.00E+00
810	GGGABAH	1.00E-06	0.00E+00	0.00E+00	0.00E+00	0.00E+00	0.00E+00
811	GGPTRCO	1.00E-06	0.00E+00	0.00E+00	0.00E+00	0.00E+00	0.00E+00
812	GGPTRCS	1.00E-06	0.00E+00	0.00E+00	0.00E+00	0.00E+00	0.00E+00
813	GHMT2r	7.54E-01	8.73E-01	8.73E-01	8.73E-01	8.73E-01	8.73E-01
814	GK1	1.64E-01	1.90E-01	1.90E-01	1.90E-01	1.90E-01	1.90E-01
815	GLBRAN2	1.00E-06	0.00E+00	0.00E+00	0.00E+00	0.00E+00	0.00E+00
816	GLCDpp	5.00E-06	0.00E+00	0.00E+00	0.00E+00	0.00E+00	0.00E+00
817	GLCNt2rpp	4.00E-06	2.84E-14	2.84E-14	2.84E-14	2.84E-14	2.84E-14
818	GLCNtex	-1.00E-06	2.84E-14	2.84E-14	2.84E-14	2.84E-14	2.84E-14
819	GLCP	1.00E-06	0.00E+00	0.00E+00	0.00E+00	0.00E+00	0.00E+00
820	GLCS1	1.07E-01	1.24E-01	1.24E-01	1.24E-01	1.24E-01	1.24E-01
821	GLCTR1	5.65E-03	6.55E-03	6.55E-03	6.55E-03	6.55E-03	6.55E-03
822	GLCTR2	5.65E-03	6.55E-03	6.55E-03	6.55E-03	6.55E-03	6.55E-03
823	GLCTR3	5.65E-03	6.55E-03	6.55E-03	6.55E-03	6.55E-03	6.55E-03
824	GLCabcpp	1.00E-06	0.00E+00	0.00E+00	0.00E+00	0.00E+00	0.00E+00
825	GLCptspp	8.16E+00	8.16E+00	8.16E+00	8.16E+00	8.16E+00	8.16E+00
826	GLCt2pp	1.00E-06	0.00E+00	0.00E+00	0.00E+00	0.00E+00	0.00E+00
827	GLCtex	8.16E+00	8.16E+00	8.16E+00	8.16E+00	8.16E+00	8.16E+00
828	GLDBRAN2	1.00E-06	0.00E+00	0.00E+00	0.00E+00	0.00E+00	0.00E+00
829	GLGC	1.07E-01	1.24E-01	1.24E-01	1.24E-01	1.24E-01	1.24E-01
830	GLNS	7.03E+00	1.40E+00	1.40E+00	1.40E+00	1.40E+00	1.40E+00
831	GLU5K	1.49E-01	1.73E-01	1.73E-01	1.73E-01	1.73E-01	1.73E-01
832	GLUABUTt7pp	2.00E-06	0.00E+00	0.00E+00	0.00E+00	0.00E+00	0.00E+00
833	GLUCYS	1.62E-04	1.79E-04	1.79E-04	1.79E-04	1.79E-04	1.79E-04
834	GLUDC	1.00E-06	0.00E+00	0.00E+00	0.00E+00	0.00E+00	0.00E+00
835	GLUDy	1.00E-06	-6.71E+00	-6.71E+00	-6.71E+00	-6.71E+00	-6.71E+00
836	GLUN	1.00E-06	0.00E+00	0.00E+00	0.00E+00	0.00E+00	0.00E+00
837	GLUPRT	3.02E-01	3.49E-01	3.49E-01	3.49E-01	3.49E-01	3.49E-01
838	GLUR	-1.91E-02	-2.21E-02	-2.21E-02	-2.21E-02	-2.21E-02	-2.21E-02
839	GLUSy	5.83E+00	0.00E+00	0.00E+00	0.00E+00	0.00E+00	0.00E+00
840	GLUTRR	3.72E-03	4.30E-03	4.30E-03	4.30E-03	4.30E-03	4.30E-03
841	GLUTRS	3.72E-03	4.30E-03	4.30E-03	4.30E-03	4.30E-03	4.30E-03
842	GLUabcpp	1.00E-06	0.00E+00	0.00E+00	0.00E+00	0.00E+00	0.00E+00
843	GLUt2rpp	1.00E-06	0.00E+00	0.00E+00	0.00E+00	0.00E+00	0.00E+00
844	GLUt4pp	1.00E-06	0.00E+00	0.00E+00	0.00E+00	0.00E+00	0.00E+00
845	GLUtex	-1.00E-06	2.84E-14	2.84E-14	2.84E-14	2.84E-14	2.84E-14
846	GLXCL	3.00E-06	0.00E+00	0.00E+00	0.00E+00	0.00E+00	0.00E+00
847	GLYALDtex	-1.00E-06	2.84E-14	2.84E-14	2.84E-14	2.84E-14	2.84E-14
848	GLYALDtpp	-1.00E-06	2.84E-14	2.84E-14	2.84E-14	2.84E-14	2.84E-14
849	GLYAT	7.00E-06	0.00E+00	0.00E+00	0.00E+00	0.00E+00	0.00E+00
850	GLYC3Pabcpp	4.00E-06	0.00E+00	0.00E+00	0.00E+00	0.00E+00	0.00E+00
851	GLYC3Pt6pp	1.00E-06	0.00E+00	0.00E+00	0.00E+00	0.00E+00	0.00E+00
852	GLYC3Ptex	-1.00E-06	2.84E-14	2.84E-14	2.84E-14	2.84E-14	2.84E-14
853	GLYCAt2rpp	-1.00E-06	2.84E-14	2.84E-14	2.84E-14	2.84E-14	2.84E-14
854	GLYCAtex	-1.00E-06	2.84E-14	2.84E-14	2.84E-14	2.84E-14	2.84E-14
855	GLYCDx	1.00E-06	0.00E+00	0.00E+00	0.00E+00	0.00E+00	0.00E+00
856	GLYCK	1.00E-06	0.00E+00	0.00E+00	0.00E+00	0.00E+00	0.00E+00
857	GLYCK2	1.00E-06	0.00E+00	0.00E+00	0.00E+00	0.00E+00	0.00E+00
858	GLYCL	3.99E-02	4.51E-02	4.51E-02	4.51E-02	4.51E-02	4.51E-02

859	GLYCLTDx	1.00E-06	0.00E+00	0.00E+00	0.00E+00	0.00E+00	0.00E+00
860	GLYCLTDy	1.00E-06	0.00E+00	0.00E+00	0.00E+00	0.00E+00	0.00E+00
861	GLYCLTt2rpp	-2.00E-06	0.00E+00	-1.00E+02	0.00E+00	0.00E+00	0.00E+00
862	GLYCLTt4pp	1.00E-06	0.00E+00	1.00E+02	0.00E+00	0.00E+00	0.00E+00
863	GLYCLTtex	-1.00E-06	0.00E+00	2.84E-14	0.00E+00	0.00E+00	0.00E+00
864	GLYCTO2	6.17E-04	7.16E-04	7.16E-04	7.16E-04	7.16E-04	7.16E-04
865	GLYCTO3	1.00E-06	0.00E+00	0.00E+00	0.00E+00	0.00E+00	0.00E+00
866	GLYCTO4	1.00E-06	0.00E+00	0.00E+00	0.00E+00	0.00E+00	0.00E+00
867	GLYCtex	-4.46E-03	2.84E-14	2.84E-14	2.84E-14	2.84E-14	2.84E-14
868	GLYCtpp	1.00E-06	-5.15E-03	-5.15E-03	-5.15E-03	-5.15E-03	-5.15E-03
869	GLYK	2.00E-06	5.15E-03	5.15E-03	5.15E-03	5.15E-03	5.15E-03
870	GLYOX	1.00E-06	0.00E+00	0.00E+00	0.00E+00	0.00E+00	0.00E+00
871	GLYOX3	1.00E-06	0.00E+00	0.00E+00	0.00E+00	0.00E+00	0.00E+00
872	GLYt2pp	1.00E+02	0.00E+00	0.00E+00	0.00E+00	0.00E+00	0.00E+00
873	GLYt2rpp	-1.00E+02	0.00E+00	0.00E+00	0.00E+00	0.00E+00	0.00E+00
874	GLYt4pp	1.00E-06	0.00E+00	0.00E+00	0.00E+00	0.00E+00	0.00E+00
875	GLYtex	-1.00E-06	0.00E+00	0.00E+00	0.00E+00	0.00E+00	0.00E+00
876	GMHEPAT	2.26E-02	2.62E-02	2.62E-02	2.62E-02	2.62E-02	2.62E-02
877	GMHEPK	2.26E-02	2.62E-02	2.62E-02	2.62E-02	2.62E-02	2.62E-02
878	GMHEPPA	2.26E-02	2.62E-02	2.62E-02	2.62E-02	2.62E-02	2.62E-02
879	GMPR	1.00E-06	0.00E+00	0.00E+00	0.00E+00	0.00E+00	0.00E+00
880	GMPS2	1.64E-01	1.90E-01	1.90E-01	1.90E-01	1.90E-01	1.90E-01
881	GND	8.02E+00	3.21E+00	3.21E+00	3.21E+00	3.21E+00	3.21E+00
882	GNK	1.00E-06	0.00E+00	0.00E+00	0.00E+00	0.00E+00	0.00E+00
883	GPDDA2	4.00E-06	0.00E+00	0.00E+00	0.00E+00	0.00E+00	0.00E+00
884	GPDDA2pp	2.00E-06	0.00E+00	0.00E+00	0.00E+00	0.00E+00	0.00E+00
885	GPDDA4	4.00E-06	0.00E+00	0.00E+00	0.00E+00	0.00E+00	0.00E+00
886	GPDDA4pp	1.00E-06	0.00E+00	0.00E+00	0.00E+00	0.00E+00	0.00E+00
887	GRTT	6.56E-04	7.61E-04	7.61E-04	7.61E-04	7.61E-04	7.61E-04
888	GRXR	1.72E-01	0.00E+00	9.95E-02	1.99E-01	1.99E-01	9.95E-02
889	GSNK	1.00E-06	0.00E+00	0.00E+00	0.00E+00	0.00E+00	0.00E+00
890	GSPMDA	1.00E-06	0.00E+00	0.00E+00	0.00E+00	0.00E+00	0.00E+00
891	GSPMDS	1.00E-06	0.00E+00	0.00E+00	0.00E+00	0.00E+00	0.00E+00
892	GTHOr	1.72E-01	0.00E+00	9.95E-02	1.99E-01	1.99E-01	9.95E-02
893	GTHPi	1.00E-06	0.00E+00	0.00E+00	0.00E+00	0.00E+00	0.00E+00
894	GTHRDHpp	6.00E-06	0.00E+00	0.00E+00	0.00E+00	0.00E+00	0.00E+00
895	GTHRDabc2pp	8.00E-06	0.00E+00	0.00E+00	0.00E+00	0.00E+00	0.00E+00
896	GTHRDabcpp	1.00E-06	0.00E+00	0.00E+00	0.00E+00	0.00E+00	0.00E+00
897	GTHRDtex	-1.00E-06	0.00E+00	0.00E+00	0.00E+00	0.00E+00	0.00E+00
898	GTHS	1.62E-04	1.79E-04	1.79E-04	1.79E-04	1.79E-04	1.79E-04
899	GTPCI	6.18E-04	7.16E-04	7.16E-04	7.16E-04	7.16E-04	7.16E-04
900	GTPCII2	3.09E-04	3.58E-04	3.58E-04	3.58E-04	3.58E-04	3.58E-04
901	GTPDPDP	1.00E-06	0.00E+00	0.00E+00	0.00E+00	0.00E+00	0.00E+00
902	GTPDPK	2.00E-06	0.00E+00	0.00E+00	0.00E+00	0.00E+00	0.00E+00
903	GTPHs	1.00E-06	0.00E+00	0.00E+00	0.00E+00	0.00E+00	0.00E+00
904	GUACYC	1.00E-06	0.00E+00	0.00E+00	0.00E+00	0.00E+00	0.00E+00
905	GUAD	1.00E-06	0.00E+00	0.00E+00	0.00E+00	0.00E+00	0.00E+00
906	GUAPRT	1.00E-06	0.00E+00	0.00E+00	0.00E+00	0.00E+00	0.00E+00
907	GUAt2pp	1.00E-06	0.00E+00	0.00E+00	0.00E+00	0.00E+00	0.00E+00
908	GUAtex	-1.00E-06	0.00E+00	0.00E+00	0.00E+00	0.00E+00	0.00E+00
909	GUAtpp	-2.00E-06	0.00E+00	0.00E+00	0.00E+00	0.00E+00	0.00E+00
910	H2Otex	-3.74E+01	-3.68E+01	-3.68E+01	-3.68E+01	-3.68E+01	-3.68E+01
911	H2Otpp	-3.74E+01	-3.69E+01	-3.69E+01	-3.68E+01	-3.68E+01	-3.69E+01
912	H2SO	1.00E-06	0.00E+00	0.00E+00	0.00E+00	0.00E+00	0.00E+00
913	H2St1pp	1.00E-06	0.00E+00	0.00E+00	0.00E+00	0.00E+00	0.00E+00
914	H2Stex	-1.00E-06	0.00E+00	0.00E+00	0.00E+00	0.00E+00	0.00E+00
915	HACD1	2.17E-01	2.52E-01	2.52E-01	2.52E-01	2.52E-01	2.52E-01
916	HACD2	2.17E-01	2.52E-01	2.52E-01	2.52E-01	2.52E-01	2.52E-01
917	HACD3	2.17E-01	2.52E-01	2.52E-01	2.52E-01	2.52E-01	2.52E-01
918	HACD4	1.18E-01	2.52E-01	2.52E-01	2.52E-01	2.52E-01	2.52E-01
919	HACD5	1.18E-01	2.52E-01	2.52E-01	2.52E-01	2.52E-01	2.52E-01
920	HACD6	8.97E-02	2.19E-01	2.19E-01	2.19E-01	2.19E-01	2.19E-01
921	HACD7	0.00E+00	1.36E-01	1.36E-01	1.36E-01	1.36E-01	1.36E-01
922	HACD8	0.00E+00	3.91E-02	3.91E-02	3.91E-02	3.91E-02	3.91E-02
923	HBZOPT	1.55E-04	1.79E-04	1.79E-04	1.79E-04	1.79E-04	1.79E-04
924	HCO3E	8.38E-01	4.51E-01	4.51E-01	4.51E-01	4.51E-01	4.51E-01
925	HCYSMT	1.00E-06	0.00E+00	0.00E+00	0.00E+00	0.00E+00	0.00E+00
926	HEMEOS	1.55E-04	1.79E-04	1.79E-04	1.79E-04	1.79E-04	1.79E-04
927	HEPK1	5.65E-03	6.55E-03	6.55E-03	6.55E-03	6.55E-03	6.55E-03
928	HEPK2	5.65E-03	6.55E-03	6.55E-03	6.55E-03	6.55E-03	6.55E-03
929	HEPT1	5.65E-03	6.55E-03	6.55E-03	6.55E-03	6.55E-03	6.55E-03
930	HEPT2	5.65E-03	6.55E-03	6.55E-03	6.55E-03	6.55E-03	6.55E-03
931	HEPT3	5.65E-03	6.55E-03	6.55E-03	6.55E-03	6.55E-03	6.55E-03

932	HEPT4	5.65E-03	6.55E-03	6.55E-03	6.55E-03	6.55E-03	6.55E-03
933	HEX1	8.00E-06	0.00E+00	0.00E+00	0.00E+00	0.00E+00	0.00E+00
934	HEX4	2.00E-06	0.00E+00	0.00E+00	0.00E+00	0.00E+00	0.00E+00
935	HEX7	2.00E-06	0.00E+00	0.00E+00	0.00E+00	0.00E+00	0.00E+00
936	HEXt2rpp	-2.00E-06	5.68E-14	5.68E-14	5.68E-14	5.68E-14	5.68E-14
937	HISTD	6.38E-02	7.39E-02	7.39E-02	7.39E-02	7.39E-02	7.39E-02
938	HISTP	6.38E-02	7.39E-02	7.39E-02	7.39E-02	7.39E-02	7.39E-02
939	HISabcpp	1.00E-06	0.00E+00	0.00E+00	0.00E+00	0.00E+00	0.00E+00
940	HISt2rpp	-2.00E-06	5.68E-14	5.68E-14	5.68E-14	5.68E-14	5.68E-14
941	HIStex	-1.00E-06	5.68E-14	5.68E-14	5.68E-14	5.68E-14	5.68E-14
942	HMBS	4.65E-04	5.37E-04	5.37E-04	5.37E-04	5.37E-04	5.37E-04
943	HOMt2pp	1.00E-06	0.00E+00	0.00E+00	0.00E+00	0.00E+00	0.00E+00
944	HOMtex	-1.00E-06	0.00E+00	0.00E+00	0.00E+00	0.00E+00	0.00E+00
945	HPPK2	6.18E-04	7.16E-04	7.16E-04	7.16E-04	7.16E-04	7.16E-04
946	HPYRI	-2.00E-06	0.00E+00	0.00E+00	0.00E+00	0.00E+00	0.00E+00
947	HPYRRx	1.00E-06	0.00E+00	0.00E+00	0.00E+00	0.00E+00	0.00E+00
948	HPYRRy	1.00E-06	0.00E+00	0.00E+00	0.00E+00	0.00E+00	0.00E+00
949	HSDy	-4.75E-01	-5.50E-01	-5.50E-01	-5.50E-01	-5.50E-01	-5.50E-01
950	HSK	3.67E-01	4.25E-01	4.25E-01	4.25E-01	4.25E-01	4.25E-01
951	HSST	1.08E-01	1.26E-01	1.26E-01	1.26E-01	1.26E-01	1.26E-01
952	HSTPT	6.38E-02	7.39E-02	7.39E-02	7.39E-02	7.39E-02	7.39E-02
953	HXAND	3.00E-06	0.00E+00	0.00E+00	0.00E+00	0.00E+00	0.00E+00
954	HXAtex	-1.00E-06	5.68E-14	5.68E-14	5.68E-14	5.68E-14	5.68E-14
955	HXCT	1.00E-06	0.00E+00	0.00E+00	0.00E+00	0.00E+00	0.00E+00
956	HXPRT	1.00E-06	0.00E+00	0.00E+00	0.00E+00	0.00E+00	0.00E+00
957	HYPOE	1.00E-06	0.00E+00	0.00E+00	0.00E+00	0.00E+00	0.00E+00
958	HYXNtex	-1.00E-06	2.84E-14	2.84E-14	2.84E-14	2.84E-14	2.84E-14
959	HYXNtpp	-1.00E-06	2.84E-14	2.84E-14	2.84E-14	2.84E-14	2.84E-14
960	Htex	1.00E-06	-7.31E+00	-7.31E+00	-7.31E+00	-7.31E+00	-7.31E+00
961	I2FE2SR	1.39E-06	1.61E-06	1.61E-06	1.61E-06	1.61E-06	1.61E-06
962	I2FE2SS	1.87E-04	2.19E-04	2.19E-04	2.19E-04	2.19E-04	2.19E-04
963	I2FE2SS2	1.73E-04	2.02E-04	2.02E-04	2.02E-04	2.02E-04	2.02E-04
964	I2FE2ST	1.56E-05	1.93E-05	1.93E-05	1.93E-05	1.93E-05	1.93E-05
965	I4FE4SR	1.73E-04	2.02E-04	2.02E-04	2.02E-04	2.02E-04	2.02E-04
966	I4FE4ST	1.73E-04	2.02E-04	2.02E-04	2.02E-04	2.02E-04	2.02E-04
967	ICDHyr	1.11E+00	4.10E+00	4.10E+00	4.10E+00	4.10E+00	4.10E+00
968	ICHORS	1.00E-06	0.00E+00	0.00E+00	0.00E+00	0.00E+00	0.00E+00
969	ICHORSi	7.78E-04	8.95E-04	8.95E-04	8.95E-04	8.95E-04	8.95E-04
970	ICHORT	4.70E-04	5.37E-04	5.37E-04	5.37E-04	5.37E-04	5.37E-04
971	ICL	2.91E+00	0.00E+00	0.00E+00	0.00E+00	0.00E+00	0.00E+00
972	ICYSDS	1.22E-03	1.42E-03	1.42E-03	1.42E-03	1.42E-03	1.42E-03
973	IDOND	1.00E-06	0.00E+00	0.00E+00	0.00E+00	0.00E+00	0.00E+00
974	IDOND2	1.00E-06	0.00E+00	0.00E+00	0.00E+00	0.00E+00	0.00E+00
975	IDONt2rpp	-2.00E-06	2.84E-14	2.84E-14	2.84E-14	2.84E-14	2.84E-14
976	IDONtex	-2.00E-06	2.84E-14	2.84E-14	2.84E-14	2.84E-14	2.84E-14
977	IG3PS	6.38E-02	7.39E-02	7.39E-02	7.39E-02	7.39E-02	7.39E-02
978	IGPDH	6.38E-02	7.39E-02	7.39E-02	7.39E-02	7.39E-02	7.39E-02
979	IGPS	3.83E-02	4.44E-02	4.44E-02	4.44E-02	4.44E-02	4.44E-02
980	ILETA	-1.96E-01	-2.27E-01	-2.27E-01	-2.27E-01	-2.27E-01	-2.27E-01
981	ILEabcpp	1.00E-06	0.00E+00	0.00E+00	0.00E+00	0.00E+00	0.00E+00
982	ILEt2rpp	-2.00E-06	5.68E-14	5.68E-14	5.68E-14	5.68E-14	5.68E-14
983	ILEtex	-1.00E-06	5.68E-14	5.68E-14	5.68E-14	5.68E-14	5.68E-14
984	IMPC	-3.65E-01	-4.23E-01	-4.23E-01	-4.23E-01	-4.23E-01	-4.23E-01
985	IMPD	1.64E-01	1.90E-01	1.90E-01	1.90E-01	1.90E-01	1.90E-01
986	INDOLEt2pp	2.00E-06	0.00E+00	0.00E+00	0.00E+00	0.00E+00	0.00E+00
987	INDOLEt2rpp	1.00E-06	0.00E+00	0.00E+00	0.00E+00	0.00E+00	0.00E+00
988	INDOLEtex	-1.00E-06	2.84E-14	2.84E-14	2.84E-14	2.84E-14	2.84E-14
989	INSH	1.00E-06	0.00E+00	0.00E+00	0.00E+00	0.00E+00	0.00E+00
990	INSK	1.00E-06	0.00E+00	0.00E+00	0.00E+00	0.00E+00	0.00E+00
991	INSt2pp	1.00E+02	0.00E+00	0.00E+00	0.00E+00	0.00E+00	0.00E+00
992	INSt2rpp	-1.00E+02	0.00E+00	0.00E+00	0.00E+00	0.00E+00	0.00E+00
993	INStex	-1.00E-06	0.00E+00	0.00E+00	0.00E+00	0.00E+00	0.00E+00
994	IPDDI	6.55E-04	0.00E+00	0.00E+00	-4.56E-03	0.00E+00	0.00E+00
995	IPDPS	4.59E-03	4.56E-03	4.56E-03	0.00E+00	4.56E-03	4.56E-03
996	IPMD	3.03E-01	3.52E-01	3.52E-01	3.52E-01	3.52E-01	3.52E-01
997	IPPMIa	-3.03E-01	-3.52E-01	-3.52E-01	-3.52E-01	-3.52E-01	-3.52E-01
998	IPPMIb	-3.03E-01	-3.52E-01	-3.52E-01	-3.52E-01	-3.52E-01	-3.52E-01
999	IPPS	3.03E-01	3.52E-01	3.52E-01	3.52E-01	3.52E-01	3.52E-01
1000	K2L4Aabcpp	1.00E-06	0.00E+00	0.00E+00	0.00E+00	0.00E+00	0.00E+00
1001	K2L4Aabctex	1.00E-06	0.00E+00	0.00E+00	0.00E+00	0.00E+00	0.00E+00
1002	KARA1	-5.89E-01	-6.82E-01	-6.82E-01	-6.82E-01	-6.82E-01	-6.82E-01
1003	KARA2	1.96E-01	2.27E-01	2.27E-01	2.27E-01	2.27E-01	2.27E-01
1004	KAS14	2.00E-06	0.00E+00	0.00E+00	0.00E+00	0.00E+00	0.00E+00

1005	KAS15	1.00E-06	0.00E+00	0.00E+00	0.00E+00	0.00E+00	0.00E+00
1006	KDOCT2	1.70E-02	1.96E-02	1.96E-02	1.96E-02	1.96E-02	1.96E-02
1007	KDOPP	1.70E-02	1.96E-02	1.96E-02	1.96E-02	1.96E-02	1.96E-02
1008	KDOPS	1.70E-02	1.96E-02	1.96E-02	1.96E-02	1.96E-02	1.96E-02
1009	Kabcpp	1.00E-06	0.00E+00	0.00E+00	0.00E+00	0.00E+00	0.00E+00
1010	Kt2pp	1.29E-01	1.49E-01	1.49E-01	1.49E-01	1.49E-01	1.49E-01
1011	Kt3pp	1.00E-06	0.00E+00	0.00E+00	0.00E+00	0.00E+00	0.00E+00
1012	Ktex	1.29E-01	1.49E-01	1.49E-01	1.49E-01	1.49E-01	1.49E-01
1013	L-LACD2	1.00E-06	0.00E+00	0.00E+00	0.00E+00	0.00E+00	0.00E+00
1014	L-LACD3	1.00E-06	0.00E+00	0.00E+00	0.00E+00	0.00E+00	0.00E+00
1015	L-LACt2rpp	-1.00E-06	2.84E-14	2.84E-14	2.84E-14	2.84E-14	2.84E-14
1016	L-LACtex	-1.00E-06	2.84E-14	2.84E-14	2.84E-14	2.84E-14	2.84E-14
1017	LA4NTpp	0.00E+00	0.00E+00	0.00E+00	0.00E+00	0.00E+00	0.00E+00
1018	LADGMDH	0.00E+00	0.00E+00	0.00E+00	0.00E+00	0.00E+00	0.00E+00
1019	LALDO2x	1.00E-06	0.00E+00	0.00E+00	0.00E+00	0.00E+00	0.00E+00
1020	LALDO3	4.00E-06	0.00E+00	0.00E+00	0.00E+00	0.00E+00	0.00E+00
1021	LALGP	0.00E+00	0.00E+00	0.00E+00	0.00E+00	0.00E+00	0.00E+00
1022	LCADi	3.00E-06	0.00E+00	0.00E+00	0.00E+00	0.00E+00	0.00E+00
1023	LCARR	1.00E-06	0.00E+00	0.00E+00	0.00E+00	0.00E+00	0.00E+00
1024	LCARS	1.00E-06	-2.84E-14	-2.84E-14	-2.84E-14	-2.84E-14	-2.84E-14
1025	LCTSt3ipp	1.00E-06	0.00E+00	0.00E+00	0.00E+00	0.00E+00	0.00E+00
1026	LCTStpp	1.00E-06	0.00E+00	0.00E+00	0.00E+00	0.00E+00	0.00E+00
1027	LDH_D	8.00E-06	0.00E+00	0.00E+00	0.00E+00	0.00E+00	0.00E+00
1028	LDH_D2	1.00E-06	0.00E+00	0.00E+00	0.00E+00	0.00E+00	0.00E+00
1029	LEUTAi	3.03E-01	3.52E-01	3.52E-01	3.52E-01	3.52E-01	3.52E-01
1030	LEUabcpp	1.00E-06	0.00E+00	0.00E+00	0.00E+00	0.00E+00	0.00E+00
1031	LEUt2rpp	-2.00E-06	5.68E-14	5.68E-14	5.68E-14	5.68E-14	5.68E-14
1032	LEUtex	-1.00E-06	5.68E-14	5.68E-14	5.68E-14	5.68E-14	5.68E-14
1033	LGTHL	1.00E-06	0.00E+00	0.00E+00	0.00E+00	0.00E+00	0.00E+00
1034	LIPACabcpp	1.00E-06	0.00E+00	0.00E+00	0.00E+00	0.00E+00	0.00E+00
1035	LIPAabcpp	3.00E-06	0.00E+00	0.00E+00	0.00E+00	0.00E+00	0.00E+00
1036	LIPAabctex	1.00E-06	0.00E+00	0.00E+00	0.00E+00	0.00E+00	0.00E+00
1037	LIPOCT	1.08E-06	2.41E-06	2.41E-06	2.41E-06	2.41E-06	2.41E-06
1038	LIPOS	2.08E-06	2.41E-06	2.41E-06	2.41E-06	2.41E-06	2.41E-06
1039	LPADSS	5.66E-03	6.55E-03	6.55E-03	6.55E-03	6.55E-03	6.55E-03
1040	LPLIPAL1A120pp	1.00E-06	0.00E+00	0.00E+00	0.00E+00	0.00E+00	0.00E+00
1041	LPLIPAL1A140pp	1.00E-06	0.00E+00	0.00E+00	0.00E+00	0.00E+00	0.00E+00
1042	LPLIPAL1A141pp	1.00E-06	0.00E+00	0.00E+00	0.00E+00	0.00E+00	0.00E+00
1043	LPLIPAL1A160pp	0.00E+00	0.00E+00	0.00E+00	0.00E+00	0.00E+00	0.00E+00
1044	LPLIPAL1A161pp	0.00E+00	0.00E+00	0.00E+00	0.00E+00	0.00E+00	0.00E+00
1045	LPLIPAL1A180pp	0.00E+00	0.00E+00	0.00E+00	0.00E+00	0.00E+00	0.00E+00
1046	LPLIPAL1A181pp	0.00E+00	0.00E+00	0.00E+00	0.00E+00	0.00E+00	0.00E+00
1047	LPLIPAL1E120pp	2.00E-06	0.00E+00	0.00E+00	0.00E+00	0.00E+00	0.00E+00
1048	LPLIPAL1E140pp	1.00E-06	0.00E+00	0.00E+00	0.00E+00	0.00E+00	0.00E+00
1049	LPLIPAL1E141pp	1.00E-06	0.00E+00	0.00E+00	0.00E+00	0.00E+00	0.00E+00
1050	LPLIPAL1E160pp	0.00E+00	0.00E+00	0.00E+00	0.00E+00	0.00E+00	0.00E+00
1051	LPLIPAL1E161pp	0.00E+00	0.00E+00	0.00E+00	0.00E+00	0.00E+00	0.00E+00
1052	LPLIPAL1E180pp	0.00E+00	0.00E+00	0.00E+00	0.00E+00	0.00E+00	0.00E+00
1053	LPLIPAL1E181pp	0.00E+00	0.00E+00	0.00E+00	0.00E+00	0.00E+00	0.00E+00
1054	LPLIPAL1G120pp	1.00E-06	0.00E+00	0.00E+00	0.00E+00	0.00E+00	0.00E+00
1055	LPLIPAL1G140pp	1.00E-06	0.00E+00	0.00E+00	0.00E+00	0.00E+00	0.00E+00
1056	LPLIPAL1G141pp	1.00E-06	0.00E+00	0.00E+00	0.00E+00	0.00E+00	0.00E+00
1057	LPLIPAL1G160pp	0.00E+00	0.00E+00	0.00E+00	0.00E+00	0.00E+00	0.00E+00
1058	LPLIPAL1G161pp	0.00E+00	0.00E+00	0.00E+00	0.00E+00	0.00E+00	0.00E+00
1059	LPLIPAL1G180pp	0.00E+00	0.00E+00	0.00E+00	0.00E+00	0.00E+00	0.00E+00
1060	LPLIPAL1G181pp	0.00E+00	0.00E+00	0.00E+00	0.00E+00	0.00E+00	0.00E+00
1061	LPLIPAL2A120	1.00E-06	0.00E+00	0.00E+00	0.00E+00	0.00E+00	0.00E+00
1062	LPLIPAL2A140	1.00E-06	0.00E+00	0.00E+00	0.00E+00	0.00E+00	0.00E+00
1063	LPLIPAL2A141	0.00E+00	0.00E+00	0.00E+00	0.00E+00	0.00E+00	0.00E+00
1064	LPLIPAL2A160	0.00E+00	0.00E+00	0.00E+00	0.00E+00	0.00E+00	0.00E+00
1065	LPLIPAL2A161	0.00E+00	0.00E+00	0.00E+00	0.00E+00	0.00E+00	0.00E+00
1066	LPLIPAL2A180	0.00E+00	0.00E+00	0.00E+00	0.00E+00	0.00E+00	0.00E+00
1067	LPLIPAL2A181	0.00E+00	0.00E+00	0.00E+00	0.00E+00	0.00E+00	0.00E+00
1068	LPLIPAL2E120	1.00E-06	0.00E+00	0.00E+00	0.00E+00	0.00E+00	0.00E+00
1069	LPLIPAL2E140	1.00E-06	0.00E+00	0.00E+00	0.00E+00	0.00E+00	0.00E+00
1070	LPLIPAL2E141	1.00E-06	0.00E+00	0.00E+00	0.00E+00	0.00E+00	0.00E+00
1071	LPLIPAL2E160	0.00E+00	0.00E+00	0.00E+00	0.00E+00	0.00E+00	0.00E+00
1072	LPLIPAL2E161	0.00E+00	0.00E+00	0.00E+00	0.00E+00	0.00E+00	0.00E+00
1073	LPLIPAL2E180	0.00E+00	0.00E+00	0.00E+00	0.00E+00	0.00E+00	0.00E+00
1074	LPLIPAL2E181	0.00E+00	0.00E+00	0.00E+00	0.00E+00	0.00E+00	0.00E+00
1075	LPLIPAL2G120	1.00E-06	0.00E+00	0.00E+00	0.00E+00	0.00E+00	0.00E+00
1076	LPLIPAL2G140	1.00E-06	0.00E+00	0.00E+00	0.00E+00	0.00E+00	0.00E+00
1077	LPLIPAL2G141	1.00E-06	0.00E+00	0.00E+00	0.00E+00	0.00E+00	0.00E+00

1078	LPLIPAL2G160	0.00E+00	0.00E+00	0.00E+00	0.00E+00	0.00E+00	0.00E+00
1079	LPLIPAL2G161	0.00E+00	0.00E+00	0.00E+00	0.00E+00	0.00E+00	0.00E+00
1080	LPLIPAL2G180	0.00E+00	0.00E+00	0.00E+00	0.00E+00	0.00E+00	0.00E+00
1081	LPLIPAL2G181	0.00E+00	0.00E+00	0.00E+00	0.00E+00	0.00E+00	0.00E+00
1082	LSERDHr	1.00E-06	0.00E+00	0.00E+00	0.00E+00	0.00E+00	0.00E+00
1083	LYSDC	1.00E-06	0.00E+00	0.00E+00	0.00E+00	0.00E+00	0.00E+00
1084	LYSabcpp	1.00E-06	0.00E+00	0.00E+00	0.00E+00	0.00E+00	0.00E+00
1085	LYSt2pp	1.00E-06	0.00E+00	0.00E+00	0.00E+00	0.00E+00	0.00E+00
1086	LYSt3pp	4.00E-06	0.00E+00	0.00E+00	0.00E+00	0.00E+00	0.00E+00
1087	LYStex	-1.00E-06	0.00E+00	0.00E+00	0.00E+00	0.00E+00	0.00E+00
1088	MACPD	1.00E-06	0.00E+00	0.00E+00	0.00E+00	0.00E+00	0.00E+00
1089	MALCOAMT	1.39E-06	1.61E-06	1.61E-06	1.61E-06	1.61E-06	1.61E-06
1090	MALS	2.91E+00	7.16E-04	7.16E-04	7.16E-04	7.16E-04	7.16E-04
1091	MALt2_2pp	1.00E-06	0.00E+00	0.00E+00	0.00E+00	0.00E+00	0.00E+00
1092	MALt2_3pp	1.00E-06	0.00E+00	0.00E+00	0.00E+00	0.00E+00	0.00E+00
1093	MALt3pp	3.00E-06	0.00E+00	0.00E+00	0.00E+00	0.00E+00	0.00E+00
1094	MALtex	-1.00E-06	0.00E+00	0.00E+00	0.00E+00	0.00E+00	0.00E+00
1095	MAN1PT2	2.00E-06	0.00E+00	0.00E+00	0.00E+00	0.00E+00	0.00E+00
1096	MCITD	2.00E-06	0.00E+00	0.00E+00	0.00E+00	0.00E+00	0.00E+00
1097	MCITL2	2.00E-06	0.00E+00	0.00E+00	0.00E+00	0.00E+00	0.00E+00
1098	MCITS	2.00E-06	0.00E+00	0.00E+00	0.00E+00	0.00E+00	0.00E+00
1099	MCOATA	5.37E-01	1.02E-01	1.02E-01	1.02E-01	1.02E-01	1.02E-01
1100	MCTP1App	7.93E-03	9.18E-03	9.18E-03	9.18E-03	9.18E-03	9.18E-03
1101	MCTP1Bpp	9.30E-04	1.08E-03	1.08E-03	1.08E-03	1.08E-03	1.08E-03
1102	MCTP2App	4.67E-04	5.40E-04	5.40E-04	5.40E-04	5.40E-04	5.40E-04
1103	MDDCP1pp	7.51E-03	8.70E-03	8.70E-03	8.70E-03	8.70E-03	8.70E-03
1104	MDDCP2pp	4.67E-04	5.40E-04	5.40E-04	5.40E-04	5.40E-04	5.40E-04
1105	MDDCP3pp	1.00E-06	0.00E+00	0.00E+00	0.00E+00	0.00E+00	0.00E+00
1106	MDDCP4pp	2.00E-06	0.00E+00	0.00E+00	0.00E+00	0.00E+00	0.00E+00
1107	MDDCP5pp	2.00E-06	0.00E+00	0.00E+00	0.00E+00	0.00E+00	0.00E+00
1108	MDDEP1pp	3.73E-03	4.32E-03	4.32E-03	4.32E-03	4.32E-03	4.32E-03
1109	MDDEP2pp	1.00E-06	0.00E+00	0.00E+00	0.00E+00	0.00E+00	0.00E+00
1110	MDDEP3pp	1.00E-06	0.00E+00	0.00E+00	0.00E+00	0.00E+00	0.00E+00
1111	MDDEP4pp	1.00E-06	0.00E+00	0.00E+00	0.00E+00	0.00E+00	0.00E+00
1112	MDH	5.99E+00	4.04E+00	4.04E+00	4.04E+00	4.04E+00	4.04E+00
1113	MDH2	1.00E-06	0.00E+00	0.00E+00	0.00E+00	0.00E+00	0.00E+00
1114	MDH3	1.00E-06	0.00E+00	0.00E+00	0.00E+00	0.00E+00	0.00E+00
1115	ME1	1.00E-06	0.00E+00	0.00E+00	0.00E+00	0.00E+00	0.00E+00
1116	ME2	8.80E-01	0.00E+00	0.00E+00	0.00E+00	0.00E+00	0.00E+00
1117	MECDPDH5	4.59E-03	5.32E-03	5.32E-03	5.32E-03	5.32E-03	5.32E-03
1118	MECDPS	4.59E-03	5.32E-03	5.32E-03	5.32E-03	5.32E-03	5.32E-03
1119	MELIBt2pp	1.00E-06	0.00E+00	0.00E+00	0.00E+00	0.00E+00	0.00E+00
1120	MELIBt3ipp	1.00E-06	0.00E+00	0.00E+00	0.00E+00	0.00E+00	0.00E+00
1121	MEOHtex	-1.39E-06	-1.61E-06	-1.61E-06	-1.61E-06	-1.61E-06	-1.61E-06
1122	MEOHtrpp	-1.39E-06	-1.61E-06	-1.61E-06	-1.61E-06	-1.61E-06	-1.61E-06
1123	MEPCT	4.59E-03	5.32E-03	5.32E-03	5.32E-03	5.32E-03	5.32E-03
1124	METAT	5.92E-03	6.86E-03	6.86E-03	6.86E-03	6.86E-03	6.86E-03
1125	METOX1s	1.00E-06	0.00E+00	0.00E+00	0.00E+00	0.00E+00	0.00E+00
1126	METOX2s	1.00E-06	0.00E+00	0.00E+00	0.00E+00	0.00E+00	0.00E+00
1127	METS	1.09E-01	1.27E-01	1.27E-01	1.27E-01	1.27E-01	1.27E-01
1128	METSOXR1	1.00E-06	0.00E+00	0.00E+00	0.00E+00	0.00E+00	0.00E+00
1129	METSOXR2	1.00E-06	0.00E+00	0.00E+00	0.00E+00	0.00E+00	0.00E+00
1130	MG2t3_2pp	5.72E-03	6.63E-03	6.63E-03	6.63E-03	6.63E-03	6.63E-03
1131	MG2tex	5.72E-03	6.63E-03	6.63E-03	6.63E-03	6.63E-03	6.63E-03
1132	MG2tpp	1.00E-06	0.00E+00	0.00E+00	0.00E+00	0.00E+00	0.00E+00
1133	MG2uabcpp	1.00E-06	0.00E+00	0.00E+00	0.00E+00	0.00E+00	0.00E+00
1134	MGSA	1.00E-06	0.00E+00	0.00E+00	0.00E+00	0.00E+00	0.00E+00
1135	MICITDr	2.00E-06	0.00E+00	0.00E+00	0.00E+00	0.00E+00	0.00E+00
1136	MINCYCtex	1.00E-06	0.00E+00	0.00E+00	0.00E+00	0.00E+00	0.00E+00
1137	MINCYCtpp	1.00E-06	0.00E+00	0.00E+00	0.00E+00	0.00E+00	0.00E+00
1138	MLDCP1App	4.20E-04	4.86E-04	4.86E-04	4.86E-04	4.86E-04	4.86E-04
1139	MLDCP1Bpp	1.00E-06	0.00E+00	0.00E+00	0.00E+00	0.00E+00	0.00E+00
1140	MLDCP2App	1.00E-06	0.00E+00	0.00E+00	0.00E+00	0.00E+00	0.00E+00
1141	MLDCP2Bpp	3.00E-06	0.00E+00	0.00E+00	0.00E+00	0.00E+00	0.00E+00
1142	MLDCP3App	9.29E-04	1.08E-03	1.08E-03	1.08E-03	1.08E-03	1.08E-03
1143	MLDEP1pp	9.29E-04	1.08E-03	1.08E-03	1.08E-03	1.08E-03	1.08E-03
1144	MLDEP2pp	1.00E-06	0.00E+00	0.00E+00	0.00E+00	0.00E+00	0.00E+00
1145	MLTG3	1.00E-06	0.00E+00	0.00E+00	0.00E+00	0.00E+00	0.00E+00
1146	MLTG4	1.00E-06	0.00E+00	0.00E+00	0.00E+00	0.00E+00	0.00E+00
1147	MLTG5	1.00E-06	0.00E+00	0.00E+00	0.00E+00	0.00E+00	0.00E+00
1148	MLTGY1pp	3.00E-06	0.00E+00	0.00E+00	0.00E+00	0.00E+00	0.00E+00
1149	MLTGY2pp	1.00E-06	0.00E+00	0.00E+00	0.00E+00	0.00E+00	0.00E+00
1150	MLTGY3pp	0.00E+00	0.00E+00	0.00E+00	0.00E+00	0.00E+00	0.00E+00

1151	MLTGY4pp	1.00E-06	0.00E+00	0.00E+00	0.00E+00	0.00E+00	0.00E+00
1152	MLTP1	-1.00E-06	0.00E+00	0.00E+00	0.00E+00	0.00E+00	0.00E+00
1153	MLTP2	-1.00E-06	0.00E+00	0.00E+00	0.00E+00	0.00E+00	0.00E+00
1154	MLTP3	-1.00E-06	0.00E+00	0.00E+00	0.00E+00	0.00E+00	0.00E+00
1155	MMCD	1.00E-06	0.00E+00	0.00E+00	0.00E+00	0.00E+00	0.00E+00
1156	MMM	1.00E-06	0.00E+00	0.00E+00	0.00E+00	0.00E+00	0.00E+00
1157	MN2t3pp	1.00E-06	0.00E+00	0.00E+00	0.00E+00	0.00E+00	0.00E+00
1158	MN2tpp	4.56E-04	5.28E-04	5.28E-04	5.28E-04	5.28E-04	5.28E-04
1159	MN6PP	1.00E-06	0.00E+00	0.00E+00	0.00E+00	0.00E+00	0.00E+00
1160	MNt2pp	1.00E-06	0.00E+00	0.00E+00	0.00E+00	0.00E+00	0.00E+00
1161	MNtex	4.56E-04	5.28E-04	5.28E-04	5.28E-04	5.28E-04	5.28E-04
1162	MOADSUx	3.41E-04	3.95E-04	3.95E-04	3.95E-04	3.95E-04	3.95E-04
1163	MOAT	5.66E-03	6.55E-03	6.55E-03	6.55E-03	6.55E-03	6.55E-03
1164	MOAT2	5.66E-03	6.55E-03	6.55E-03	6.55E-03	6.55E-03	6.55E-03
1165	MOAT3C	5.65E-03	6.55E-03	6.55E-03	6.55E-03	6.55E-03	6.55E-03
1166	MOBDabcpp	9.49E-05	1.10E-04	1.10E-04	1.10E-04	1.10E-04	1.10E-04
1167	MOBDtex	9.49E-05	1.10E-04	1.10E-04	1.10E-04	1.10E-04	1.10E-04
1168	MOCDS	4.85E-06	5.62E-06	5.62E-06	5.62E-06	5.62E-06	5.62E-06
1169	MOCOS	9.01E-05	1.04E-04	1.04E-04	1.04E-04	1.04E-04	1.04E-04
1170	MOGDS	4.85E-06	5.62E-06	5.62E-06	5.62E-06	5.62E-06	5.62E-06
1171	MOHMT	3.99E-04	4.63E-04	4.63E-04	4.63E-04	4.63E-04	4.63E-04
1172	MOX	9.87E-04	9.73E-04	9.73E-04	1.15E-03	1.15E-03	9.73E-04
1173	MPTAT	1.70E-04	1.98E-04	1.98E-04	1.98E-04	1.98E-04	1.98E-04
1174	MPTG	9.33E-03	1.08E-02	1.08E-02	1.08E-02	1.08E-02	1.08E-02
1175	MPTG2	4.67E-04	5.40E-04	5.40E-04	5.40E-04	5.40E-04	5.40E-04
1176	MPTS	1.70E-04	1.98E-04	1.98E-04	1.98E-04	1.98E-04	1.98E-04
1177	MPTSS	3.41E-04	3.95E-04	3.95E-04	3.95E-04	3.95E-04	3.95E-04
1178	MSAR	1.00E-06	0.00E+00	0.00E+00	0.00E+00	0.00E+00	0.00E+00
1179	MTAN	4.68E-03	5.42E-03	5.42E-03	5.42E-03	5.42E-03	5.42E-03
1180	MTHFC	6.67E-01	7.71E-01	7.71E-01	7.71E-01	7.71E-01	7.71E-01
1181	MTHFD	6.67E-01	7.71E-01	7.71E-01	7.71E-01	7.71E-01	7.71E-01
1182	MTHFR2	1.09E-01	1.27E-01	1.27E-01	1.27E-01	1.27E-01	1.27E-01
1183	MTHTHFSs	9.30E-04	1.08E-03	1.08E-03	1.08E-03	1.08E-03	1.08E-03
1184	NACODA	1.00E-06	0.00E+00	0.00E+00	0.00E+00	0.00E+00	0.00E+00
1185	NADDP	3.00E-06	0.00E+00	0.00E+00	0.00E+00	0.00E+00	0.00E+00
1186	NADH10	1.00E-06	0.00E+00	0.00E+00	0.00E+00	0.00E+00	0.00E+00
1187	NADH16pp	1.32E+01	2.55E+01	2.55E+01	2.55E+01	2.55E+01	2.55E+01
1188	NADH17pp	1.00E-06	0.00E+00	0.00E+00	0.00E+00	0.00E+00	0.00E+00
1189	NADH18pp	1.00E-06	0.00E+00	0.00E+00	0.00E+00	0.00E+00	0.00E+00
1190	NADH5	1.00E-06	0.00E+00	0.00E+00	0.00E+00	0.00E+00	0.00E+00
1191	NADH9	1.00E-06	0.00E+00	0.00E+00	0.00E+00	0.00E+00	0.00E+00
1192	NADK	3.11E-04	3.59E-04	3.59E-04	3.59E-04	3.59E-04	3.59E-04
1193	NADN	1.00E-06	0.00E+00	0.00E+00	0.00E+00	0.00E+00	0.00E+00
1194	NADPHQR2	1.00E-06	0.00E+00	0.00E+00	0.00E+00	0.00E+00	0.00E+00
1195	NADPHQR3	1.00E-06	0.00E+00	0.00E+00	0.00E+00	0.00E+00	0.00E+00
1196	NADPHQR4	1.00E-06	0.00E+00	0.00E+00	0.00E+00	0.00E+00	0.00E+00
1197	NADPPPS	1.00E-06	0.00E+00	0.00E+00	0.00E+00	0.00E+00	0.00E+00
1198	NADS1	1.58E-03	1.83E-03	1.83E-03	1.83E-03	1.83E-03	1.83E-03
1199	NADTRHD	1.00E-06	0.00E+00	0.00E+00	0.00E+00	0.00E+00	0.00E+00
1200	NAMNPP	2.00E-06	0.00E+00	0.00E+00	0.00E+00	0.00E+00	0.00E+00
1201	NAt3_1p5pp	1.00E-06	0.00E+00	0.00E+00	0.00E+00	0.00E+00	0.00E+00
1202	NAt3_2pp	1.00E-06	0.00E+00	0.00E+00	0.00E+00	0.00E+00	0.00E+00
1203	NAt3pp	1.00E+02	1.00E+02	1.00E+02	1.00E+02	0.00E+00	1.00E+02
1204	NDPK1	5.19E-01	0.00E+00	2.66E+00	6.22E-01	6.22E-01	2.66E+00
1205	NDPK2	2.77E-01	3.41E-01	3.41E-01	3.41E-01	3.41E-01	3.41E-01
1206	NDPK3	9.58E-02	1.32E-01	1.32E-01	1.32E-01	1.32E-01	1.32E-01
1207	NDPK4	2.28E-02	2.65E-02	2.65E-02	2.65E-02	2.65E-02	2.65E-02
1208	NDPK5	1.78E-02	0.00E+00	-2.84E-14	-2.84E-14	-2.84E-14	-2.84E-14
1209	NDPK6	1.72E-02	0.00E+00	0.00E+00	0.00E+00	0.00E+00	0.00E+00
1210	NDPK7	1.78E-02	0.00E+00	0.00E+00	0.00E+00	0.00E+00	0.00E+00
1211	NDPK8	1.72E-02	0.00E+00	0.00E+00	0.00E+00	0.00E+00	-2.84E-14
1212	NH4tex	7.28E+00	8.44E+00	8.44E+00	8.44E+00	8.44E+00	8.44E+00
1213	NH4tpp	7.28E+00	8.44E+00	8.44E+00	8.44E+00	8.44E+00	8.44E+00
1214	NHFRBO	1.00E-06	0.00E+00	0.00E+00	0.00E+00	0.00E+00	0.00E+00
1215	NI2abcpp	1.00E-06	0.00E+00	0.00E+00	0.00E+00	0.00E+00	0.00E+00
1216	NI2t3pp	1.00E-06	0.00E+00	0.00E+00	0.00E+00	0.00E+00	0.00E+00
1217	NI2tex	2.13E-04	2.47E-04	2.47E-04	2.47E-04	2.47E-04	2.47E-04
1218	NI2tpp	2.14E-04	2.47E-04	2.47E-04	2.47E-04	2.47E-04	2.47E-04
1219	NI2uabcpp	1.00E-06	0.00E+00	0.00E+00	0.00E+00	0.00E+00	0.00E+00
1220	NMNAT	1.00E-06	0.00E+00	0.00E+00	0.00E+00	0.00E+00	0.00E+00
1221	NMNDA	1.00E-06	0.00E+00	0.00E+00	0.00E+00	0.00E+00	0.00E+00
1222	NMNN	1.00E-06	0.00E+00	0.00E+00	0.00E+00	0.00E+00	0.00E+00
1223	NNAM	2.00E-06	0.00E+00	0.00E+00	0.00E+00	0.00E+00	0.00E+00

1224	NNATr	1.58E-03	1.83E-03	1.83E-03	1.83E-03	1.83E-03	1.83E-03
1225	NNDPR	1.58E-03	1.83E-03	1.83E-03	1.83E-03	1.83E-03	1.83E-03
1226	NOVBCNtex	1.00E-06	0.00E+00	0.00E+00	0.00E+00	0.00E+00	0.00E+00
1227	NOVBCNtpp	1.00E-06	0.00E+00	0.00E+00	0.00E+00	0.00E+00	0.00E+00
1228	NTD1	1.00E-06	0.00E+00	0.00E+00	0.00E+00	0.00E+00	0.00E+00
1229	NTD10	3.00E-06	0.00E+00	0.00E+00	0.00E+00	0.00E+00	0.00E+00
1230	NTD11	3.00E-06	0.00E+00	0.00E+00	0.00E+00	0.00E+00	0.00E+00
1231	NTD12	1.00E-06	0.00E+00	0.00E+00	0.00E+00	0.00E+00	0.00E+00
1232	NTD2	3.00E-06	0.00E+00	0.00E+00	0.00E+00	0.00E+00	0.00E+00
1233	NTD3	1.00E-06	0.00E+00	0.00E+00	0.00E+00	0.00E+00	0.00E+00
1234	NTD4	4.00E-06	0.00E+00	0.00E+00	0.00E+00	0.00E+00	0.00E+00
1235	NTD5	3.00E-06	0.00E+00	0.00E+00	0.00E+00	0.00E+00	0.00E+00
1236	NTD6	2.00E-06	0.00E+00	0.00E+00	0.00E+00	0.00E+00	0.00E+00
1237	NTD7	5.00E-06	0.00E+00	0.00E+00	0.00E+00	0.00E+00	0.00E+00
1238	NTD8	1.00E-06	0.00E+00	0.00E+00	0.00E+00	0.00E+00	0.00E+00
1239	NTD9	1.00E-06	0.00E+00	0.00E+00	0.00E+00	0.00E+00	0.00E+00
1240	NTP1	1.00E-06	0.00E+00	0.00E+00	0.00E+00	0.00E+00	0.00E+00
1241	NTP10	1.00E-06	0.00E+00	0.00E+00	0.00E+00	0.00E+00	0.00E+00
1242	NTP3	1.00E-06	0.00E+00	0.00E+00	0.00E+00	0.00E+00	0.00E+00
1243	NTP5	1.00E-06	0.00E+00	0.00E+00	0.00E+00	0.00E+00	0.00E+00
1244	NTPP1	2.00E-06	0.00E+00	0.00E+00	0.00E+00	0.00E+00	0.00E+00
1245	NTPP10	1.00E-06	0.00E+00	0.00E+00	0.00E+00	0.00E+00	0.00E+00
1246	NTPP11	1.00E-06	0.00E+00	0.00E+00	0.00E+00	0.00E+00	0.00E+00
1247	NTPP2	1.00E-06	0.00E+00	0.00E+00	0.00E+00	0.00E+00	0.00E+00
1248	NTPP3	2.00E-06	0.00E+00	0.00E+00	0.00E+00	0.00E+00	0.00E+00
1249	NTPP4	1.00E-06	0.00E+00	0.00E+00	0.00E+00	0.00E+00	0.00E+00
1250	NTPP5	3.00E-06	0.00E+00	0.00E+00	0.00E+00	0.00E+00	0.00E+00
1251	NTPP6	1.00E-06	0.00E+00	0.00E+00	0.00E+00	0.00E+00	0.00E+00
1252	NTPP7	1.00E-06	0.00E+00	0.00E+00	0.00E+00	0.00E+00	0.00E+00
1253	NTPP8	1.00E-06	0.00E+00	0.00E+00	0.00E+00	0.00E+00	0.00E+00
1254	NTPP9	1.00E-06	0.00E+00	0.00E+00	0.00E+00	0.00E+00	0.00E+00
1255	NTPTP1	1.00E-06	0.00E+00	0.00E+00	0.00E+00	0.00E+00	0.00E+00
1256	NTPTP2	1.00E-06	0.00E+00	0.00E+00	0.00E+00	0.00E+00	0.00E+00
1257	O2tex	1.87E+01	1.45E+01	1.45E+01	1.45E+01	1.45E+01	1.45E+01
1258	O2tpp	1.87E+01	1.45E+01	1.45E+01	1.45E+01	1.45E+01	1.45E+01
1259	OAADC	1.00E-06	0.00E+00	0.00E+00	0.00E+00	0.00E+00	0.00E+00
1260	OBTFL	1.00E-06	0.00E+00	0.00E+00	0.00E+00	0.00E+00	0.00E+00
1261	OCBT	1.99E-01	2.31E-01	2.31E-01	2.31E-01	2.31E-01	2.31E-01
1262	OCTDPS	4.64E-04	5.37E-04	5.37E-04	5.37E-04	5.37E-04	5.37E-04
1263	OCTNLL	1.00E-06	0.00E+00	0.00E+00	0.00E+00	0.00E+00	0.00E+00
1264	OGMEACPD	1.39E-06	1.61E-06	1.61E-06	1.61E-06	1.61E-06	1.61E-06
1265	OGMEACPR	1.39E-06	1.61E-06	1.61E-06	1.61E-06	1.61E-06	1.61E-06
1266	OGMEACPS	1.39E-06	1.61E-06	1.61E-06	1.61E-06	1.61E-06	1.61E-06
1267	OHPBAT	1.55E-04	1.79E-04	1.79E-04	1.79E-04	1.79E-04	1.79E-04
1268	OHPHM	1.55E-04	1.79E-04	1.79E-04	1.79E-04	1.79E-04	1.79E-04
1269	OMBZLM	1.55E-04	1.79E-04	1.79E-04	1.79E-04	1.79E-04	1.79E-04
1270	OMCDC	3.03E-01	3.52E-01	3.52E-01	3.52E-01	3.52E-01	3.52E-01
1271	OMMBLHX	1.54E-04	1.79E-04	1.79E-04	1.79E-04	1.79E-04	1.79E-04
1272	OMMBLHX3	1.00E-06	0.00E+00	0.00E+00	0.00E+00	0.00E+00	0.00E+00
1273	OMPDC	2.22E-01	2.57E-01	2.57E-01	2.57E-01	2.57E-01	2.57E-01
1274	OMPHHX	1.54E-04	1.79E-04	1.79E-04	1.79E-04	1.79E-04	1.79E-04
1275	OMPHHX3	1.00E-06	0.00E+00	0.00E+00	0.00E+00	0.00E+00	0.00E+00
1276	OPHBDC	1.55E-04	1.79E-04	1.79E-04	1.79E-04	1.79E-04	1.79E-04
1277	OPHHX	1.54E-04	1.79E-04	1.79E-04	1.79E-04	1.79E-04	1.79E-04
1278	OPHHX3	1.00E-06	0.00E+00	0.00E+00	0.00E+00	0.00E+00	0.00E+00
1279	OPMEACPD	1.39E-06	1.61E-06	1.61E-06	1.61E-06	1.61E-06	1.61E-06
1280	OPMEACPR	1.39E-06	1.61E-06	1.61E-06	1.61E-06	1.61E-06	1.61E-06
1281	OPMEACPS	1.39E-06	1.61E-06	1.61E-06	1.61E-06	1.61E-06	1.61E-06
1282	ORNDC	2.77E-02	3.21E-02	3.21E-02	3.21E-02	3.21E-02	3.21E-02
1283	ORNabcpp	1.00E-06	0.00E+00	0.00E+00	0.00E+00	0.00E+00	0.00E+00
1284	ORNtex	-1.00E-06	0.00E+00	0.00E+00	0.00E+00	0.00E+00	0.00E+00
1285	ORPT	-2.22E-01	-2.57E-01	-2.57E-01	-2.57E-01	-2.57E-01	-2.57E-01
1286	OXAMTC	1.00E-06	0.00E+00	0.00E+00	0.00E+00	0.00E+00	0.00E+00
1287	P5CD	1.00E-06	0.00E+00	0.00E+00	0.00E+00	0.00E+00	0.00E+00
1288	P5CR	1.49E-01	1.73E-01	1.73E-01	1.73E-01	1.73E-01	1.73E-01
1289	PA120abcpp	2.00E-06	0.00E+00	0.00E+00	0.00E+00	0.00E+00	0.00E+00
1290	PA140abcpp	2.00E-06	0.00E+00	0.00E+00	0.00E+00	0.00E+00	0.00E+00
1291	PA141abcpp	1.00E-06	0.00E+00	0.00E+00	0.00E+00	0.00E+00	0.00E+00
1292	PA160abcpp	1.00E-06	0.00E+00	0.00E+00	0.00E+00	0.00E+00	0.00E+00
1293	PA161abcpp	1.00E-06	0.00E+00	0.00E+00	0.00E+00	0.00E+00	0.00E+00
1294	PA180abcpp	1.00E-06	0.00E+00	0.00E+00	0.00E+00	0.00E+00	0.00E+00
1295	PA181abcpp	1.00E-06	0.00E+00	0.00E+00	0.00E+00	0.00E+00	0.00E+00
1296	PANTS	3.99E-04	4.63E-04	4.63E-04	4.63E-04	4.63E-04	4.63E-04

1297	PAPA120	1.00E-06	0.00E+00	0.00E+00	0.00E+00	0.00E+00	0.00E+00
1298	PAPA120pp	1.00E-06	0.00E+00	0.00E+00	0.00E+00	0.00E+00	0.00E+00
1299	PAPA140	1.00E-06	0.00E+00	0.00E+00	0.00E+00	0.00E+00	0.00E+00
1300	PAPA140pp	1.00E-06	0.00E+00	0.00E+00	0.00E+00	0.00E+00	0.00E+00
1301	PAPA141	1.00E-06	0.00E+00	0.00E+00	0.00E+00	0.00E+00	0.00E+00
1302	PAPA141pp	1.00E-06	0.00E+00	0.00E+00	0.00E+00	0.00E+00	0.00E+00
1303	PAPA160	1.00E-06	0.00E+00	0.00E+00	0.00E+00	0.00E+00	0.00E+00
1304	PAPA160pp	2.00E-06	0.00E+00	0.00E+00	0.00E+00	0.00E+00	0.00E+00
1305	PAPA161	1.00E-06	0.00E+00	0.00E+00	0.00E+00	0.00E+00	0.00E+00
1306	PAPA161pp	2.00E-06	0.00E+00	0.00E+00	0.00E+00	0.00E+00	0.00E+00
1307	PAPA180	1.00E-06	0.00E+00	0.00E+00	0.00E+00	0.00E+00	0.00E+00
1308	PAPA180pp	3.00E-06	0.00E+00	0.00E+00	0.00E+00	0.00E+00	0.00E+00
1309	PAPA181	1.00E-06	0.00E+00	0.00E+00	0.00E+00	0.00E+00	0.00E+00
1310	PAPA181pp	2.00E-06	0.00E+00	0.00E+00	0.00E+00	0.00E+00	0.00E+00
1311	PAPPT3	1.91E-02	2.21E-02	2.21E-02	2.21E-02	2.21E-02	2.21E-02
1312	PAPSR	1.00E-06	1.99E-01	9.95E-02	0.00E+00	0.00E+00	9.95E-02
1313	PAPSR2	1.72E-01	0.00E+00	9.95E-02	1.99E-01	1.99E-01	9.95E-02
1314	PDE1	1.00E-06	0.00E+00	0.00E+00	0.00E+00	0.00E+00	0.00E+00
1315	PDE4	1.00E-06	0.00E+00	0.00E+00	0.00E+00	0.00E+00	0.00E+00
1316	PDH	1.00E-06	6.42E+00	6.42E+00	6.42E+00	6.42E+00	6.42E+00
1317	PDX5PO2	1.54E-04	0.00E+00	0.00E+00	1.79E-04	1.79E-04	0.00E+00
1318	PDX5POi	1.00E-06	1.79E-04	1.79E-04	0.00E+00	0.00E+00	1.79E-04
1319	PDX5PS	1.55E-04	1.79E-04	1.79E-04	1.79E-04	1.79E-04	1.79E-04
1320	PDXPP	1.00E-06	0.00E+00	0.00E+00	0.00E+00	0.00E+00	0.00E+00
1321	PE120abcpp	4.00E-06	0.00E+00	0.00E+00	0.00E+00	0.00E+00	0.00E+00
1322	PE140abcpp	3.00E-06	0.00E+00	0.00E+00	0.00E+00	0.00E+00	0.00E+00
1323	PE141abcpp	3.00E-06	0.00E+00	0.00E+00	0.00E+00	0.00E+00	0.00E+00
1324	PE160abcpp	2.20E-02	2.55E-02	2.55E-02	2.55E-02	2.55E-02	2.55E-02
1325	PE161abcpp	1.71E-02	1.99E-02	1.99E-02	1.99E-02	1.99E-02	1.99E-02
1326	PE180abcpp	0.00E+00	0.00E+00	0.00E+00	0.00E+00	0.00E+00	0.00E+00
1327	PE181abcpp	8.84E-03	1.02E-02	1.02E-02	1.02E-02	1.02E-02	1.02E-02
1328	PERD	1.55E-04	1.79E-04	1.79E-04	1.79E-04	1.79E-04	1.79E-04
1329	PETNT161pp	1.00E-06	0.00E+00	0.00E+00	0.00E+00	0.00E+00	0.00E+00
1330	PETNT181pp	1.00E-06	0.00E+00	0.00E+00	0.00E+00	0.00E+00	0.00E+00
1331	PFK	4.75E+00	5.34E+00	0.00E+00	0.00E+00	4.79E+00	0.00E+00
1332	PFK_3	1.00E-06	9.01E-01	6.24E+00	6.24E+00	9.01E-01	5.69E+00
1333	PFL	2.06E+01	0.00E+00	0.00E+00	0.00E+00	0.00E+00	0.00E+00
1334	PG120abcpp	3.00E-06	0.00E+00	0.00E+00	0.00E+00	0.00E+00	0.00E+00
1335	PG140abcpp	3.00E-06	0.00E+00	0.00E+00	0.00E+00	0.00E+00	0.00E+00
1336	PG141abcpp	3.00E-06	0.00E+00	0.00E+00	0.00E+00	0.00E+00	0.00E+00
1337	PG160abcpp	7.47E-03	8.66E-03	0.00E+00	8.66E-03	8.66E-03	0.00E+00
1338	PG161abcpp	5.81E-03	0.00E+00	0.00E+00	6.73E-03	6.73E-03	0.00E+00
1339	PG180abcpp	1.00E-06	0.00E+00	0.00E+00	0.00E+00	0.00E+00	0.00E+00
1340	PG181abcpp	2.99E-03	3.47E-03	3.47E-03	3.47E-03	3.47E-03	3.47E-03
1341	PGAMT	-4.96E-02	-5.74E-02	-5.74E-02	-5.74E-02	-5.74E-02	-5.74E-02
1342	PGCD	1.18E+00	1.32E+00	1.32E+00	1.32E+00	1.32E+00	1.32E+00
1343	PGI	1.00E-06	4.79E+00	4.79E+00	4.79E+00	4.79E+00	4.79E+00
1344	PGK	-1.17E+01	-1.30E+01	-1.30E+01	-1.30E+01	-1.30E+01	-1.30E+01
1345	PGL	8.02E+00	3.21E+00	3.21E+00	3.21E+00	3.21E+00	3.21E+00
1346	PGM	-1.05E+01	-1.17E+01	-1.17E+01	-1.17E+01	-1.17E+01	-1.17E+01
1347	PGMT	-1.35E-01	-1.57E-01	-1.57E-01	-1.57E-01	-1.57E-01	-1.57E-01
1348	PGP120abcpp	1.00E-06	0.00E+00	0.00E+00	0.00E+00	0.00E+00	0.00E+00
1349	PGP140abcpp	1.00E-06	0.00E+00	0.00E+00	0.00E+00	0.00E+00	0.00E+00
1350	PGP141abcpp	1.00E-06	0.00E+00	0.00E+00	0.00E+00	0.00E+00	0.00E+00
1351	PGP160abcpp	1.00E-06	0.00E+00	8.66E-03	0.00E+00	0.00E+00	8.66E-03
1352	PGP161abcpp	1.00E-06	6.73E-03	6.73E-03	0.00E+00	0.00E+00	6.73E-03
1353	PGP180abcpp	1.00E-06	0.00E+00	0.00E+00	0.00E+00	0.00E+00	0.00E+00
1354	PGP181abcpp	1.00E-06	0.00E+00	0.00E+00	0.00E+00	0.00E+00	0.00E+00
1355	PGPP120	2.00E-06	0.00E+00	0.00E+00	0.00E+00	0.00E+00	0.00E+00
1356	PGPP120pp	1.00E-06	0.00E+00	0.00E+00	0.00E+00	0.00E+00	0.00E+00
1357	PGPP140	2.00E-06	0.00E+00	0.00E+00	0.00E+00	0.00E+00	0.00E+00
1358	PGPP140pp	1.00E-06	0.00E+00	0.00E+00	0.00E+00	0.00E+00	0.00E+00
1359	PGPP141	2.00E-06	0.00E+00	0.00E+00	0.00E+00	0.00E+00	0.00E+00
1360	PGPP141pp	1.00E-06	0.00E+00	0.00E+00	0.00E+00	0.00E+00	0.00E+00
1361	PGPP160	1.14E-02	1.32E-02	4.58E-03	1.32E-02	1.32E-02	4.58E-03
1362	PGPP160pp	1.00E-06	0.00E+00	8.66E-03	0.00E+00	0.00E+00	8.66E-03
1363	PGPP161	8.89E-03	3.57E-03	3.57E-03	1.03E-02	1.03E-02	3.57E-03
1364	PGPP161pp	1.00E-06	6.73E-03	6.73E-03	0.00E+00	0.00E+00	6.73E-03
1365	PGPP180	1.00E-06	0.00E+00	0.00E+00	0.00E+00	0.00E+00	0.00E+00
1366	PGPP180pp	1.00E-06	0.00E+00	0.00E+00	0.00E+00	0.00E+00	0.00E+00
1367	PGPP181	4.58E-03	5.31E-03	5.31E-03	5.31E-03	5.31E-03	5.31E-03
1368	PGPP181pp	1.00E-06	0.00E+00	0.00E+00	0.00E+00	0.00E+00	0.00E+00
1369	PGSA120	3.00E-06	0.00E+00	0.00E+00	0.00E+00	0.00E+00	0.00E+00

1370	PGSA140	3.00E-06	0.00E+00	0.00E+00	0.00E+00	0.00E+00	0.00E+00
1371	PGSA141	3.00E-06	0.00E+00	0.00E+00	0.00E+00	0.00E+00	0.00E+00
1372	PGSA160	1.14E-02	1.32E-02	1.32E-02	1.32E-02	1.32E-02	1.32E-02
1373	PGSA161	8.89E-03	1.03E-02	1.03E-02	1.03E-02	1.03E-02	1.03E-02
1374	PGSA180	2.00E-06	0.00E+00	0.00E+00	0.00E+00	0.00E+00	0.00E+00
1375	PGSA181	4.58E-03	5.31E-03	5.31E-03	5.31E-03	5.31E-03	5.31E-03
1376	PHEMEabcpp	1.00E-06	0.00E+00	0.00E+00	0.00E+00	0.00E+00	0.00E+00
1377	PHEMEtiex	1.00E-06	0.00E+00	0.00E+00	0.00E+00	0.00E+00	0.00E+00
1378	PHETA1	-1.25E-01	-1.45E-01	-1.45E-01	-1.45E-01	-1.45E-01	-1.45E-01
1379	PHEt2rpp	-1.00E-06	2.84E-14	2.84E-14	2.84E-14	2.84E-14	2.84E-14
1380	PHEtex	-1.00E-06	2.84E-14	2.84E-14	2.84E-14	2.84E-14	2.84E-14
1381	PIt2rpp	-1.00E-06	7.51E-01	7.60E-01	7.45E-01	7.45E-01	7.60E-01
1382	PItex	6.43E-01	7.45E-01	7.45E-01	7.45E-01	7.45E-01	7.45E-01
1383	PIuabcpp	6.43E-01	0.00E+00	0.00E+00	0.00E+00	0.00E+00	0.00E+00
1384	PLIPA1A120pp	1.00E-06	0.00E+00	0.00E+00	0.00E+00	0.00E+00	0.00E+00
1385	PLIPA1A140pp	1.00E-06	0.00E+00	0.00E+00	0.00E+00	0.00E+00	0.00E+00
1386	PLIPA1A141pp	0.00E+00	0.00E+00	0.00E+00	0.00E+00	0.00E+00	0.00E+00
1387	PLIPA1A160pp	0.00E+00	0.00E+00	0.00E+00	0.00E+00	0.00E+00	0.00E+00
1388	PLIPA1A161pp	0.00E+00	0.00E+00	0.00E+00	0.00E+00	0.00E+00	0.00E+00
1389	PLIPA1A180pp	0.00E+00	0.00E+00	0.00E+00	0.00E+00	0.00E+00	0.00E+00
1390	PLIPA1A181pp	0.00E+00	0.00E+00	0.00E+00	0.00E+00	0.00E+00	0.00E+00
1391	PLIPA1E120pp	2.00E-06	0.00E+00	0.00E+00	0.00E+00	0.00E+00	0.00E+00
1392	PLIPA1E140pp	2.00E-06	0.00E+00	0.00E+00	0.00E+00	0.00E+00	0.00E+00
1393	PLIPA1E141pp	2.00E-06	0.00E+00	0.00E+00	0.00E+00	0.00E+00	0.00E+00
1394	PLIPA1E160pp	0.00E+00	0.00E+00	0.00E+00	0.00E+00	0.00E+00	0.00E+00
1395	PLIPA1E161pp	0.00E+00	0.00E+00	0.00E+00	0.00E+00	0.00E+00	0.00E+00
1396	PLIPA1E180pp	0.00E+00	0.00E+00	0.00E+00	0.00E+00	0.00E+00	0.00E+00
1397	PLIPA1E181pp	0.00E+00	0.00E+00	0.00E+00	0.00E+00	0.00E+00	0.00E+00
1398	PLIPA1G120pp	2.00E-06	0.00E+00	0.00E+00	0.00E+00	0.00E+00	0.00E+00
1399	PLIPA1G140pp	2.00E-06	0.00E+00	0.00E+00	0.00E+00	0.00E+00	0.00E+00
1400	PLIPA1G141pp	2.00E-06	0.00E+00	0.00E+00	0.00E+00	0.00E+00	0.00E+00
1401	PLIPA1G160pp	0.00E+00	0.00E+00	0.00E+00	0.00E+00	0.00E+00	0.00E+00
1402	PLIPA1G161pp	0.00E+00	0.00E+00	0.00E+00	0.00E+00	0.00E+00	0.00E+00
1403	PLIPA1G180pp	0.00E+00	0.00E+00	0.00E+00	0.00E+00	0.00E+00	0.00E+00
1404	PLIPA1G181pp	0.00E+00	0.00E+00	0.00E+00	0.00E+00	0.00E+00	0.00E+00
1405	PLIPA2A120pp	1.00E-06	0.00E+00	0.00E+00	0.00E+00	0.00E+00	0.00E+00
1406	PLIPA2A140pp	1.00E-06	0.00E+00	0.00E+00	0.00E+00	0.00E+00	0.00E+00
1407	PLIPA2A141pp	1.00E-06	0.00E+00	0.00E+00	0.00E+00	0.00E+00	0.00E+00
1408	PLIPA2A160pp	0.00E+00	0.00E+00	0.00E+00	0.00E+00	0.00E+00	0.00E+00
1409	PLIPA2A161pp	0.00E+00	0.00E+00	0.00E+00	0.00E+00	0.00E+00	0.00E+00
1410	PLIPA2A180pp	0.00E+00	0.00E+00	0.00E+00	0.00E+00	0.00E+00	0.00E+00
1411	PLIPA2A181pp	0.00E+00	0.00E+00	0.00E+00	0.00E+00	0.00E+00	0.00E+00
1412	PLIPA2E120pp	2.00E-06	0.00E+00	0.00E+00	0.00E+00	0.00E+00	0.00E+00
1413	PLIPA2E140pp	1.00E-06	0.00E+00	0.00E+00	0.00E+00	0.00E+00	0.00E+00
1414	PLIPA2E141pp	1.00E-06	0.00E+00	0.00E+00	0.00E+00	0.00E+00	0.00E+00
1415	PLIPA2E160pp	0.00E+00	0.00E+00	0.00E+00	0.00E+00	0.00E+00	0.00E+00
1416	PLIPA2E161pp	0.00E+00	0.00E+00	0.00E+00	0.00E+00	0.00E+00	0.00E+00
1417	PLIPA2E180pp	0.00E+00	0.00E+00	0.00E+00	0.00E+00	0.00E+00	0.00E+00
1418	PLIPA2E181pp	0.00E+00	0.00E+00	0.00E+00	0.00E+00	0.00E+00	0.00E+00
1419	PLIPA2G120pp	1.00E-06	0.00E+00	0.00E+00	0.00E+00	0.00E+00	0.00E+00
1420	PLIPA2G140pp	1.00E-06	0.00E+00	0.00E+00	0.00E+00	0.00E+00	0.00E+00
1421	PLIPA2G141pp	1.00E-06	0.00E+00	0.00E+00	0.00E+00	0.00E+00	0.00E+00
1422	PLIPA2G160pp	0.00E+00	0.00E+00	0.00E+00	0.00E+00	0.00E+00	0.00E+00
1423	PLIPA2G161pp	0.00E+00	0.00E+00	0.00E+00	0.00E+00	0.00E+00	0.00E+00
1424	PLIPA2G180pp	0.00E+00	0.00E+00	0.00E+00	0.00E+00	0.00E+00	0.00E+00
1425	PLIPA2G181pp	0.00E+00	0.00E+00	0.00E+00	0.00E+00	0.00E+00	0.00E+00
1426	PMANM	-1.00E-06	0.00E+00	0.00E+00	0.00E+00	0.00E+00	0.00E+00
1427	PMDPHT	3.09E-04	3.58E-04	3.58E-04	3.58E-04	3.58E-04	3.58E-04
1428	PMEACPE	1.39E-06	1.61E-06	1.61E-06	1.61E-06	1.61E-06	1.61E-06
1429	PMPK	1.56E-04	1.79E-04	1.79E-04	1.79E-04	1.79E-04	1.79E-04
1430	PNTK	3.99E-04	4.63E-04	4.63E-04	4.63E-04	4.63E-04	4.63E-04
1431	POAACR	1.00E-06	0.00E+00	0.00E+00	0.00E+00	0.00E+00	0.00E+00
1432	POR5	-1.16E+01	8.63E-02	8.63E-02	8.63E-02	8.63E-02	8.63E-02
1433	POX	1.00E-06	0.00E+00	0.00E+00	0.00E+00	0.00E+00	0.00E+00
1434	PPA	2.49E+00	2.88E+00	2.88E+00	2.88E+00	2.88E+00	2.88E+00
1435	PPA2	1.58E-04	0.00E+00	0.00E+00	0.00E+00	0.00E+00	0.00E+00
1436	PPAKr	1.00E-06	0.00E+00	0.00E+00	0.00E+00	0.00E+00	0.00E+00
1437	PPBNGS	1.86E-03	2.15E-03	2.15E-03	2.15E-03	2.15E-03	2.15E-03
1438	PPC	1.00E-06	2.35E+00	2.35E+00	2.35E+00	2.35E+00	2.35E+00
1439	PPCDC	3.99E-04	4.63E-04	4.63E-04	4.63E-04	4.63E-04	4.63E-04
1440	PPCK	1.00E-06	0.00E+00	0.00E+00	0.00E+00	0.00E+00	0.00E+00
1441	PPCSCT	1.00E-06	0.00E+00	0.00E+00	0.00E+00	0.00E+00	0.00E+00
1442	PPGPPDP	2.00E-06	0.00E+00	0.00E+00	0.00E+00	0.00E+00	0.00E+00

1443	PPK2r	1.00E-06	-1.79E-04	-1.79E-04	-1.79E-04	-1.79E-04	-1.79E-04
1444	PPKr	1.00E-06	-2.84E-14	-2.84E-14	-2.84E-14	-2.84E-14	-2.84E-14
1445	PPM	1.00E-06	-7.33E-01	-6.68E-03	-7.33E-01	-7.33E-01	-6.68E-03
1446	PPM2	7.00E-06	0.00E+00	0.00E+00	0.00E+00	0.00E+00	0.00E+00
1447	PPNCL2	3.99E-04	4.63E-04	4.63E-04	4.63E-04	4.63E-04	4.63E-04
1448	PPND	9.30E-02	1.08E-01	1.08E-01	1.08E-01	1.08E-01	1.08E-01
1449	PPNDH	1.25E-01	1.45E-01	1.45E-01	1.45E-01	1.45E-01	1.45E-01
1450	PPPGO	1.00E-06	0.00E+00	0.00E+00	0.00E+00	0.00E+00	0.00E+00
1451	PPPGO3	3.09E-04	3.58E-04	3.58E-04	3.58E-04	3.58E-04	3.58E-04
1452	PPS	1.00E-06	0.00E+00	0.00E+00	0.00E+00	0.00E+00	0.00E+00
1453	PRAGSr	3.02E-01	3.49E-01	3.49E-01	3.49E-01	3.49E-01	3.49E-01
1454	PRAIS	3.02E-01	3.49E-01	3.49E-01	3.49E-01	3.49E-01	3.49E-01
1455	PRAIi	3.83E-02	4.44E-02	4.44E-02	4.44E-02	4.44E-02	4.44E-02
1456	PRAMPC	6.38E-02	7.39E-02	7.39E-02	7.39E-02	7.39E-02	7.39E-02
1457	PRASCSi	3.01E-01	3.49E-01	3.49E-01	3.49E-01	3.49E-01	3.49E-01
1458	PRATPP	6.38E-02	7.39E-02	7.39E-02	7.39E-02	7.39E-02	7.39E-02
1459	PRFGS	3.02E-01	3.49E-01	3.49E-01	3.49E-01	3.49E-01	3.49E-01
1460	PRMICI	6.38E-02	7.39E-02	7.39E-02	7.39E-02	7.39E-02	7.39E-02
1461	PROD2	1.00E-06	0.00E+00	0.00E+00	0.00E+00	0.00E+00	0.00E+00
1462	PROabcpp	1.00E-06	0.00E+00	0.00E+00	0.00E+00	0.00E+00	0.00E+00
1463	PROt2rpp	-1.00E+02	-1.00E+02	0.00E+00	-1.00E+02	0.00E+00	-1.00E+02
1464	PROt4pp	1.00E+02	1.00E+02	0.00E+00	1.00E+02	0.00E+00	1.00E+02
1465	PROtex	-1.00E-06	2.84E-14	0.00E+00	2.84E-14	0.00E+00	2.84E-14
1466	PRPPS	6.33E-01	0.00E+00	7.27E-01	0.00E+00	0.00E+00	7.27E-01
1467	PSCVT	2.58E-01	2.99E-01	2.99E-01	2.99E-01	2.99E-01	2.99E-01
1468	PSD120	3.00E-06	0.00E+00	0.00E+00	0.00E+00	0.00E+00	0.00E+00
1469	PSD140	2.00E-06	0.00E+00	0.00E+00	0.00E+00	0.00E+00	0.00E+00
1470	PSD141	2.00E-06	0.00E+00	0.00E+00	0.00E+00	0.00E+00	0.00E+00
1471	PSD160	3.06E-02	3.55E-02	3.55E-02	3.55E-02	3.55E-02	3.55E-02
1472	PSD161	2.38E-02	2.76E-02	2.76E-02	2.76E-02	2.76E-02	2.76E-02
1473	PSD180	0.00E+00	0.00E+00	0.00E+00	0.00E+00	0.00E+00	0.00E+00
1474	PSD181	1.23E-02	1.42E-02	1.42E-02	1.42E-02	1.42E-02	1.42E-02
1475	PSERT	1.18E+00	1.32E+00	1.32E+00	1.32E+00	1.32E+00	1.32E+00
1476	PSP_L	1.18E+00	1.32E+00	1.32E+00	1.32E+00	1.32E+00	1.32E+00
1477	PSSA120	3.00E-06	0.00E+00	0.00E+00	0.00E+00	0.00E+00	0.00E+00
1478	PSSA140	2.00E-06	0.00E+00	0.00E+00	0.00E+00	0.00E+00	0.00E+00
1479	PSSA141	2.00E-06	0.00E+00	0.00E+00	0.00E+00	0.00E+00	0.00E+00
1480	PSSA160	3.06E-02	3.55E-02	3.55E-02	3.55E-02	3.55E-02	3.55E-02
1481	PSSA161	2.38E-02	2.76E-02	2.76E-02	2.76E-02	2.76E-02	2.76E-02
1482	PSSA180	0.00E+00	0.00E+00	0.00E+00	0.00E+00	0.00E+00	0.00E+00
1483	PSSA181	1.23E-02	1.42E-02	1.42E-02	1.42E-02	1.42E-02	1.42E-02
1484	PTA2	1.00E-06	0.00E+00	0.00E+00	0.00E+00	0.00E+00	0.00E+00
1485	PTAr	-4.10E-01	-4.75E-01	-4.75E-01	-4.75E-01	-4.75E-01	-4.75E-01
1486	PTPATi	3.99E-04	4.63E-04	4.63E-04	4.63E-04	4.63E-04	4.63E-04
1487	PTRCORNt7pp	-3.00E-06	0.00E+00	0.00E+00	0.00E+00	0.00E+00	0.00E+00
1488	PTRCTA	1.00E-06	0.00E+00	0.00E+00	0.00E+00	0.00E+00	0.00E+00
1489	PTRCabcpp	1.00E-06	0.00E+00	0.00E+00	0.00E+00	0.00E+00	0.00E+00
1490	PTRCt2pp	1.00E-06	0.00E+00	0.00E+00	0.00E+00	0.00E+00	0.00E+00
1491	PTRCtex	-1.00E-06	0.00E+00	0.00E+00	0.00E+00	0.00E+00	0.00E+00
1492	PUNP1	1.00E-06	-6.68E-03	-6.68E-03	-6.68E-03	-6.68E-03	-6.68E-03
1493	PUNP2	1.00E-06	0.00E+00	0.00E+00	0.00E+00	0.00E+00	0.00E+00
1494	PUNP3	1.00E-06	0.00E+00	0.00E+00	0.00E+00	0.00E+00	0.00E+00
1495	PUNP4	2.00E-06	0.00E+00	0.00E+00	0.00E+00	0.00E+00	0.00E+00
1496	PUNP5	1.00E-06	0.00E+00	0.00E+00	0.00E+00	0.00E+00	0.00E+00
1497	PUNP6	2.00E-06	0.00E+00	0.00E+00	0.00E+00	0.00E+00	0.00E+00
1498	PUNP7	1.00E-06	0.00E+00	0.00E+00	0.00E+00	0.00E+00	0.00E+00
1499	PYAM5PO	2.00E-06	0.00E+00	0.00E+00	0.00E+00	0.00E+00	0.00E+00
1500	PYDAMK	1.00E-06	0.00E+00	0.00E+00	0.00E+00	0.00E+00	0.00E+00
1501	PYDXK	1.00E-06	0.00E+00	0.00E+00	0.00E+00	0.00E+00	0.00E+00
1502	PYDXNK	1.00E-06	0.00E+00	0.00E+00	0.00E+00	0.00E+00	0.00E+00
1503	PYDXPP	1.00E-06	0.00E+00	0.00E+00	0.00E+00	0.00E+00	0.00E+00
1504	PYK	1.82E+00	5.47E-01	5.47E-01	5.47E-01	0.00E+00	0.00E+00
1505	PYNP2r	1.00E-06	0.00E+00	0.00E+00	0.00E+00	0.00E+00	0.00E+00
1506	PYROX	1.00E-06	0.00E+00	0.00E+00	0.00E+00	0.00E+00	0.00E+00
1507	PYRt2rpp	-1.00E-06	2.84E-14	2.84E-14	2.84E-14	2.84E-14	2.84E-14
1508	PYRtex	-1.00E-06	2.84E-14	2.84E-14	2.84E-14	2.84E-14	2.84E-14
1509	QUIN2tex	-1.00E-06	2.84E-14	2.84E-14	2.84E-14	2.84E-14	2.84E-14
1510	QUIN2tpp	-1.00E-06	2.84E-14	2.84E-14	2.84E-14	2.84E-14	2.84E-14
1511	QUINDH	-1.00E-06	2.84E-14	2.84E-14	2.84E-14	2.84E-14	2.84E-14
1512	QULNS	1.58E-03	1.83E-03	1.83E-03	1.83E-03	1.83E-03	1.83E-03
1513	R15BPK	4.00E-06	7.27E-01	0.00E+00	7.27E-01	7.27E-01	0.00E+00
1514	R1PK	4.00E-06	7.27E-01	0.00E+00	7.27E-01	7.27E-01	0.00E+00
1515	R5PP	1.00E-06	0.00E+00	0.00E+00	0.00E+00	0.00E+00	0.00E+00

1516	RBFK	1.55E-04	1.79E-04	1.79E-04	1.79E-04	1.79E-04	1.79E-04
1517	RBFSa	6.18E-04	7.16E-04	7.16E-04	7.16E-04	7.16E-04	7.16E-04
1518	RBFSb	3.09E-04	3.58E-04	3.58E-04	3.58E-04	3.58E-04	3.58E-04
1519	RBK	6.00E-06	0.00E+00	0.00E+00	0.00E+00	0.00E+00	0.00E+00
1520	RFAMPtex	1.00E-06	0.00E+00	0.00E+00	0.00E+00	0.00E+00	0.00E+00
1521	RFAMPtpp	1.00E-06	0.00E+00	0.00E+00	0.00E+00	0.00E+00	0.00E+00
1522	RHAT1	5.65E-03	6.55E-03	6.55E-03	6.55E-03	6.55E-03	6.55E-03
1523	RHCCE	9.30E-04	1.08E-03	1.08E-03	1.08E-03	1.08E-03	1.08E-03
1524	RNDR1	1.72E-02	0.00E+00	0.00E+00	0.00E+00	0.00E+00	0.00E+00
1525	RNDR1b	1.00E-06	0.00E+00	0.00E+00	0.00E+00	0.00E+00	0.00E+00
1526	RNDR2	1.78E-02	0.00E+00	0.00E+00	0.00E+00	0.00E+00	0.00E+00
1527	RNDR2b	1.00E-06	0.00E+00	0.00E+00	0.00E+00	0.00E+00	0.00E+00
1528	RNDR3	1.78E-02	0.00E+00	0.00E+00	0.00E+00	0.00E+00	0.00E+00
1529	RNDR3b	1.00E-06	0.00E+00	0.00E+00	0.00E+00	0.00E+00	0.00E+00
1530	RNDR4	1.72E-02	0.00E+00	0.00E+00	0.00E+00	0.00E+00	0.00E+00
1531	RNDR4b	1.00E-06	0.00E+00	0.00E+00	0.00E+00	0.00E+00	0.00E+00
1532	RNTR1c2	1.00E-06	1.99E-02	1.99E-02	1.99E-02	1.99E-02	1.99E-02
1533	RNTR2c2	1.00E-06	2.06E-02	2.06E-02	2.06E-02	2.06E-02	2.06E-02
1534	RNTR3c2	1.00E-06	2.06E-02	2.06E-02	2.06E-02	2.06E-02	2.06E-02
1535	RNTR4c2	1.00E-06	1.99E-02	1.99E-02	1.99E-02	1.99E-02	1.99E-02
1536	RPE	4.82E+00	1.53E+00	1.53E+00	1.53E+00	1.53E+00	1.53E+00
1537	RPI	-3.18E+00	-1.66E+00	-1.66E+00	-1.66E+00	-1.66E+00	-1.66E+00
1538	S2FE2SR	0.00E+00	0.00E+00	0.00E+00	0.00E+00	0.00E+00	0.00E+00
1539	S2FE2SS	2.00E-06	0.00E+00	0.00E+00	0.00E+00	0.00E+00	0.00E+00
1540	S2FE2SS2	1.00E-06	0.00E+00	0.00E+00	0.00E+00	0.00E+00	0.00E+00
1541	S2FE2ST	1.00E-06	0.00E+00	0.00E+00	0.00E+00	0.00E+00	0.00E+00
1542	S4FE4SR	1.00E-06	0.00E+00	0.00E+00	0.00E+00	0.00E+00	0.00E+00
1543	S4FE4ST	1.00E-06	0.00E+00	0.00E+00	0.00E+00	0.00E+00	0.00E+00
1544	S7PI	2.26E-02	2.62E-02	2.62E-02	2.62E-02	2.62E-02	2.62E-02
1545	SADH	1.00E-06	0.00E+00	0.00E+00	0.00E+00	0.00E+00	0.00E+00
1546	SADT2	1.72E-01	1.99E-01	1.99E-01	1.99E-01	1.99E-01	1.99E-01
1547	SCYSDS	6.00E-06	0.00E+00	0.00E+00	0.00E+00	0.00E+00	0.00E+00
1548	SDPDS	2.50E-01	2.90E-01	2.90E-01	2.90E-01	2.90E-01	2.90E-01
1549	SDPTA	-2.50E-01	-2.90E-01	-2.90E-01	-2.90E-01	-2.90E-01	-2.90E-01
1550	SEPHCHCS	3.09E-04	3.58E-04	3.58E-04	3.58E-04	3.58E-04	3.58E-04
1551	SERASr	4.76E-04	5.37E-04	5.37E-04	5.37E-04	5.37E-04	5.37E-04
1552	SERAT	1.72E-01	1.99E-01	1.99E-01	1.99E-01	1.99E-01	1.99E-01
1553	SERD_D	1.00E-06	0.00E+00	0.00E+00	0.00E+00	0.00E+00	0.00E+00
1554	SERD_L	1.00E-06	0.00E+00	0.00E+00	0.00E+00	0.00E+00	0.00E+00
1555	SERt2rpp	-1.00E+02	0.00E+00	0.00E+00	0.00E+00	0.00E+00	0.00E+00
1556	SERt4pp	1.00E+02	0.00E+00	0.00E+00	0.00E+00	0.00E+00	0.00E+00
1557	SERtex	-1.00E-06	0.00E+00	0.00E+00	0.00E+00	0.00E+00	0.00E+00
1558	SGDS	1.00E-06	0.00E+00	0.00E+00	0.00E+00	0.00E+00	0.00E+00
1559	SGSAD	1.00E-06	0.00E+00	0.00E+00	0.00E+00	0.00E+00	0.00E+00
1560	SHCHCS3	3.09E-04	3.58E-04	3.58E-04	3.58E-04	3.58E-04	3.58E-04
1561	SHCHD2	1.55E-04	1.79E-04	1.79E-04	1.79E-04	1.79E-04	1.79E-04
1562	SHCHF	1.55E-04	1.79E-04	1.79E-04	1.79E-04	1.79E-04	1.79E-04
1563	SHK3Dr	2.58E-01	2.99E-01	2.99E-01	2.99E-01	2.99E-01	2.99E-01
1564	SHKK	2.58E-01	2.99E-01	2.99E-01	2.99E-01	2.99E-01	2.99E-01
1565	SHSL1	1.08E-01	1.26E-01	1.26E-01	1.26E-01	1.26E-01	1.26E-01
1566	SO4t2pp	1.75E-01	2.02E-01	2.02E-01	2.02E-01	2.02E-01	2.02E-01
1567	SO4tex	1.75E-01	2.02E-01	2.02E-01	2.02E-01	2.02E-01	2.02E-01
1568	SOTA	1.00E-06	0.00E+00	0.00E+00	0.00E+00	0.00E+00	0.00E+00
1569	SPMDabcpp	1.00E-06	0.00E+00	0.00E+00	0.00E+00	0.00E+00	0.00E+00
1570	SPMDt3pp	2.00E-06	0.00E+00	0.00E+00	0.00E+00	0.00E+00	0.00E+00
1571	SPMDtex	-1.00E-06	0.00E+00	0.00E+00	0.00E+00	0.00E+00	0.00E+00
1572	SPMS	4.68E-03	5.42E-03	5.42E-03	5.42E-03	5.42E-03	5.42E-03
1573	SSALx	1.00E-06	0.00E+00	0.00E+00	0.00E+00	0.00E+00	0.00E+00
1574	SSALy	1.00E-06	0.00E+00	0.00E+00	0.00E+00	0.00E+00	0.00E+00
1575	SUCBZL	3.09E-04	3.58E-04	3.58E-04	3.58E-04	3.58E-04	3.58E-04
1576	SUCBZS	3.09E-04	3.58E-04	3.58E-04	3.58E-04	3.58E-04	3.58E-04
1577	SUCCt2_2pp	1.00E-06	0.00E+00	0.00E+00	0.00E+00	0.00E+00	0.00E+00
1578	SUCCt2_3pp	1.00E-06	0.00E+00	0.00E+00	0.00E+00	0.00E+00	0.00E+00
1579	SUCCt3pp	2.00E-06	0.00E+00	0.00E+00	0.00E+00	0.00E+00	0.00E+00
1580	SUCCtex	-1.00E-06	2.84E-14	2.84E-14	2.84E-14	2.84E-14	2.84E-14
1581	SUCDi	3.27E+00	3.49E+00	3.49E+00	3.49E+00	3.23E+00	3.49E+00
1582	SUCOAS	1.00E-06	-2.81E+00	-2.81E+00	-2.81E+00	-2.81E+00	-2.81E+00
1583	SULRi	1.72E-01	1.99E-01	1.99E-01	1.99E-01	1.99E-01	1.99E-01
1584	SULabcpp	1.00E-06	0.00E+00	0.00E+00	0.00E+00	0.00E+00	0.00E+00
1585	T2DECAI	9.91E-02	0.00E+00	0.00E+00	0.00E+00	0.00E+00	0.00E+00
1586	TALA	2.53E+00	0.00E+00	-5.34E+00	-5.34E+00	0.00E+00	-4.79E+00
1587	TDP	1.00E-06	0.00E+00	0.00E+00	0.00E+00	0.00E+00	0.00E+00
1588	TDPADGAT	0.00E+00	0.00E+00	0.00E+00	0.00E+00	0.00E+00	0.00E+00

1589	TDPAGTA	0.00E+00	0.00E+00	0.00E+00	0.00E+00	0.00E+00	0.00E+00
1590	TDPDRE	5.65E-03	6.55E-03	6.55E-03	6.55E-03	6.55E-03	6.55E-03
1591	TDPDRR	5.65E-03	6.55E-03	6.55E-03	6.55E-03	6.55E-03	6.55E-03
1592	TDPGDH	5.65E-03	6.55E-03	6.55E-03	6.55E-03	6.55E-03	6.55E-03
1593	TDSK	5.66E-03	6.55E-03	6.55E-03	6.55E-03	6.55E-03	6.55E-03
1594	THD2pp	3.20E+00	0.00E+00	0.00E+00	0.00E+00	0.00E+00	0.00E+00
1595	THDPS	2.50E-01	2.90E-01	2.90E-01	2.90E-01	2.90E-01	2.90E-01
1596	THFAT	1.00E-06	0.00E+00	0.00E+00	0.00E+00	0.00E+00	0.00E+00
1597	THIORDXi	1.00E-06	0.00E+00	0.00E+00	0.00E+00	0.00E+00	0.00E+00
1598	THMDt2pp	1.00E+02	1.00E+02	0.00E+00	0.00E+00	0.00E+00	0.00E+00
1599	THMDt2rpp	-1.00E+02	-1.00E+02	2.84E-14	2.84E-14	2.84E-14	2.84E-14
1600	THMDtex	-1.00E-06	2.84E-14	2.84E-14	2.84E-14	2.84E-14	2.84E-14
1601	THRA2i	1.00E-06	0.00E+00	0.00E+00	0.00E+00	0.00E+00	0.00E+00
1602	THRAi	1.00E-06	0.00E+00	0.00E+00	0.00E+00	0.00E+00	0.00E+00
1603	THRD	1.00E-06	0.00E+00	0.00E+00	0.00E+00	0.00E+00	0.00E+00
1604	THRD_L	1.96E-01	2.27E-01	2.27E-01	2.27E-01	2.27E-01	2.27E-01
1605	THRS	3.67E-01	4.25E-01	4.25E-01	4.25E-01	4.25E-01	4.25E-01
1606	THRabcpp	1.00E-06	0.00E+00	0.00E+00	0.00E+00	0.00E+00	0.00E+00
1607	THRt2pp	4.00E-06	0.00E+00	0.00E+00	0.00E+00	0.00E+00	0.00E+00
1608	THRt2rpp	1.00E-06	0.00E+00	0.00E+00	0.00E+00	0.00E+00	0.00E+00
1609	THRt4pp	1.00E-06	0.00E+00	0.00E+00	0.00E+00	0.00E+00	0.00E+00
1610	THRtex	-1.00E-06	2.84E-14	2.84E-14	2.84E-14	2.84E-14	2.84E-14
1611	THYMt3pp	1.00E-06	0.00E+00	0.00E+00	0.00E+00	0.00E+00	0.00E+00
1612	THYMtex	-1.00E-06	0.00E+00	0.00E+00	0.00E+00	0.00E+00	0.00E+00
1613	THZPSN3	1.55E-04	1.79E-04	1.79E-04	1.79E-04	1.79E-04	1.79E-04
1614	TKT1	2.55E+00	9.27E-01	9.27E-01	9.27E-01	9.27E-01	9.27E-01
1615	TKT2	2.27E+00	6.02E-01	6.02E-01	6.02E-01	6.02E-01	6.02E-01
1616	TMDK1	1.00E-06	0.00E+00	0.00E+00	0.00E+00	0.00E+00	0.00E+00
1617	TMDPP	1.00E-06	0.00E+00	0.00E+00	0.00E+00	0.00E+00	0.00E+00
1618	TMDS	1.72E-02	1.99E-02	1.99E-02	1.99E-02	1.99E-02	1.99E-02
1619	TMPK	1.56E-04	1.79E-04	1.79E-04	1.79E-04	1.79E-04	1.79E-04
1620	TMPPP	1.55E-04	1.79E-04	1.79E-04	1.79E-04	1.79E-04	1.79E-04
1621	TPI	4.63E+00	6.11E+00	6.11E+00	6.11E+00	6.11E+00	6.11E+00
1622	TRDR	6.99E-02	1.99E-01	9.95E-02	0.00E+00	0.00E+00	9.95E-02
1623	TRE6PH	1.00E-06	0.00E+00	0.00E+00	0.00E+00	0.00E+00	0.00E+00
1624	TRE6PP	1.00E-06	0.00E+00	0.00E+00	0.00E+00	0.00E+00	0.00E+00
1625	TRE6PS	2.00E-06	0.00E+00	0.00E+00	0.00E+00	0.00E+00	0.00E+00
1626	TREH	1.00E-06	0.00E+00	0.00E+00	0.00E+00	0.00E+00	0.00E+00
1627	TRPAS2	1.00E-06	-4.44E-02	-4.44E-02	-4.44E-02	-4.44E-02	-4.44E-02
1628	TRPS1	3.83E-02	0.00E+00	0.00E+00	0.00E+00	0.00E+00	0.00E+00
1629	TRPS2	1.00E-06	0.00E+00	0.00E+00	0.00E+00	0.00E+00	0.00E+00
1630	TRPS3	1.00E-06	4.44E-02	4.44E-02	4.44E-02	4.44E-02	4.44E-02
1631	TRPt2rpp	-1.00E-06	2.84E-14	2.84E-14	2.84E-14	2.84E-14	2.84E-14
1632	TRPtex	-1.00E-06	2.84E-14	2.84E-14	2.84E-14	2.84E-14	2.84E-14
1633	TRSARr	1.00E-06	0.00E+00	0.00E+00	0.00E+00	0.00E+00	0.00E+00
1634	TTRCYCtex	1.00E-06	0.00E+00	0.00E+00	0.00E+00	0.00E+00	0.00E+00
1635	TTRCYCtpp	1.00E-06	0.00E+00	0.00E+00	0.00E+00	0.00E+00	0.00E+00
1636	TYRL	1.55E-04	1.79E-04	1.79E-04	1.79E-04	1.79E-04	1.79E-04
1637	TYRTA	-9.30E-02	-1.08E-01	-1.08E-01	-1.08E-01	-1.08E-01	-1.08E-01
1638	TYRt2rpp	-1.00E-06	2.84E-14	2.84E-14	2.84E-14	2.84E-14	2.84E-14
1639	TYRtex	-1.00E-06	2.84E-14	2.84E-14	2.84E-14	2.84E-14	2.84E-14
1640	U23GAAT	1.13E-02	1.31E-02	1.31E-02	1.31E-02	1.31E-02	1.31E-02
1641	UAAGDS	1.91E-02	2.21E-02	2.21E-02	2.21E-02	2.21E-02	2.21E-02
1642	UACMAMO	0.00E+00	0.00E+00	0.00E+00	0.00E+00	0.00E+00	0.00E+00
1643	UAG2E	0.00E+00	-2.84E-14	-2.84E-14	-2.84E-14	-2.84E-14	-2.84E-14
1644	UAGAAT	1.13E-02	1.31E-02	1.31E-02	1.31E-02	1.31E-02	1.31E-02
1645	UAGCVT	1.91E-02	2.21E-02	2.21E-02	2.21E-02	2.21E-02	2.21E-02
1646	UAGDP	4.96E-02	5.74E-02	5.74E-02	5.74E-02	5.74E-02	5.74E-02
1647	UAGPT3	1.91E-02	2.21E-02	2.21E-02	2.21E-02	2.21E-02	2.21E-02
1648	UAMAGS	1.91E-02	2.21E-02	2.21E-02	2.21E-02	2.21E-02	2.21E-02
1649	UAMAS	1.91E-02	2.21E-02	2.21E-02	2.21E-02	2.21E-02	2.21E-02
1650	UAPGR	1.91E-02	2.21E-02	2.21E-02	2.21E-02	2.21E-02	2.21E-02
1651	UDCPDP	1.91E-02	2.21E-02	2.21E-02	2.21E-02	2.21E-02	2.21E-02
1652	UDCPDPS	3.81E-05	4.42E-05	4.42E-05	4.42E-05	4.42E-05	4.42E-05
1653	UDCPDPpp	0.00E+00	0.00E+00	0.00E+00	0.00E+00	0.00E+00	0.00E+00
1654	UDCPPtppi	0.00E+00	0.00E+00	0.00E+00	0.00E+00	0.00E+00	0.00E+00
1655	UDPGD	0.00E+00	0.00E+00	0.00E+00	0.00E+00	0.00E+00	0.00E+00
1656	UDPGDC	0.00E+00	0.00E+00	0.00E+00	0.00E+00	0.00E+00	0.00E+00
1657	UDPKAAT	0.00E+00	-2.84E-14	-2.84E-14	-2.84E-14	-2.84E-14	-2.84E-14
1658	UGLYCH	1.00E-06	0.00E+00	0.00E+00	0.00E+00	0.00E+00	0.00E+00
1659	UGMDDS	1.91E-02	2.21E-02	2.21E-02	2.21E-02	2.21E-02	2.21E-02
1660	UHGADA	1.13E-02	1.31E-02	1.31E-02	1.31E-02	1.31E-02	1.31E-02
1661	ULA4NFT	0.00E+00	0.00E+00	0.00E+00	0.00E+00	0.00E+00	0.00E+00

1662	ULA4Ntppi	0.00E+00	0.00E+00	0.00E+00	0.00E+00	0.00E+00	0.00E+00
1663	UM3PL	5.00E-06	0.00E+00	0.00E+00	0.00E+00	0.00E+00	0.00E+00
1664	UM4PCP	2.00E-06	0.00E+00	0.00E+00	0.00E+00	0.00E+00	0.00E+00
1665	UM4PL	2.00E-06	0.00E+00	0.00E+00	0.00E+00	0.00E+00	0.00E+00
1666	UMPK	2.47E-01	2.86E-01	2.86E-01	2.86E-01	2.86E-01	2.86E-01
1667	UPLA4FNF	0.00E+00	0.00E+00	0.00E+00	0.00E+00	0.00E+00	0.00E+00
1668	UPLA4FNT	0.00E+00	0.00E+00	0.00E+00	0.00E+00	0.00E+00	0.00E+00
1669	UPP3MT	1.55E-04	1.79E-04	1.79E-04	1.79E-04	1.79E-04	1.79E-04
1670	UPP3S	4.65E-04	5.37E-04	5.37E-04	5.37E-04	5.37E-04	5.37E-04
1671	UPPDC1	3.10E-04	3.58E-04	3.58E-04	3.58E-04	3.58E-04	3.58E-04
1672	UPPRT	3.00E-06	0.00E+00	0.00E+00	0.00E+00	0.00E+00	0.00E+00
1673	URACPAH	1.00E-06	0.00E+00	0.00E+00	0.00E+00	0.00E+00	0.00E+00
1674	URAt2pp	1.00E+02	0.00E+00	0.00E+00	0.00E+00	0.00E+00	0.00E+00
1675	URAt2rpp	-1.00E+02	0.00E+00	0.00E+00	0.00E+00	0.00E+00	0.00E+00
1676	URAtex	-1.00E-06	0.00E+00	0.00E+00	0.00E+00	0.00E+00	0.00E+00
1677	URDGLYCD	1.00E-06	0.00E+00	0.00E+00	0.00E+00	0.00E+00	0.00E+00
1678	UREAtex	-1.00E-06	0.00E+00	0.00E+00	0.00E+00	0.00E+00	0.00E+00
1679	UREAtpp	-1.00E-06	0.00E+00	0.00E+00	0.00E+00	0.00E+00	0.00E+00
1680	URIC	3.00E-06	0.00E+00	0.00E+00	0.00E+00	0.00E+00	0.00E+00
1681	URIH	1.00E-06	0.00E+00	0.00E+00	0.00E+00	0.00E+00	0.00E+00
1682	URIK2	1.00E-06	0.00E+00	0.00E+00	0.00E+00	0.00E+00	0.00E+00
1683	URIt2pp	1.00E+02	0.00E+00	0.00E+00	0.00E+00	0.00E+00	0.00E+00
1684	URIt2rpp	-1.00E+02	0.00E+00	0.00E+00	0.00E+00	0.00E+00	0.00E+00
1685	URItex	-1.00E-06	0.00E+00	0.00E+00	0.00E+00	0.00E+00	0.00E+00
1686	USHD	5.66E-03	6.55E-03	6.55E-03	6.55E-03	6.55E-03	6.55E-03
1687	VALTA	-1.00E+02	0.00E+00	0.00E+00	-7.71E-01	-7.71E-01	0.00E+00
1688	VALabcpp	1.00E-06	0.00E+00	0.00E+00	0.00E+00	0.00E+00	0.00E+00
1689	VALt2rpp	-2.00E-06	5.68E-14	5.68E-14	5.68E-14	5.68E-14	5.68E-14
1690	VALtex	-1.00E-06	5.68E-14	5.68E-14	5.68E-14	5.68E-14	5.68E-14
1691	VPAMTr	-9.97E+01	3.30E-01	3.30E-01	-4.41E-01	-4.41E-01	3.30E-01
1692	XAND	3.00E-06	0.00E+00	0.00E+00	0.00E+00	0.00E+00	0.00E+00
1693	XANt2pp	1.00E-06	0.00E+00	0.00E+00	0.00E+00	0.00E+00	0.00E+00
1694	XANtex	-1.00E-06	0.00E+00	0.00E+00	0.00E+00	0.00E+00	0.00E+00
1695	XANtpp	-2.00E-06	0.00E+00	0.00E+00	0.00E+00	0.00E+00	0.00E+00
1696	XPPT	2.00E-06	0.00E+00	0.00E+00	0.00E+00	0.00E+00	0.00E+00
1697	XTSNH	1.00E-06	0.00E+00	0.00E+00	0.00E+00	0.00E+00	0.00E+00
1698	XTSNt2rpp	-1.00E-06	2.84E-14	2.84E-14	2.84E-14	2.84E-14	2.84E-14
1699	XTSNtex	-1.00E-06	2.84E-14	2.84E-14	2.84E-14	2.84E-14	2.84E-14
1700	XYLI2	1.00E-06	0.00E+00	0.00E+00	0.00E+00	0.00E+00	0.00E+00
1701	ZN2abcpp	1.00E-06	0.00E+00	0.00E+00	0.00E+00	0.00E+00	0.00E+00
1702	ZN2t3pp	1.00E-06	0.00E+00	0.00E+00	0.00E+00	0.00E+00	0.00E+00
1703	ZN2tpp	2.26E-04	2.60E-04	2.60E-04	2.60E-04	2.60E-04	2.60E-04
1704	ZNabcpp	1.00E-06	0.00E+00	0.00E+00	0.00E+00	0.00E+00	0.00E+00
1705	Zn2tex	2.25E-04	2.60E-04	2.60E-04	2.60E-04	2.60E-04	2.60E-04

S2-1 Table. Mapping of metabolic fluxes.

Generally, metabolic networks include reactions defined by assuming the forward direction is the normally occurring one. In ^{13}C-MFA some reactions are lumped, which hinders a direct comparison of flux values. If that happens, the flux of said lumped reaction in ^{13}C-MFA is assumed to be the same for the two component reactions in the GSM. When one of those two reactions is defined in the GSM as the equivalent reverse reaction, the sign of the flux value is corrected, allowing a proper comparison between predicted flux distributions with GSMs and experimental ^{13}C-MFA values. *Since the metabolic network for ^{13}C-MFA did not specify the cofactor, both reactions were included in the mapping (one automatically shut down in TFA).

GSM name (Salvy, Fengos et al. 2018)	GSM definition (Salvy, Fengos et al. 2018)	^{13}C-MFA definition (Ishii, Nakahigashi et al. 2007)	^{13}C-MFA flux value (Ishii, Nakahigashi et al. 2007)	Corrected flux value
ACALD	acald_c + coa_c + nad_c <=> accoa_c + h_c + nadh_c	AcCoA -> Ethanol	0.1	-0.1
ACONTa	cit_c <=> acon-C_c + h2o_c	CIT -> ICT	85.9	85.9
ACONTb	acon-C_c + h2o_c <=> icit_c	CIT -> ICT	85.9	85.9
ACKr	ac_c + atp_c + h_c <=> actp_c + adp_c	AcCoA -> Acetate	0	0
AKGDH	akg_c + coa_c + nad_c -> co2_c + nadh_c + succoa_c	2-KG -> SUC + CO2	62.5	62.5
ALCD2x	etoh_c + nad_c <=> acald_c + h_c + nadh_c	AcCoA -> Ethanol	0.1	-0.1
CS	accoa_c + h2o_c + oaa_c -> cit_c + coa_c + h_c	AcCoA + OAA -> CIT	85.9	85.9
EDA	2ddg6p_c -> g3p_c + pyr_c	6-PG -> G3P + PYR	0	0
EDD	6pgc_c -> 2ddg6p_c + h2o_c	6-PG -> G3P + PYR	0	0
ENO	2pg_c <=> h2o_c + pep_c	3PG <-> PEP	161.7	161.7
FBA	fdp_c <=> dhap_c + g3p_c	F1,6P -> DHAP + G3P	85.3	85.3
FUM	fum_c + h2o_c <=> mal-L_c	FUM -> MAL	77.5	77.5

GSM name (Salvy, Fengos et al. 2018)	GSM definition (Salvy, Fengos et al. 2018)	^{13}C-MFA definition (Ishii, Nakahigashi et al. 2007)	^{13}C-MFA flux value (Ishii, Nakahigashi et al. 2007)	Corrected flux value
G6PDH2r	g6p_c + nadp_c <=> 6pgl_c + h_c + nadph_c	G6P -> 6PG	20.5	20.5
GAPD	g3p_c + nad_c + pi_c <=> 13dpg_c + nadh_c	G3P -> 3PG	172	172
GLCptspp	pep_c + glc-D_p <=> g6p_c + pyr_c	Glucose + PEP -> G6P + PYR	100	100
GND	6pgc_c + nadp_c -> co2_c + nadph_c + ru5p-D_c	6PG -> Ru5P + CO2	20.5	20.5
ICDHyr	icit_c + nadp_c <=> akg_c + co2_c + nadph_c	ICT -> 2-KG + CO2	70.9	70.9
ICL	icit_c -> glx_c + succ_c	ICT -> Glyoxylate + SUC	15	15
LDH_D	lac-D_c + nad_c <=> h_c + nadh_c + pyr_c	PYR -> Lactate	0	0
MALS	accoa_c + glx_c + h2o_c -> coa_c + h_c + mal-L_c	Glyoxylate + AcCoA -> MAL	15	15
MDH	mal-L_c + nad_c <=> h_c + nadh_c + oaa_c	MAL <-> OAA	89.1	89.1
ME1*	mal-L_c + nad_c -> co2_c + nadh_c + pyr_c	MAL -> PYR + CO2	3.4	3.4
ME2*	mal-L_c + nadp_c -> co2_c + nadph_c + pyr_c	MAL -> PYR + CO2	3.4	3.4
PDH	coa_c + nad_c + pyr_c <=> accoa_c + co2_c + nadh_c	PYR -> AcCoA + CO2	129.4	129.4
PFK	atp_c + f6p_c <=> adp_c + fdp_c	F6P -> F1,6P	85.3	85.3
PGI	g6p_c <=> f6p_c	G6P <-> F6P	78	78

GSM name (Salvy, Fengos et al. 2018)	GSM definition (Salvy, Fengos et al. 2018)	^{13}C-MFA definition (Ishii, Nakahigashi et al. 2007)	^{13}C-MFA flux value (Ishii, Nakahigashi et al. 2007)	Corrected flux value
PGK	3pg_c + atp_c + h_c <=> 13dpg_c + adp_c	G3P -> 3PG	172	-172
PGL	6pgl_c + h2o_c -> 6pgc_c + h_c	G6P -> 6PG	20.5	20.5
PGM	2pg_c <=> 3pg_c	3PG <-> PEP	161.7	-161.7
PPC	co2_c + h2o_c + pep_c -> 2 h_c + oaa_c + pi_c	PEP + CO2 <-> OAA	10.6	10.6
PTAr	accoa_c + h_c + pi_c <=> actp_c + coa_c	AcCoA -> Acetate	0	0
PYK	adp_c + pep_c <=> atp_c + pyr_c	PEP -> PYR	47.3	47.3
RPE	ru5p-D_c <=> xu5p-D_c	Ru5P -> X5P	8.1	8.1
RPI	r5p_c <=> ru5p-D_c	Ru5P -> R5P	12.4	-12.4
SUCDi	q8_c + succ_c -> fum_c + q8h2_c	SUC -> FUM	77.5	77.5
SUCOAS	atp_c + coa_c + succ_c <=> adp_c + pi_c + succoa_c	2-KG -> SUC + CO2	62.5	62.5
TALA	g3p_c + s7p_c <=> e4p_c + f6p_c	S7P + G3P <-> E4P + F6P	5.6	5.6
TKT1	r5p_c + xu5p-D_c <=> g3p_c + s7p_c	R5P + X5P <-> S7P + G3P	5.6	5.6
TKT2	e4p_c + xu5p-D_c <=> f6p_c + g3p_c	X5P + E4P <-> F6P + G3P	2.5	2.5
TPI	dhap_c <=> g3p_c	DHAP -> G3P	85.3	85.3

S2-2 Table. List of files used in this study.

These include files from the matTFA toolbox (Salvy, Fengos et al. 2018) (here only showing the ones that were modified), functions from the MATLAB community (Mathworks) and original code. The compatibility MATLAB-CPLEX was checked in IBM's website (https://www.ibm.com/software/reports/compatibility/clarity/softwarePrereqsMatrix.html)

File name	Comment	Based on/ source
calcDGis.m	Changes made so that parameter values will be those set for the global variables	Same file name, matTFA toolbox
calcDGsp.m	Changes made so that parameter values will be those set for the global variables	Same file name, matTFA toolbox
calcDGspA.m	Changes made so that parameter values will be those set for the global variables	Same file name, matTFA toolbox
calcDGspecie.m	Changes made so that parameter values will be those set for the global variables	Same file name, matTFA toolbox
calcDGtpt_RHS.m	Changes made so that parameter values will be those set for the global variables	Same file name, matTFA toolbox
calcpka.m	Changes made so that parameter values will be those set for the global variables	Same file name, matTFA toolbox
convToTFA.m	Changes made so that parameter values will be those set for the global variables	Same file name, matTFA toolbox
debye_hueckel.m	Temperature/Salinity dependent function to calculate parameter A	This study
def_analysis_E_coli.m	Increased number of parameters and parameter values. Automated analysis of all the combinations. Deleted sections focusing on plotting changes of directionalities originally included. Comparison with ^{13}C-MFA and experimental metabolomics data was added, as well as ways to evaluate the goodness-of-fit and the concordance	tutorial.m, matTFA toolbox
density_sw.m + densityH2O.m	This function applies an internationally accepted equation of state of sea water (Siedler and Peters 1986). Here, we use the equation of state for a pressure of one standard atmosphere which corrects the pure water reference by salinity contributions. Range of validity: 0 <= S <= 42 g/kg and -2 <= T <= 40 ℃. It is important to note that for the thermophilic case, a T value beyond the range limit was used (72 ℃)	This study

KendallCoef.m	The original script did not account for ties: here MATLAB's function 'tiedrank' was used	https://uk.mathworks.com/matlabcentral/fileexchange/27833-compute-the-kendall-s-coefficient-of-concordance-of-the-matrix-x
permittivityH2O.m + permittivityH2OS.m	Computation of the temperature-dependent static permittivity (dielectric constant) for water with dissolved salt (Meissner and Wentz 2004)	This study
phc.m	List of physical constants and conversion factors (Mohr, Newell et al. 2015)	This study
prefactor_A.m	Plot of predicted values for the parameter A according to two approaches: a (i) T-dependent function, and a (ii) T/S-dependent function	This study
prepModelforTFA.m	Changes made so that parameter values will be those set for the global variables. In addition, there were problems regarding duplicates in metFormulas. A molecule (set molecular formula) can have different similar forms (R/S,...). In the T. thermophilus GSM they are considered as separate molecules, but in Thermo DB (matTFA) they are not. The way this file was design is based on using an index (assuming there would be no duplicates) – changed it so that it considers the first value of a vector of indexes (since they all refer to the same Gibbs free energy values anyway)	Same file name, matTFA toolbox

S2-3 Table. Full factorial design.

Six parameters with two levels each were considered, yielding 64 different combinations. Run #3 recreates the conditions of the original matTFA.

Run	t (°C) (0 = 25, 1= 37)	I (M) (0 = 0, 1= 0.25)	S (g/kg) (0 = 0, 1= 13.74)	Parameter A (0 = t-dependent, 1 = t/S-dependent)	Adjustment method (0 = DH, 1= Davies)	[met] (0 = only ATP, ADP, AMP as matTFA, 1 = experimental values)
1	0	0	0	0	0	0
2	1	0	0	0	0	0
3	0	1	0	0	0	0
4	1	1	0	0	0	0
5	0	0	1	0	0	0
6	1	0	1	0	0	0
7	0	1	1	0	0	0
8	1	1	1	0	0	0
9	0	0	0	1	0	0
10	1	0	0	1	0	0
11	0	1	0	1	0	0
12	1	1	0	1	0	0
13	0	0	1	1	0	0
14	1	0	1	1	0	0
15	0	1	1	1	0	0
16	1	1	1	1	0	0
17	0	0	0	0	1	0
18	1	0	0	0	1	0
19	0	1	0	0	1	0

20	1	1	0	0	1	0
21	0	0	1	0	1	0
22	1	0	1	0	1	0
23	0	1	1	0	1	0
24	1	1	1	0	1	0
25	0	0	0	1	1	0
26	1	0	0	1	1	0
27	0	1	0	1	1	0
28	1	1	0	1	1	0
29	0	0	1	1	1	0
30	1	0	1	1	1	0
31	0	1	1	1	1	0
32	1	1	1	1	1	0
33	0	0	0	0	0	1
34	1	0	0	0	0	1
35	0	1	0	0	0	1
36	1	1	0	0	0	1
37	0	0	1	0	0	1
38	1	0	1	0	0	1
39	0	1	1	0	0	1
40	1	1	1	0	0	1
41	0	0	0	1	0	1
42	1	0	0	1	0	1
43	0	1	0	1	0	1
44	1	1	0	1	0	1
45	0	0	1	1	0	1
46	1	0	1	1	0	1
47	0	1	1	1	0	1
48	1	1	1	1	0	1
49	0	0	0	0	1	1
50	1	0	0	0	1	1
51	0	1	0	0	1	1

52	1	1	0	0	1	1
53	0	0	1	0	1	1
54	1	0	1	0	1	1
55	0	1	1	0	1	1
56	1	1	1	0	1	1
57	0	0	0	1	1	1
58	1	0	0	1	1	1
59	0	1	0	1	1	1
60	1	1	0	1	1	1
61	0	0	1	1	1	1
62	1	0	1	1	1	1
63	0	1	1	1	1	1
64	1	1	1	1	1	1

S2-4 Table. Tests characterisation and ranking.

A 2^6 full factorial design was tested in mod-matTFA, where 26/64 runs were unsuccessful. The remaining 38/64 converged into common optimal solutions, which depend on the results considered for grouping. All test yielded the same flux distribution in flux balance analysis (FBA), but 5 different ones are available for thermodynamics based flux analysis (TFA). These are reduced to 4 when only considering reactions in the central carbon metabolism (those mapped onto the ^{13}C-MFA results, S1 Table). With regards to the predicted concentration values, 9 different set are possible when considering either the full list of metabolites, or just those with an experimental counterpart. The joint ranking is based on the position of each run in two different rankings (correlation coefficient at the fluxomics level, and at the metabolomics level). A Kendall's W $\approx$ 0.81, showing a notable agreement between both rankings. *(run #3) Reflects the conditions used in the original matTFA.

Run	sol FBA	sol TFA	sol TFA central	sol Conc	sol Conc match	r flux.	r met	t (0 = 25, 1 = 37)	I (0 = 0, 1 = 0.25)	S (0 = 0, 1 = 13.74)	A (0 = t-dep, 1 = t/S-dep)	Adj (0 = DH, 1 = Davies)	[met] (0 = default, 1 = experimental)	Joint rank
20	1	5	4	6	6	0.95	0.18	1	1	0	0	1	0	62.5
24	1	5	4	6	6	0.95	0.18	1	1	1	0	1	0	62.5
52	1	5	4	6	6	0.95	0.18	1	1	0	0	1	1	62.5
56	1	5	4	6	6	0.95	0.18	1	1	1	0	1	1	62.5
28	1	5	4	7	7	0.95	0.17	1	1	0	1	1	0	59.5
60	1	5	4	7	7	0.95	0.17	1	1	0	1	1	1	59.5
12	1	3	3	4	4	0.90	0.17	1	1	0	1	0	0	56.5
32	1	3	3	9	9	0.90	0.17	1	1	1	1	1	0	56.5
44	1	3	3	4	4	0.90	0.17	1	1	0	1	0	1	56.5
64	1	3	3	9	9	0.90	0.17	1	1	1	1	1	1	56.5
3*	1	2	2	2	2	0.90	0.15	0	1	0	0	0	0	51.5
7	1	2	2	2	2	0.90	0.15	0	1	1	0	0	0	51.5
31	1	4	2	8	8	0.90	0.15	0	1	1	1	1	0	51.5
35	1	2	2	2	2	0.90	0.15	0	1	0	0	0	1	51.5
39	1	2	2	2	2	0.90	0.15	0	1	1	0	0	1	51.5
63	1	4	2	8	8	0.90	0.15	0	1	1	1	1	1	51.5
1	1	1	1	1	1	0.94	0.08	0	0	0	0	0	0	40.5
5	1	1	1	1	1	0.94	0.08	0	0	1	0	0	0	40.5

Run	sol FBA	sol TFA	sol TFA central	sol Conc	sol Conc match	r flux.	r met	t (0 = 25, 1 = 37)	I (0 = 0, 1 = 0.25)	S (0 = 0, 1 = 13.74)	A (0 = t-dep, 1 = t/S-dep)	Adj (0 = DH, 1 = Davies)	[met] (0 = default, 1 = experimental)	Joint rank
9	1	1	1	1	1	0.94	0.08	0	0	0	1	0	0	40.5
13	1	1	1	1	1	0.94	0.08	0	0	1	1	0	0	40.5
17	1	1	1	1	1	0.94	0.08	0	0	0	0	1	0	40.5
21	1	1	1	1	1	0.94	0.08	0	0	1	0	1	0	40.5
25	1	1	1	1	1	0.94	0.08	0	0	0	1	1	0	40.5
29	1	1	1	1	1	0.94	0.08	0	0	1	1	1	0	40.5
33	1	1	1	1	1	0.94	0.08	0	0	0	0	0	1	40.5
37	1	1	1	1	1	0.94	0.08	0	0	1	0	0	1	40.5
41	1	1	1	1	1	0.94	0.08	0	0	0	1	0	1	40.5
45	1	1	1	1	1	0.94	0.08	0	0	1	1	0	1	40.5
49	1	1	1	1	1	0.94	0.08	0	0	0	0	1	1	40.5
53	1	1	1	1	1	0.94	0.08	0	0	1	0	1	1	40.5
57	1	1	1	1	1	0.94	0.08	0	0	0	1	1	1	40.5
61	1	1	1	1	1	0.94	0.08	0	0	1	1	1	1	40.5
4	1	3	3	3	3	0.90	0.16	1	1	0	0	0	0	30.5
8	1	3	3	3	3	0.90	0.16	1	1	1	0	0	0	30.5
36	1	3	3	3	3	0.90	0.16	1	1	0	0	0	1	30.5
40	1	3	3	3	3	0.90	0.16	1	1	1	0	0	1	30.5
15	1	4	2	5	5	0.90	0.14	0	1	1	1	0	0	27.5
47	1	4	2	5	5	0.90	0.14	0	1	1	1	0	1	27.5

Supporting information Chapter 3

Table S3-1. Tests performed with FBA.

Tests differ on the weight values for each reaction in the field *c* of the model (Schellenberger, Que et al. 2011), where in all cases* they add up to 1. Three main objective functions were selected: (i) maximisation of the biomass yield (R_BIOMASS_LM3), (ii) maximisation of the ATP production by the flagellum (R_ATPS4r), (iii) maximisation of VSG formation, represented by a glycosylphosphatidylinositol (GPI) anchor sink (R_lipidSINK_HYPO). *To minimise the sum of fluxes, all reactions have a weight of '1'.

Test number	Weight biomass formation	Weight ATP synthesis	Weight VSG production	Weight any other reaction
1	0	0	1	0
2	0	0.25	0.75	0
3	0	0.5	0.5	0
4	0	0.75	0.25	0
5	0	1	0	0
6	0.25	0	0.75	0
7	0.25	0.25	0.5	0
8	0.25	0.5	0.25	0
9	0.25	0.75	0	0
10	0.5	0	0.5	0
11	0.5	0.25	0.25	0
12	0.5	0.5	0	0
13	0.75	0	0.25	0
14	0.75	0.25	0	0
15	1	0	0	0
16	1	1	1	1

Table S3-2. Different problem definitions converge into similar optimal solutions.

Non-redundant tests were identified. Apart from ATP synthesis in the cell membrane (*flux ATP synthesis*), for all of the solutions there was also ATP production in the mitochondria (R_ATPSm), but not via the flagellum (R_ATPS3v). Flux values in units of mmol/gDCW-h.

Solution	Test number(s)	Flux biomass formation	Flux ATP synthesis	Flux VSG production
1	1	0	100	20
2	2	0	100	20
3	3, 4	0	100	20
4	5	0	100	0.7
5	6	2.9	100	20
6	7	5.5	100	18.95
7	8	22.7	100	5.41
8	9, 12, 14	26.6	100	0
9	10	22.7	100	5.4
10	11	26.4	100	0.6
11	13	26.6	100	0
12	15	26.6	100	0
13	16	0	100	0

Table S3-3. Reactions of interest.

Ranked by their occurrence ('Oc.') over non-redundant tests. Only 33/240 potential targets were identified in at least half of the tests (7/13), and most of them have a gene annotated in the GSM used. Druggability data ('Drugg.') ranges from 0 to 1. Some reactions are also choke points in humans (HumanCyc v. 21.5, https://humancyc.org/) (Romero, Wagg et al. 2004): *C* (consuming side) and *P* (producing side), include the EC number in brackets. † A similar reaction was also selected, but no gene or protein was identified either ('R_RXN3O__45__458') (Dataset S3-1). * Available 3D structural data in Table S3-4. Since the workflow was based on reaction essentiality (as opposed to gene essentiality), some choke points lack UniProt IDs. As not all potential drug targets have been genetically and structurally characterised, this pipeline could also be used to guide further research on less studied reactions.

Oc	Reaction (GSM)	Gene(s) (GSM)	Drugg. (TDR)	Protein (TriTrypDB)	UniprotID (TriTrypDB)	Studied/ Tested	Choke point human
12	R_ENO	Tb927.10.2890	-	* Enolase	Q38BV6	(Avilán, Gualdrón-López et al. 2011)	-
		Tb927.11.16410	-	Enolase, putative	Q381E5	(Avilán, Gualdrón-López et al. 2011)	
12	R_PGM	Tb927.10.7930	-	* 2,3-bisphosphoglycerate-independent phosphoglycerate mutase	Q38AH1	-	-
		Tb927.11.10340	-	Serine/threonine-protein phosphatase PGAM5, mitochondrial, putative	Q383P5	-	-
		Tb927.11.11490	-	2,3-bisphosphoglycerate-independent phosphoglycerate mutase-like protein, putative	Q383C9	-	-
		Tb927.5.3580	-	Phosphoglycerate mutase protein, putative	Q57UA8	(Fuad, Fothergill-Gilmore et al. 2011)	-
12	† R_RXN3	-	-	(Phyto)sphingosine kinase	-	(Pasternack, Sharma	-

	O__45__504					et al. 2015)	
		Tb927.10.3260	-	Long-chain-fatty-acid--CoA ligase 5 (EC 6.2.1.3) (Long-chain acyl-CoA synthetase 5) (LACS 5), putative	Q38BS1	(Allmann, Mazet et al. 2014)	-
		Tb927.11.4490	-	long-chain-fatty-acid-CoA ligase, putative	Q385W8	(Kaur, Tiwari et al. 2011)	C (6.2.1.-)
12	R_FACOAL1	Tb927.9.4190	-	fatty acyl CoA syntetase 1	Q9U404	(Jiang, Ingersoll et al. 2000)	-
		Tb927.9.4200	-	fatty acyl CoA synthetase 2	Q9U403	(Jiang, Ingersoll et al. 2000)	-
		Tb927.9.4210	0.3	fatty acyl CoA synthetase 3	Q38FB8	(Jiang, Ingersoll et al. 2000)	-
		Tb927.10.3260	-	Long-chain-fatty-acid--CoA ligase 5 (EC 6.2.1.3) (Long-chain acyl-CoA synthetase 5) (LACS 5), putative	Q38BS1	(Allmann, Mazet et al. 2014)	-
		Tb927.11.4490	-	long-chain-fatty-acid-CoA ligase, putative	Q385W8	(Kaur, Tiwari et al. 2011)	C (6.2.1.-)
12	R_FACOAL140	Tb927.9.4190	-	fatty acyl CoA syntetase 1	Q9U404	(Jiang, Ingersoll et al. 2000)	-
		Tb927.9.4200	-	fatty acyl CoA synthetase 2	Q9U403	(Jiang, Ingersoll et al. 2000)	-
		Tb927.9.4210	0.3	fatty acyl CoA synthetase 3	Q38FB8	(Jiang, Ingersoll et al. 2000)	-
11	R_ETHAK	Tb927.11.2090	0.3	choline kinase	Q386V0		
11	R_ETAPCT	Tb927.11.14140	-	ethanolamine-phosphate cytidylyltransferase	Q382C3		

11	R_FACOAL180	Tb927.10.3260	-	Long-chain-fatty-acid--CoA ligase 5 (EC 6.2.1.3) (Long-chain acyl-CoA synthetase 5) (LACS 5), putative	Q38BS1	(Allmann, Mazet et al. 2014)	-
		Tb927.11.4490	-	long-chain-fatty-acid-CoA ligase, putative	Q385W8	(Kaur, Tiwari et al. 2011)	C (6.2.1.-)
		Tb927.9.4190	-	fatty acyl CoA syntetase 1	Q9U404	(Jiang, Ingersoll et al. 2000)	-
		Tb927.9.4200	-	fatty acyl CoA synthetase 2	Q9U403	(Jiang, Ingersoll et al. 2000)	-
		Tb927.9.4210	0.3	fatty acyl CoA synthetase 3	Q38FB8	(Jiang, Ingersoll et al. 2000)	-
11	R_FACOAL181	Tb927.10.3260	-	Long-chain-fatty-acid--CoA ligase 5 (EC 6.2.1.3) (Long-chain acyl-CoA synthetase 5) (LACS 5), putative	Q38BS1	(Allmann, Mazet et al. 2014)	-
		Tb927.11.4490	-	long-chain-fatty-acid-CoA ligase, putative	Q385W8	(Kaur, Tiwari et al. 2011)	C (6.2.1.-)
		Tb927.9.4190	-	fatty acyl CoA syntetase 1	Q9U404	(Jiang, Ingersoll et al. 2000)	-
		Tb927.9.4200	-	fatty acyl CoA synthetase 2	Q9U403	(Jiang, Ingersoll et al. 2000)	-
		Tb927.9.4210	0.3	fatty acyl CoA synthetase 3	Q38FB8	(Jiang, Ingersoll et al. 2000)	-
11	R_FACOAL182	Tb927.10.3260	-	Long-chain-fatty-acid--CoA ligase 5 (EC 6.2.1.3) (Long-chain acyl-CoA synthetase 5) (LACS 5), putative	Q38BS1	(Allmann, Mazet et al. 2014)	-
		Tb927.11.4490	-	long-chain-fatty-acid-CoA ligase, putative	Q385W8	(Kaur, Tiwari et al. 2011)	C (6.2.1.-)

		Tb927.9.4190	-	fatty acyl CoA syntetase 1	Q9U404	(Jiang, Ingersoll et al. 2000)	-
		Tb927.9.4200	-	fatty acyl CoA synthetase 2	Q9U403	(Jiang, Ingersoll et al. 2000)	-
		Tb927.9.4210	0.3	fatty acyl CoA synthetase 3	Q38FB8	(Jiang, Ingersoll et al. 2000)	-
8	R_2__46__3__(...)	Tb927.4.3160	0.6	Dihydroxyacetone phosphate acyltransferase, putative	Q583Z3	(Zufferey, Pirani et al. 2017)	P (2.3.1.42)
8	R_CHLPCTD	Tb927.10.12810	-	Cholinephosphate cytidylyltransferase A, putative	Q388W5	-	P (2.7.7.15)
8	R_2__46__7__(...)	Tb927.9.1610	-	CDP-diacylglycerol--inositol 3-phosphatidyltransferase, putative	Q38FY6	-	-
8	R_ALKYLGLYCER(...)	Tb927.6.1500	0.3	Alkyl-dihydroxyacetone phosphate synthase	Q585R0	(Zomer, Opperdoes et al. 1995)	-
8	R_CHOLK	Tb927.5.1140	-	Choline/ethanolamine kinase	Q57W59	(Gibellini, Hunter et al. 2008, Major, Denton et al. 2013)	-
8	R_GTHS	Tb927.7.4000	-	* glutathione synthetase, putative	Q57UN0	(Alsford, Turner et al. 2011)	-
8	R_ORNDC	Tb927.11.13730	1	* ornithine decarboxylase	Q382G4	(Bacchi, Nathan et al. 1980)	-
8	R_DAGCPT_LM	Tb927.10.8900	-	choline/ethanolamine phosphotransferase (CEPT)	Q38A84	-	C (2.7.8.22)

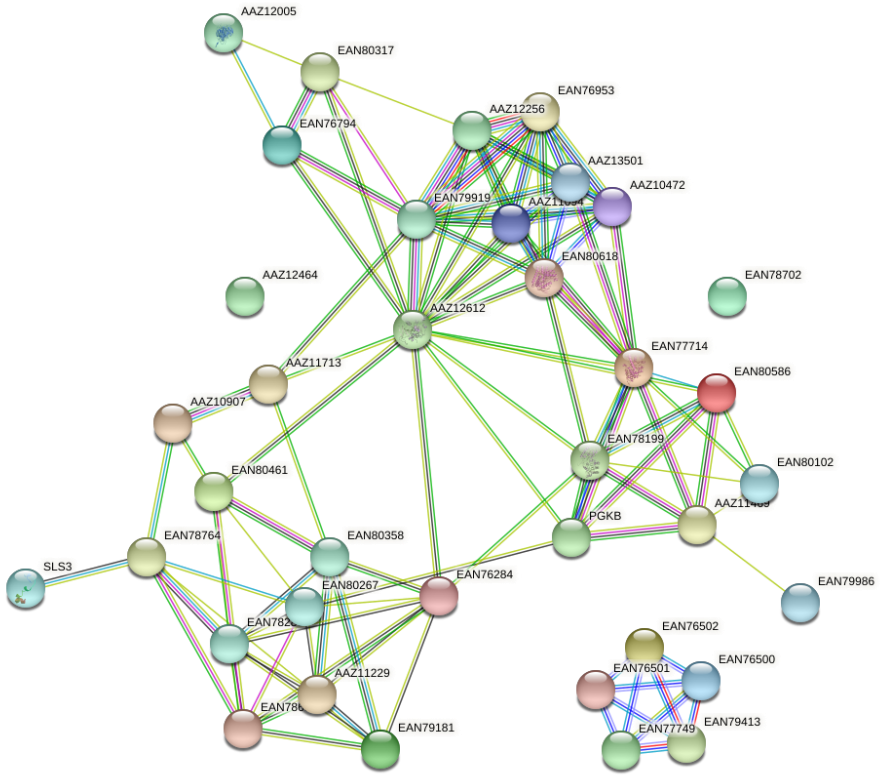
8	R_1akg3p acyltransfe rase	Tb927.11.15150	0.6	1-acyl-sn-glycerol-3-phosphate acyltransferase, putative	Q381S0	-	-
8	R_AKG3P O_LM	-	-	Acylglycerone- phosphate reductase	-	-	-
8	R_EAPT _LM	Tb927.10.13290	-	Ethanolamine phosphotransferase (EPT)	Q388R8	-	-
8	R_AKAG PP_LM	Tb927.10.13930	-	Phosphatidic acid phosphatase, putative	Q388K6	(Pasternac k, Sharma et al. 2015)	-
8	R_IPCS_ LM	Tb927.9.9390	-	Sphingomyelin/ceramide phosphorylethanolamine synthase	Q38E55	(Major, Denton et al. 2013)	-
8	R_DAGA T_LM	Tb927.11.13220	-	Phospholipid:diacylglycerol acyltransferase-like protein	Q382L4	-	-
8	R_ADMD C	Tb927.6.4410	0.6	S-adenosylmethionine decarboxylase	-	(Willert and Phillips 2008)	P (4.1.1.50)
		Tb927.6.4460	0.6	S-adenosylmethionine decarboxylase	-	(Willert and Phillips 2008)	P (4.1.1.50)
		Tb927.6.4470	-	* S-adenosylmethionine decarboxylase proenzyme	Q587B3	(Willert and Phillips 2008)	P (4.1.1.50)
8	R_SPMS	Tb927.9.7770	0.8	spermidine synthase	Q38EH6	(Xiao, McCloskey et al. 2009)	-
8	R_TMDS	Tb927.7.5480	1	bifunctional dihydrofolate reductase-thymidylate synthase	Q582G3	(Gibson, Dewar et al. 2016)	-

7	R_GCVP__45__RXN	Tb927.7.1910	-	Pyridoxal phosphate containing glycine decarboxylase, putative (glycine cleavage system P protein)	Q57V19	-	-
7	R_GCVT__45__RXN	Tb927.11.9670	-	Aminomethyltransferase, mitochondrial, putative	Q383W2	-	-
		Tb927.9.9840	-	Lipoic acid containing carrier protein, putative	Q38E17	-	-
7	R_PGK	Tb927.1.710	0.8	* phosphoglycerate kinase	Q4GZG3	(Bressi, Choe et al. 2000)	-
7	R_RXN__45__8629	Tb927.11.16730	0.5	Dihydrolipoyl dehydrogenase	Q381B3	-	-
		Tb927.3.4390	-	Dihydrolipoamide dehydrogenase	Q580K3	-	-
		Tb927.4.5040	-	Dihydrolipoamide dehydrogenase	Q584K1	-	-
		Tb927.8.7380	-	Dihydrolipoamide dehydrogenase, point mutation	Q57YU0	-	-
		Tb927.4.5050	-	Dihydrolipoamide dehydrogenase, pseudogene, putative	-	-	-

Table S3-4. Structurally characterised native proteins.

Protein	UniProt ID	PDB ID
2,3-bisphosphoglycerate-independent phosphoglycerate mutase	Q38AH1	3NVL
Glutathione synthetase, putative	Q57UN0	2WYO
S-adenosylmethionine decarboxylase proenzyme-like, putative	Q587B3	5TVF
Enolase (2-phospho-D-glycerate hydro-lyase)	Q38BV6	2PTW
Ornithine decarboxylase	Q382G4	1NJJ
Phosphoglycerate kinase	Q4GZG3	13PK

Figure S3-1. Network of genes codifying for reactions of interest.

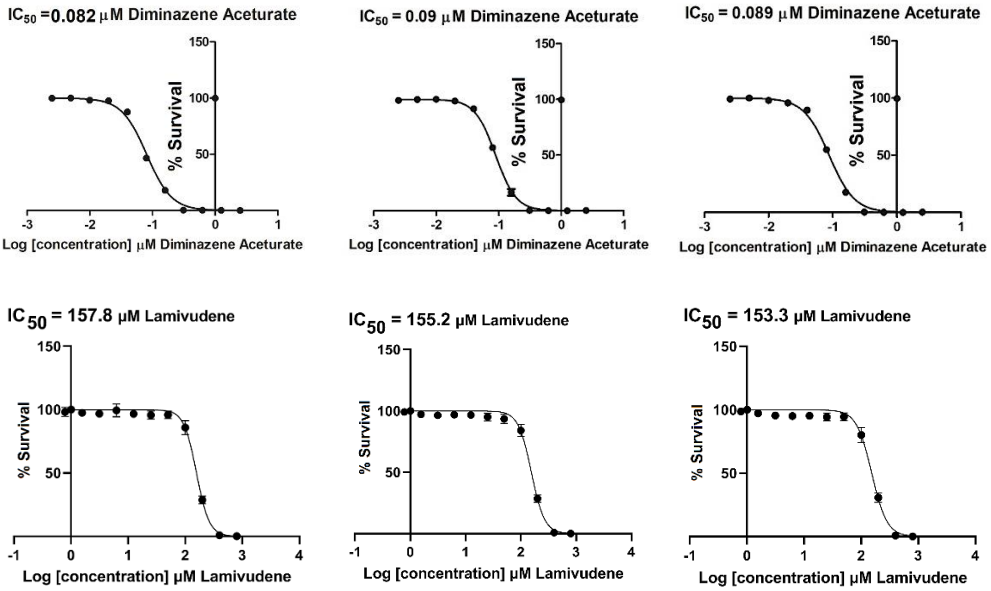


As generated by STRING (Szklarczyk, Gable et al. 2019). A PPI enrichment p-value: $< 1.0^{-16}$ suggests proteins are biologically connected as a group (at least partially). Legend as shown in the site: EAN80586: Enolase, putative (507 aa), EAN77714: Enolase (429 aa), EAN76502: Fatty acyl CoA synthetase 3 (702 aa), EAN80461: 1-acyl-sn-glycerol-3-phosphate acyltransferase protein, putative (271 aa), EAN79181: Choline/ethanolamine kinase, putative (431 aa), EAN78702: Uncharacterised protein; Belongs to the CDP-alcohol phosphatidyltransferase class-I family (412 aa), EAN76794: Spermidine synthase, putative (298 aa), EAN76500: Fatty acyl CoA syntetase 1 (698 aa), AAZ11094 Dihydrolipoamide dehydrogenase, putative (605 aa), AAZ10472: Dihydrolipoamide dehydrogenase, putative (505 aa), EAN76284: CDP-diacylglycerol--inositol 3-phosphatidyltransferase; Phosphatidyltransferase, putative (217 aa), EAN76501: Fatty acyl CoA synthetase 2 (708 aa), EAN78655: Cholinephosphate cytidylyltransferase A, putative (506 aa), EAN80618:Dihydrolipoyl dehydrogenase (477 aa), AAZ10907: Dihydroxyacetone phosphate acyltransferase, putative (1242 aa), AAZ11229: Choline/ethanolamine kinase, putative (628 aa), AAZ11713: Alkyl-dihydroxyacetone phosphate synthase (613 aa), EAN76953: Glycine cleavage system H protein; The H protein shuttles the methylamine group of glycine from the P protein to the T protein; Belongs to the GcvH family (138 aa), AAZ11469: Phosphoglycerate mutase protein, putative (185 aa), EAN78764: Phosphatidic acid phosphatase, putative (332 aa), EAN80317: Ornithine decarboxylase; Belongs to the Orn/Lys/Arg decarboxylase class-II

family (445 aa), EAN79413: Long-chain-fatty acid-CoA ligase protein, putative (665 aa), EAN78199: 2,3-bisphosphoglycerate-independent phosphoglycerate mutase (551 aa), AAZ12612: Bifunctional dihydrofolate reductase-thymidylate synthase; Bifunctional enzyme. Involved in de novo dTMP biosynthesis. Key enzyme in folate metabolism (527 aa), PGKB: Phosphoglycerate kinase (420 aa), EAN77749: Fatty acyl CoA synthetase, putative (703 aa), AAZ12464: Glutathione synthetase, putative (555 aa), AAZ12256: Glycine cleavage system P protein; The glycine cleavage system catalyzes the degradation of glycine (970 aa), AAZ12005: S-adenosylmethionine decarboxylase proenzyme-like, putative (325 aa), EAN79919: Aminomethyltransferase; The glycine cleavage system catalyzes the degradation of glycine; Belongs to the GcvT family (375 aa), EAN80358: Ethanolamine-phosphate cytidylyltransferase, putative (384 aa), EAN78286: Ethanolaminephosphotransferase, putative; Belongs to the CDP-alcohol phosphatidyltransferase class-I family (432 aa), EAN80267: Phospholipid:diacylglycerol acyltransferase-like protein (639 aa), SLS3: Phosphatidylcholine:ceramide cholinephosphotransferase 3; Bidirectional lipid cholinephosphotransferase capable of converting phosphatidylcholine (PC) and ceramide to sphingomyelin (SM) and diacylglycerol (DAG) and vice versa. Direction is dependent on the relative concentrations of DAG and ceramide as phosphocholine acceptors. Directly and specifically recognizes the choline head group on the substrate. Also requires two fatty chains on the choline-P donor molecule in order to be recognized efficiently as a substrate. Does not function strictly as a SM synthase. [...] (322 aa), EAN80102: 2,3-bisphosphoglycerate-independent phosphoglycerate mutase-like protein, putative (747 aa), EAN79986: Phosphoglycerate mutase-like protein (304 aa), and AAZ13501: Dihydrolipoamide dehydrogenase, point mutation (546 aa).

Figure S3-2. Drug sensitivity testing results.

Drugs and the control were tested in triplicate. Top row (diminazene aceturate, $\overline{IC_{50}} = 0.087 \pm 0.004\ \mu M$), and bottom row (lamivudine, $\overline{IC_{50}} = 155.4 \pm 2.3\ \mu M$.



Supporting information Chapter 4

Table S4-1. Single tandem repeat genotyping of GIN-28, GCE-28, GIN-31 and GCE-31 patient-derived primary lines isolated from the GBM 5ALA invasive edge (GIN) and contrast enhanced core (GCE). DNA was isolated from each sample and genetic characteristics determined by PCR-single-locus-technology, utilizing 21 independent PCR-systems. The GIN-28 line compared across two passages (p11 and p33), showed identical STR genotypes, with 20/21 DNA systems matching the STR genotype from primary invasive margin GBM tissue (T28.3) from which the cells were derived. GIN-31 p11 cells fully retain the genotype from primary invasive margin GBM tissue (T31.5) from which the cells were derived; GIN-31 p33 retains a matched STR genotype in 13/21 loci, with amplifications acquired in culture likely a result of the 22 passages between this sample and early passage. The GCE-28 line compared across two passages (p16 and p19), showed identical STR genotypes, with 20/21 DNA systems matching the STR genotype from primary invasive margin GBM tissue (T28.3) from which the cells were derived. The GCE-31 line compared across two passages (p7 and p16), showed identical STR genotypes, and fully retains the genotype from primary invasive margin GBM tissue (T31.5) from which the cells were derived. Collectively these results confirm that the cell lines utilized in this study have not been cross-contaminated with any other cell line and the primary lines derived from the GBM invasive margin and core regions, broadly retain the genotype of the tumour. Materials & Methods - Cell line authentication of the, GIN-28, GCE-28, GIN-31 and GCE-31 patient-derived primary lines were determined by PCR-single-locus-technology, utilizing 21 independent PCR-systems (Eurofins, Germany).

DNA-System	DNA-criteria T28.2 CL181019_025	DNA-criteria GIN-28 p11 CL18019_021	DNA-criteria GIN-28 p33 CL18019_022	DNA-criteria GCE-28 p16 CL18019_023	DNA-criteria GIN-28 p19 CL18019_024	DNA-criteria T31.5 CL18019_030	DNA-criteria GIN-31 p11 CL18019_026	DNA-criteria GIN-31 p31 CL18019_027	DNA-criteria GCE-31 p7 CL18019_028	DNA-criteria GCE-31 p16 CL18019_029
AM	X,Y	X,Y	X,Y	X,Y	X,Y	X,X	X,X	X,X	X,X	X,X
D3S1358	14,17	14,17	14,17	14,17	14,17	16,18	16,18	16,18	16,18	16,18
D1S1656	12,16	12,16	12,16	12,16	12,16	12,15	12,15	12,15	12,15	12,15
D6S1043	11,13	11,13	11,13	11,13	11,13	12,18	12,18	12,18	12,18	12,18
D13S317	11,12	11,12	11,12	11,12	11,12	13,13	11,13	11,13	11,13	11,13
Penta E	7,17	7,17	7,17	7,17	7,17	7,12	7,12	7,12	7,12	7,12
D16S539	9,12	9,12	9,12	9,12	9,12	10,11	10,11	10,11	10,11	10,11
D18S51	14,17	14,17	14,17	14,17	14,17	17,18	17,18	16,17,18	17,18	17,18
D2S1338	19,23	19,23	19,23	19,23	19,23	19,25	19,25	11,19,25	19,25	19,25
CSF1PO	11,13	11,13	11,13	11,13	11,13	11,12	11,12	11,12	11,12	11,12
Penta D	12,13,14	12,14	12,14	12,14	12,14	11,12	11,12	11,12	11,12	11,12
TH01	6,9,3	6,9,3	6,9,3	6,9,3	6,9,3	6,9	6,9	6,9	6,9	6,9
vWA	14,15	14,15	14,15	14,15	14,15	14,18	14,18	14,15,18,21	14,18	14,18
D21S11	27,33	27,33	27,33	27,33	27,33	29,29	29,29	29,29	29,29	29,29
D7S820	8,10	8,10	8,10	8,10	8,10	7,10	7,10	7,10	7,10	7,10
D5S818	11,12	11,12	11,12	11,12	11,12	11,12	11,12	11.1,12	11,12	11,12
TPOX	8,11	8,11	8,11	8,11	8,11	9,9	9,9	9,9	9,9	9,9
D8S1179	10,14	10,14	10,14	10,14	10,14	11,13	11,13	11,13,14.1	11,13	11,13
D12S391	20,21	20,21	20,21	20,21	20,21	23,23	17,23	16,17,22.3,23	17,23	17,23
D19S433	13,14	14,14	14,14	14,14	14,14	12,?	12,15	12,13.1,15	12,15	12,15
FGA	23,25	23,25	23,25	23,25	23,25	22,26	22,26	19.3,22,26	22,26	22,26

Table S4-2. Example of reaction of interest: 'HMR_6436'. This reaction along with 'HMR_6453' are related to *ACSF2* (ENSG00000167107), a gene indirectly targeted by afuresertib. More information about the metabolites can be found at https://metabolicatlas.org.

Metabolite symbol	Metabolite name	Comment
m01096m[m]	5-carboxy-alpha-chromanol [Mitochondria]	Exclusively produced by 'HMR_6453'. Exclusively consumed by 'HMR_6436'.
m01371m[m]	ATP [Mitochondria]	-
m01597m[m]	CoA [Mitochondria]	-
m02040m[m]	H2O [Mitochondria]	-
m02552m[m]	NAD+ [Mitochondria]	-
m02630m[m]	O2 [Mitochondria]	-
	→	
m00766m[m]	3-carboxy-alpha-chromanol [Mitochondria]	Exclusively produced by 'HMR_6436'. Exclusively consumed by 'HMR_6438' (transport to cytosol).
m01334m[m]	AMP [Mitochondria]	-
m02039m[m]	H+ [Mitochondria]	-
m02041m[m]	H2O2 [Mitochondria]	-
m02553m[m]	NADH [Mitochondria]	-
m02759m[m]	PPi [Mitochondria]	-
m02774m[m]	propanoyl-CoA [Mitochondria]	-

Dataset S4-1. Genes of interest lacking a cognate ligand, according to the multiple databases checked in this study. All the entries refer to upregulated genes in the tumour related to extended choke points and/or topologically important reactions.

Gene Symbol	Gene id	Gene name	Relevance (sum)
COQ6	ENSG00000119723	coenzyme Q6, monooxygenase	163
CYP4V2	ENSG00000145476	cytochrome P450 family 4 subfamily V member 2	163
AASDH	ENSG00000157426	aminoadipate-semialdehyde dehydrogenase	119
ACOT2	ENSG00000119673	acyl-CoA thioesterase 2	119
ACSF3	ENSG00000176715	acyl-CoA synthetase family member 3	119
HADHB	ENSG00000138029	hydroxyacyl-CoA dehydrogenase trifunctional multienzyme complex subunit beta	119
HSD17B4	ENSG00000133835	hydroxysteroid 17-beta dehydrogenase 4	119
SLC27A4	ENSG00000167114	solute carrier family 27 member 4	119
ACSBG1	ENSG00000103740	acyl-CoA synthetase bubblegum family member 1	86
CPOX	ENSG00000080819	coproporphyrinogen oxidase	45
MMAA	ENSG00000151611	metabolism of cobalamin associated A	35
CYP26B1	ENSG00000003137	cytochrome P450 family 26 subfamily B member 1	28
EPRS1	ENSG00000136628	glutamyl-prolyl-tRNA synthetase 1	19
CDS2	ENSG00000101290	CDP-diacylglycerol synthase 2	16
NME2	ENSG00000243678	NME/NM23 nucleoside diphosphate kinase 2	10
ABHD5	ENSG00000011198	abhydrolase domain containing 5, lysophosphatidic acid acyltransferase	9
AGPAT4	ENSG00000026652	1-acylglycerol-3-phosphate O-acyltransferase 4	9
CARS1	ENSG00000110619	cysteinyl-tRNA synthetase 1	9
DDX19B	ENSG00000157349	DEAD-box helicase 19B	9
FARSA	ENSG00000179115	phenylalanyl-tRNA synthetase subunit alpha	9

GARS1	ENSG00000106105	glycyl-tRNA synthetase 1	9
GUSB	ENSG00000169919	glucuronidase beta	9
IARS1	ENSG00000196305	isoleucyl-tRNA synthetase 1	9
KARS1	ENSG00000065427	lysyl-tRNA synthetase 1	9
LARS1	ENSG00000133706	leucyl-tRNA synthetase 1	9
LCLAT1	ENSG00000172954	lysocardiolipin acyltransferase 1	9
MARS1	ENSG00000166986	methionyl-tRNA synthetase 1	9
MBOAT2	ENSG00000143797	membrane bound O-acyltransferase domain containing 2	9
NARS1	ENSG00000134440	asparaginyl-tRNA synthetase 1	9
NUP133	ENSG00000069248	nucleoporin 133	9
NUP153	ENSG00000124789	nucleoporin 153	9
NUP160	ENSG00000030066	nucleoporin 160	9
NUP188	ENSG00000095319	nucleoporin 188	9
NUP214	ENSG00000126883	nucleoporin 214	9
NUP42	ENSG00000136243	nucleoporin 42	9
NUP43	ENSG00000120253	nucleoporin 43	9
NUP54	ENSG00000138750	nucleoporin 54	9
NUP58	ENSG00000139496	nucleoporin 58	9
NUP62	ENSG00000213024	nucleoporin 62	9
NUP88	ENSG00000108559	nucleoporin 88	9
NUP93	ENSG00000102900	nucleoporin 93	9
NUP98	ENSG00000110713	nucleoporin 98 and 96 precursor	9
PLPP1	ENSG00000067113	phospholipid phosphatase 1	9
PLPP3	ENSG00000162407	phospholipid phosphatase 3	9
PLPP5	ENSG00000147535	phospholipid phosphatase 5	9
PLPPR2	ENSG00000105520	phospholipid phosphatase related 2	9

PLPPR4	ENSG00000117600	phospholipid phosphatase related 4	9
POM121	ENSG00000196313	POM121 transmembrane nucleoporin	9
QARS1	ENSG00000172053	glutaminyl-tRNA synthetase 1	9
RANBP2	ENSG00000153201	RAN binding protein 2	9
RARS1	ENSG00000113643	arginyl-tRNA synthetase 1	9
SARS1	ENSG00000031698	seryl-tRNA synthetase 1	9
SEC13	ENSG00000157020	SEC13 homolog, nuclear pore and COPII coat complex component	9
SEH1L	ENSG00000085415	SEH1 like nucleoporin	9
TARS1	ENSG00000113407	threonyl-tRNA synthetase 1	9
TPK1	ENSG00000196511	thiamin pyrophosphokinase 1	9
TPR	ENSG00000047410	translocated promoter region, nuclear basket protein	9
WARS1	ENSG00000140105	tryptophanyl-tRNA synthetase 1	9
SLC5A6	ENSG00000138074	solute carrier family 5 member 6	8
ABCB6	ENSG00000115657	ATP binding cassette subfamily B member 6 (Langereis blood group)	6
SLC29A2	ENSG00000174669	solute carrier family 29 member 2	6
SLC46A1	ENSG00000076351	solute carrier family 46 member 1	6
APIP	ENSG00000149089	APAF1 interacting protein	4
COX4I1	ENSG00000131143	cytochrome c oxidase subunit 4I1	4
COX5B	ENSG00000135940	cytochrome c oxidase subunit 5B	4
COX6A1	ENSG00000111775	cytochrome c oxidase subunit 6A1	4
COX6B1	ENSG00000126267	cytochrome c oxidase subunit 6B1	4
COX6C	ENSG00000164919	cytochrome c oxidase subunit 6C	4
COX7A1	ENSG00000161281	cytochrome c oxidase subunit 7A1	4
COX7A2	ENSG00000112695	cytochrome c oxidase subunit 7A2	4
COX7B	ENSG00000131174	cytochrome c oxidase subunit 7B	4
COX8A	ENSG00000176340	cytochrome c oxidase subunit 8A	4

CRAT	ENSG00000095321	carnitine O-acetyltransferase	4
DGUOK	ENSG00000114956	deoxyguanosine kinase	4
GUK1	ENSG00000143774	guanylate kinase 1	4
MRI1	ENSG00000037757	methylthioribose-1-phosphate isomerase 1	4
MYBBP1A	ENSG00000132382	MYB binding protein 1a	4
NME3	ENSG00000103024	NME/NM23 nucleoside diphosphate kinase 3	4
NME6	ENSG00000172113	NME/NM23 nucleoside diphosphate kinase 6	4
NME7	ENSG00000143156	NME/NM23 family member 7	4
POLE4	ENSG00000115350	DNA polymerase epsilon 4, accessory subunit	4
POLG	ENSG00000140521	DNA polymerase gamma, catalytic subunit	4
POLG2	ENSG00000256525	DNA polymerase gamma 2, accessory subunit	4
POLL	ENSG00000166169	DNA polymerase lambda	4
POLM	ENSG00000122678	DNA polymerase mu	4
REV3L	ENSG00000009413	REV3 like, DNA directed polymerase zeta catalytic subunit	4
DAGLA	ENSG00000134780	diacylglycerol lipase alpha	3
DAGLB	ENSG00000164535	diacylglycerol lipase beta	3
GALE	ENSG00000117308	UDP-galactose-4-epimerase	3
LIPE	ENSG00000079435	lipase E, hormone sensitive type	3
RRM2B	ENSG00000048392	ribonucleotide reductase regulatory TP53 inducible subunit M2B	3
TXN2	ENSG00000100348	thioredoxin 2	3
ABHD6	ENSG00000163686	abhydrolase domain containing 6, acylglycerol lipase	2
CPT1C	ENSG00000169169	carnitine palmitoyltransferase 1C	2

Dataset S4-2. Top 30 identified chemicals of interest, ranked according to their relevance (Figure 4.1). In general, readily approved drugs, rather than natural products, were selected for the *in vitro* tests. Interactions have been codified as follows: affects cotreatment (A. cotreat.), affects expression (A. exp.), decreases expression (D. exp.), decreases reaction (D. reac.), increases activity (I. act.), increases expression (I. exp.), increases metabolic processing (I. metab.), inhibitor (Inhib.), predicted (-).

#	Database	Drug/ Chemical	Relevance	Gene(s)	Interaction(s) (predicted "-")	Information
1	CTD	GW 4064	1247	*ACAA2* *ACOT7* *ACOT8* *ACOX1* *ACSL3* *ACSL4* *ACSL5* *AGPAT1* *CPT1A* *ECHS1*	A. cotreat., D. exp. A. cotreat., D. exp. A. cotreat., D. exp. A. cotreat., D. exp. A. cotreat., D. exp. A. cotreat., D. exp. I. exp. A. cotreat., D. exp. A. cotreat., D. exp. A. cotreat., D. exp.	- Interaction: (Pant, Rondini et al. 2019) - Description: synthetic chemical, agonist of Farnesoid X receptor (a nuclear receptor). FXR is normally expressed in the liver and the intestine, but has been found in human CAFs (cancer-associated fibroblasts). Drugbank: (-). - Mechanism: activating it by GW4064 suppressed proliferation and induced apoptosis in colorectal cancer cells (Hotta, Sakatani et al. 2019), and decreased CAF migration, stress-fiber formation and contractility in breast cancer (Barone, Vircillo et al. 2018). - Application to GBM: it was generally assumed GBM is not related to CAFs, but a recent study suggested otherwise, but only for 5-26% of cells in GBM (Rick, Nguyen et al. 2019).

							FASN	A. cotreat., D. exp.	
							GPAT4	A. cotreat., D. exp.	
							HADH	A. cotreat., D. exp.	
							HADHA	A. cotreat., D. exp.	
							LPIN1	A. cotreat., D. exp.	
							LPIN2	A. cotreat., D. exp.	
							SLC27A1	A. cotreat., D. exp.	
2	CTD			obeticholic acid		899	*ACAA1*	I. exp.	- Description: semi-synthetic bile acid derivative, agonist of FXR (Dash, Figler et al. 2017). Drugbank: DB05990. - Mechanism: interferes with IL-6/STAT3 signalling pathway in vitro, supressing proliferation and metastasis in hepatocellular carcinoma (Attia, Tawfiq et al. 2017), and induced tumour necrosis/cell proliferation inhibition in human cholangiocarcinoma (Di Matteo, Nevi et al. 2019). - Application to GBM: none relevant.
							ACAA2	I. exp.	
							ACOX1	I. exp.	
							ACOX3	I. exp.	
							ACSL1	D. exp.	
							ACSL4	I. exp.	
							ACSL5	I. exp.	
							ACSL6	I. exp.	
							AGPAT5	D. exp.	
							CPT1A	D. exp., D. reac.	
							FASN	I. exp., D. reac.	
							GAPDH	D. exp.	
							GPAM	D. exp.	
							LPIN1	D. exp.	
							LPIN2	D. exp.	
							TXN	D. exp.	
							TXNRD2	D. exp.	
3	CTD			coumestrol		677	*AAAS*	A. cotreat., I. exp.	- Description: natural product (phytoestrogen) (Dip, Lenz et al. 2009). Drugbank: (-).
							AARS1	I. exp.	

ABHD12	A. cotreat., I. exp.
ACAA2	A. cotreat., D. exp.
ACOT7	A. cotreat., I. exp.
ACSL3	D. exp.
AGPAT3	D. exp.
CDS1	A. cotreat., D. exp.
FARSB	I. exp.
GLE1	A. cotreat., I. exp.
GPAT4	A. cotreat., I. exp.
HADH	A. cotreat., I. exp.
MGLL	A. cotreat., D. exp.
MMAB	I. exp.
NDC1	A. cotreat., I. exp.
NUP107	A. cotreat., I. exp.
NUP155	A. cotreat., I. exp.
NUP205	I. exp.
NUP210	A. cotreat., I. exp.
NUP35	I. exp.
NUP50	I. exp.
NUP85	I. exp.
PKM	A. cotreat., I. exp.
POLA1	A. cotreat., I. exp.
POLA2	A. cotreat., I. exp.
POLD2	A. cotreat., I. exp.
POLD3	A. cotreat., I. exp.
POLE	A. cotreat., I. exp.
POLE3	A. cotreat., I. exp.
POLI	A. cotreat., D. exp.

- Mechanism: direct targeting of haspin kinase, anti-cancer effects against skin melanoma, lung cancer and colon cancer cell growth (Kim, Lee et al. 2017). Additionally, it can induce ROS generation, DNA damage, G1/S cell cycle arrest, up-regulation of Bax and apoptosis induction via caspase-dependent mitochondrial mediated pathway (breast cancer cells (Zafar, Singh et al. 2018)), plus a plethora of other mechanisms (Lim, Jeong et al. 2017).
- Application to GBM: it can cross the blood brain barrier and may exert a neuroprotective effect (Canal Castro, Pagnussat et al. 2012).

				RAE1	I. exp.	
				RFC5	A. cotreat., I. exp.	
				RRM1	A. cotreat., I. exp.	
				SLC29A1	A. cotreat., I. exp.	
				TENT4A	I. exp.	
				VARS1	I. exp.	
4	CTD	afuresertib	385	*ACSF2*	I. exp.	- Description: orally bioavailable inhibitor of the serine/threonine protein kinase Akt (protein kinase B) with potential antineoplastic activity (Yamaji, Ota et al. 2017). Drugbank: DB11648. - Mechanism: overcomes chemotherapy platinum-resistance (ovarian cancer, (Blagden, Hamilton et al. 2019)), and enhanced cisplatin treatment of malignant pleural mesothelioma cells (Yamaji, Ota et al. 2017). - Application to GBM: loss of *PTEN* function or activation of *PIK3CA or PIK3R1* due to mutations provoke an almost uniform activation of PI3K/AKT/mTOR (Brennan, Verhaak et al. 2013, Le Rhun, Preusser et al. 2019).
				ACSL5	I. exp.	
				FARSB	D. exp.	
				LPIN1	I. exp.	
				MMAB	I. exp.	
				PNPLA2	I. exp.	
				POLA2	D. exp.	
				POLD4	I. exp.	
				SLC27A1	I. exp.	
				SLC29A1	D. exp.	
5	CTD	Tolcapone	172	*ACSL1*	D. exp.	- Description: medication for Parkinson's disease, it can penetrate the blood brain barrier, but it provokes liver toxicity (Grünig, Felser et al. 2018). Drugbank: DB00323. - Mechanism: inhibits Catechol-O-methyltransferase (COMT) and kills neuroblastoma (NB) cells in preclinical models (Maser, Rich et al. 2017,Pinheiro, 2019 #1256). - Application to GBM: by proximity to neuroblastoma.
				ACSL5	D. exp.	
6	CTD	VER 155008	146	*DARS1*	A. cotreat., I. exp.	- Description: HSP70 inhibitor (Marrugal, Ferrer et al. 2019). Drugbank: (-). - Mechanism: proven pleiotropic effect in breast cancer, including the downregulation of TFGb (Lee, Ouzounova et al. 2019)
				FARSB	A. cotreat., I. exp.	
				HSD17B10	A. cotreat., D. exp.	

				YARS1	A. cotreat., D. exp.	- Application to GBM: TGFb is related to migration, invasion and angiogenesis in GBM (Le Rhun, Preusser et al. 2019). However, high HSP70 levels have been correlated to a better clinical outcome (Lämmer, Delbridge et al. 2019).
7	CTD	pyrrolidine dithiocarbamic acid (PDTC)	128	*HADHA*	A. cotreat., I. exp., D. reac.	- Description: anticonvulsant, a neuroprotective agent, a radical scavenger, an antineoplastic agent and a NF-kappaB inhibitor (Hardy and Hunt 2004). Drugbank: (-). - Mechanism: helps fighting doxorubicin resistance and NF-kappaB activation by doxorubicin (Park, Lee et al. 2018). - Application to GBM: targeting *NF-κB* and *STAT3* has been suggested as a potential therapeutic approach to treat GBM (McFarland, Gray et al. 2013).
				HARS1	A. cotreat., D. exp., D. reac.	
				HSD17B10	-	- Description: coumarin derivative extracted from natural plants. Drugbank: (-). - Mechanism: down-regulation of c-myc, Cyclin D1 and NF-κB in lung cancer (Zhu, Gu et al. 2018), and induction of apoptosis in gastric cancer cells through IGF-1/PI3K/Akt mediated mitochondrial apoptosis pathway (Wang, Lu et al. 2017). - Application to GBM: IGF-1/PI3K/Akt does not seem to have been targeted in the literature
8	DGI	Esculetin	123	*POLK*	-	

8	DGI	Pyrogallol	123	*HSD17B10*	-	- Description: natural polyphenol. Drugbank: (-). - Mechanism: antitumor effect in hepatocellular carcinoma cells via *miR-134* activation-mediated S phase arrest, plus inhibiting *PI3K/AKT/Skp2/cMyc* signalling (Ahn, Im et al. 2019) - Application to GBM: miR-134 is commonly deregulated in human gliomas, and restoring its function promotes apoptosis, inhibits cell proliferation, invasion and migration (Niu, Yang et al. 2013)
				POLK	-	
9	DGI	Boldine	119	*HSD17B10*	-	- Description: aporphine alkaloid of *Peumus boldus*. Drugbank: (-). - Mechanism: antioxidant activity and provokes the upregulation of pro-apoptotic proteins (Subramaniam, Kannan et al. 2019), plus inhibiting telomerase at non-toxic concentrations (Kazemi Noureini and Tanavar 2015, Kazemi Noureini, Kheirabadi et al. 2018). - Application to GBM: increasing cleaved caspase-3 enhanced apoptosis in a GBM cell line (Hwang, Park et al. 2019).
9	DGI	Chelerythrine	119	*HSD17B10*	-	- Description: natural benzo[c]phenanthridine alkaloid and a widely used broad-range protein kinase C inhibitor which has anti-cancer effect on various types of human cancer cells (He, Zhuo et al. 2020). Drugbank: (-). - Mechanism: modulation of the MMP/TIMP/NF-κB system (suppresses proliferation and metastasis of human prostate cancer cells, (Yang, Zhang et al. 2020)) and induces apoptosis via ROS-mediated endoplasmic reticulum stress and STAT3 pathways (human renal cell carcinoma, (He, Zhuo et al. 2020)). - Application to GBM: they do not seem to have been targeted
9	DGI	Diflunisal	119	*HSD17B10*	-	- Description: anti-inflammatory drug. Drugbank: DB00861. - Mechanism: inhibition of p300 lysine acetyltransferase activity - Application to GBM: using another inhibitor of p300 (C646) did not yield a significant reduction of invasiveness in U87 cell line (GBM) (Fahey, Korytowski et al. 2019).

9	DGI	Formononetin	119	*HSD17B10*	-	- Description: isoflavone from red clovers and the Chinese herb *Astragalus membranaceus*. Drugbank: DB15335. - Mechanism: induction of apoptosis and cell cycle arrest, thus suppressing cell proliferation (Tay, Tan et al. 2019). It affects a plethora of targets (Ong, Shanmugam et al. 2019). - Application to GBM: some of those targets could be of interest.
9	DGI	gatifloxacin	119	*HSD17B10*	-	- Description: 7-piperazinylquinolone antibacterial (fluoroquinolone). Drugbank: DB01044. - Mechanism: induction of apoptosis, and cell cycle arrest at the S/G2 stage for multiple cell lines (Ahadi and Emami 2020). - Application to GBM: generic cancer targets
9	DGI	karanjin	119	*HSD17B10*	-	- Description: furanoflavanoids. Drugbank: (-). - Mechanism: Induction of G2/M arrest and apoptosis (Roy, Pal et al. 2019) - Application to GBM: generic cancer targets
9	DGI	purvalanol A	119	*HSD17B10*	-	- Description: highly selective inhibitor of Cdc2 [also known as cyclin-dependent kinase 1 (CDK1)]. Drugbank: DB04751. - Mechanism: highly selective inhibitor of Cdc2 [also known as cyclin-dependent kinase 1 (CDK1)] (Chen, Liao et al. 2017), induction of apoptosis and autophagy in HeLa cervical cancer cells (Ozfiliz-Kilbas, Sarikaya et al. 2018). - Application to GBM: generic cancer targets
10	CTD	methylselenic acid	114	*ACSL3* *NME1* *NME4* *POLA1* *RFC5* *RRM1* *TXNRD1*	A. exp. D. exp. D. exp. D. exp. D. exp. A. exp. I. metab.	- Description: selenium derivative (Zhao, Whitfield et al. 2004). Drugbank: (-). - Mechanism: targets GDF15 in prostate cancer cells (Zhang, Hu et al. 2019), inhibition of the JAK2/STAT3 pathway (Qiu, Zhang et al. 2019) - Application to GBM: JAK2/STAT3 is a known target for GBM (Stechishin, Luchman et al. 2013, Zheng, Han et al. 2014)

11	CTD	Pinosylvin	23	*COX5A* *COX7C* *HMOX2* *NUP35*	D. exp. D. exp. I. exp. D. exp.	- Description: pre-infectious stilbenoid toxin (Park, Chung et al. 2013). Drugbank: (-). - Mechanism: enhances cell death in leukemia cells by down-regulating AMPKα (Song, Seo et al. 2018), reduces cell migration and invasion of oral cancer carcinoma by regulating matrix metalloproteinase-2 expression and extracellular signal-regulated kinase pathway (Chen, Liu et al. 2019) - Application to GBM: targeting matrix metalloproteinase-2 and -9 to reduce growth and invasion has been suggested (Kast and Halatsch 2012).
12	CTD	geraniol	17	*AHCTF1* *POLA1* *POLE*	D. exp. D. exp. D. exp.	- Description: dietary monoterpene alcohol (Lee, Park et al. 2016). Drugbank: DB14183 - Mechanism: growth suppression by down-regulation of E2F8 (prostate cancer, (Lee, Park et al. 2016)) - Application to GBM: generic cancer target
13	DGI	3-O-methylquercetin (Isorhamnetin)	16	*POLB* *POLH*	- -	- Description: flavonoid. Drugbank: (-) - Mechanism: promotes mitochondrial fission and apoptosis by translocation of *CaMKII*, plus affecting multiple signalling pathways (breast cancer, (Hu, Zhang et al. 2019)) - Application to GBM: *CaMKII* has been appointed as a potential novel target to eliminate GSCs [Glioblastoma stem-like cells] (Shin, Lee et al. 2019).

				POLI	-	
				POLK	-	
13	DGI	eupafolin	16	*POLB* *POLH* *POLI* *POLK*	-	- Description: flavonoid from *Artemisia vulgaris* L. Drugbank: (-) - Mechanism: supresses TOPK (T-LAK cell-originated protein kinase), provoking a reduction of histone H3 and Ki67, and an increase of cleaved caspase-3 (Fan, Tao et al. 2019) - Application to GBM: targeting *TOPK* has been suggested as a treatment for GBM (Hayashi, Hayakawa et al. 2018). Increasing cleaved caspase-3 enhanced apoptosis in a GBM cell line (Hwang, Park et al. 2019)
13	DGI	hispidin	16	*POLB* *POLH* *POLI* *POLK*		- Description: natural compound from edible mushrooms. Drugbank: (-) - Mechanism: inhibit tubulin polymerization by modulating microtubule regulatory proteins, caspase-independent death in cancer cells but not in normal ones (Lv, Zhou et al. 2017) - Application to GBM: generic cancer target
13	DGI	Prexasertib	16	*CDS1*	Inhib.	- Description: small ATP-competitive selective inhibitor of CHK1 and CHK2 (Angius, Tomao et al. 2020). Drugbank: DB12008 - Mechanism: small ATP-competitive selective inhibitor of CHK1 and CHK2 (Angius, Tomao et al. 2020).

13	DGI	Taxifolin	16	*POLB* *POLH* *POLI* *POLK*	-	- Application to GBM: this drug sensitizes to PARP inhibition in ovarian cancer models (Parmar, Kochupurakkal et al. 2019). PARP inhibition for GBM has been shown to overcome apoptotic resistance (Karpel-Massler, Pareja et al. 2014). Similarly, other drugs shown in this list are based on using cleaved caspase-3 to cleave PARP to an inactive form (boldine and eupafolin). This drug also increases the sensitivity to gemcitabine (pancreatic cancer cells, (Morimoto, Takada et al. 2020)), a drug used for GBM but which generate chemoresistance (Bastiancich, Bastiat et al. 2018).
14	DGI	Isoorientin	8	*POLI* *POLK*	- -	- Description: flavonoid Drugbank: DB02224. - Mechanism: promotes mesenchymal to epithelial transition via β-catenin signalling (the reverse process of EMT, related to metastasis), by down-regulating β-catenin (Li, Hu et al. 2019). - Application to GBM: targeting β-catenin signalling has been suggested as a therapeutic approach for GBM, where it could affect migration (Sareddy, Pratap et al. 2019)
15	DGI	Crocin	4	*POLK*	-	- Description: C-glycosyl flavone Drugbank: (-) - Mechanism: increases levels of cleaved-caspase-3 and cle-PARP, inducing apoptosis in lung cancer (Xu, Shen et al. 2020) - Application to GBM: as explained for other drugs in this list, cle-cas-3 and cle-PARP are of interest for GBM
						- Description: Drugbank: DB11874 - Mechanism: inhibits the migration, invasion, and epithelial-mesenchymal transition of gastric cancer cells by increasing the expression of miR-320 (Zhou, Xu et al. 2019) - Application to GBM: miR-320 overexpression promoted apoptosis in glioma cells (Li, Ma et al. 2018)

16	DGI	dequalinium chloride	4	*POLB*	-	- Description: antiseptic and disinfectant (bactericidal and fungicidal activity). Drugbank: DB04209 - Mechanism: blocks DNA synthesis and sensitizes cancer cells to DNA damage agents (Cheng, Lo et al. 2018) - Application to GBM: generic cancer targets
16	DGI	Rhamnetin	4	*POLK*	-	- Description: flavonoid Drugbank: (-) - Mechanism: induced apoptosis by the miR-34a/Notch-1 signalling pathway in human breast cancer (Lan, Wang et al. 2019) - Application to GBM: overexpression of miR-34a (Lan, Wang et al. 2019) could be an interesting approach, since it is a transcriptional target downregulated in GBM compared to normal brain, and transient expression in GBM inhibited growth in a xenograft (Lino, Merlo et al. 2010). However, a clinical trial based on reintroducing this tumour suppressive miRNA provoked immune-related adverse effects, so it was terminated (Bahreyni-Toossi, Dolat et al. 2019).
17	CTD	Scutellarin	3	*PKM*	I. act.	- Description: flavonoid Drugbank: (-) - Mechanism: inhibited cell migration and invasion in bladder cancer models (Lv, Liu et al. 2019), plus reversing growth and epithelial-mesenchymal transition (EMT) in colon cancer (Yang, Zhao et al. 2017). - Application to GBM: the ETM has been recently linked to GBM's invasiveness (Iser, Pereira et al. 2017).
17	CTD	Yessotoxin	3	*PKM*	I. exp.	- Description: marine toxin. Drugbank: (-) - Mechanism:, mitotic catastrophe in murine brain tumour (Korsnes and Korsnes 2017) - Application to GBM: induction of Paraptosis-like cell death in glioma cells (Rubiolo, López-Alonso et al. 2014)

Other contributions

Required Gene Set for Autotrophic Growth of *Clostridium autoethanogenum* (Woods, Humphreys Christopher et al.), third author.

A genome-scale metabolic model of Cupriavidus necator H16 integrated with TraDIS and transcriptomic data reveals metabolic insights for biotechnological applications (Pearcy, Garavaglia et al. 2022), eighth author.

Metabolic engineering in *Clostridium autoethanogenum*, in collaboration with François Seys (School of Life Sciences) for a project on genetic editing tools in *C. autoethanogenum*, an industrially relevant acetogenic bacterium (Humphreys, McLean et al. 2015). Results were used for his thesis, for an oral communication (*Multiplex Base Editing in Acetogens targeting non-canonical PAMs*, Synthetic Biology UK 2021 November 23, 2021) and a publication (in preparation). A script was developed in MATLAB R2017b to identify lethal mutations for the following nucleases:

Nuclease(s)	Protospacer Adjacent Motifs (PAMs) class	PAM
Cas9, nCas9	NGG	AGG CGG GGG TGG
xCas9, Cas9-NG	NGD	AGA CGA GGA TGA AGT CGT GGT TGT AGG CGG GGG TGG
xCas9, Cas9-NG	NG	AG CG GG TG
Spy-Mac	NAA	AAA CAA GAA TAA
Cas9-VQR	NGA	AGA CGA GGA TGA

The algorithm can be summarised as follows. Base editors read both the sense and the antisense strands in direction 5'-3'. However, the impact of a C-to-T substitution and the creation of a STOP codon is noted in the sense strand (TGA, TAG or TAA), even if the tool has recognized a PAM and modified an editing window in the antisense strand. Extra steps are needed when handling and mutating the antisense strand, so the consistency with the reading frame (in the sense strand) is only considered at the end.

The protospacer and the editing window are defined as the sequences -21 to -1 and -19 to -16 from the PAM, respectively. The distance of the PAM from the first base pair of the CDS (coding region) was measured as the size of the sequence in between them, divided by the full size of the CDS. A threshold of 75% was selected to remove PAMs too far in the CDS.

Column number	Sense strand	Antisense strand
1	CDS name	CDS name
2	CDS sequence	CDS sequence (flipped and complementary)
3	CDS length	CDS length
4	Direction	Direction
5	PAM	PAM
6	PAM class	PAM class
7	PAM position	PAM position
8	PAM % distance	PAM % distance (corrected)
9	Protospacer (-21, -1)	Protospacer (-21, -1)
10	Reading frame-consistent protospacer	Equivalent PAM position in the reverse complementary strand
11	Sequence pre-editing window	Sequence pre-editing window
12	Sequence editing window	Sequence editing window
13	Sequence post-editing window	Sequence post-editing window
14	Mutant editing window	Mutant editing window
15	Mutant protospacer (starting on reading frame-consistent codon)	Mutant protospacer
16	Confirmation of STOP codon being reading frame-consistent	Obtain flipped and complementary (mutant 'sense' strand)
17	STOP codons found	Mutant protospacer (starting on reading frame-consistent codon)
18	-	Confirmation of STOP codon being reading frame-consistent
19	-	STOP codons found

For illustrating purposes, a few locus tags have been selected, indicating the protospacer (yellow), the PAM (blue), the editing window (underlined) and the STOP codon (red):

CLAU_0001 (CDS, sense)

Wild type: 5' – (...) AGA AAT CAA ATA ACA GGG AAA ACT GAA (...) – 3'

Mutant: 5' – (...) AGA AAT TAA ATA ACA GGG AAA ACT GAA (...) – 3'

CLAU_0003 (CDS, sense)

Wild type: 5' – (...) GGA TAT CAG GAC ATA AGA TTT AAC GTT (...) – 3'

Mutant: 5' – (...) GGA TAT TAG GAC ATA AGA TTT AAC GTT (...) – 3'

CLAU_0002 (CDS, antisense)

Wild type: 5' – (...) TTCCCAAGAGGGATTGAAAAATAA (...) – 3'

Mutant: 5' – (...) TTTTTAAGAGGGATTGAAAAATAA (...) – 3'

Mutant 'sense' strand: 5' – (...) TTT TTC AAT CCC TCT TAA AAA (...) – 3'

CLAU_0006 (CDS, antisense)

Wild type: 5' – (...) TTTAACCAATTTTCTACATAAAAA (...) – 3'

Mutant: 5' – (...) TTTAATCAATTTTCTACATAAAAA (...) – 3'

Mutant 'sense' strand: 5' – (...) TAT GTA GAA AAT TGA TTA (...) – 3'

Publications

PLOS COMPUTATIONAL BIOLOGY

RESEARCH ARTICLE

Physicochemical and metabolic constraints for thermodynamics-based stoichiometric modelling under mesophilic growth conditions

Claudio Tomi-Andrino[1,2,3], Rupert Norman[2], Thomas Millat[2], Philippe Soucaille[2,4,5,6], Klaus Winzer[2], David A. Barrett[1], John King[3], Dong-Hyun Kim[1]*

1 Centre for Analytical Bioscience, Advanced Materials and Healthcare Technologies Division, School of Pharmacy, University of Nottingham, Nottingham, United Kingdom, **2** Nottingham BBSRC/EPSRC Synthetic Biology Research Centre (SBRC), School of Life Sciences, BioDiscovery Institute, University of Nottingham, Nottingham, United Kingdom, **3** Nottingham BBSRC/EPSRC Synthetic Biology Research Centre (SBRC), School of Mathematical Sciences, University of Nottingham, Nottingham, United Kingdom, **4** INSA, UPS, INP, Toulouse Biotechnology Institute, (TBI), Université de Toulouse, Toulouse, France, **5** INRA, UMR792, Toulouse, France, **6** CNRS, UMR5504, Toulouse, France

* dong-hyun.kim@nottingham.ac.uk

Check for updates

OPEN ACCESS

Citation: Tomi-Andrino C, Norman R, Millat T, Soucaille P, Winzer K, Barrett DA, et al. (2021) Physicochemical and metabolic constraints for thermodynamics-based stoichiometric modelling under mesophilic growth conditions. PLoS Comput Biol 17(1): e1007694. https://doi.org/10.1371/journal.pcbi.1007694

Editor: Costas D. Maranas, The Pennsylvania State University, UNITED STATES

Received: January 29, 2020

Accepted: December 28, 2020

Published: January 25, 2021

Copyright: © 2021 Tomi-Andrino et al. This is an open access article distributed under the terms of the Creative Commons Attribution License, which permits unrestricted use, distribution, and reproduction in any medium, provided the original author and source are credited.

Data Availability Statement: All relevant files are available from Nottingham SBRC's GitHub profile (https://github.com/SBRCNottingham/Impact-of-Physicochemical-Parameters-on-thermodynamics-based-FBA).

Funding: This work was supported by the Biotechnology and Biological Sciences Research Council [grant number BB/L013940/1]; and the Engineering and Physical Sciences Research Council [grant number BB/L013940/1]. We thank

Abstract

Metabolic engineering in the post-genomic era is characterised by the development of new methods for metabolomics and fluxomics, supported by the integration of genetic engineering tools and mathematical modelling. Particularly, constraint-based stoichiometric models have been widely studied: (i) flux balance analysis (FBA) (*in silico*), and (ii) metabolic flux analysis (MFA) (*in vivo*). Recent studies have enabled the incorporation of thermodynamics and metabolomics data to improve the predictive capabilities of these approaches. However, an in-depth comparison and evaluation of these methods is lacking. This study presents a thorough analysis of two different *in silico* methods tested against experimental data (metabolomics and ^{13}C-MFA) for the mesophile *Escherichia coli*. In particular, a modified version of the recently published matTFA toolbox was created, providing a broader range of physicochemical parameters. Validating against experimental data allowed the determination of the best physicochemical parameters to perform the TFA (Thermodynamics-based Flux Analysis). An analysis of flux pattern changes in the central carbon metabolism between ^{13}C-MFA and TFA highlighted the limited capabilities of both approaches for elucidating the anaplerotic fluxes. In addition, a method based on centrality measures was suggested to identify important metabolites that (if quantified) would allow to further constrain the TFA. Finally, this study emphasised the need for standardisation in the fluxomics community: novel approaches are frequently released but a thorough comparison with currently accepted methods is not always performed.

the University of Nottingham for supporting the PhD studentship of CTA. The funders had no role in study design, data collection and analysis, decision to publish, or preparation of the manuscript.

Competing interests: The authors have declared that no competing interests exist.

Author summary

Biotechnology has benefitted from the development of high throughput methods characterising living systems at different levels (e.g. concerning genes or proteins), allowing the industrial production of chemical commodities. Recently, focus has been placed on determining reaction rates (or metabolic fluxes) in the metabolic network of certain microorganisms, in order to identify bottlenecks hindering their exploitation. Two main approaches are commonly used, termed metabolic flux analysis (MFA) and flux balance analysis (FBA), based on measuring and estimating fluxes, respectively. While the influence of thermodynamics in living systems was accepted several decades ago, its application to study biochemical networks has only recently been enabled. In this sense, a multitude of different approaches constraining well-established modelling methods with thermodynamics has been suggested. However, physicochemical parameters are generally not properly adjusted to the experimental conditions, which might affect their predictive capabilities. In this study, we have explored the reliability of currently available tools by investigating the impact of varying said parameters in the simulation of metabolic fluxes and metabolite concentration values. Additionally, our in-depth analysis allowed us to highlight limitations and potential solutions that should be considered in future studies.

Introduction

Metabolic engineering aims to improve microbial strains by considering comprehensive metabolic pathways in their entirety rather than overexpressing a single gene [1]. To improve the strains, hypothesis-driven studies have attempted to rationally identify gene targets and to evaluate the effects of those changes in the network [2,3]. However, the complex nature of cellular metabolism and its regulation demands a holistic understanding, i.e. a data-driven approach [1–3]. Combining metabolic engineering with systems biology and mathematical modelling allows for an optimisation of entire cellular networks considering further downstream processes at early stages [4].

This systematic framework exploits information regarding the metabolic state, which comprises the metabolome (complete set of low-molecular-weight metabolites (<1.5 kDa)) and the fluxome (or metabolic activity, distribution of rates of conversion/transport in the metabolic network) [5,6]. Kinetic modelling can yield metabolic fluxes from metabolomics data, but lack of high-quality enzymatic parameters and computational limitations (e.g. time-consuming processes) hinder its application [7–9]. Performing an elementary flux mode analysis (EFMA) to decompose the metabolic network into minimal subsets allowing to maintain the steady state provides useful information [10]. However, the combinatorial explosion makes the algorithm computationally expensive and therefore limits the size of the network that can be analysed [10,11]. Alternatively, stoichiometric modelling can provide a flux distribution for larger networks without any kinetic or metabolomics information [12]. Briefly, a metabolic (quasi) steady state for intracellular concentration values (C) is assumed, so that the stoichiometric matrix (S) (including the stoichiometric coefficients of metabolites in each reaction of the metabolic network) constrains the set of metabolic fluxes (v) [13]:

$$\frac{dC}{dt} = S \times v \cong 0 \tag{1}$$

Two main approaches to solve this equation can be found: (i) flux balance analysis (FBA), normally applied to large models (genome-scale model, GSM) [14] or (ii) metabolic flux

Table 1. Comparison of frequently used approaches in fluxomics. Parameter *A* is used in the extended Debye-Hückel equation.

	^{13}C-MFA	FBA	TFA
Metabolic network size	small	GSM	GSM
Flux distribution	generated	generated	generated
Uptake rate	Yes	Yes	Yes
Specific growth rate, μ (h^{-1})	-	Yes	Yes
Gibbs free energy of formation ($\Delta G_f^{'}$)	-	-	Experimental [32], or GCM [33]
Temperature, *t* (˚C)	-	-	25
Ionic strength, *I* (M)	-	-	0.25
Salinity, S (g/kg)	-	-	-
Adjustment method	-	-	Extended Debye-Hückel
Parameter *A*	-	-	T-dependent
Metabolite concentration values	-	-	Constraint or predicted
Problem formulation	least square regression [13]	LP [14]	MILP [20]

13 **C-MFA**, ^{13}C metabolic flux analysis; **FBA**, flux balance analysis; **GCM**, group contribution method; **GSM**, genome-scale model; **LP**, linear programming; **MILP**, mixed-integer linear programming; **TFA**, thermodynamics-based flux analysis.

https://doi.org/10.1371/journal.pcbi.1007694.t001

analysis (MFA), used for smaller metabolic networks (mainly the central carbon metabolism) (Table 1). FBA solves the underdetermined system represented in Eq 1 by maximising or minimising the value of an assumed objective function [14]. A plethora of different objectives has been described in the literature [15]. Three of them can be highlighted: maximisation of biomass yield ($Y_{X/S}$, equal to the ratio growth rate/substrate uptake rate), maximisation of ATP yield, and minimisation of sum of fluxes, which have been suggested to compete in the regulation of bacterial metabolism [16]. Hence, selecting an adequate one/multi-dimensional objective function when analysing a GSM will depend on the growth conditions to be simulated in FBA. In general, measured extracellular metabolic rates (e.g. substrate uptake) are insufficient to properly constrain the intracellular metabolic fluxes [13]. In contrast, MFA is based on a least-squares-regression problem, normally solved by exploiting experimental mass isotopomer distribution (MID) of proteinogenic amino acids (^{13}C-MFA) [13]. Since this approach requires fewer assumptions and uses more experimental information than FBA, ^{13}C-MFA is considered to be the *gold standard* in fluxomics [17]. However, current applicability (central carbon metabolism), and technical/computational complexity (particularly for autotrophic growth [18]) limit its usage.

The set of constraints characterising stoichiometric modelling approaches (Eq 1) is insufficient to guarantee thermodynamically feasible results in the flux solution space [19,20]. Both FBA and ^{13}C-MFA assume most reactions to be reversible [13,21]: in the first case directionalities are dictated by the optimal flux distribution (which depends on the *a priori* chosen objective function [14]), whereas in ^{13}C-MFA they are determined by the MIDs [22]. The flux-force relationship (thermodynamic displacement from the equilibrium [23]) links thermodynamic potentials and fluxes (Eq 2):

$$\Delta_r G' = \Delta_r G'^{o} + RT\ln Q = RT\ln(Q/k_{eq}) = -RT\ln(J^+/J^-) \quad (2)$$

where $\Delta_r G'$ and $\Delta_r G'^{o}$ are the Gibbs free energies of reactions (the latter referring to adjusted standard conditions), Q and k_{eq} are the ratio of products to reactant concentrations or activities (the latter at equilibrium) and (J^+/J^-) is the relative forward-to-backward flux [22].

Four main approaches exploiting thermodynamics data can be highlighted: (i) energy balance analysis (EBA), where pre-selecting $\Delta_r G'$ bounds leads to biased results [24], (ii) network-embedded thermodynamic (NET) analysis, that needs pre-assigned directionalities (e.g. obtained by FBA) and evaluates the thermodynamic consistency [25], (iii) max-min driving force (MDF), which needs a flux distribution as input data to predict metabolite concentration values [26], and (iv) thermodynamically-constrained FBA. Two methods were developed in the latter approach: thermodynamics-based flux analysis (TFA), and an optimization problem allowing to obtain a thermodynamically flux-minimised (TR-fluxmin) solution. TFA directly yields a thermodynamically feasible FBA solution (e.g. by maximising $Y_{X/S}$) and simulates metabolomics data [20,27]. In contrast, TR-fluxmin is based on the minimisation of sum of fluxes in the system whilst applying a penalty score for *in silico* metabolite concentration values [21]. Other recent approaches are based on alternative constraints, such as setting an upper limit on the Gibbs energy dissipation rate [28], or only provide information regarding reaction directionalities [29]. With regards to EFMA, even though using thermodynamics reduces the aforementioned limitations due to combinatorial explosion, the network size is still a limiting factor [30].

MDF and TFA are generally performed using eQuilibrator [26] and matTFA [20], respectively. Since matTFA can be directly used to analyse a GSM, it was selected for this study. Three features should be highlighted: (i) unique values for temperature ($25^{\circ}C$) are considered, (ii) salinity (S) is not taken into account when calculating parameter A, and (iii) Gibbs free energy values are adjusted for ionic strength (I) using the extended Debye-Hückel equation (Table 1). It should be noted that in [20], $I = 0.25$ M and no salinity were assumed to study *E. coli* (with a cytosol in the interval 0.15–0.20 M [27]), where the extended Debye-Hückel is only valid for $I < 0.1$ M [31].

This study was based on determining the impact of varying and adjusting the physicochemical parameters (t, I and S) on the predictive capabilities of TFA under mesophilic growth conditions. In order to do so, a modified matTFA was developed by increasing the number of parameters and parameter values that were originally considered [20]. To validate the results, a comparison with published ^{13}C-MFA and metabolomics data was performed. In particular, flux pattern changes between *in vivo* and *in silico* fluxes in the central carbon metabolism were analysed, with a focus on the anaplerotic reactions. In addition, a method based on centrality measures was suggested to identify important metabolites that (if quantified) would allow to further constrain the TFA.

Materials and methods

Metabolic network, mapping of metabolic fluxes and experimental data

Mesophilic growth conditions were studied by selecting a GSM for *Escherichia coli* (str. K-12 substr. MG1655): *i*JO1366, which has proven to predict phenotypes in a wide range of growth conditions [34]. For the sake of consistency, metabolomics and fluxomics data were obtained from the same experiment (S1 Dataset and S1 Table) [35]. Briefly, cells were grown in glucose-limited chemostats at $37^{\circ}C$ with minimal medium and a fixed specific growth rate (μ) of 0.20 h^{-1}. The experimental glucose uptake rate (2.93 mmol $gDCW^{-1}$ h^{-1}) was used as a constraint, leaving the default lower and upper bounds for transport reactions. Maximisation of the biomass yield was selected as the objective function, and no flux value was forced through the biomass reactions ($v_{biomass}$). Directionalities of resulting flux values from TFA were compared on a reaction-by-reaction case against *in vivo* fluxes from ^{13}C-MFA, for which a mapping and directionality correction step was needed (S1 Table).

Generation of experimental design

The original matTFA toolbox uses unique values for t and I [20], and S is not taken into account (Table 1). To explore their potential impact in the predictive capabilities, a modified matTFA (mod-matTFA) allowing to consider alternative parameters values and methods was created (Table 2). For the sake of reproducibility [36], the complete list of files used in this study was collected in S2 Table, and are publicly available in *Nottingham SBRC*'s GitHub profile (https://github.com/SBRCNottingham/Impact-of-Physicochemical-Parameters-on-thermodynamics-based-FBA). Analyses were performed using the COBRA toolbox [37] in MATLAB R2016b with the solver CPLEX 12.8.0 to ensure compatibility.

Since I affects the Gibbs energy of formation, an adjustment from the reference state ($\Delta_f G_j^o$) was needed to obtain the standard transformed Gibbs energy of formation ($\Delta_f G_j^{to}$) [32]. In the original matTFA [20] and other studies [26,28] the extended Debye-Hückel equation was used to adjust the Gibbs free energy values, with a proven validity for $I < 0.1$ M [31](Eq 3). The parameter B was assumed to be constant, with a value of 1.6 $mol^{-1/2}L^{1/2}$ [27,32]. Mod-matTFA also explored the impact of using the Davies equation ($\beta = 0.3$) (Eq 4) as an alternative adjustment approach, with a tested validity for $I < 0.5$ M [31].

$$\Delta_f G_j^{to}(I) = \Delta_f G_j^o + N_H(j)RT\ln(10)\mathrm{pH} - RT\left(\frac{A\sqrt{I}}{1+B\sqrt{I}}\right)(z_j^2 - N_H(j)) \quad (3)$$

$$\Delta_f G_j^{to}(I) = \Delta_f G_j^o + N_H(j)RT\ln(10)\mathrm{pH} - RT\left(\frac{A\sqrt{I}}{1+\sqrt{I}} - \beta I\right)(z_j^2 - N_H(j)) \quad (4)$$

Both formulas include terms correcting the pH and I, where $N_H(j)$ is the number of hydrogen atoms in species j, R is the gas constant, T is the absolute temperature and z_j refers to the charge of the species [32]. Applying the Gibbs-Helmholtz equation would be necessary to account for temperature different from standard conditions, i.e. 25˚C, but the lack of measured changes in enthalpy (ΔH^o) for all the metabolites prevents from doing so [38]. Hence, variations from 25˚C to 37˚C were assumed to be small, as shown elsewhere [39]. The parameter A is normally assumed to be constant [27]or calculated using a temperature-dependent function

Table 2. Factors considered in mod-matTFA. Values 0/1 refer to the binary codification for the full factorial design (S3 Table). In total, 2^6 combinations were tested.

Temperature, t (˚C)	(0): 25 (1): 37
Ionic strength, I (M)	(0): 0 (1): 0.25
Salinity, S (g/kg)	(0): 0 (1): 13.74
Adjustment method	(0): Extended Debye-Hückel equation (1): Davies equation
Parameter A	(0): T-dependent* (1): T,S-dependent
Metabolite concentration values	(0): Default matTFA (1): experimental data

* T is temperature in K. There is a 'default matTFA' constraint regarding set concentrations values for cofactors (AMP, ADP and ATP) as included in the original matTFA code. 'Experimental data' refers to the use of published metabolomics data (S2 Dataset), setting the lower and upper bound for the simulation as 90–110% of the concentration values.

https://doi.org/10.1371/journal.pcbi.1007694.t002

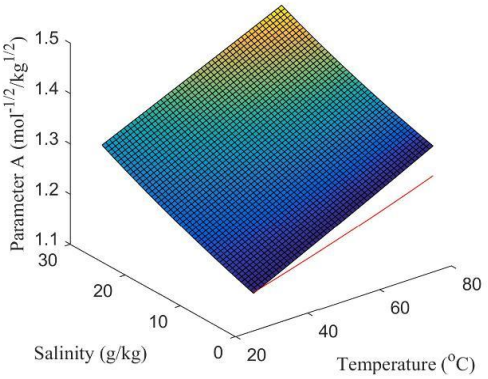


Fig 1. Calculation of the parameter *A*. The red line refers to the temperature-dependent function (Eq 5), whereas the surface is the temperature/salinity-dependent function (Eq 6).

https://doi.org/10.1371/journal.pcbi.1007694.g001

(Eq 5) [20,26], and the impact of using a temperature/salinity-dependent function (Eq 6) [38] was also tested in this study (Fig 1).

$$A(\mathrm{mol}^{-1/2}\mathrm{kg}^{1/2}) = 1.10708 - 1.54508 \times 10^{-3}T + 5.95584 \times 10^{-6}T^2 \quad (5)$$

$$A(\mathrm{mol}^{-1/2}\mathrm{kg}^{1/2}) = \frac{F^3\sqrt{2\varepsilon_0 R^3}}{4\pi\varepsilon_0 N_A} \times \left(\frac{\rho_{sw}(t,S)}{(\varepsilon_{sw}(t,S)T)^3}\right)^{1/2} \quad (6)$$

where the first term in (Eq 6) includes physical constants (Faraday's constant (F), vacuum permittivity (ε_0), gas constant (R) and Avogadro's constant (N_A)), and the second is the temperature (T in K and t in °C), and salinity (S) dependent functions to calculate the density (ρ_{sw}) [40]and the relative permittivity (ε_{sw}) [41]for seawater (S2 Table).

In general, consistency in units between parameters A ($\mathrm{mol}^{-1/2}\mathrm{kg}^{1/2}$) and B ($\mathrm{mol}^{-1/2}\mathrm{L}^{1/2}$) is achieved by assuming 1 kg = 1 L. In this study, an expression for seawater (Eq 7) [42]was used to estimate a salinity value by considering a buoyant density (ρ) for bacterial cells of 1.11 kg/L [43]. For I, a value of 0.25 M was used (Table 2).

$$I(\mathrm{M}) \times \rho(\mathrm{kg/L}) = \frac{19.92 \times \mathrm{S}}{1000 - 1.005 \times \mathrm{S}} \quad (7)$$

Assessment of fluxomics and metabolomics predictive capabilities

Mesophilic growth conditions for *E. coli* were selected as a case study to explore the impact of metabolic and physiochemical constraints on the predictive capabilities of TFA at the fluxomics and metabolomics level. Accordingly, 64 different factor combinations (Table 2) were tested using mod-matTFA. It is important to note that not all test yielded a solution where cell growth was achieved (i.e. $v_{\mathrm{biomass}} > 0$ mmol $\mathrm{gDCW}^{-1}\,\mathrm{h}^{-1}$). Since different factor combinations converged into the same set of solutions, tests were characterised at the fluxomics and

metabolomics levels by considering either the full set of values, or the subset with an experimental counterpart.

Results yielding feasible solutions were also compared against ^{13}C-MFA flux values (S1 Table) and experimental metabolomics data (S1 Dataset), respectively. A goodness-of-fit analysis based on the Pearson correlation coefficient (r) was performed, as shown in [44]. In order to identify the test(s) with the best predictive capabilities at both levels, they were separately ranked according to two criteria: (i) correlation coefficient at the fluxomics level, and (ii) correlation coefficient at the metabolomics level. The concordance between results was assessed by the Kendall's W statistics (S2 Table), where a value of 0 means no agreement of ranking position with respect to each criterion, and a value of 1 indicates total agreement. This statistics is a normalisation of the Friedman test, which simply tests whether samples are from the same population or not [45]. Finally, a joint ranking after weighting the ranking position according to each criterion was considered (the higher the score, the better the correlation in both the fluxomics and metabolomics levels).

Thermodynamics-enriched network analysis

The constraining capacity of metabolites is not uniform, and depends on their connectivity in the network [20,46]. To further constrain the model, a priority list of metabolites to be quantified should be considered when designing the metabolomics protocol. In this study, the suitability of the selected dataset for this purpose was analysed (S1 Dataset). The importance of each metabolite in the network was measured by means of PageRank as implemented in MATLAB. This algorithm was developed by Google [47]and has been recently applied to metabolic networks [48]. In this sense, the presence of over-represented metabolites (e.g. proton donor) biases centrality measures [48]. Therefore, a removal of these *currency* [49], *side* [48]or *pool* [50]metabolites from the network was performed (S1 Appendix).

Non-redundant flux distributions from TFA were selected and subjected to network simplification and correction. Briefly, only active metabolites and reactions were kept, and stoichiometric coefficients were corrected so that they reflected the flux direction of each reaction. Centrality measures require a graph G, defined as a pair $G = (V, E)$, where the vertices (or nodes) V are the metabolites, and the edges E the reactions connecting them. The stoichiometric matrix was converted into an adjacency matrix using an in-house script (S1 Appendix), which was later used to generate a G ready for the PageRank analysis. The final lists of metabolites were ranked by their centrality score, and the top 50% compared against the list of available experimental values.

Results and discussion

In the last two decades, biotechnology and systems biology have benefitted from the development of ^{13}C-MFA and FBA to measure and estimate intracellular metabolic fluxes in industrially relevant bacteria. Although the influence of thermodynamics in living systems has been considered for several decades, its application to study biochemical networks has been only recently enabled [24,32]. In this sense, a multitude of different approaches constraining well-established modelling approaches with thermodynamics have been suggested. Given its relevance, this study focused on analysing TFA (performed by matTFA toolbox [20]). This study aimed at: (i) assessing and improving TFA's reliability of predicting metabolic fluxes and metabolite concentration values, and (ii) identifying important metabolites to further constrain the model. In order to do so, (i) the published matTFA toolbox was modified to include a broader range of parameters (and parameter values) as well as alternative equations and

Table 3. Relative factor importance. The type of analysis depended on the nature of the response: *classification* was selected for TFA (full), TFA (match ^{13}C-MFA), concentration values (full) and concentration values (match experimental), and *regression* for r (fluxomics) and r (metabolomics). The former was suited for categorical responses (i.e. which solution is achieved, as shown in S4 Table), and the latter for continuous responses (for Pearson's r, from -1 to +1).

	TFA (full)	TFA (match ^{13}C-MFA)	Concentration values (full)	Concentration values (match experimental)	r (fluxomics)	r (metabolomics)
t **(˚*C*)**	95.7	50.0	50.0	50.0	29.8	60.4
I **(M)**	95.7	100.0	100.0	100.0	100.0	100.0
S (g/kg)	19.9	7.8	27.5	27.5	-	-
Parameter *A*	-	1.0	50.0	50.0	2.6	-
Adjustment method	100.0	52.1	44.4	44.4	52.3	0.9
[met]	-	-	-	-	-	-

https://doi.org/10.1371/journal.pcbi.1007694.t003

constraints (Table 2), and (ii) an in-house script was developed to perform a GSM-wide network analysis exploiting TFA-derived reaction directionalities.

Evaluation of the reliability of predicted flux and concentration values

A full factorial design comprising 2^6 tests (Table 2) was applied in TFA to constrain the GSM *i*JO1366 [34], selecting the maximisation of biomass yield as the objective function. An experimental glucose uptake rate was set (2.93 mmol gDCW^{-1} h^{-1}), reaching a $\mu \approx 0.28$ h^{-1} (the experimental was 0.20 h^{-1}) for all FBA and TFA tests. Overall, 26/64 tests were unsuccessful (no cell growth), and the remaining 38/64 converged into common optimal solutions (S4 Table). At the fluxomics level, a single flux distribution was achieved in FBA for all tests, whereas for TFA a different number of non-redundant solutions were found: 5 (when considering all reactions) or 4 (only those with an experimental counterpart). Likewise, at the metabolomics level, the 38 tests were reduced to 9 optimal solutions. Results were tested against available experimental data (^{13}C-MFA [35,51]and metabolomics [35]) by calculating the Pearson correlation coefficient. Therefore, each successful test was characterised by the optimal solutions it achieved and the correlation coefficients at both the fluxomics and metabolomics levels.

The importance of each factor was assessed by means of decision trees (CART in Minitab 19) (Table 3). Briefly, models were built considering categorical predictors (the factors after the codification (S3 Table)) and responses: the importance of a factor measured the improvement on the model when using it to split the data. Accordingly, the relative importance was calculated with respect to the best predictor (Table 3). The *I* (M) was the top one for all responses except for *TFA (full)*, where it equalized *t* (˚*C*) at 95.7% and was second to the adjustment method. In all cases, using either default concentrations values for AMP, ADP and ATP (as included in the original matTFA), or experimental data made no difference. As a result, tests only differing in this factor showed the same correlations with experimental data (Table 4).

Correlation coefficients for FBA in all tests was $r \approx 0.02$, whereas for TFA it varied within the range from 0.90 to 0.95. A reaction-by-reaction comparison of flux directionalities in central metabolism showed inherent differences between ^{13}C-MFA and FBA/TFA, as discussed in the last section of this study. At the metabolomics level, it ranged from 0.08 to 0.18 (S4 Table). Tests were ranked independently by both criteria, showing a notable agreement in their positions (Kendall's W $\approx$ 0.81). Scoring the position according to each criterion allowed creating a joint ranking to identify the test(s) with the best predictive capability at both levels (Table 4). Four tests held the first position, since they all converged into the same optimal solutions (S4

Table 4. Tests with the highest score in the joint ranking. The full list is available in (S4 Table). *(run #3) reflects the conditions used in the original matTFA.

Rank sum	62.5				59.5		56.5				51.5
Correlation coefficient TFA vs. ^{13}C-MFA	0.95				0.95		0.90				0.90
Correlation coefficient metabolomics	0.18				0.17		0.17				0.15
Run number	20	24	52	56	28	60	32	64	12	44	3*
t (°C) (0 = 25, 1 = 37)	1	1	1	1	1	1	1	1	1	1	0
I (M) (0 = 0, 1 = 0.25)	1	1	1	1	1	1	1	1	1	1	1
S (g/kg) (0 = 0, 1 = 13.74)	0	1	0	1	0	0	1	1	0	0	0
Parameter A (0 = t-dependent, 1 = t/S-dependent)	0	0	0	0	1	1	1	1	1	1	0
Adjustment method (0 = DH, 1 = Davies)	1	1	1	1	1	1	1	1	0	0	0
[met] (0 = default, 1 = experimental values)	0	0	1	1	0	1	0	1	0	1	0

Davies, Davies equation; **DH**, extended Debye-Hückel equation; **[met]**, metabolite concentration values. Values of 0 and 1 in the headers refer to the binary codification from the full factorial design (S3 Table). *Run #3 represents the analytical conditions from the original matTFA, added here as a reference. There is a 'default matTFA' constraint regarding set concentrations values for AMP, ADP and ATP, as included in the original matTFA script. 'Experimental values' refers to the use of published metabolomics data (S1 Dataset). Correlation coefficient values were rounded to the closest integer for ranking purposes.

https://doi.org/10.1371/journal.pcbi.1007694.t004

Table). Specifically, $t = 37^{\circ}C$, $I = 0.25$ M and the Davies equations as adjustment method were used. Following the relative factor importance (Table 3), correlation coefficients were not affected by S and the selection of concentration values.

This analysis showed that adjusting the physicochemical parameters to the experimental conditions did improve the predictive capabilities of TFA, but certain technical limitations at both levels need to be discussed. The nature of ^{13}C-MFA only allows determining the flux distribution in the central carbon metabolism by considering amino acid synthesis [13], which has been noted to be very robust against changes in the intermediate metabolite concentrations [52,53]. The recent discovery of non-enzymatic metabolism-like reactions suggests that current metabolic networks evolved from prebiotic reaction sequences. Therefore, a well-established flux distribution in the central pathways can be expected [54]. In order to discern among tests, focus on highly variable flux values should be promoted, but the variance among them was low (S2 Dataset). In fact, only 36/1679 showed a variance greater than zero, where 6 reactions had an experimental counterpart to compare against. Optimal solutions for all tests were similar (reducing the discerning capacity), which explained the overall high correlation coefficients for all tests. Therefore, results from the comparison of predicted and experimental metabolite concentration values are paramount to better understand the impact of varying the physicochemical parameters.

Regarding the metabolomics level, the 9 non-redundant solutions were subjected to a similar analysis. Likewise, only 46/972 metabolites had a variance among tests greater than zero (S3 Dataset), out of which 7 were quantified: L-aspartate, phosphoenolpyruvate, ATP, L-valine, pyruvate, $NADP^+$, and FAD. Reliable quantitation of energy-carrying molecules and redox cofactors is not easily achievable, given the inherent cell dynamics (e.g. cell cycle and cell size variations) and degradation during extraction [55–63]. Since the correlation coefficients were calculated using a dataset blind to highly variable metabolites (e.g. 3-phosphohydroxypyruvate ranged four orders of magnitude), resulting values were similar for different factor

Table 5. Quantified metabolites in the top 50% of PageRank (PR) based analysis. The last position in the ranking (#622) was L-Tyrosine (PR score = 0.0004), which had been quantified. The full list can be found in (S4 Dataset).

Quantile	Ranking position	Metabolite	Node	PR score
10%	1	L-Glutamate	glu-L_c	0.0172
	2	Pyruvate	pyr_c	0.0126
	4	D-Fructose 6-phosphate	f6p_c	0.0079
	6	Acetyl-CoA	accoa_c	0.0071
	7	L-Methionine	met-L_c	0.0071
	23	Succinyl-CoA	succoa_c	0.0046
	44	L-Serine	ser-L_c	0.0034
30%	69	Dihydroxyacetone phosphate	dhap_c	0.0029
	70	L-Tryptophan	trp-L_c	0.0029
	88	Phosphoenolpyruvate	pep_c	0.0026
	103	S-Adenosyl-L-methionine	amet_c	0.0024
	129	L-Alanine	ala-L_c	0.0021
	157	L-Histidine	his-L_c	0.0020
	161	D-Glucose 1-phosphate	g1p_c	0.0019
	177	L-Proline	pro-L_c	0.0019
	181	3-Phospho-D-glycerate	3pg_c	0.0018
50%	249	D-Fructose 1,6-bisphosphate	fdp_c	0.0016
	258	L-Leucine	leu-L_c	0.0015

https://doi.org/10.1371/journal.pcbi.1007694.t005

combinations (Table 4). Thus, said metabolites should be quantified to deconvolute the impact of using default or experimental concentration values in the predictive capabilities.

Other limitations refer to the design of the tool itself. This method does not consider other complex phenomena affecting the thermodynamic feasibility of metabolic pathways, such as Mg complexation with metabolites, or compound dissociation into more than two protonated species [19,20](as shown in the file *calcDGspecies.m*). In addition, Gibbs free energy values are relaxed when no feasible solution is found, so the constraining power of experimental metabolite concentration values is reduced [20]. Related to this, an approach allowing to identify metabolites to further constrain the model was developed in this study (next section). Finally, it should be noted that to apply matTFA to thermophilic species (e.g. *Thermus thermophilus*, a potential non-model metabolic engineering platform [64]), recent methods to adjust Gibbs free energies to high temperatures should be considered [65].

Identification of central metabolites to further constrain the model

Successful tests converged into 5 solutions at the fluxomics level (S4 Table), which are structurally equivalent. Therefore, a single stoichiometric matrix was considered for further analysis. After the simplification step (removal of inactive metabolites and reactions, as well as side compounds) 622/1805 metabolites were left in the network. The experimental dataset included information about 44 metabolites (S1 Dataset), out of which 34 were also considered in the simplified network, and the rest was discarded as side compounds.

PageRank scores were calculated, allowing to identify metabolites in the top 50% for which experimental data was available (Table 5). Overall, 18/34 quantified metabolites were in the top 50%, with only 7 in the top 10%. The lack of high centrality for most metabolites explains the aforementioned result, where tests only differing in the set of concentrations values used as a constraint (default ATP/ADP/AMP or experimental) led to the same optimal solution (e.g. tests 20 and 52, Table 3).

The priority list is led by L-glutamate, pyruvate, 2-oxoglutarate (not quantified), D-fructose-6-phosphate and glyceraldehyde 3-phosphate (not quantified). Both L-glutamate and 2-oxoglutarate participate in the assimilation of nitrogen in *E. coli*, where the former also plays a role as nitrogen donor in the biosynthesis of nucleic acids [66]. The latter along with the rest (except for glyceraldehyde 3-phosphate), and acetyl-CoA are important biosynthetic precursors used in modelling [49]. Accordingly, other metabolites participating in central pathways such as glycolysis (glyceraldehyde 3-phosphate, dihydroxyacetone phosphate, etc.) and protein biosynthesis (amino acids) were also identified. Important metabolites highlighted here agree with results from the seminal work by Wagner et al. [49], where they used a smaller network (317 vs. 931 reactions). Due to computational costs, other attempts specifically focusing on the constraining capacity with regards to TFA (Thermodynamics-based Metabolite Sensitivity Analysis, TMSA) are also limited by the network size (156 reactions in [46]). In particular, this approach identified pyruvate as the most significant metabolite in terms of reducing the variability in the thermodynamic properties of reactions, and attributed it to its high connectivity in the network. Other important compounds included phosphate, NAD^+, NADH, CO_2, menaquinol-8, menaquinone-8 and D-lactate. All but the latter were classified as side compounds for this study (and therefore excluded (S1 Appendix)), since the centrality measures are biased by ubiquitous metabolites [48].

The impact of the inherent dynamics (cell cycle and cell ageing) has been pointed out as a source of metabolic heterogeneity in clonal microbial populations [55]. In a chemostat, cells are maintained at the exponential growth phase, but the cell cycle is not synchronised across single cells unless forced [56,57]. In *E. coli*, concentration values for NAD(P)H oscillate along the cell cycle [58], and ATP concentration values show an asymmetric distribution across single cells in a continuous culture [59]. From a metabolomics point of view, an unbiased extraction and quantitation method is yet to be developed [60]. Particularly, ATP/ADP/AMP quantitation require specific culture conditions [61], and nicotinamides parallel protocols to avoid degradation. Overall, the method developed here generated a priority list to be considered when selecting a metabolomics protocol aiming at providing data to further constrain a model in TFA.

Reaction directionalities in the central carbon metabolism

Finally, flux pattern changes between *in vivo* and *in silico* fluxes in the central carbon metabolism were analysed, with a particular focus on the anaplerotic reactions. The 'anaplerotic node' (Fig 2) consists of carboxylation/decarboxylation reactions including intermediates participating in the tricarboxylic acid (TCA) cycle that are used for biosynthesis of amino acids [67]. Given the fact similar MIDs (from proteinogenic amino acids) can be obtained from different precursors, ^{13}C-MFA has been noted to show a limited capability to elucidate fluxes around the anaplerotic node [52,68,69]. In order to evaluate changes in reaction directionalities, the available *in vivo* fluxes were tested against their equivalents in the simulated TFA flux distributions (S1 Table). Overall, 13/40 flux directions disagree between approaches (Table 6).

Discrepancies in flux pattern between methods are caused by both differences in the structure of the metabolic networks and the way the problem is defined (Table 1). On the one hand, *i*JO1366 includes 8 reactions concerning the anaplerotic node and the glyoxylate shunt: PPC and PPCK (between phosphoenolpyruvate and oxaloacetate), PYK and PPS (between phosphoenolpyruvate and pyruvate), ME1 and ME2 (between pyruvate and malate) (Fig 2), and finally ICL and MALS (from isocitrate to malate, via glyoxylate). In contrast, the metabolic network used for the ^{13}C-MFA did not consider PPCK and PPS (S1 Table), which could affect the determination of fluxes to/from phosphoenolpyruvate. Since ^{13}C-MFA is based on lumped

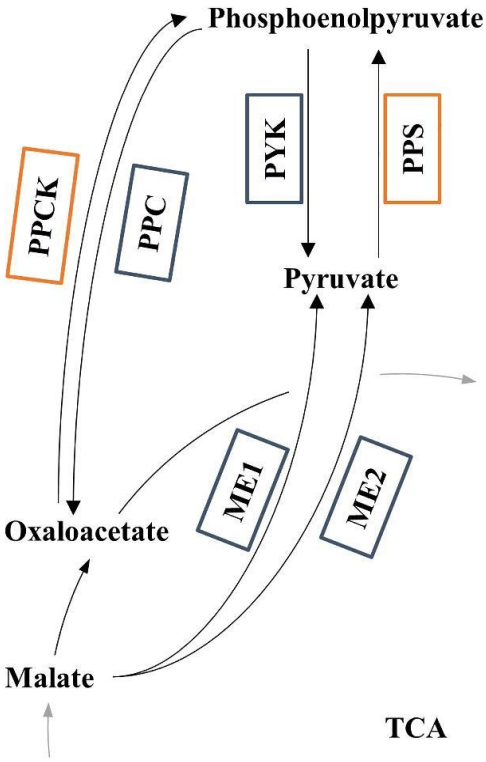


Fig 2. Anaplerotic node for *E. coli*. Set of carboxylation/decarboxylation reactions including phosphoenolpyruvate, pyruvate, oxaloacetate, and malate. Arrows indicate the expected direction of carbon fluxes. Boxes refer to reactions: blue when they are defined in both the GSM and the metabolic network used for ^{13}C-MFA, and orange when they are exclusively considered in the GSM. In the latter case no mapping was possible (S1 Table).

https://doi.org/10.1371/journal.pcbi.1007694.g002

reaction, branched pathways are not taken into account [13]. Thus, having a smaller range of alternative pathways than FBA/TFA may affect the estimation of flux values.

On the other hand, *in silico* flux distributions are the result of optimising the system according to the chosen objective function. Accordingly, when maximising the biomass production (which requires ATP), FBA and TFA promote pathways that reduce wasting ATP in the optimal solution [14]. For instance, PPCK (ATP-consuming reaction) carried no flux. In contrast, experimental data from *E. coli* grown on glucose has proven that both PPC and PPCK (which constitute a *futile cycle*) are active and play a role in metabolic regulations [70]. However,

Table 6. Flux pattern changes between ^{13}C-MFA data and matTFA predictions.

Reaction (GSM)	Definition (GSM)	Definition (^{13}C-MFA)	Direction (^{13}C-MFA)	Corrected direction (^{13}C-MFA)	Direction (TFA)
ACALD	acald_c + coa_c + nad_c ↔ accoa_c + h_c + nadh_c	AcCoA → Ethanol	+	-	0
ACKr	ac_c + atp_c + h_c ↔ actp_c + adp_c	AcCoA → Acetate	0	0	+
ACONTb	acon-C_c + h2o_c < = > icit_c	CIT -> ICT	+	+	0/+
ALCD2x	etoh_c + nad_c ↔ acald_c + h_c + nadh_c	AcCoA → Ethanol	+	-	+
FBA	fdp_c ↔ dhap_c + g3p_c	F1,6P → DHAP + G3P	+	+	0/+
ICL	icit_c → glx_c + succ_c	ICT → Glyoxylate + SUC	+	+	0
ME1	mal-L_c + nad_c → co2_c + nadh_c + pyr_c	MAL → PYR + CO2	+	+	0
ME2	mal-L_c + nadp_c → co2_c + nadph_c + pyr_c	MAL → PYR + CO2	+	+	0
PFK	atp_c + f6p_c < = > adp_c + fdp_c	F6P -> F1,6P	+	+	0/+
PTAr	accoa_c + h_c + pi_c ↔ actp_c + coa_c	AcCoA → Acetate	0	0	-/0
PYK	adp_c + pep_c ↔ atp_c + pyr_c	PEP → PYR	+	+	0/+
SUCOAS	atp_c + coa_c + succ_c ↔ adp_c + pi_c + succoa_c	2-KG → SUC + CO2	+	+	-
TALA	g3p_c + s7p_c ↔ e4p_c + f6p_c	S7P + G3P ↔ E4P + F6P	+	+	-/0

Where +, flux in the forward direction; -, flux in the reverse direction; 0, no flux. *Corrected direction*, refers to the adjustments due to differences in the definition of the reaction between ^{13}C-MFA and GSM (S1 Table). For example the case of ALCD2x: *in vivo* flux (^{13}C-MFA) suggests production of ethanol, whereas the *in silico* one (GSM/TFA) predicts consumption of ethanol. Since reactions are defined in opposite directions, a correction becomes necessary. Discrepancy between corrected directions and predicted ones allowed an automated identification of flux pattern changes.

https://doi.org/10.1371/journal.pcbi.1007694.t006

given the fact that ICL and ME1/ME2 do not generate any ATP, fluxes are shut down in the simulated flux distributions (as shown in [52]). In this sense, it should be noted that stochastic events or regulatory processes have been suggested to provoke a variation of the fluxes through PPCK and ME1/ME2 [71]. FBA/TFA also faced problems regarding the overflow metabolism: acetate was predicted to be produced (PTAr and ACKr), as opposed to the lack of flux according to ^{13}C-MFA.

Even though flux pattern changes between predicted and experimentally determined intracellular fluxes were present, TFA offered a reliable prediction of intracellular fluxes (Table 4). This overall consistency has been noted in the literature by comparing an array of different objective functions and constraints (based on split ratios rather than on mapping on a reaction-by-reaction case) [15]. A combination of both approaches to overcome their limitations and different flux space solutions has also been suggested [72,73]. However, fluxes concerning the TCA cycle, the glyoxylate shunt and acetate secretion have proven to be difficult to predict [15], as also shown in this study. Similarly, other reactions are also affected by the substrate uptake rate: ALCD2x becomes unidirectional at high glucose levels [28].

In addition, the nonlinear dependency of the anaplerotic fluxes on the growth rate has been reported in the literature, limiting the reliability of conclusions from experiments using single dilution rates [70,71]. Particularly, metabolic fluxes through the aforementioned futile cycle are expected to be active under glucose-limited growth conditions [74], rather than being totally shut down (Fig 2). In this sense, a higher degree of consistency between predicted and experimental flux distributions could have been achieved by (i) focusing on data from cultures with high dilution rates, so that futile cycle activity is lowered and the flux distribution becomes closer to the optimal solution, or (ii) applying further constraints to properly model the anaplerotic reactions [75]. The first option is limited by the lack of published data at both

the metabolomics and fluxomics levels from the same experiment, and the second one by the lack of implementation.

Consequently, it was assumed that the high correlation coefficient achieved for TFA against *in vivo* fluxomics data ($r \approx 0.9$) was high enough to enable the analyses on the impact of varying the physicochemical parameters in the predictive capabilities. Studying flux pattern changes on a reaction-by-reaction basis also allowed to confirm previously reported limitations from both ^{13}C-MFA and FBA/TFA with regards to the anaplerotic node [68,69,75]. Thus, metabolites in the node are expected to be directly affected.

Conclusions

This study showed that the predictive capabilities of TFA can be potentially improved by using physicochemical parameters closer to the experimental conditions and adequate equations. In addition, we proposed a method based on centrality measures to identify important metabolites allowing to further constrain the TFA. In contrast to previous attempts, our strategy is not limited by the size of the network and is computationally cheap. Therefore, a preliminary TFA could be considered when designing a metabolomics protocol to maximise the constraining power of the experimental concentration values. Overall, our study stressed the necessity of performing an in-depth assessment of available methods in the fluxomics field. For instance, interesting published potential solutions to known problems (e.g. elucidation of the anaplerotic fluxes) should be integrated with the widely used approaches. This should increase the degree of standardisation in the community, allowing to cross-validate novel strategies and improving the reliability of the simulated data.

Supporting information

S1 Appendix. Generation of directed graphs and side compounds.
(DOCX)

S1 Dataset. Metabolomics Keio database.
(XLSX)

S2 Dataset. Variation of flux values among tests.
(XLSX)

S3 Dataset. Variation of concentration values among tests.
(XLSX)

S4 Dataset. PageRank scores.
(XLSX)

S1 Table. Mapping of metabolic fluxes.
(DOCX)

S2 Table. List of files used in this study.
(DOCX)

S3 Table. Full factorial design for the mesophilic growth conditions.
(DOCX)

S4 Table. Tests characterisation and ranking.
(DOCX)

Acknowledgments

We thank Nicole Pearcy for her helpful comments.

Author Contributions

Conceptualization: Claudio Tomi-Andrino, Thomas Millat, Klaus Winzer, Dong-Hyun Kim.

Data curation: Claudio Tomi-Andrino.

Formal analysis: Claudio Tomi-Andrino.

Methodology: Claudio Tomi-Andrino, Rupert Norman, Thomas Millat, Philippe Soucaille.

Project administration: Claudio Tomi-Andrino.

Resources: Klaus Winzer, David A. Barrett, John King, Dong-Hyun Kim.

Software: Claudio Tomi-Andrino, Rupert Norman, Thomas Millat.

Supervision: Klaus Winzer, David A. Barrett, John King, Dong-Hyun Kim.

Writing – original draft: Claudio Tomi-Andrino.

Writing – review & editing: Claudio Tomi-Andrino, Rupert Norman, Thomas Millat, Philippe Soucaille, Klaus Winzer, David A. Barrett, John King, Dong-Hyun Kim.

References

1. Stephanopoulos G, Alper H, Moxley J. Exploiting biological complexity for strain improvement through systems biology. Nat Biotechnol. 2004; 22(10):1261–7. https://doi.org/10.1038/nbt1016 PMID: 15470466
2. Kell DB, Oliver SG. Here is the evidence, now what is the hypothesis? The complementary roles of inductive and hypothesis-driven science in the post-genomic era. BioEssays. 2003; 26:99–105.
3. Dai Z, Nielsen J. Advancing metabolic engineering through systems biology of industrial microorganisms. Curr Opin Biotechnol. 2015; 36:8–15. https://doi.org/10.1016/j.copbio.2015.08.006 PMID: 26318074
4. Park JH, Lee SY, Kim TY, Kim HU. Application of systems biology for bioprocess development. Trends Biotechnol. 2008; 26(8):404–12. https://doi.org/10.1016/j.tibtech.2008.05.001 PMID: 18582974
5. Toya Y, Shimizu H. Flux analysis and metabolomics for systematic metabolic engineering of microorganisms. Biotechnol Adv. 2013; 31(6):818–26. https://doi.org/10.1016/j.biotechadv.2013.05.002 PMID: 23680193
6. Kim DH, Achcar F, Breitling R, Burgess KE, Barrett MP. LC-MS-based absolute metabolite quantification: application to metabolic flux measurement in trypanosomes. Metabolomics. 2015; 11(6):1721–32. https://doi.org/10.1007/s11306-015-0827-2 PMID: 26491423
7. Cortassa S, Caceres V, Bell LN, O'Rourke B, Paolocci N, Aon MA. From metabolomics to fluxomics: a computational procedure to translate metabolite profiles into metabolic fluxes. Biophysical Journal. 2015; 108(1):163–72. https://doi.org/10.1016/j.bpj.2014.11.1857 PMID: 25564863
8. van Eunen K, Kiewiet JAL, Westerhoff HV, Bakker BM. Testing Biochemistry Revisited: How In Vivo Metabolism Can Be Understood from In Vitro Enzyme Kinetics. PLoS Comput Biol. 2012; 8(4). https://doi.org/10.1371/journal.pcbi.1002483 PMID: 22570597
9. Tomar N, De RK. Comparing methods for metabolic network analysis and an application to metabolic engineering. Gene. 2013; 521(1):1–14. https://doi.org/10.1016/j.gene.2013.03.017 PMID: 23537990
10. Zanghellini J, Ruckerbauer D, Hanscho M, Jungreuthmayer C. Elementary flux modes in a nutshell: Properties, calculation and applications. Biotechnol J. 2013; 8:1009–16. https://doi.org/10.1002/biot.201200269 PMID: 23788432
11. Jol S, Kummel A, Terzer M, Stelling J, Heinemann M. System-Level Insights into Yeast Metabolism by Thermodynamic Analysis of Elementary Flux Modes. PLoS Comput Biol. 2012; 8(3). https://doi.org/10.1371/journal.pcbi.1002415 PMID: 22416224
12. Feist AM, Herrgard MJ, Thiele I, Reed JL, Palsson BO. Reconstruction of biochemical networks in microorganisms. Nat Rev Microbiol. 2009; 7(2):129–43. https://doi.org/10.1038/nrmicro1949 PMID: 19116616

13. Antoniewicz MR. Methods and advances in metabolic flux analysis: a mini-review. J Ind Microbiol Biotechnol. 2015; 42(3):317–25. https://doi.org/10.1007/s10295-015-1585-x PMID: 25613286
14. Orth JD, Thiele I, Palsson BO. What is flux balance analysis? Nat Biotechnol. 2010; 28(3):245–8. https://doi.org/10.1038/nbt.1614 PMID: 20212490
15. Schuetz R, Kuepfer L, Sauer U. Systematic evaluation of objective functions for predicting intracellular fluxes in Escherichia coli. Molecular Systems Biology. 2007; 3(119). https://doi.org/10.1038/msb4100162 PMID: 17625511
16. Schuetz R, Zamboni N, Zampieri M, Heinemann M, Sauer M. Multidimensional optimality of microbial metabolism. Science. 2012; 336:601–4. https://doi.org/10.1126/science.1216882 PMID: 22556256
17. Long CP, Antoniewicz MR. High-resolution 13C metabolic flux analysis. Nat Protoc. 2019; 14:2856–77. https://doi.org/10.1038/s41596-019-0204-0 PMID: 31471597
18. Wiechert W, Noh K. Isotopically non-stationary metabolic flux analysis: complex yet highly informative. Curr Opin Biotechnol. 2013; 24(6):979–86. https://doi.org/10.1016/j.copbio.2013.03.024 PMID: 23623747
19. Vojinović V, Von Stockar U. Influence of uncertainties in pH, pMg, activity coefficients, metabolite concentrations, and other factors on the analysis of the thermodynamic feasibility of metabolic pathways. Biotechnol Bioeng. 2009; 103(4):780–95. https://doi.org/10.1002/bit.22309 PMID: 19365870
20. Salvy P, Fengos G, Ataman M, Pathier T, Soh KC, Hatzimanikatis V. pyTFA and matTFA a Python package and a Matlab toolbox for Thermodynamics-based Flux Analysis. Bioinformatics. 2018; 35 (1):167–9.
21. Hoppe A, Hoffmann S, Holzhütter H-G. Including metabolite concentrations into flux balance analysis: thermodynamic realizability as a constraint on flux distributions in metabolic networks. BMC Syst Biol. 2007; 1(23). https://doi.org/10.1186/1752-0509-1-23 PMID: 17543097
22. Park JO, Rubin SA, Xu YF, Amador-Noguez D, Fan J, Shlomi T, et al. Metabolite concentrations, fluxes and free energies imply efficient enzyme usage. Nat Chem Biol. 2016; 12. https://doi.org/10.1038/nchembio.2077 PMID: 27159581
23. Ataman M, Hatzimanikatis V. Heading in the right direction: thermodynamics-based network analysis and pathway engineering. Curr Opin Biotechnol. 2015; 36:176–82. https://doi.org/10.1016/j.copbio.2015.08.021 PMID: 26360871
24. Beard DA, Babson E, Curtis E, Qian H. Thermodynamic constraints for biochemical networks. J Theor Biol. 2004; 228:327–33. https://doi.org/10.1016/j.jtbi.2004.01.008 PMID: 15135031
25. Kümmel A, Panke S, Heinemann M. Putative regulatory sites unraveled by network-embedded thermodynamic analysis of metabolome data. Mol Syst Biol. 2006. https://doi.org/10.1038/msb4100074 PMID: 16788595
26. Flamholz A, Noor E, Bar-Even A, Milo R. eQuilibrator—the biochemical thermodynamics calculator. Nucleic Acids Res. 2012; 40:D770–D5. https://doi.org/10.1093/nar/gkr874 PMID: 22064852
27. Henry CS, Broadbelt LJ, Hatzimanikatis V. Thermodynamics-Based Metabolic Flux Analysis. Biophys J. 2007; 92:1792–805. https://doi.org/10.1529/biophysj.106.093138 PMID: 17172310
28. Niebel B, Leupold S, Heinemann M. An upper limit on Gibbs energy dissipation governs cellular metabolism. Nat Metab. 2019; 1:125–32. https://doi.org/10.1038/s42255-018-0006-7 PMID: 32694810
29. Fleming RM, Thiele I. von Bertalanffy 1.0: a COBRA toolbox extension to thermodynamically constrain metabolic models. Bioinformatics. 2011; 27(1):142–3. https://doi.org/10.1093/bioinformatics/btq607 PMID: 21115436
30. Gerstl M, Jungreuthmayer C, Zanghellini J. tEFMA: computing thermodynamically feasible elementary flux modes in metabolic networks. Bioinformatics. 2015; 31(13):2232–4. https://doi.org/10.1093/bioinformatics/btv111 PMID: 25701571
31. Simonin J-P. Thermodynamic consistency in the modeling of speciation in selfcomplexing electrolytes. Ind Eng Chem Res. 2017; 56:9721–33.
32. Alberty RA. Thermodynamics of Biochemical Reactions: John Wiley & Sons; 2005.
33. Jankowski K, Henry CS, Broadbelt LJ, Hatzimanikatis V. Group contribution method for thermodynamic analysis of complex metabolic networks. Biophys J. 2008; 95:1487–99. https://doi.org/10.1529/biophysj.107.124784 PMID: 18645197
34. Orth JD, Conrad TM, Na J, Lerman JA, Nam H, Feist AM, et al. A comprehensive genome-scale reconstruction of Escherichia coli metabolism—2011. Mol Syst Biol. 2011; 7(535).
35. Ishii N, Nakahigashi K, Baba T, Robert M, Soga T, Kanai A, et al. Multiple high-throughput analyses monitor the response of E.coli to perturbations. Science. 2007; 316(5824):593–7. https://doi.org/10.1126/science.1132067 PMID: 17379776

36. Sandve GK, Nekrutenko A, Taylor J, Hovig E. Ten Simple Rules for Reproducible Computational Research. PLoS Comput Biol. 2013; 9(10). https://doi.org/10.1371/journal.pcbi.1003285 PMID: 24204232

37. Schellenberger J, Que R, Fleming RM, Thiele I, Orth JD, Feist AM, et al. Quantitative prediction of cellular metabolism with constraint-based models: the COBRA Toolbox v2.0. Nat Protoc. 2011; 6(9):1290–307. https://doi.org/10.1038/nprot.2011.308 PMID: 21886097

38. Atkins P, Paula Jd. Equilibrium electrochemistry. Atkins' physical chemistry. 7th ed. United States: Oxford University Press; 2002.

39. Fleming RM, Thiele I, Nasheuer HP. Quantitative assignment of reaction directionality in constraint-based models of metabolism: Application to Escherichia coli. Biophys Chem. 2009; 145:47–56. https://doi.org/10.1016/j.bpc.2009.08.007 PMID: 19783351

40. Siedler G, Peters H. Physical properties (general) of sea water. Oceanography. Landolt-Börnstein: Numerical data and functional relationships in science and technology. V/ 3a. Berlin: Springer; 1986. p. 233–64.

41. Meissner T, Wentz FJ. The complex dielectric constant of pure and sea water from microwave satellite observations. IEEE T Geosci Remote. 2004; 42(9):1836–49.

42. Millero FJ, Leung WH. Thermodynamics of seawater at one atmosphere. Am J Sci. 1976; 276:1035–77.

43. Baldwin WW, Myer R, Powell N, Anderson E, Koch AL. Buoyant density of Escherichia coli is determined solely by the osmolarity of the culture medium. Arch Microbiol. 1995; 164:155–7. https://doi.org/10.1007/s002030050248 PMID: 8588736

44. Pandey V, Hadadi N, Hatzimanikatis V. Enhanced flux prediction by integrating relative expression and relative metabolite abundance into thermodynamically consistent metabolic models. PLoS Comput Biol. 2019; 15(5). https://doi.org/10.1371/journal.pcbi.1007036 PMID: 31083653

45. Field A. Discovering statistic using SPSS. 3rd ed: SAGE Publications; 2009.

46. Kiparissides A, Hatzimanikatis V. Thermodynamics-based Metabolite Sensitivity Analysis in metabolic networks. Metab Eng. 2017; 39:117–27. https://doi.org/10.1016/j.ymben.2016.11.006 PMID: 27845184

47. Page L B, Motwani R W. The PageRank Citation Ranking: Bringing Order to the Web. In: InfoLab S, editor. Stanford, CA, USA1998.

48. Frainay C, Aros S, Chazalviel M, Garcia T, Vinson F, Weiss N, et al. MetaboRank: network-based recommendation system to interpret and enrich metabolomics results. Bioinformatics. 2018; 35(2):274–83.

49. Wagner A, Fell D. The small world inside large metabolic networks. Proc Biol Sci. 2001; 268:1803–10. https://doi.org/10.1098/rspb.2001.1711 PMID: 11522199

50. Beguerisse-Díaz M, Bosque G, Oyarzún D, Picó J, Barahona M. Flux-dependent graphs for metabolic networks. NPJ Syst Biol Appl. 2018; 4(32). https://doi.org/10.1038/s41540-018-0067-y PMID: 30131869

51. Cordova LT, Cipolla RM, Swarup A, Long CP, Antoniewicz MR. 13C metabolic flux analysis of three divergent extremely thermophilic bacteria: Geobacillus sp. LC300, Thermus thermophilus HB8, and Rhodothermus marinus DSM 4252. Metab Eng. 2017; 44:182–90. https://doi.org/10.1016/j.ymben.2017.10.007 PMID: 29037779

52. Toya Y, Ishii N, Nakahigashi K, Hirasawa T, Soga T, Tomita M, et al. 13C-metabolic flux analysis for batch culture of Escherichia coli and its pyk and pgi gene knockout mutants based on mass isotopomer distribution of intracellular metabolites. Biotechnol Prog. 2010; 26(4):975–92. https://doi.org/10.1002/btpr.420 PMID: 20730757

53. Costenoble R, Muller D, Barl T, van Gulik WM, van Winden WA, Reuss M, et al. 13C-Labeled metabolic flux analysis of a fed-batch culture of elutriated Saccharomyces cerevisiae. FEMS Yeast Res. 2007; 7(4):511–26. https://doi.org/10.1111/j.1567-1364.2006.00199.x PMID: 17355600

54. Ralser M. An appeal to magic? The discovery of a non-enzymatic metabolism and its role in the origins of life. Biochem J. 2018; 475:2577–92. https://doi.org/10.1042/BCJ20160866 PMID: 30166494

55. Takhaveev V, Heinemann M. Metabolic heterogeneity in clonal microbial populations. Curr Opin Microbiol. 2018; 45:30–8. https://doi.org/10.1016/j.mib.2018.02.004 PMID: 29477028

56. Goodwin BC. Synchronization of Escherichia coli in a chemostat by periodic phosphate feeding. Eur J Biochem. 1969; 10:511–4. https://doi.org/10.1111/j.1432-1033.1969.tb00718.x PMID: 4899926

57. Massie TM, Blasius B, Weithoff G, Gaedke U, Fussmann GF. Cycles, phase synchronization, and entrainment in single-species phytoplankton populations. P Natl Acad Sci USA. 2010; 107(9):4236–41.

58. Zhang Z, Milias-Argeitis A, Heinemann M. Dynamic single-cell NAD(P)H measurement reveals oscillatory metabolism throughout the E. coli cell division cycle. Sci Rep. 2018; 8(2162).

59. Yaginuma H, Kawai S, Tabata KV, Tomiyama K, Kakizuka A, Komatsuzaki T, et al. Diversity in ATP concentrations in a single bacterial cell population revealed by quantitative single-cell imaging. Sci Rep. 2014; 4(6522).

60. Gao P, Xu G. Mass-spectrometry-based microbial metabolomics: recent developments and applications. Anal Bioanal Chem. 2015; 407(3):669–80. https://doi.org/10.1007/s00216-014-8127-7 PMID: 25216964

61. Rabinowitz JD, Kimball E. Acidic Acetonitrile for Cellular Metabolome Extraction from Escherichia coli. Anal Chem. 2007; 79:6167–73. https://doi.org/10.1021/ac070470c PMID: 17630720

62. Lu W, Wang L, Chen L, Hui S, Rabinowitz JD. Extraction and Quantitation of Nicotinamide adenine dinucleotide redox cofactors. Antioxidants & redox signaling. 2018; 28(3):167–79. https://doi.org/10.1089/ars.2017.7014 PMID: 28497978

63. Barber F, Ho P-Y, Murray AW, Amir A. Details matter: noise and model structure set the relationship between cell size and cell cycle timing. Front Cell Dev Biol. 2017; 5(92). https://doi.org/10.3389/fcell.2017.00092 PMID: 29164112

64. Crosby JR, Laemthong T, Lewis AM, Straub CT, Adams MW, Kelly RM. Extreme thermophiles as emerging metabolic engineering platforms. Curr Opin Biotechnol. 2019; 59:55–64. https://doi.org/10.1016/j.copbio.2019.02.006 PMID: 30875665

65. Dun B, Zhang Z, Grubner S, Yurkovich J, Palsson B, Zielinski D. Temperature-Dependent Estimation of Gibbs Energies Using an Updated Group-Contribution Method. Biophys J. 2018; 114:2691–702. https://doi.org/10.1016/j.bpj.2018.04.030 PMID: 29874618

66. van Heeswijk W, V. Westerhoff H, Boogerd F. Nitrogen Assimilation in Escherichia coli: Putting Molecular Data into a Systems Perspective. Microbiol Mol Biol Rev. 2013; 77(4):628–95. https://doi.org/10.1128/MMBR.00025-13 PMID: 24296575

67. Sauer U, Eikmanns BJ. The PEP-pyruvate-oxaloacetate node as the switch point for carbon flux distribution in bacteria. FEMS Microbiol Rev. 2005; 29:765–94. https://doi.org/10.1016/j.femsre.2004.11.002 PMID: 16102602

68. Kappelmann J, Wiechert W, Noack S. Cutting the Gordian Knot: Identifiability of anaplerotic reactions in Corynebacterium glutamicum by means of (13) C-metabolic flux analysis. Biotechnol Bioeng. 2015; 113 (3). https://doi.org/10.1002/bit.25833 PMID: 26375179

69. Fischer E, Zamboni N, Sauer U. High-throughput metabolic flux analysis based on gas chromatography–mass spectrometry derived 13C constraints. Anal Biochem. 2004; 325(2):308–16. https://doi.org/10.1016/j.ab.2003.10.036 PMID: 14751266

70. Yang C, Hua Q, Baba T, Mori H, Shimizu K. Analysis of Escherichia coli anaplerotic metabolism and its regulation mechanisms from the metabolic responses to altered dilution rates and phosphoenolpyruvate carboxykinase knockout. Biotechnol Bioeng. 2003; 84(2):129–44. https://doi.org/10.1002/bit.10692 PMID: 12966569

71. Nanchen A, Schicker A, Sauer U. Nonlinear dependency of intracellular fluxes on growth rate in miniaturized continuous cultures of Escherichia coli. Appl Environ Microb. 2006; 72(2):1164–72. https://doi.org/10.1128/AEM.72.2.1164-1172.2006 PMID: 16461663

72. Williams TCR, Poolman MG, Howden AJM, Schwarzlander M, Fell DA, Ratcliffe RG, et al. A genome-scale metabolic model accurately predicts fluxes in central carbon metabolism under stress conditions. Plant Physiol. 2010; 154:311–23. https://doi.org/10.1104/pp.110.158535 PMID: 20605915

73. Chen X, Alonso AP, Allen DK, Reed JL, Shachar-Hill Y. Synergy between (13)C-metabolic flux analysis and flux balance analysis for understanding metabolic adaptation to anaerobiosis in E. coli. Metab Eng. 2011; 13(1):38–48. https://doi.org/10.1016/j.ymben.2010.11.004 PMID: 21129495

74. Sauer U, Lasko DR, Fiaux J, Hochuli M, Glaser R, Szyperski T, et al. Metabolic flux ratio analysis of genetic and environmental modulations of Escherichia coli central carbon metabolism. J Bacteriol. 1999; 181(21):6679–88. https://doi.org/10.1128/JB.181.21.6679-6688.1999 PMID: 10542169

75. Myoung Park J, Yong Kim T, Yup Lee S. Prediction of metabolic fluxes by incorporating genomic context and flux-converging pattern analyses. P Natl Acad Sci USA. 2010; 107(33):14931–6.

scientific reports

Check for updates

OPEN

Metabolic modeling-based drug repurposing in Glioblastoma

Claudio Tomi-Andrino[1,2,3], Alina Pandele[4], Klaus Winzer[2], John King[3], Ruman Rahman[4] & Dong-Hyun Kim[1]✉

The manifestation of intra- and inter-tumor heterogeneity hinders the development of ubiquitous cancer treatments, thus requiring a tailored therapy for each cancer type. Specifically, the reprogramming of cellular metabolism has been identified as a source of potential drug targets. Drug discovery is a long and resource-demanding process aiming at identifying and testing compounds early in the drug development pipeline. While drug repurposing efforts (i.e., inspecting readily available approved drugs) can be supported by a mechanistic rationale, strategies to further reduce and prioritize the list of potential candidates are still needed to facilitate feasible studies. Although a variety of '*omics*' data are widely gathered, a standard integration method with modeling approaches is lacking. For instance, flux balance analysis is a metabolic modeling technique that mainly relies on the stoichiometry of the metabolic network. However, exploring the network's topology typically neglects biologically relevant information. Here we introduce *Transcriptomics-Informed Stoichiometric Modelling And Network analysis* (TISMAN) in a recombinant innovation manner, allowing identification and validation of genes as targets for drug repurposing using glioblastoma as an exemplar.

Cancer is the first or second cause of premature death in 70% of countries[1]. Tumors are characterized by multiple biological capabilities conferring cellular proliferation and metastasis (dissemination to other tissues and colonization), where metabolic reprogramming is crucial to fulfil biosynthetic requirements underlying these phenotypes[2]. The disparity of oxygen and nutrient availability within the surrounding tumor microenvironment promotes different metabolic states amongst cells, which show a continuum in gene expression within sub-clonal populations[3]. Consequently, metabolic dependencies and vulnerabilities are shaped by the cell lineage and the environment, rather than being universal[4]. Isocitrate dehydrogenase-1 wild-type Glioblastoma (GBM) is the most aggressive brain tumor in adults[5], characterized by a high degree of invasiveness through brain parenchyma[6]. Different subtypes and transcriptional subpopulations may co-exist within the same tumor, where a quiescent subpopulation of GBM stem cells (GSC) can facilitate the development of radio- or chemo-resistance, leading to inevitable disease relapse[7–9]. Therefore, novel therapeutic approaches should aim to target all cell lineages[10], block GSC differentiation[11], or combine both strategies[9]. In particular, recent studies have shown the suitability of chemicals disrupting energy metabolism in GBM[12] or blocking de novo pyrimidine synthesis in GSC[13]. Conversely, the application of immunotherapy and many drug compounds is hindered by the impermeability of the blood–brain–barrier[14].

Phenotypic screening of compound libraries can help identify putative drug candidates, albeit being a costly process and requiring further target deconvolution steps[15]. Although gene essentiality is used as a proxy for potential drug targeting, its context-dependent and evolvable nature hinders its usage, for example: (i) genetic ablation affects both the catalytic activity (which may not be essential) and any other function (e.g. essential structural); (ii) incomplete knockdown or off-target effects; (iii) genetic divergence of cell lines from the original tumor; (iv) metabolic response of cells to non-physiological growth conditions[16–19].

Whilst simulating ligand–target interactions (molecular docking) provides a shortlist of compounds to be tested, the scarcity of structural data limits its application[20]. In addition, this approach prevents the identification of compounds indirectly affecting metabolism, for example by altering the expression levels of multiple genes[21]. Therefore, information-rich computational strategies to generate manageable lists of drug candidates should be considered as a viable complement to the drug discovery phase. The set of metabolic fluxes (i.e., metabolic or

[1]Centre for Analytical Bioscience, Advanced Materials and Healthcare Technologies Division, School of Pharmacy, University of Nottingham, Nottingham NG7 2RD, UK. [2]Nottingham BBSRC/EPSRC Synthetic Biology Research Centre (SBRC), School of Life Sciences, BioDiscovery Institute, University of Nottingham, Nottingham NG7 2RD, UK. [3]Nottingham BBSRC/EPSRC Synthetic Biology Research Centre (SBRC), School of Mathematical Sciences, University of Nottingham, Nottingham NG7 2RD, UK. [4]Children's Brain Tumour Research Centre, Biodiscovery Institute, School of Medicine, University of Nottingham, Nottingham NG7 2RD, UK. ✉email: dong-hyun.kim@nottingham.ac.uk

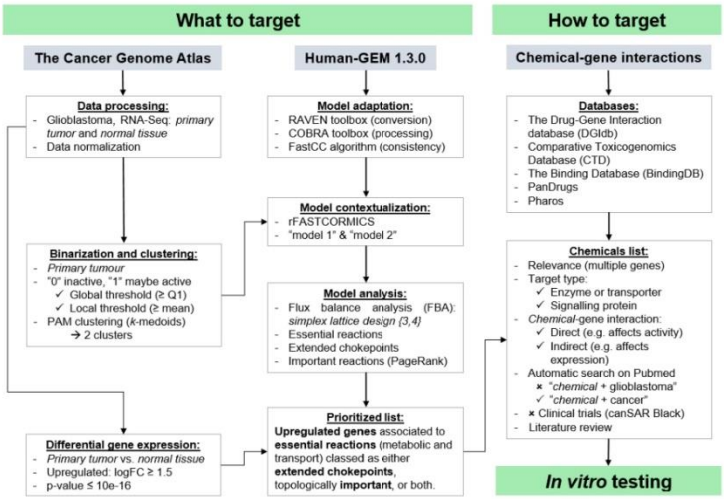


Figure 1. TISMAN (Transcriptomics-Informed Stoichiometric Modelling And Network analysis), the workflow developed in this study. It comprised three main parts (what to target, how to target and in vitro testing), where both MATLAB and R scripts were used.

transport reaction rates) can be either estimated via ^{13}C metabolic flux analysis (^{13}C-MFA) for the central carbon metabolism or modelled by applying flux balance analysis (FBA) to a genome-scale model (GSM).

A GSM consists of a stoichiometric matrix connecting metabolites (substrates and products) with reactions, where the latter are associated with genes following the gene-protein-reaction formalism[22]. FBA predicts a flux distribution upon the optimization for a biological task (normally the biomass formation), represented by a reaction in the GSM[23]. Whilst ^{13}C-MFA mainly informs about the central carbon metabolism[4,24], transcriptomics data can be applied to obtain cell-specific models from GSMs and can predict in silico gene essentiality[25–27]. Other strategies based on network analysis allow identification of highly connected reactions or reactions which exclusively consume/produce a metabolite (choke points) that if inhibited, would potentially disrupt metabolism[28].

To this end, we developed *Transcriptomics-Informed Stoichiometric Modelling And Network analysis* (TISMAN), a recombinant innovation introducing the concept of "extended choke point" and exploiting biologically-rich information aiming at developing a workflow providing a stringent search of potential drug targets and compounds to be tested for GBM as an exemplar disease type. Briefly, published data were exploited to build condition specific GBM metabolic models, which were analyzed to identify and rank the reactions of interest according to different indicative criteria. Several chemical-gene interaction databases were used to identify and prioritize approved drugs or experimental compounds either directly targeting proteins or indirectly affecting the corresponding gene expression levels. Chemicals with a proven impact against other cancer types but which have not been tested for GBM, were prioritized for experimental validation using patient-derived GBM in vitro models.

Materials and methods

The workflow developed in this study comprised three main parts (Fig. 1): (i) "what to target": identification of either metabolic or transport (e.g., between cellular compartments) reactions of interest; (ii) "how to target": identification of chemicals (readily available approved drugs or experimental compounds); (iii) in vitro validation of the selected compounds. Briefly, transcriptomics data from GBM tumors was used to: (a) contextualize a generic human GSM, yielding two GBM-specific models; (b) identify up-regulated genes. Next, the models were subjected to FBA to identify essential reactions, and the network topology was inspected to pinpoint certain features (choke points and centrality). Overall, the workflow aimed to identify proteins that if targeted, would potentially hinder cellular metabolism, impairing tumor metabolic viability and/or invasion. Chemicals targeting metabolism either directly (i.e., affecting the activity) or indirectly (i.e., affecting gene expression) were ranked, with five candidates prioritized for in vitro testing. Files and scripts for MATLAB and R can be found in Github (https://github.com/CTA-code/TISMAN).

What to target. *Transcriptomics data analysis.* Data processing: RNA-Seq data for GBM and healthy counterpart astrocytic tissue (herein referred to as 'primary tumor' and 'normal tissue') was obtained from the Cancer Genome Atlas (TCGA) database (https://portal.gdc.cancer.gov/) and processed using the R package TCGAbiolinks[29]. This information was used for two independent steps, binarization and clustering. Expression data from *primary tumor* was binarized by considering two simultaneous thresholds: (i) global (≥ Q1) across all genes and samples, and (ii) local (≥ mean), which was gene-specific across samples. Genes were flagged as either *maybe active* ("1") or *inactive* ("0") if fulfilling both criteria or not, respectively, so that each sample was codified by a binary vector[25]. Next, R's PAM function (Partitioning Around Medoids, or *k*-medoids) was used to cluster the data into two groups (optimal number of clusters according to the Silhouette method), yielding a representative binary vector (or medoid) for each cluster[30]. Focusing on upregulated genes in cancerous tissue compared to normal tissue is a widely used strategy to identify potential therapeutic genes[31]. Therefore, both *primary tumor* and *normal tissue* datasets were used to determine the differential gene expression: genes with logFC ≥ 1.5 and p-value ≤ 10^{-16} were deemed upregulated in the tumor[32].

Stoichiometric modeling and network analysis. Model adaptation: the latest version of a human GSM (Human-GEM 1.3.0, comprising 13,417 reactions, 10,135 metabolites and 3,628 genes[33]) was converted and adapted to a COBRA toolbox paradigm by using the RAVEN toolbox[34] and the COBRA toolbox[22]. Next, a consistent model was generated by FastCC prior to the contextualization step, so that all reactions were active (i.e., nonzero flux) for at least one feasible flux distribution[35].

Model contextualization: the two medoids were used with rFASTCORMICS[27] to build two cancer-specific models (COBRA toolbox v. 2, with IBM CPLEX 12.8 in MATLAB R2016b run in Windows 10 to ensure solver compatibility).

Model analysis: an upper bound of 2 mmol/gDW-h was set for the oxygen uptake rate, as suggested for previous cancer models[36,37]. For the sake of modelling a variety of metabolic states, several objective functions were considered: maximization of the biomass yield ('biomass_human'), maximization of the ATP yield ('HMR_4358'), and maximization of 1-phosphatidyl-1D-myo-inositol-4-phosphate production ('HMR_6552'), a lipid which induces curvature in the lipid membrane[38]. The latter reaction is catalyzed by synaptojanin 2 (*SYNJ2*) a polyphosphoinositide phosphatase related to GBM invasion[39] and a mediator of metastasis in breast cancer[40]. Instead solving a multi-objective linear problem[41], the weighted global criterion method was used to reformulate it as a single objective problem directly solvable by FBA[23,42]. Therefore, a simplex lattice design for FBA was designed by varying the weight of the three reactions, allowing to study the aforementioned three objective functions and mixtures amongst them in 15 single objective problems (Fig. 2A). In addition, an extra case for the minimization of the sum of fluxes was considered, yielding 16 final tests. Since certain optimal solutions were the same, the number of non-redundant solutions for each model was calculated. Reactions of interest fulfilled several criteria (Fig. 2C): related to an upregulated gene in the tumor; essential reaction; extended choke point and/or topologically important. Considering the full GSM and the flux through the biomass reaction when maximizing for it in FBA, a reaction was deemed essential for a test (same network, different objective function(s)) when shutting it down (no flux through allowed) caused a ≥ 5% reduction of said metabolic flux. Conversely, topological aspects were studied by exploring reduced metabolic networks. A condition-specific model was generated for each unique flux distribution produced by FBA, so that the stoichiometric matrix only comprised active elements (reactions and metabolites). Single choke points were identified as reactions associated exclusively with producing or consuming a metabolite. Double choke points were then defined as reactions associated exclusively with producing and consuming metabolites. To ensure a more stringent selection criterion, the concept of extended choke points was introduced, defined as double choke points surrounded by single choke points (consuming and producing) (Fig. 2B). Alternatively, topologically important reactions were identified by MATLAB's in-built PageRank function[43]. This analysis was applied to a directed graph (i.e., considering the flux direction) derived from an adjacency matrix, where the centrality of the nodes (reactions) was determined. Directly calculating the adjacency matrix from the stoichiometric matrix would yield a metabolite-centric graph (metabolites as nodes)[44]. Therefore, an intermediate step converting the stoichiometric matrix into its conjugate transpose (reactions as nodes) was included prior to generating the adjacency matrix.

Prioritized list: reactions of interest for each medoids were identified by independently selecting those identified as extended choke points in at least half of the non-redundant optimal solutions (occurrence), and those within the top 10% of central reactions according to PageRank. Finally, results from both medoids were combined by summation of occurrence or centrality scores, respectively.

How to target. *Identification of relevant drugs and chemicals.* Five databases were used, either programmatically or manually: *The Drug-Gene Interaction database* (DGIdb) Nov 2020, v4.2.0[45]; *Comparative Toxicogenomics Database* (CTD), Oct 2020[46]; *The Binding Database* (BindingDB), Nov 2020[47]; *PanDrugs*, version: 2018.11.7[48]; and *Pharos*, version 3.2.0[49]. To exploit published chemical–gene interactions, a gene-centric list of potential candidates was generated from the reactions of interest. Since a gene may participate in several reactions, occurrence and centrality scores for each gene were normalized and separately summated. Similarly, as a chemical may target (directly or indirectly) one or several genes (Fig. 2D), drug-centric lists were created, and a final relevance score was calculated as the sum of occurrences and centrality scores. Automatic searches on Pubmed were performed to identify which drugs have been tested for cancers (except for GBM), followed by a literature review and search for clinical trials in canSAR[50] to finally select five compounds for in vitro testing.

In vitro testing. *Cell culture.* **G**lioblastoma **IN**vasive margin (GIN28, GIN31) and **G**lioblastoma **C**ontrast-**E**nhanced core (GCE28, GCE31) cell lines have been previously derived at Queen's Medical Centre, Nottingham,

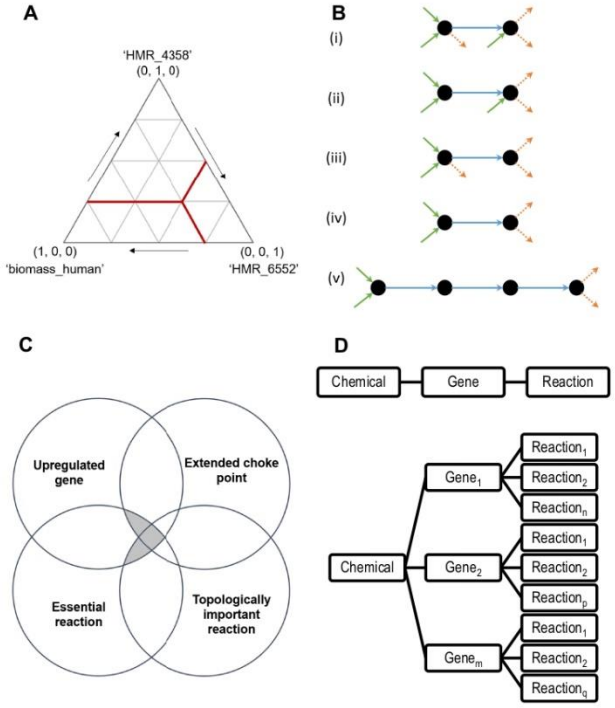


Figure 2. Strategies to identify gene targets for drug repurposing. (**A**) Simplex lattice design {3, 4} for objective function weight values distribution. Each outer vertex represents a case where a single objective function is selected: maximization of the biomass yield ('biomass_human'), maximization of the ATP yield ('HMR_4358'), and maximization of 1-phosphatidyl-1D-myo-inositol-4-phosphate production ('HMR_6552'). For illustrative purposes, the test comprising weight values (0.25, 0.25, 0.50) is labeled in red. (**B**) Examples of metabolites-reactions relationships (dots and arrows, respectively). The blue arrows represent the production of the metabolite on the right from the metabolite on the left. Inward green arrows refer to production reactions from metabolites not drawn, while outward orange dotted arrows represent consumption reactions. (i) Not a choke point, (ii) single choke point on the consumption side, (iii) single choke point on the production side, (iv) double choke point, and (v) extended choke point. (**C**) Venn diagram showing the subsets of reactions of interest. In all cases, reactions (metabolic or of transport) were essential and carried out by proteins related to upregulated genes, as well as identified as extended choke point and/or topologically important reactions. (**D**) (Top) Direct chemical–gene interaction, where a compound affects the activity of a single protein (e.g., an inhibitor). (**D**) (Bottom) Indirect chemical–gene interaction, where a single compound targets an element such as a signaling protein, that leads to changes in the expression levels of multiple genes, thus affecting several reactions in a pleiotropic manner.

authenticated using short tandem repeat genotyping (Supplementary Table S1) and used at passages 21–29, 27–36, 15–23 and 28–37, respectively[51,52]. Cell lines were cultured using adherent T75 flasks (Corning) in Dulbecco's Modified Eagle Medium (Gibco) supplemented with 10% FBS (Sigma-Aldrich) and incubated under humidified growth conditions at 37 °C and 5% CO_2.

Metabolic viability assay. All cell lines were seeded in 96 well plates (Costar) at 5×10^3 cells/well and incubated for 24 h prior to treatment. Cells were treated with afuresertib (Selleckchem), isorhamnetin (Merck), formon-

onetin (Merck), pyrogallol (Merck) and taxifolin (Merck) in a 16-point dose response (n = 6) over 72 h, with concentrations ranging from 1 to 500 µM. Appropriate vehicle (0.1% DMSO) and positive cell death controls (10% DMSO) were used. Viability was assessed by adding 1:10 PrestoBlue (ThermoFisher) over 45 min and measuring the resulting fluorescence at 544/590 nm (excitation/emission) on a FLUOstar Omega microplate reader (BMG LABTECH). Fluorescence intensity was normalized against that of control wells to determine percentage viability of drug-treated cells.

Invasion assay. The ability of the compounds to inhibit invasion was investigated for all cell lines using a Transwell collagen barrier assay. 24 well ThinCert™ 8 µm cell culture inserts (Greiner) were coated with 10 µg of mouse collagen IV (Cultrex, Trevigen) and incubated at 37 °C overnight. Cells were seeded at 13,500–15,000 cells/insert in 0% FBS DMEM with added treatment and allowed to invade towards 10% FBS DMEM over 24 h at 37 °C and 5% CO_2. Invasion of untreated cells towards 10% and 0% FBS was used as controls. Following incubation, non-invading cells were removed from the top chamber using a cotton swab and media was replaced in the bottom chamber with 1:10 PrestoBlue in 0% DMEM and incubated for 45 min with fluorescence measured at 544/590 nm. Number of invading cells was extrapolated from a standard curve comparing fluorescence intensity to cell seeding density (serially diluted from 20,000 to 234 cells/well). Finally, percentage invasion was calculated as the ratio of the number of invading cells to number of seeded cells.

Statistical analysis. Statistical data analysis and curve fitting was performed using GraphPad Prism (v8.4.3). Statistical significance was analyzed via one-way ANOVA with $p < 0.05$ considered significant. Inhibitory concentration values (IC_{50} and IC_{25} for afuresertib and taxifolin, respectively) were generated from sigmoidal dose–response curves with upper and lower 95% confidence intervals.

Results and discussion

This study revealed three main outcomes: a widely applicable workflow based on metabolic modelling and network analysis (TISMAN), a list of potential drug targets for further investigation, and repurposing of drug compounds exerting inhibitory effects on GBM metabolic viability and invasion. Accessible high throughput sequencing of biopsies transformed the usage of RNA-sequencing in neuro-oncology practice[53]. Therefore, transcriptomics data was used to generate two contextualized models from a generic human GSM[25–27], and to identify upregulated genes in cancerous cells[32]. Specifically, GBMs comprise pro-tumorigenic subpopulations of stem cells able to develop resistance to therapy[7–9,54]. While using FBA to obtain in silico gene essentiality is not a novel idea[23], defining an appropriate objective function for normal and cancerous tissues to elucidate differences cannot be easily done[2,55]. Therefore, our analyses focused on cancer-specific models under an array of metabolic states and considering only reactions related to genes upregulated in GBM versus normal tissue. Conversely, recent metabolic modelling studies for GBM solely focused on the maximization of biomass yield, but generated c. 140 patient-derived GSMs[56].

Identification of genes of interest. A final list of 168 upregulated genes associated with essential reactions classed as extended chokepoints and/or topologically important, was generated. Specifically, 74 genes contained hits in the chemical-gene interaction databases (Fig. 3). The remaining 94/168 genes had no reported chemical–gene interactions, so they were deemed as potential drug targets yet to be explored (Dataset S1)[58].

Given the genetic heterogeneity which manifests within GBM[7–9,54], predicted genes of interest were compared against modelling and experimental approaches applied to cancerous tissue or specific subpopulations (Fig. 4). In Larsson et al. (Fig. 4A), patient-derived GSMs for GBM were generated from transcriptomics data, and gene essentiality predicted by FBA[56]. Two of the genes pinpointed for the low survival models agreed with our results: *ACOT8* (acyl-CoA thioesterase 8) and *GPAT4* (glycerol-3-phosphate acyltransferase 4), both related to lipid metabolism. The former is targeted by three drugs with antineoplastic activity which decrease its expression: doxorubicin[52,59], orlistat[60,61], and paclitaxel[60,62]. *GPAT4* is the only gene of the *GPAT* family expressed in the brain, and it has recently been identified as a potential drug target for treating obesity-associated depression[63].

A subpopulation of GSC can facilitate developing resistance to therapy, promoting disease relapse[7–9]. In Richards et al.[9] certain marker genes for intra-GSC clusters were identified, some of which were also highlighted in this work as potential drug targets (Fig. 4B): *ACSF2* (acyl-CoA Synthetase Family Member 2), *MGLL* (monoglyceride lipase), and *PKM* (pyruvate kinase M1/2). Although *ACSF2* is functionally associated with fatty acid metabolism, *ACSF2* did not affect cell anchorage-dependent growth in U87 GBM cells[64]. *MGLL* is highly expressed in the brain and in aggressive cancers and its role in self-renewal and tumorigenic behavior has been demonstrated in murine models for GBM, where pharmacological inhibition of the translated protein showed promising results[65]. Finally, overexpression of pyruvate kinase M1/2 is a trait occurring in brain tumors but not in other cancers, where it is involved in metabolic and signaling functions that promote cell proliferation, migration and chemoresistance. Knocking down *PKM* alters central carbon metabolism and decreases the activation of oncogenes, thus making it a viable therapy target[66].

Other genes of interest also identified by both Richards et al.[9] and this study, currently lack (i) extensive evidence of therapeutic relevance to treating cancer and/or (ii) cognate ligands or compounds affecting their expression levels (or outdated chemical–gene interactions in databases): *ACSBG1* (acyl-CoA synthetase bubblegum family member 1), *COX6A1* (cytochrome c oxidase subunit 6A1), *GUSB* (glucuronidase beta), *HADHB* (acetyl-CoA acyltransferase), as well as multiple nucleoporins (*NUP58, NUP107, NUP155, NUP205* and *NUP201*). A recent study in renal cell carcinoma cells showed that *ACSBG1* induces ferroptosis, an iron-dependent regulated cell death proposed as a therapeutic approach for cancer treatment[69]. This mechanism plays a pro-tumorigenic effect in GBM by promoting necrosis, which is a sign of poor prognosis[70]. Interestingly, depleting *ACSL4*

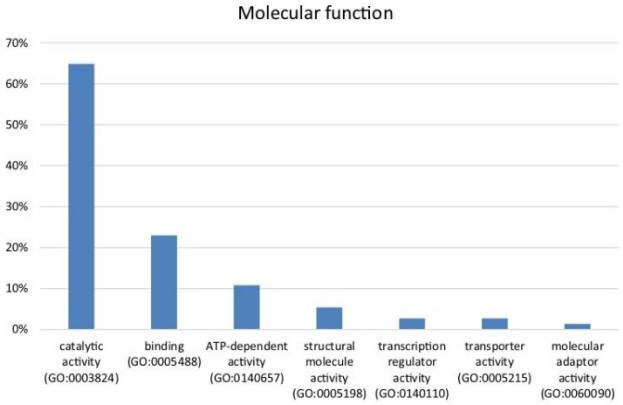


Figure 3. Functional classification of the 74 genes of interest. Using the PANTHER Classification System (17.0)[58] showed that 65% of the 74 aforementioned genes have a catalytic function, which relates to the underlying metabolic modelling to TISMAN. A functional enrichment analysis performed in STRING v11[57] identified oxidase and ligase activity in lipid metabolism to be particularly prevalent in this gene list.

(acyl-CoA synthetase long chain family member 4), a gene highlighted by the workflow, also inhibited tumor necrosis[70]. *COX6A1*, has been reported as an anti-apoptotic gene in U373MG GBM cells, involved in mitochondrial energy metabolism[71]. *HADHB* is involved in fatty acid β-oxidation, and gene knockdown in a colon carcinoma cell line decreased cell proliferation and increased sensitivity to the monoclonal antibody cetuximab[72]. Regarding the aforementioned nucleoporins, even though there is a known link to cancer[73], targeting membrane proteins remains a challenge[74].

Radial glia (RG) cells are located in the ventricular zone during embryonic development and in the subventricular zone in the adult brain. In Wang et al., RG-like cells were found to play a role in the initiation or maintenance of adult GBM[54]. Specifically, two subpopulations of RG cells were identified: ventricular RG-like and outer RG-like, and upregulated RG genes are consistent with our results (Fig. 4C). Firstly, only one gene for ventricular RG-like was found in this study. *ACSL6* (acyl-CoA Synthetase Long Chain Family Member 6) is predominately expressed in the brain, where it participates in omega-3 fatty acid metabolism (crucial for correct brain function)[75]. Six genes were highlighted as outer RG-like: *ABHD6* (Abhydrolase Domain-Containing Protein 6), *CYP4V2* (cytochrome P450 family 4 subfamily V member 2), *FASN* (fatty acid synthase), *POLH* (DNA polymerase eta), *MGLL* and *ACSBG1*[54]. *ABHD6* is an endocannabinoid hydrolase with oncogenic functions, knockdown of which, reduces metastatic seeding in murine models[76,77]. *CYP4V2* metabolizes fatty acids; however, as mutants with an impaired activity are the cause of multiple diseases (e.g. Bietti's crystalline dystrophy), this gene may not be a suitable drug target[78]. Regarding *FASN*, it is known to be highly expressed in GBM, where its inhibition in vitro and in vivo by means of a saffron-derived compound, induced cell death and impaired migration[79]. *POLH* is a DNA repair gene associated with correcting UV-induced damage, and its deficiency increases the risk of developing skin cancer[80]. Conversely, ovarian cancer stem cells survive cisplatin treatment due to an enhanced *POLH* expression, leading to tumor relapse[81]. Lastly, the remaining two genes identified as outer RG-like (*MGLL* and *ACSBG1*) are also marker genes for intra-GSC clusters, as discussed above.

Targeting transcription factors driving characteristic biological capabilities of cancer remains an attractive therapeutic approach[21]. 47/168 genes of interest had entries in RegNetwork (Fig. 4D), a database for regulatory information last updated in 2019[67]. Interestingly, 21 of these genes were related to the *MYC* family oncogene, which regulates a plethora of cellular functions and has been subjected to targeting studies at different levels[82]. Specifically, *MYC* maintains GSC[83] and downregulating *MYC* promotes GBM autophagy[84]. Similarly, 13 genes are modulated by *PPARα*[67], a transcription factor whose depletion inhibits tumor cell proliferation and induces senescence[85]. Overall, genes of interest identified by the workflow agreed with published attempts to find potential drug targets for GBM. Therefore, the validation of its predictive capabilities should foster more research into the aforementioned genes whose relevance to GBM has been poorly studied (e.g., *ACSBG1*). Improving the workflow by adding more biological information (such as epigenomics, proteomics or survival data) would allow further refining of potential drug targets to enable in vitro and in vivo efficacy characterizations.

Selection of chemicals and in vitro testing. The goal of TISMAN is to facilitate drug repurposing projects by generating a prioritized list of potential drug targets to identify chemicals for testing in an efficient

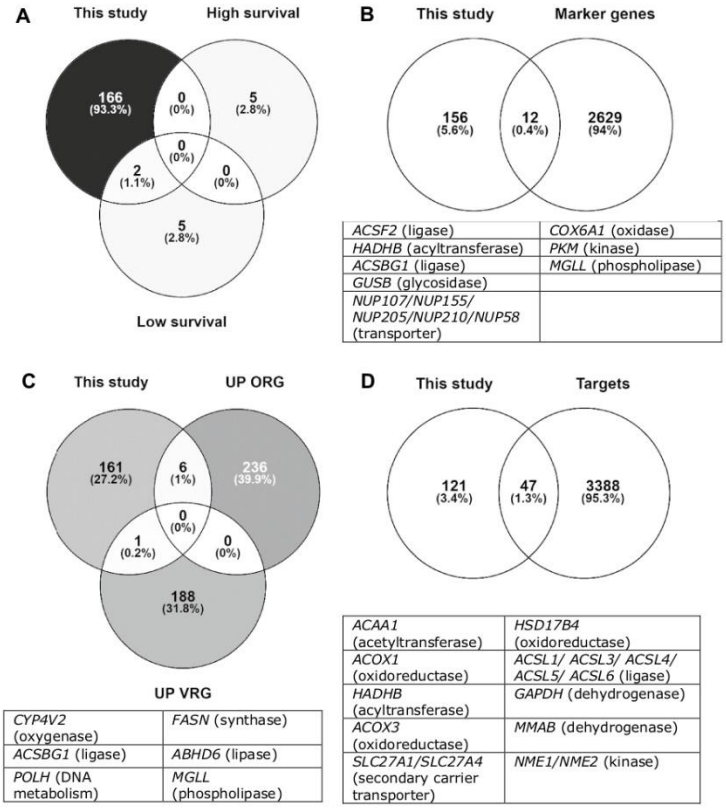


Figure 4. Comparison of genes of interest identified in this study against published works: (**A**) Larsson et al.[56], which highlighted essential genes for models for high and low survival, (**B**) Richards et al.[9], where the list of marker genes comprises the top 50 genes for each one of the 86 intra-GSC clusters, (**C**) Wang et al.[54], where upregulated genes for outer RG-like and ventricular RG-like (UP ORG and UP VRG, respectively) were considered, and (**D**) Liu et al.[67], where "targets" comprise both genes and miRNAs. Diagrams were made using Venny[68]. Panels B, C and D include tables informing about the protein type (most of them are enzymes).

and timely manner. Multiple gene–chemical interactions databases were combined and used to identify relevant compounds, ranking them by the number of genes they interacted with (directly and/or indirectly, Fig. 2). Next, a literature search allowed selection based upon proven efficacy for other cancer types, but which have not yet been tested for GBM (Fig. 1).This approach reduced thousands of gene-chemical interactions to a ranked list of 30 compounds, allowing a detailed inspection of each one of them. Upon considering reported results, five chemicals were selected based on their potential effects on cell viability and invasion in GBM: afuresertib, pyrogallol, isorhamnetin, formononetin, and taxifolin (Table 1).

Afuresertib is an orally bioavailable inhibitor of the serine/threonine protein kinase Akt pathway[86] that can resensitize ovarian cancer to platinum-based chemotherapy[87] and enhanced cisplatin treatment of mesothelioma cells[88]. The PI3K/AKT/mTOR pathway is related to metabolism, proliferation and migration, and is generally active in GBM[89]. Pyrogallol is a natural polyphenol with antitumor effects in hepatocellular carcinoma via the upregulation of miR-134[90]. This microRNA is deregulated in GBM (U87 cells), and overexpressing it inhibited

Position in priority list (relevance)	Drug/chemical	Gene name	Gene symbol	Gene relevance	Interaction(s) (predicted "–")
4 (385)	Afuresertib	Acyl-CoA synthetase family member 2	*ACSF2*	119	Increases exp
		Acyl-CoA synthetase long chain family member 5	*ACSL5*	86	Increases exp
		Phenylalanyl-TRNA synthetase subunit beta	*FARSB*	9	Decreases exp
		Lipin 1	*LPIN1*	9	Increases exp
		Metabolism of cobalamin associated B	*MMAB*	26	Increases exp
		Patatin like phospholipase domain containing 2	*PNPLA2*	3	Increases exp
		DNA polymerase alpha 2, accessory subunit	*POLA2*	4	Decreases exp
		DNA polymerase delta 4, accessory subunit	*POLD4*	4	Increases exp
		Solute carrier family 27 member 1. Long-chain fatty acid transport protein 1	*SLC27A1*	119	Increases exp
		Solute carrier family 29 member 1. Equilibrative nucleoside transporter 1	*SLC29A1*	6	Decreases exp
8 (123)	Pyrogallol	Hydroxysteroid 17-beta dehydrogenase 10	*HSD17B10*	119	–
		DNA polymerase kappa	*POLK*	4	–
9 (119)	Formononetin	Hydroxysteroid 17-beta dehydrogenase 10	*HSD17B10*	119	–
13 (16)	3-*O*-methylquercetin (Isorhamnetin)	DNA polymerase beta	*POLB*	4	–
		DNA polymerase eta	*POLH*	4	–
		DNA polymerase iota	*POLI*	4	–
		DNA polymerase kappa	*POLK*	4	–
13 (16)	Taxifolin	DNA polymerase beta	*POLB*	4	–
		DNA polymerase eta	*POLH*	4	–
		DNA Polymerase iota	*POLI*	4	–
		DNA Polymerase kappa	*POLK*	4	–

Table 1. Selected chemicals from the priority list for in vitro testing. Interactions for afuresertib were derived from *Comparative Toxicogenomics Database* (CTD) Oct 2020[46], and interactions for all other compounds derived from *The Drug-Gene Interaction database* (DGIdb) Nov 2020, v4.2.0[45]. Gene relevance refers to the summation of the occurrence (extended choke point) and the topological importance (centrality score by PageRank). The stoichiometry of a reaction related to *ACSF2* can be found in Supplementary Table S2.

cell proliferation and invasion[91]. Formononetin is an isoflavone affecting multiple signaling pathways with proven antitumorigenic properties in a rat glioma cell line[92,93]. 3-*O*-methylquercetin (isorhamnetin) is a flavonoid that inhibits cell proliferation and invasion, and induces apoptosis in triple-negative breast cancer cells[94]. Finally, taxifolin (also a flavonoid) down-regulates β-catenin, thus promoting mesenchymal to epithelial transition—the reverse process is the epithelial to mesenchymal transition, related to metastasis. Specifically, this compound inhibited cell proliferation and invasion in breast cancer cell lines[95]. Knockdown of PELP1, a β-catenin coactivator, proved both elements to be crucial for GBM progression in a murine model[96]. Even though interesting candidates were identified in the databases, some instances referred to predicted interactions with DNA polymerases rather than stating the aforementioned actual effects (Table 1). Well-curated and maintained databases would greatly benefit drug repurposing efforts, and researchers should consider updating the chemical-gene interaction entries based upon new data.

Two in vitro tests were performed to assess the effects of the selected chemicals on metabolic viability and invasiveness of four patient-derived GBM cell lines, as a means to validate this innovative in silico pipeline. Afuresertib was identified as the most potent drug inhibiting proliferation (Fig. 5A), while taxifolin showed a modest but significant effect on cell sensitization (Fig. 5B). No significant effect on proliferation was observed after treatment with isorhamnetin, formononetin and pyrogallol at 72 h. Regarding the invasion assays, afuresertib was the only compound to significantly inhibit invasion at IC_{50}, impairing invasion by 86.7% ($p < 0.001$) and 74.5% ($p < 0.0001$) in GIN28 and GIN31 GBM invasive margin cells, respectively, and by 25.6% ($p = 0.017$) and 18% ($p = 0.028$) in corresponding GCE28 and GCE31 counterpart cell lines derived from the central tumor core. At 500 µM, isorhamnetin significantly reduced invasion by 25.2% ($p = 0.0036$) in GIN28 and 34.2% ($p = 0.0011$) in GCE28. A significant reduction in invading cells was also observed in GIN28 and GCE28 cell lines upon treatment with formononetin at 500 µM, impairing invasion by 26.8% ($p = 0.0042$) and 14.7% ($p = 0.0193$), respectively. While taxifolin demonstrated an antiproliferative effect across all cell lines, a significant effect on invasion was only observed in GCE28 ($p = 0.0034$) when used at 500 µM, reducing invasion to 15.5% (Fig. 5C–F).

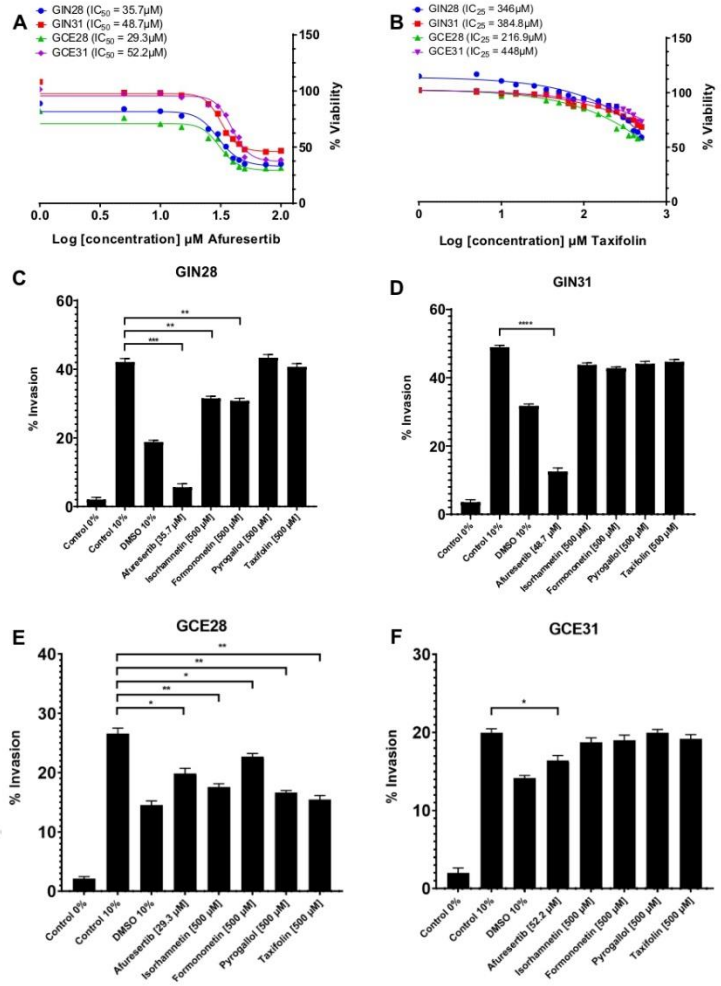


Figure 5. In vitro assessment of identified compounds for drug repurposing as validation of in silico workflow. (**A**,**B**) Metabolic viability was assessed for afuresertib (**A**) and taxifolin (**B**) in a 96-well 16-point dose response assay across four patient-derived GBM lines. PrestoBlue was used to assess metabolic viability after 72 h and data is presented as the mean percent viability compared to DMSO-treated controls (n = 6). Afuresertib was identified as the most potent drug inhibiting proliferation at IC_{50} values of 35.7 μM, 48.7 μM, 29.3 μM and 52.2 μM for the GIN28, GIN31, GCE28 and GCE31 cell lines, respectively (**A**). Taxifolin showed a modest but significant effect on cell sensitisation generating IC_{25} values of 346 μM, 384.8 μM, 216.9 μM, 448 μM on GIN28, GIN31, GCE28 and GCE31 cell lines, respectively (**B**). (**C**–**F**) Effects on invasion in GBM invasive margin (GIN28, GIN31) and GBM Contrast-Enhanced core (GCE28, GCE31) cell lines following treatment with four compounds at 500 μM and afuresertib at IC50 concentration. Invasion towards 0% FBS (Control 0%) on untreated cells and DMSO treated (DMSO 10%) controls were also included. Data is presented as mean percent invasion ± SEM compared to number of seeded cells after 24 h incubation. Significance was tested by one-way ANOVA (*$p < 0.05$, **$p < 0.01$, ***$p < 0.001$, **** $p < 0.0001$) comparing each data set to control 10% (invasion towards 10% FBS; n = 3).

Therefore, afuresertib should be considered for in vitro studies to understand the underlying mechanisms to different responses, as well to assess the effect on GSCs, potentially leading to further in vivo studies to characterize its pre-clinical suitability. Collectively, in vitro assessment identifies 2/5 tested compounds as impairing metabolic viability, and 3/5 tested compounds as impairing invasion. Considering both intra- and inter-tumor heterogeneity which manifests in GBM, and thereby the likely biological variation in TCGA transcriptomics data compared to the patient-derived GBM lines used in this study, validation of 40% and 60% of repurposed compounds for anti-proliferative and anti-invasion effects, represents an effective hit rate and validates TISMAN as an in silico workflow to expedite compound prioritization at a drug discovery phase. Furthermore, identified genes lacking targeting molecules should be considered in structural studies to enable and exploit molecular docking efforts.

Received: 1 November 2021; Accepted: 10 June 2022
Published online: 01 July 2022

References

1. World Health Organization. (Geneva, 2020).
2. Hanahan, D. & Weinberg, R. Hallmarks of cancer: The next generation. *Cell* **144**, 646–674. https://doi.org/10.1016/j.cell.2011.02.013 (2011).
3. Hausser, J. & Alon, U. Tumour heterogeneity and the evolutionary trade-offs of cancer. *Nat. Rev. Cancer* **20**, 247–257 (2020).
4. Chen, P.-H. *et al.* Metabolic diversity in human non-small cell lung cancer cells. *Mol. Cell* **76**, 838–851. https://doi.org/10.1016/j.molcel.2019.08.028 (2019).
5. Jemal, A., Siegel, R., Xu, J. & Ward, E. Cancer statistics, 2010. *CA Cancer J. Clin.* **60**, 277–300. https://doi.org/10.3322/caac.20073 (2010).
6. Petrecca, K., Guiot, M., Panet-Raymond, V. & Souhami, L. Failure pattern following complete resection plus radiotherapy and temozolomide is at the resection margin in patients with glioblastoma. *J. Neurooncol.* **111**, 19–23. https://doi.org/10.1007/s11060-012-0983-4 (2013).
7. Neftel, C. *et al.* An integrative model of cellular states, plasticity, and genetics for glioblastoma. *Cell* **178**, 835-849.e821. https://doi.org/10.1016/j.cell.2019.06.024 (2019).
8. Chen, J. *et al.* A restricted cell population propagates glioblastoma growth after chemotherapy. *Nature* **488**, 522–526. https://doi.org/10.1038/nature11287 (2012).
9. Richards, L. M. *et al.* Gradient of developmental and injury response transcriptional states defines functional vulnerabilities underpinning glioblastoma heterogeneity. *Nat. Cancer* **2**, 157–173. https://doi.org/10.1038/s43018-020-00154-9 (2021).
10. Couturier, C. P. *et al.* Single-cell RNA-seq reveals that glioblastoma recapitulates a normal neurodevelopmental hierarchy. *Nat. Commun.* **11**, 3406. https://doi.org/10.1038/s41467-020-17186-5 (2020).
11. Castellan, M. *et al.* Single-cell analyses reveal YAP/TAZ as regulators of stemness and cell plasticity in glioblastoma. *Nat. Cancer* **2**, 174–188. https://doi.org/10.1038/s43018-020-00150-z (2021).
12. Polson, E. S. *et al.* KHS101 disrupts energy metabolism in human glioblastoma cells and reduces tumor growth in mice. *Sci. Transl. Med.* **10**, eaar2718. https://doi.org/10.1126/scitranslmed.aar2718 (2018).
13. Wang, X. *et al.* Targeting pyrimidine synthesis accentuates molecular therapy response in glioblastoma stem cells. *Sci. Transl. Med.* **11**, eaau4972. https://doi.org/10.1126/scitranslmed.aau4972 (2019).
14. McCrorie, P. *et al.* Biomedical engineering approaches to enhance therapeutic delivery for malignant glioma. *J. Control. Release* **328**, 917–931. https://doi.org/10.1016/j.jconrel.2020.11.022 (2020).
15. Moffat, J. G., Vincent, F., Lee, J. A., Eder, J. & Prunotto, M. Opportunities and challenges in phenotypic drug discovery: An industry perspective. *Nat. Rev. Drug Discov.* **16**, 531–543. https://doi.org/10.1038/nrd.2017.111 (2017).
16. Faubert, B. *et al.* Lactate metabolism in human lung tumors. *Cell* **171**, 358–371. https://doi.org/10.1016/j.cell.2017.09.019 (2017).
17. Nilsson, A., Haanstra, J., Teusink, B. & Nielsen, J. Metabolite depletion affects flux profiling of cell lines. *Trends Biochem. Sci.* **43**, 395–397. https://doi.org/10.1016/j.tibs.2018.03.009 (2018).
18. Rancati, G., Moffat, J., Typas, A. & Pavelka, N. Emerging and evolving concepts in gene essentiality. *Nat. Rev. Genet.* **19**, 34–49. https://doi.org/10.1038/nrg.2017.74 (2018).
19. Lin, A. & Sheltzer, J. M. Discovering and validating cancer genetic dependencies: Approaches and pitfalls. *Nat. Rev. Genet.* **21**, 671–682. https://doi.org/10.1038/s41576-020-0247-7 (2020).
20. Adasme, M. F., Parisi, D., Sveshnikova, A. & Schroeder, M. Structure-based drug repositioning: Potential and limits. *Semin. Cancer Biol.* https://doi.org/10.1016/j.semcancer.2020.01.010 (2020).
21. Bushweller, J. H. Targeting transcription factors in cancer—From undruggable to reality. *Nat. Rev. Cancer* **19**, 611–624. https://doi.org/10.1038/s41568-019-0196-7 (2019).
22. Schellenberger, J. *et al.* Quantitative prediction of cellular metabolism with constraint-based models: The COBRA Toolbox v2.0. *Nat. Protoc.* **6**, 1290–1307. https://doi.org/10.1038/nprot.2011.308 (2011).
23. Orth, J. D., Thiele, I. & Palsson, B. O. What is flux balance analysis?. *Nat. Biotechnol.* **28**, 245–248. https://doi.org/10.1038/nbt.1614 (2010).
24. Ahn, E., Kumar, P., Mukha, D., Tzur, A. & Shlomi, T. Temporal fluxomics reveals oscillations in TCA cycle flux throughout the mammalian cell cycle. *Mol. Syst. Biol.* **13**, 953. https://doi.org/10.15252/msb.20177763 (2017).
25. Richelle, A., Joshi, C. & Lewis, N. E. Assessing key decisions for transcriptomic data integration in biochemical networks. *PLoS Comput. Biol.* https://doi.org/10.1371/journal.pcbi.1007185 (2019).
26. Opdam, S. *et al.* A systematic evaluation of methods for tailoring genome-scale metabolic models. *Cell Syst.* **4**, 318–329. https://doi.org/10.1016/j.cels.2017.01.010 (2017).
27. Pires Pacheco, M. *et al.* Identifying and targeting cancer-specific metabolism with network-based drug target prediction. *EBioMedicine* **43**, 98–106. https://doi.org/10.1016/j.ebiom.2019.04.046 (2019).
28. Csermely, P., Korcsmáros, T., Kiss, H., London, G. & Nussinov, R. Structure and dynamics of molecular networks: A novel paradigm of drug discovery. A comprehensive review. *Pharmacol. Ther.* **138**, 333–408. https://doi.org/10.1016/j.pharmthera.2013.01.016 (2013).
29. Colaprico, A. *et al.* TCGAbiolinks: An R/Bioconductor package for integrative analysis of TCGA data. *Nucleic Acids Res.* https://doi.org/10.1093/nar/gkv1507 (2016).
30. Schubert, E. & Rousseeuw, P. J. In *Similarity Search and Applications*. (eds. Giuseppe, A., Claudio, G., Vincent, O., & Miloš, R.) 171–187 (Springer International Publishing).
31. Yoshimaru, T., Nakamura, Y. & Katagiri, T. Functional genomics for breast cancer drug target discovery. *J. Hum. Genet.* **66**, 927–935. https://doi.org/10.1038/s10038-021-00962-6 (2021).
32. Maié, T. & Ticconi, F. *Analysis of Cancer Genome Atlas in R*, Retrieved from https://costalab.ukaachen.de/open_data/Bioinformatics_Analysis_in_R_2019/BIAR_D3/handout.html (2019). Accessed 20 Nov 2020.

33. Robinson, J. *et al.* An atlas of human metabolism. *Sci. Signal.* https://doi.org/10.1126/scisignal.aaz1482 (2020).
34. Agren, R. *et al.* The RAVEN toolbox and its use for generating a genome-scale metabolic model for *Penicillium chrysogenum*. *PLoS Comput. Biol.* https://doi.org/10.1371/journal.pcbi.1002980 (2013).
35. Vlassis, N., Pires Pacheco, M. & Sauter, T. Fast reconstruction of compact context-specific metabolic network models. *PLoS Comput. Biol.* https://doi.org/10.1371/journal.pcbi.1003424 (2014).
36. Zielinski, D. *et al.* Systems biology analysis of drivers underlying hallmarks of cancer cell metabolism. *Sci. Rep.* https://doi.org/10.1038/srep41241 (2017).
37. Wagner, B., Venkataraman, S. & Buettner, G. The rate of oxygen utilization by cells. *Free Radic. Biol. Med.* **51**, 700–712. https://doi.org/10.1016/j.freeradbiomed.2011.05.024 (2011).
38. Furse, S. *et al.* Lipid membrane curvature induced by distearoyl phosphatidylinositol 4-phosphate. *Soft Matter* **8**, 3090–3093. https://doi.org/10.1039/C2SM07358G (2012).
39. Chuang, Y. *et al.* Role of synaptojanin 2 in glioma cell migration and invasion. *Cancer Res.* **64**, 8271–8275 (2004).
40. Ben-Chetrit, N. *et al.* Synaptojanin 2 is a druggable mediator of metastasis and the gene is overexpressed and amplified in breast cancer. *Sci. Signal.* https://doi.org/10.1126/scisignal.2005537 (2015).
41. Budinich, M., Bourdon, J., Larhlimi, A. & Eveillard, D. A multi-objective constraint-based approach for modeling genome-scale microbial ecosystems. *PLoS One* **12**, e0171744. https://doi.org/10.1371/journal.pone.0171744 (2017).
42. Marler, R. T. & Arora, J. S. Survey of multi-objective optimization methods for engineering. *Struct. Multidiscip. Optim.* **26**, 369–395. https://doi.org/10.1007/s00158-003-0368-6 (2004).
43. Page, L. B. & Motwani, R. W. (ed Stanford InfoLab) (1998).
44. Tomi-Andrino, C. *et al.* Physicochemical and metabolic constraints for thermodynamics-based stoichiometric modelling under mesophilic growth conditions. *PLoS Comput. Biol.* **17**, e1007694. https://doi.org/10.1371/journal.pcbi.1007694 (2021).
45. Freshour, S. *et al.* Integration of the Drug–Gene Interaction Database (DGIdb 4.0) with open crowdsource efforts. *Nucleic Acid Res.* https://doi.org/10.1093/nar/gkaa1084 (2020).
46. Davis, A. *et al.* Comparative toxicogenomics database (CTD): Update 2021. *Nucleic Acid Res.* https://doi.org/10.1093/nar/gkaa891 (2020).
47. Gilson, M. *et al.* BindingDB in 2015: A public database for medicinal chemistry, computational chemistry and systems pharmacology. *Nucleic Acid Res.* **44**, D1045–D1053. https://doi.org/10.1093/nar/gkv1072 (2016).
48. Piñeiro-Yáñez, E. *et al.* PanDrugs: A novel method to prioritize anticancer drug treatments according to individual genomic data. *Genome Med.* https://doi.org/10.1186/s13073-018-0546-1 (2018).
49. Sheils, T. *et al.* TCRD and Pharos 2021: Mining the human proteome for disease biology. *Nucleic Acid Res.* https://doi.org/10.1093/nar/gkaa993 (2020).
50. Mitsopoulos, C. *et al.* canSAR: Update to the cancer translational research and drug discovery knowledgebase. *Nucleic Acids Res.* **49**, D1074–D1082. https://doi.org/10.1093/nar/gkaa1059 (2020).
51. Greco, C. *et al.* Development of Pyrazolo[3,4-d]pyrimidine kinase inhibitors as potential clinical candidates for glioblastoma multiforme. *ACS Med. Chem. Lett.* **11**, 657–663. https://doi.org/10.1021/acsmedchemlett.9b00530 (2020).
52. Vasey, C. E. *et al.* Polymer pro-drug nanoparticles for sustained release of cytotoxic drugs evaluated in patient-derived glioblastoma cell lines and in situ gelling formulations. *Pharmaceutics*. https://doi.org/10.3390/pharmaceutics13020208 (2021).
53. Rogawski, D., Vitanza, N., Gauthier, A., Ramaswamy, V. & Koschmann, C. Integrating RNA sequencing into neuro-oncology practice. *Transl. Res.* **189**, 93–104. https://doi.org/10.1016/j.trsl.2017.06.013 (2017).
54. Wang, R. *et al.* Adult human glioblastomas harbor radial glia-like cells. *Stem Cell Rep.* **14**, 338–350. https://doi.org/10.1016/j.stemcr.2020.01.007 (2020).
55. Folger, O. *et al.* Predicting selective drug targets in cancer through metabolic networks. *Mol. Syst. Biol.* https://doi.org/10.1038/msb.2011.35 (2011).
56. Larsson, I., Uhlén, M., Zhang, C. & Mardinoglu, A. Genome-scale metabolic modeling of glioblastoma reveals promising targets for drug development. *Front. Genet.* https://doi.org/10.3389/fgene.2020.00381 (2020).
57. Szklarczyk, D. *et al.* STRING v11: Protein-protein association networks with increased coverage, supporting functional discovery in genome-wide experimental datasets. *Nucleic Acids Res.* **47**, D607–D613. https://doi.org/10.1093/nar/gky1131 (2019).
58. Mi, H., Muruganujan, A. & Thomas, P. D. PANTHER in 2013: Modeling the evolution of gene function, and other gene attributes, in the context of phylogenetic trees. *Nucleic Acids Res.* **41**, D377-386. https://doi.org/10.1093/nar/gks1118 (2013).
59. Jung, S. H. *et al.* Acyl-CoA thioesterase 7 is involved in cell cycle progression via regulation of PKCζ–p53–p21 signaling pathway. *Cell Death Dis.* **8**, e2793–e2793. https://doi.org/10.1038/cddis.2017.202 (2017).
60. You, B. J. *et al.* Orlistat displays antitumor activity and enhances the efficacy of paclitaxel in human hepatoma Hep3B cells. *Chem. Res. Toxicol.* **32**, 255–264. https://doi.org/10.1021/acs.chemrestox.8b00269 (2019).
61. Grube, S. *et al.* Overexpression of fatty acid synthase in human gliomas correlates with the WHO tumor grade and inhibition with Orlistat reduces cell viability and triggers apoptosis. *J. Neurooncol.* **118**, 277–287. https://doi.org/10.1007/s11060-014-1452-z (2014).
62. Ganipineni, L. P. *et al.* Paclitaxel-loaded multifunctional nanoparticles for the targeted treatment of glioblastoma. *J. Drug Target* **27**, 614–623. https://doi.org/10.1080/1061186x.2019.1567738 (2019).
63. Huang, Y.-Q., Wang, Y., Hu, K., Lin, S. & Lin, X.-H. Hippocampal glycerol-3-phosphate acyltransferases 4 and BDNF in the progress of obesity-induced depression. *Front. Endocrinol.* https://doi.org/10.3389/fendo.2021.667773 (2021).
64. Pei, Z. *et al.* Acyl-CoA synthetase VL3 knockdown inhibits human glioma cell proliferation and tumorigenicity. *Cancer Res.* **69**, 9175–9182. https://doi.org/10.1158/0008-5472.CAN-08-4689 (2009).
65. Yin, J. *et al.* ARS2/MAGL signaling in glioblastoma stem cells promotes self-renewal and M2-like polarization of tumor-associated macrophages. *Nat. Commun.* **11**, 2978. https://doi.org/10.1038/s41467-020-16789-2 (2020).
66. Verma, H., Cholia, R. P., Kaur, S., Dhiman, M. & Mantha, A. K. A short review on cross-link between pyruvate kinase (PKM2) and Glioblastoma Multiforme. *Metab. Brain Dis.* **36**, 751–765. https://doi.org/10.1007/s11011-021-00690-y (2021).
67. Liu, Z.-P., Wu, C., Miao, H. & Wu, H. RegNetwork: An integrated database of transcriptional and post-transcriptional regulatory networks in human and mouse. *Database* https://doi.org/10.1093/database/bav095 (2015).
68. Oliveros, J. C. *Venny. An interactive tool for comparing lists with Venn's diagrams.* https://bioinfogp.cnb.csic.es/tools/venny/index.html (2007–2015). Accessed 1 Aug 2021.
69. Xie, S. *et al.* Metabolic control by heat stress determining cell fate to ferroptosis for effective cancer therapy. *ACS Nano* **15**, 7179–7194. https://doi.org/10.1021/acsnano.1c00380 (2021).
70. Yee, P. P. *et al.* Neutrophil-induced ferroptosis promotes tumor necrosis in glioblastoma progression. *Nat. Commun.* **11**, 5424. https://doi.org/10.1038/s41467-020-19193-y (2020).
71. Eun, S. Y. *et al.* Identification of cytochrome c oxidase subunit 6A1 as a suppressor of Bax-induced cell death by yeast-based functional screening. *Biochem. Biophys. Res. Commun.* **373**, 58–63. https://doi.org/10.1016/j.bbrc.2008.05.178 (2008).
72. Hu, T.-T. *et al.* Detection of genes responsible for cetuximab sensitization in colorectal cancer cells using CRISPR-Cas9. Biosci. Rep. https://doi.org/10.1042/BSR20201125 (2020).
73. Köhler, A. & Hurt, E. Gene regulation by nucleoporins and links to cancer. *Mol. Cell* **38**, 6–15. https://doi.org/10.1016/j.molcel.2010.01.040 (2010).

74. The International Transporter Consortium. Membrane transporters in drug development. *Nat. Rev. Drug Discov.* **9**, 215–236. https://doi.org/10.1038/nrd3028 (2010).
75. Fernandez, R. F. *et al.* Acyl-CoA synthetase 6 enriches the neuroprotective omega-3 fatty acid DHA in the brain. *Proc. Natl. Acad. Sci.* **115**, 12525. https://doi.org/10.1073/pnas.1807958115 (2018).
76. Miralpeix, C. *et al.* Carnitine palmitoyltransferase 1C negatively regulates the endocannabinoid hydrolase ABHD6 in mice, depending on nutritional status. *Br. J. Pharmacol.* **178**, 1507–1523. https://doi.org/10.1111/bph.15377 (2021).
77. Tang, Z. *et al.* Enhanced monoacylglycerol lipolysis by ABHD6 promotes NSCLC pathogenesis. *EBioMedicine* **53**, 102696. https://doi.org/10.1016/j.ebiom.2020.102696 (2020).
78. Jarrar, Y. B. & Lee, S.-J. Molecular functionality of cytochrome P450 4 (CYP4) genetic polymorphisms and their clinical implications. *Int. J. Mol. Sci.* https://doi.org/10.3390/ijms20174274 (2019).
79. Colapietro, A. *et al.* Crocetin extracted from saffron shows antitumor effects in models of human glioblastoma. *Int. J. Mol. Sci.* https://doi.org/10.3390/ijms21020423 (2020).
80. Di Lucca, J. *et al.* Variants of the xeroderma pigmentosum variant gene (POLH) are associated with melanoma risk. *Eur. J. Cancer* **45**, 3228–3236. https://doi.org/10.1016/j.ejca.2009.04.034 (2009).
81. Srivastava, A. K. *et al.* Enhanced expression of DNA polymerase eta contributes to cisplatin resistance of ovarian cancer stem cells. *Proc. Natl. Acad. Sci. U. S. A.* **112**, 4411–4416. https://doi.org/10.1073/pnas.1421365112 (2015).
82. Chen, H., Liu, H. & Qing, G. Targeting oncogenic Myc as a strategy for cancer treatment. *Signal Transduct. Target. Ther.* **3**, 5. https://doi.org/10.1038/s41392-018-0008-7 (2018).
83. Wang, J. *et al.* c-Myc is required for maintenance of glioma cancer stem cells. *PLoS One* **3**, e3769. https://doi.org/10.1371/journal.pone.0003769 (2008).
84. Ke, X. X., Zhang, R., Zhong, X., Zhang, L. & Cui, H. Deficiency of G9a inhibits cell proliferation and activates autophagy via transcriptionally regulating c-Myc expression in glioblastoma. *Front. Cell Dev. Biol.* **8**, 593964. https://doi.org/10.3389/fcell.2020.593964 (2020).
85. Chen, Y. *et al.* PPARα regulates tumor cell proliferation and senescence via a novel target gene carnitine palmitoyltransferase 1C. *Carcinogenesis* **38**, 474–483. https://doi.org/10.1093/carcin/bgx023 (2017).
86. Spencer, A. *et al.* The novel AKT inhibitor afuresertib shows favorable safety, pharmacokinetics, and clinical activity in multiple myeloma. *Blood* **124**, 2190–2195. https://doi.org/10.1182/blood-2014-03-559963 (2014).
87. Blagden, S. P. *et al.* Phase IB dose escalation and expansion study of AKT inhibitor afuresertib with carboplatin and paclitaxel in recurrent platinum-resistant ovarian cancer. *Clin. Cancer Res.* **25**, 1472–1478. https://doi.org/10.1158/1078-0432.Ccr-18-2277 (2019).
88. Yamaji, M. *et al.* Novel ATP-competitive Akt inhibitor afuresertib suppresses the proliferation of malignant pleural mesothelioma cells. *Cancer Med.* **6**, 2646–2659. https://doi.org/10.1002/cam4.1179 (2017).
89. Le Rhun, E. *et al.* Molecular targeted therapy of glioblastoma. *Cancer Treat. Rev.* https://doi.org/10.1016/j.ctrv.2019.101896 (2019).
90. Ahn, H. *et al.* Antitumor effect of pyrogallol via miR-134 mediated S phase arrest and inhibition of PI3K/AKT/Skp2/cMyc signaling in hepatocellular carcinoma. *Int. J. Mol. Sci.* https://doi.org/10.3390/ijms20163985 (2019).
91. Niu, C. S., Yang, Y. & Cheng, C. D. MiR-134 regulates the proliferation and invasion of glioblastoma cells by reducing Nanog expression. *Int. J. Oncol.* **42**, 1533–1540. https://doi.org/10.3892/ijo.2013.1844 (2013).
92. Tay, K. C. *et al.* Formononetin: A review of its anticancer potentials and mechanisms. *Front. Pharmacol.* **10**, 820. https://doi.org/10.3389/fphar.2019.00820 (2019).
93. Ong, S. K. L. *et al.* Focus on formononetin: Anticancer potential and molecular targets. *Cancers (Basel).* https://doi.org/10.3390/cancers11050611 (2019).
94. Hu, J. *et al.* ROS-mediated activation and mitochondrial translocation of CaMKII contributes to Drp1-dependent mitochondrial fission and apoptosis in triple-negative breast cancer cells by isorhamnetin and chloroquine. *J. Exp. Clin. Cancer Res.* **38**, 225. https://doi.org/10.1186/s13046-019-1201-4 (2019).
95. Li, J. *et al.* Taxifolin inhibits breast cancer cells proliferation, migration and invasion by promoting mesenchymal to epithelial transition via β-catenin signaling. *Life Sci.* **232**, 116617. https://doi.org/10.1016/j.lfs.2019.116617 (2019).
96. Sareddy, G. R. *et al.* PELP1 promotes glioblastoma progression by enhancing Wnt/β-catenin signaling. *Neurooncol. Adv.* **1**, vdz042. https://doi.org/10.1093/noajnl/vdz042 (2019).

Acknowledgements

This work was supported by the Biotechnology and Biological Sciences Research Council [Grant number BB/L013940/1], the Engineering and Physical Sciences Research Council [Grant number BB/L013940/1] and The Stoneygate Trust [Grant number CARO/SS/2016/CC1], through its Career Catalyst to RR. We thank the University of Nottingham for supporting the PhD studentship of CTA. The funders had no role in study design, data collection and analysis, decision to publish, or preparation of the manuscript.

Author contributions

C.T.A. and D.H.K. designed research; C.T.A. designed and performed the modelling; A.P. and R.R. designed the experimental setup; A.P. performed the experiments; C.T.A. and A.P. analyzed data; C.T.A., A.P., K.W., J.K., R.R., and D.H.K. wrote the paper.

Competing interests

The authors declare no competing interests.

Additional information

Supplementary Information The online version contains supplementary material available at https://doi.org/10.1038/s41598-022-14721-w.

Correspondence and requests for materials should be addressed to D.-H.K.

Reprints and permissions information is available at www.nature.com/reprints.

Publisher's note Springer Nature remains neutral with regard to jurisdictional claims in published maps and institutional affiliations.


Open Access This article is licensed under a Creative Commons Attribution 4.0 International License, which permits use, sharing, adaptation, distribution and reproduction in any medium or format, as long as you give appropriate credit to the original author(s) and the source, provide a link to the Creative Commons licence, and indicate if changes were made. The images or other third party material in this article are included in the article's Creative Commons licence, unless indicated otherwise in a credit line to the material. If material is not included in the article's Creative Commons licence and your intended use is not permitted by statutory regulation or exceeds the permitted use, you will need to obtain permission directly from the copyright holder. To view a copy of this licence, visit http://creativecommons.org/licenses/by/4.0/.

© The Author(s) 2022